Dissertation

submitted to the
Combined Faculties for the Natural Sciences and for Mathematics
of the Ruperto-Carola University of Heidelberg, Germany
for the degree of
Doctor of Natural Sciences

presented by
Pablo Luján Miralles, M.Sc.
born in Valencia, Spain

Oral examination:
July 4th, 2017

New roles for the phosphatase PRL-3 in epithelial architecture maintenance and endocytosis

Referees:

Dr. Christian Häring, EMBL Heidelberg

Prof. Dr. Ana Martín Villalba, Heidelberg University

The present work was carried out under the supervision of Dr. Maja Köhn at the European Molecular Biology Laboratory (EMBL) in Heidelberg, Germany, between July 2013 and June 2017.

A mi madre

"I have always been more interested in experiment, than in accomplishment."

Orson Welles

Acknowledgments

Foremost, I would like to express my sincere gratitude to my principal supervisor, Dr. Maja Köhn, for giving me the opportunity to develop a challenging and gratifying subject for my PhD thesis in her laboratory, for her continuous support, motivation, guidance, and her trust on me giving me freedom of action. My sincere thanks also to my thesis advisory committee members, Prof. Dr. Ana Martín Villalba, Dr. Christian Häring and Dr. Nassos Typas, for bringing new fresh ideas when and the distended atmosphere during the meetings. I also thank our collaborator Dr. Britta Brügger, Dr. Anne-Claude Gavin and Dr. Haralabia Boleti for their scientific support and expertise in different fields. Special thanks are dedicated to Marco Hennrich for the mass spectrometry collaboration, Aris Doukas for his knowledge transfer in *L. tarentolae* and showing me the wonders of Greece, Amy Cooke for teaching me polysome fractionation and shRNA stable cell line development, Stefan Terjung for his patience in the microscope and Malte Paulsen and Diana Ordonez for all their help in flow cytometry and shearing with me their love for the field.

I also would like to thank all my current and past colleagues in the Köhn laboratory, specifically Pablo Rios and Jeremy Chojnacki for all the moments of fun inside and outside work.

I want to thanks also all my precious friends Adrián, Aleix, Altozano, Balle, Cencillo, César, Victor, Manel, Xavi, Miguel and Laura and to my family. I specially give infinite thanks to Teresa, my wife, my partner in science and life and who gave me the apple of my eyes, my daughter Mia. Thanks for being always there supporting every crazy idea I had and my nerdy hobbies. And also to my father for being always there, in the good and bad moments, and for supporting me in every decision I did in my life.

Finally, I would like to thank the person to whom the manuscript is dedicated to: my mother. Thanks for inculcating your passion for science and life. This is the product of your love and perseverance during my education and knowing that you would be proud of me fills me of joy.

Publications

Parts of this work have been published or submitted to publication:

Lujan, P.*, Varsano, G.*, Rubio, T., Hennrich, M.L., Sachsenheimer, T., Gálvez-Santisteban, M., Martín-Belmonte, F., Gavin, A.C., Brügger, B., Köhn, M. (2016) PRL-3 disrupts epithelial architecture by altering the post-mitotic midbody position. *J Cell Sci.* **129**(21), 4130-42.

Fahs, S., **Lujan, P.**, Köhn, M. (2016) Approaches to study phosphatases. *ACS Chem. Biol.* **11**(11), 2944-61

Lujan, P.*, Rubio, T.*, Varsano, G., Köhn, M. A new mechanism to alter the post-mitotic midbody position revealed by studying the cancer-promoting phosphatase PRL-3 in polarized cells. *Comm. Int. Biol.* (Accepted)

Lujan, P., Rios, P., Müller, H.M., Lüchtenborg, C., Sachsenheimer, T., Brügger, B., Nickel, W., Köhn, M. PRL-3 enhances clathrin-mediated endocytosis by PI(4,5)P_2 dephosphorylation. (Submitted within 2017)

* Co-first authorship

Table of contents

Figures and table index

Abbreviations

5' UTR – 5' untranslated region

5-ptase – 5' phosphatase type IV

ACTB – Actin B

AMIS – Apical membrane initiation site

AP2 – Adaptor protein 2

aPKC – atypical protein kinase C

ARAP2 – Ankyrin repeat and PH domain

Arf1 – ADP-ribosylation factor 1

Arf6 – ADP-ribosylation factor 6

Arg – Arginine

BAR – Bin/Amphiphysin/Rvs

Bcl-2 – B-cell lymphoma 2

BFA – Brefeldin A

BRAG2 – Brefeldin A-resistant Arf

BSA – Bovin serum albumin

Caco-2 – Caucasian colon adenocarcinoma -2 cells

Cav-1 – Caveolin-1

CCP – Clathrin-coated pit

Cdc42 – Cell division control protein 42

CDE – Clathrin-dependent endocytosis

Cep55 – Centrosomal protein 55

Cep55 – Centrosomal protein 55

CHMP – Charged multivesicular body protein

CLTB – Clathrin light chain B

CNNM – Ancient conserved domain protein/cyclin M

CPC – Chromosomal passenger complex

CRE – Common recycling endosome

Ctrl – Control

Cys – Cysteine

Dab2 – Disable homolog 2

DAPI – 4' ,6-Diamidine-2' -phenylindole

DMSO – Dimethyl sulfoxide

DSP – Dual specificity phosphatase

DTT – Dithiothreitol

E. coli – *Escherichia coli*

ECM – Extracellular matrix

EDTA – Ethylenediaminetetracetic acid

EE – Early endosome

EF2 – Elongation factor 2

EGFR – Epithelial growth factor receptor

EGTA – Ethylene glycol-bis(β-aminoethyl ether)-N,N,N',N'-tetraacetic acid

EMT – Epithelial-mesenchymal transition

EPS15 – EGFR pathway substrate 15

ERM – Ezrin/Radixin/Moesin

ESCRT – Endosomal sorting complexes required for transport

FA – Focal adhesion

FACS – Fluorescence-activated cell sorting

FAK – Focal adhesion kinase

FCHO – FCH domain only

Fwd – Forward

GAP – GTPase activating protein

GDI – Guanosine nucleotide dissociation factor

GEF – Guanine nucleotide exchange factor

GFP – Green fluorescent protein

GPCR – G protein-coupled receptors

GST – Gluthatione S-transferase

GTP – Guanosine triphosphate

Gαi – Guanine-nucleotide protein α i

HAD – Haloacid dehalogenases

HCT116 – Western Blot

Hek293 – Human embryonic kidney 293 cells

HeLa – Henrietta Lacks cells

His – Histidine

HSC70 – ATPase heat shock cognate 70

HUVEC – Human umbilical vein endothelial cells

INPP4A/B – PI(3,4)P_2–specific inositol 4-phosphatase

IPTG – isopropyl β-D-1 thiogalactopyranoside

KD – knocked down

KIF – Kinesin

KLC1 – Kinesin light chain 1

KHC – Kinesin heavy chain

LC – Liquid chromatography

L. tarentolae – *Leishmania tarentolae*

MCF-10A – Michigan Cancer Foundation-10A cells

MCF-7 – Michigan Cancer Foundation-7 cells

MDCK – Madin-Darby canine kidney cells

MEF2C – Myocyte enhancer factor 2C

MESG – 2-amino-6-mercapto-7-methylpurine riboside

MKLP1 – Mitotic kinesin-like protein 1

MKLP1 – Mitotic kinesin-like protein1

MS – Mass spectrometry

NES – Nuclear export signal

NHERF-1 – Sodium-hydrogen exchanger regulatory factor 1

Par3 – Partitioning defective 3

Par6 – Partitioning defective 6

PC – Phosphatidylcholine

PCBP1 – PolyC-RNA-binding protein 1

PDGF – Platelet-derived growth factor

PFA – Paraformadehyde

PH PLCδ – Plekstrin homology domain of phospholipase Cδ

PI – Phosphatidylinositol

PI – Propidium iodide

PI(3,4,5)P_3 – Phosphatidylinositol 3,4,5-triphosphate

PI(4,5)P_2 – Phosphatidylinositol 4,5-biphosphate

PI3K – Phosphoinositide 3-kinase

PI4K – Phosphoinositide 4-kinase

PI4P – Phosphatidylinositol 4-phosphate

PI5K – Phosphoinositide 5-kinase

PIP – Phosphatidylinositol phosphate

PIP_2 – Phosphatidylinositol biphosphates

PIP5Kα – Phosphatidylinositol 4-phosphate 5-kinase type I alpha

PKP2 – Plakophilin-2

PKP4 – Plakophilin-4

Plk1 – Polo-like kinase 1

PNP – Nucleoside phosphorylase

Podxl – Podocalyxin precursor

PRC1 – Protein regulator of cytokinesis 1

PRL-1 – Phosphatase of regenerating liver -1

PRL-3 – Phosphatase of regenerating liver -3

pS – phosphoserine

PSTP – Protein serine/threonine phosphatase

PTEN – Phosphatase and tensin homolog

PTM – Post-translational modifications

Rab – Ras-related in brain

Rabin8 – Rab8 GEF

Rac – Ras-related C3 botulinum toxin substrate

REEP – Receptor expression-enhancing protein

Rev – Reverse

RhoA – Ras homolog family member A

RNase – Ribonuclease

RPM – Revolutions per minute

RT-PCR – Reverse transcription polymerase chain reaction

SDS-PAGE – Sodium dodecyl sulfate polyacrylamide gel electrophoresis

SH3 – SRC homology 3

SHIP2 – SH2 domain containing inositol 5-phosphatase

shRNA – short hairpin ribonucleic acid

siRNA – small interfering ribonucleic acid

Smad3 – mothers against decapentaplegic homolog 3

SN – Supernatant

Snj1 – Synaptojanin-p170

SNX9 – Sorting nexin 9

SRRM2 – Serine/arginine matrix protein 2

Swiss 3T3 – Swiss albino mouse embryo tissue

t-SNARE – *N*-ethylmaleimide-sensitive factor attachment receptors associated with target membrane

TCA – Trichloroacetic acid

TFNβ – transforming growth factor

TIAM1 – T-cell lymphoma invasion and metastasis 1

TPR – Tetratricopeptide

ULK3 – Unc-51-like kinase 3

VDAC1 – Voltage-dependent anion channel 1

VEGF – Vascular endothelial growth factor

VSP4 – Vacuolar protein sorting-associated 4

WB – Western Blot

WT – Wild type

YTH – YT51-B homology

YTHDC1 – YTH domain-containing-protein 1

Abstract

Phosphorylation and dephosphorylation of proteins and lipids are the major post-translational modifications involved in virtually all molecular signaling pathways in the cell and are catalyzed by kinases and phosphatases respectively. Abnormal variation in kinase and phosphatase activity leads to the development of several human diseases. Phosphatase of regenerating liver (PRL)-3 is a dual specificity phosphatase that has been related to cell proliferation, migration, invasion, and epithelial to mesenchymal transition. Interestingly, while PRL-3 is aberrantly overexpressed in primary and metastatic tumors, it is barely expressed at all in healthy human tissue. Therefore, PRL-3 represents a promising therapeutic target in cancer treatment and an emerging prognostic marker for tumor progression. However, finding robust PRL-3 substrate candidates remains a challenge in the field. The aim of the present work is to gain insight in both the cellular and molecular pathways where PRL-3 is involved.

The first part of this project is focused on the characterization of the role of PRL-3 in epithelial cell polarity using organotypic 3D-culture systems. We show that overexpression of PRL-3 disrupts epithelial architecture by promoting the development of cysts with ectopic lumens that arise from mispositioned midbodies. Furthermore, we propose a novel cellular mechanism where midbodies are retained in the lateral membrane due to acceleration of cytokinesis driven by PRL-3 overexpression.

The second part of the work deals with investigating PRL-3 PI(4,5)P2 phosphatase activity in cells, which was previously established in vitro. Here, we demonstrate this activity in vivo with a novel technique developed for this purpose. Moreover, we prove that the low phosphoinositide phosphatase activity of PRL-3 and its specific interaction with PI(4,5)P2 are essential for enhancing clathrin-mediated internalization.

In conclusion, we show that PRL-3 overexpression disrupts epithelial cell polarization probably by accelerating cytokinesis, and we demonstrate that it is a phosphoinositide phosphatase, increasing clathrin-dependent endocytosis.

Zusammenfassung

Phosphorylierung und Dephosphorylierung von Proteinen und Lipiden sind die häufigsten posttranslationalen Modifikationen, die in allen molekularen Signalwegen der Zelle involviert sind und durch Kinasen beziehungsweise Phosphatasen katalysiert werden. Eine Fehlfunktion der Kinase- oder Phosphataseaktivität kann zur Entwicklung verschiedenster Krankheiten führen. Die „Phosphatase of regenerating liver" PRL-3 ist eine doppelspezifische Phosphatase, die mit Metastasierung sowie den zu Grunde liegenden Prozessen wie Zellvermehrung, Migration, Invasion und dem Übergang von Epithel- zu Mesenchymgewebe in Verbindung gebracht wird. Während PRL-3 in primären Tumoren und Metastasen überexprimiert wird, ist die Expression im gesunden menschlichen Gewebe kaum nachweisbar. Daher repräsentiert PRL-3 einen vielversprechenden therapeutischen Ansatzpunkt in der Krebstherapie und dient als Marker zur Erkennung von Tumorprogression. Die Erforschung von bisher weitestgehend unbekannten PRL-3 Substraten ist jedoch noch immer im Fokus der aktuellen Forschung in diesem Bereich. Das Ziel der vorliegenden Arbeit ist es daher, weitere Einblicke in die Funktion von PRL-3 hinsichtlich zellbiologischer sowie molekularer Signalwege zu gewinnen.

Im ersten Teil des Projekts wird die Rolle von PRL-3 in der Polarität von Epithelzellen mit der Verwendung von Organ-repräsentierenden 3D Kultursystemen charakterisiert. Wir zeigen, dass eine Überexpression von PRL-3 die Epithelarchitektur der Zelle zerstört: So weisen die sich im 3D System entwickelnden Zysten, ausgehend von falsch lokalisierten Midbodies, ekotopische Lumen auf. Desweiteren demonstrieren wir einen neuen zellulären Mechanismus, bei welchem es, ausgelöst durch PRL-3 Überexpression, zu einer Beschleunigung der Zytokinese und einer daraus resultierender Ansammlung von Midbodies in der lateralen Zellmembran kommt.

Der zweite Teil der Arbeit befasst sich mit der Erforschung der PRL-3 $PI(4,5)P_2$ Phosphatase Aktivität innerhalb von Zellen, die zuvor bereits in vitro gezeigt werden konnte. Mit der Verwendung einer neuen, speziell für diesen Zweck entwickelten Technik ist es uns möglich die Dephosphorylierung auch in vivo zu demonstrieren. Außerdem können wir nachweisen, dass sowohl die niedrige Phosphoinositid Phosphatase Aktivität von PRL-3 als auch die spezifische Wechselwirkung von PRL-3 mit $PI(4,5)P_2$ essentiell für eine verbesserte Clathrin-vermittelte Endozytose sind.

Zusammenfassend zeigen wir, dass die Überexpression von PRL-3 zu einer Störung der Polarität von Epithelzellen führt, vermutlich durch eine Beschleunigung der Zytokinese. Desweiteren demonstrieren wir PRL-3 als eine Phosphoinositide Phosphatase, welche die Clathrin-vermittelte Endozytose erhöht.

1. Introduction

1.1. Protein phosphatases

In eukaryotic cells, rapid responses to external stimuli, besides internal homeostasis preservation, are achieved through an integrated network of fine-tuned intracellular signaling pathways based on post-translational modifications (PTMs) that increases the functional complexity and dynamism of the proteome (Snider, 2013; Knorre *et al.*, 2009; Cohen, 2002). Among the different types of PTMs, phosphorylation plays a central role in all intracellular processes by activating or inhibiting protein enzymatic activity, modifying protein subcellular localization, and changing protein-protein interaction affinity. Protein phosphorylation mainly occurs on hydroxyl-containing residues: tyrosine, serine, and threonine (Cohen, 2002; Hendriks *et al.*, 2013). Protein kinases are the enzymes that catalyze the covalent binding of a phosphoryl group to these residues, while protein phosphatases act as their counterpart by transferring the phosphate group from the phosphorylated amino acid to a water molecule (Cohen, 2002). Furthermore, phosphorylation is not an event restricted to proteins: kinases and phosphatases are also involved in the regulation of signal transduction affecting the phosphorylation of non-protein substrates, such as phosphatidylinositol phosphates (PIPs) (Majerus and York, 2009) or carbohydrates for proper starch and glycogen metabolism (Worby *et al.*, 2006; Romá-Mateo *et al.*, 2016).

1.1.1. Protein phosphatase superfamilies

While protein kinases have evolved from a common ancestor, protein phosphatases do not share any structural similarities and apparently, evolved independently (Tonks, 2006; Alonso et al., 2004). Historically, phosphatases can be classified into three superfamilies based on the enzymatic mechanism, although this is still currently being refined due to their complexity and new discoveries in the field (Fahs *et al.*, 2016; Li *et al.*, 2013; Duan *et al.*, 2015; Liberti *et al.*, 2013).

1. **Protein serine/threonine phosphatases (PSTPs):** Catalysis strictly requires the presence of metal ions in the enzyme active site and proceeds with direct phosphate hydrolysis, without an intermediate. Within PSTPs families phosphoprotein phosphatases (PPPs) and protein phosphatase 2C (PP2C) the active site is highly conserved, so substrate specificity is achieved by regulatory subunit interaction with the catalytic subunit, rather than by specific amino acid sequence recognition (Shi, 2009; Brautigan, 2013).

2. **Haloacid dehalogenase (HAD):** Catalytic activity is driven by a nucleophile superfamily in which the nucleophilic aspartic acid in the active site is an absolute requirement for the activity (Seifried *et al.*, 2013).

3. **Protein tyrosine phosphatase (PTP):** This is the largest superfamily with 96 members sharing the consensus catalytic signature motif His-Cys-X_5-Arg (X= any amino acid). The active site contains a cysteine that forms a phosphoenzyme intermediate with the substrate (Tonks, 2006; Tonks, 2013; Li *et al.*, 2013). The enzymatic mechanism is explained in more detail in the next section, as the subject of this thesis belongs to this family.

1.1.2. Protein Tyrosine Phosphatases

Protein dephosphorylation reactions driven by a PTP are a two-step mechanism. First, the thiol group of the catalytic cysteine acts as a nucleophile and attacks the phosphorus atom of the phosphate group. A conserved aspartic acid residue from a flanking loop facilitates this first step by acting as an acid while, in the second step, it acts as a general base, activating a water molecule that hydrolyses the phosphocysteine intermediate (Fig. 1) (Tremblay, 2009; Tonks, 2013). Within the PTP superfamily, two classes can be distinguished.

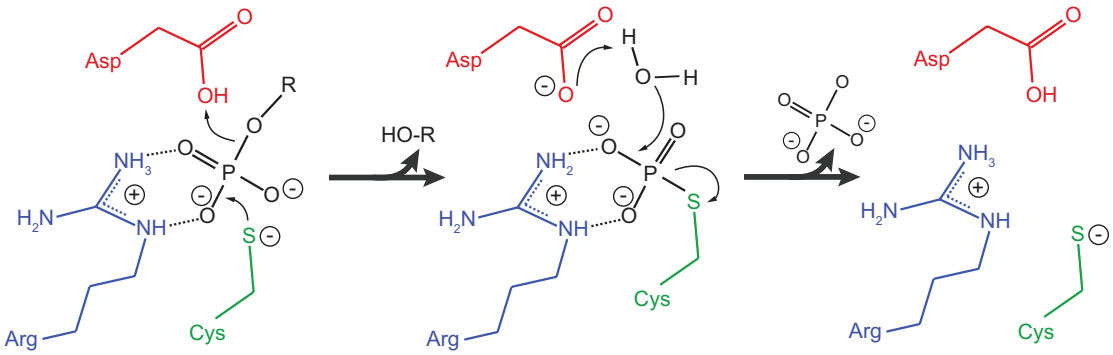

Figure 1. *Catalytic mechanism of protein tyrosine phosphatases. Relevant active site amino acids are drawn using the Lesk color scheme. R = substrate.*

- **Classical PTP family:** These cytoplasmic, as well as transmembrane, enzymes are characterized by phosphotyrosine specificity (Tonks, 2006; Tonks, 2013). Most

of the function, structure, and regulation findings have been revealed through the study of PTP1B, which is considered the prototype for this family (Tonks, 2003).

- **Dual Specificity Phosphatases (DSPs):** These enzymes are a heterogeneous group of non-transmembrane proteins characterized by a shallow catalytic pocket able to accommodate phosphotyrosine residues but also phosphoserine, phosphothreonine, and non-protein substrates (Pulido *et al.*, 2013; Patterson *et al.*, 2009; Tonks, 2013; Worby *et al.*, 2006). Phosphatase and tensin homolog (PTEN) is one of the most remarkable example of DSPs with a broad range of substrate specificity due to a catalytic pocket that is large enough to accommodate phosphotyrosine, phosphoserine, phosphothreonine, and the head group of PIPs (Song *et al.*, 2012; Maehama, 1998; Tamguney and Stokoe, 2007; Zhang *et al.*, 2012).

1.2. Phosphatases of regenerating liver (PRLs)

PRL phosphatases (*PTP4A* genes) belong to the DSP family. They comprise three small (20 kDa), single domain members (PRL-1, PRL-2, and PRL-3) that share high sequence identity. As a PTP, PRLs contain the conserved catalytic signature within a shallow active site that is unusually hydrophobic (Rios *et al.*, 2013; Al-Aidaroos and Zeng, 2010; Bessette *et al.*, 2008). PRLs contain a CaaX prenylation motif at the C-terminus (a is an aliphatic amino acid and X is any amino acid). The prenyl modification is unique within PTPs and essential for their anchoring to the cell membrane (Q Zeng *et al.*, 2000). Close to the lipidation motif, a basic amino acid-containing section, known as the polybasic sequence, is required for their plasma membrane localization, and it could also serve as a Golgi apparatus export signal (Parmar *et al.*, 2014), although this has not yet been proven. The catalytic activity of PRLs is redox-regulated by the formation of an intramolecular disulfide bond between the catalytic cysteine (Cys104) and the conserved Cys49, which is similar to other DSPs, such as PTEN (Boivin and Tonks, 2010; Skinner *et al.*, 2009). PRLs are involved in molecular pathways related to cell proliferation, migration, invasion, tumor growth, and metastasis (Fig. 2) (Rios *et al.*, 2013; Bessette *et al.*, 2008; Stephens *et al.*, 2005), which make them a unique class of oncogenic phosphatases that might

play a causative role in tumor development and metastasis (Guzińska-Ustymowicz and Pryczynicz, 2011).

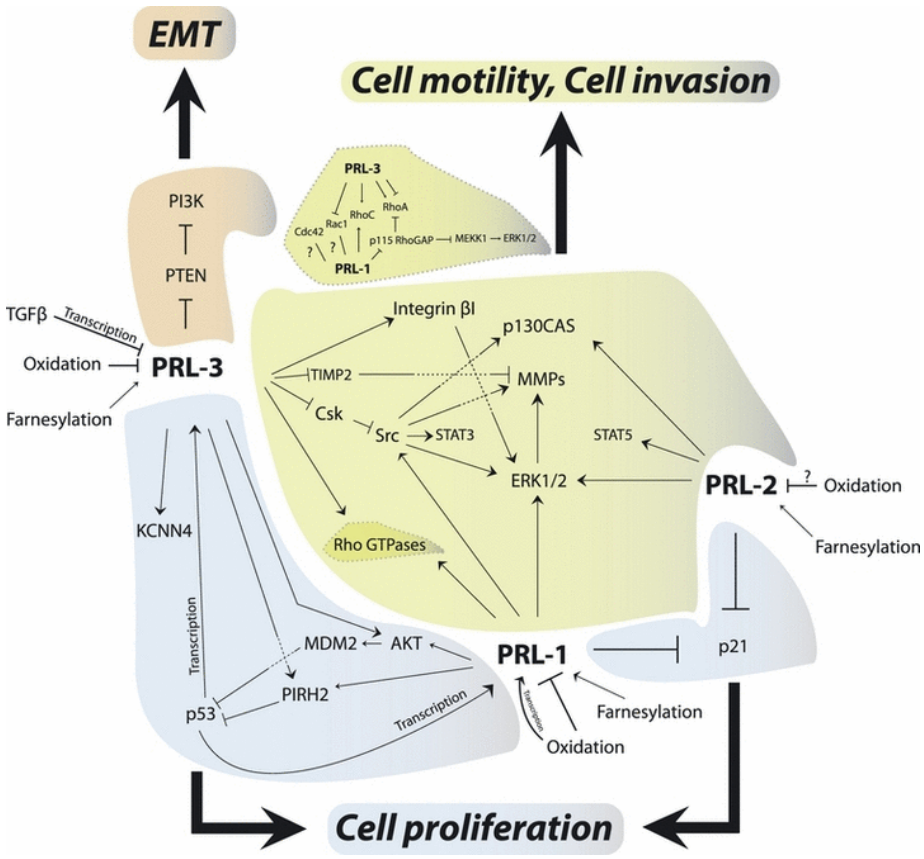

Figure 2. *The signaling network of the PRL phosphatase family. Several signaling pathways involved in epithelial mesenchymal transition (EMT) (orange), cell migration/invasion (green), and proliferation (blue) are affected upon PRLs' presence. Arrows and lines indicate indirect effects due to the absence of known substrates. Adapted by permission from John Wiley: The FEBS Journal (Rios et al.), copyright (2013).*

The main difference among PRLs is the distinct pattern of tissue distribution. Whereas PRL-1 and PRL-2 are ubiquitously expressed in adult human tissues (Dumaual *et al.*, 2006), PRL-3 seems to be much more restricted. Although PRL-3 mRNA is found in most tissues, with higher levels in heart and skeletal muscle (Mele *et al.*, 2015, www.gtexprotal.org, www.proteinatlas.com), the actual protein has only been confirmed in rat fetal heart tissue and mouse fetal intestine, adult heart, skeletal muscle, brain, pancreas and lung (Matter *et al.*, 2001; Guo *et al.*, 2006; Zimmerman *et al.*, 2014).

1.3. Phosphatases of regenerating liver -3 (PRL-3)

1.3.1. Subcellular localization of PRL-3

PRL-3 is mainly found in the plasma membrane, Golgi apparatus, endosomes, and to a lesser extent, in the endoplasmic reticulum (Rios *et al.*, 2013; Qi Zeng *et al.*, 2000; Krndija *et al.*, 2012). This particular subcellular localization is governed by its C-terminal lipidation and polybasic sequence. Unlike PRL-1 and PRL-2, the CaaX motif of PRL-3 contains two consecutives cysteines. The farnesylation of the first cysteine facilitates the palmitoylation on the second one leading to a unique double lipidation within the PRL family (Nishimura and Linder, 2013; Rubio and Köhn, 2016). Protein palmitoylation was proven to be a plasma membrane traffic signal (Linder and Deschenes, 2007). Nevertheless, polybasic sequence deletion inhibits PRL-3 plasma membrane localization, while a non-palmitoylable PRL-3 mutant (PRL-3 C171S) does not show a different cellular distribution compared to WT (data unpublished), suggesting that plasma membrane localization might be exclusively driven by the polybasic sequence.

1.3.2. Regulation of PRL-3 expression

The aforementioned discrepancy between mRNA and protein expression in several human tissues can only be explained by the extremely restricted regulation of PRL-3 levels at the transcriptional, translational, and post-translational stages (Fig. 3). Several possible scenarios have been reported in the past providing data often difficult to integrate, considering the different experimental conditions used. Some examples are discussed here.

1.3.2.1. Transcriptional regulation

Vascular endothelial growth factor (VEGF) stimulation activates PRL-3 transcription through the transcription factor myocyte enhancer factor 2C (MEF2C) (Fig. 3). However, this was only investigated in human umbilical vein endothelial cells (HUVEC) (Xu *et al.*, 2011). On the other hand, PRL-3 is able to up-regulate VEGF expression in lung cancer cell lines, together suggesting the possibility of a positive feedback loop for PRL-3 transcriptional regulation (Ming *et al.*, 2009). PRL-3 has also been postulated as a direct transcriptional target gene of tumor suppressor p53 (Fig.

3), although opposing results have been observed in different cell lines, suggesting that it is cell-type specific (Basak *et al.*, 2008; Min *et al.*, 2010). Moreover, PRL-3 may also be negatively regulated at the transcription level by transforming growth factor (TGFβ) (Fig. 3) through mothers against decapentaplegic homolog (Smad3) (Jiang *et al.*, 2011). Since TGFβ is often found to be comprised in cancer, it could explain PRL-3 aberrant expression in several kinds of tumors (see also section *1.3.4.*).

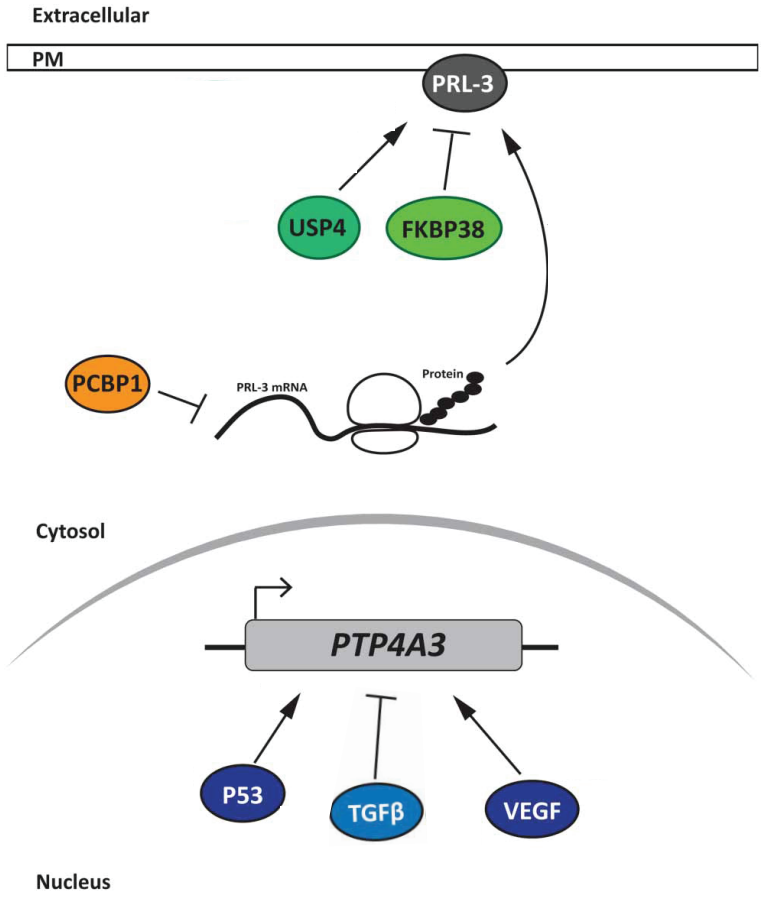

Figure 3. *Regulation of PRL-3 expression in cells. Final PRL-3 protein content in cells is tightly regulated at the transcriptional (blue), translational (orange), and post-translational stages (green). Adapted by permission from Portland Press: Biochemical Society Transactions Journal (Rubio and Köhn), copyright (2016).*

1.3.2.2. Translational regulation

PRL-3 mRNA contains triple GCCCAG motifs in the 5' untranslated region (5'-UTR) that interacts with PolyC-RNA-binding protein (PCBP1) retarding PRL-3 mRNA incorporation into the ribosome (Fig. 3). Therefore, PCBP1 overexpression

inhibits PRL-3 translation, and an inverse correlation between protein levels of PRL-3 and PCBP1 has been observed in primary tumors (Wang *et al.*, 2010).

1.3.2.3. Post-translational regulation

PRL-3 protein stability is also tightly regulated and repressed via proteasome degradation upon ubiquitination. FK506-binding protein (FKBP38) interaction with PRL-3 leads to the ubiquitination of the phosphatase (Myung-Suk Choi *et al.*, 2011), while the ubiquitin-specific protease (USP4) is in charge of deubiquitination (Xing *et al.*, 2016) (Fig. 3). The oncogenic abundance of the PRL-3 protein has been correlated with the presence or deletion of many ubiquitination-related proteins (Myung-Suk Choi *et al.*, 2011; Xing *et al.*, 2016).

1.3.3. Physiological roles of PRL-3

Unfortunately, physiological functions of PRL-3 remains unclear as its investigation faces technical challenge (Ríos *et al.*, 2014; Fahs *et al.*, 2016). PRL-3 knockout mice have not provided clear conclusions since they do not present any clear phenotype during development or adult life, with the only exception being a small perturbation in the ratio of gender in offspring (Zimmerman *et al.*, 2013). However, deletion of PRL-2 in mice leads to severe fetal growth retardation due to reduced placental development (Dong *et al.*, 2012), suggesting that the functions of the two phosphatases do not overlap *in vivo*.

1.3.4. Oncogenic roles of PRL-3

Historically, PRL-3 was first found highly overexpressed in several kinds of metastatic lesions derived from colorectal cancer, whereas it was not detected in the primary tumor nor in the normal colorectal epithelium, establishing PRL-3 as a metastasis-associated phosphatase (Saha *et al.*, 2001). However, numerous recent studies have correlated aberrant PRL-3 expression with both metastasis and also primary tumor formation with a poor prognosis outcome in multiple epithelial-related (breast, gastric, colon, ovarian, prostate, kidney, bladder, and lung) and non-epithelial-related cancers like acute myeloid and lymphoblastic leukemia (Al-Aidaroos and Zeng, 2010; Bessette *et al.*, 2008; Guzińska-Ustymowicz and Pryczynicz, 2011;

Stephens *et al.*, 2005; Cheng *et al.*, 2013; Ren *et al.*, 2009; Sun *et al.*, 2017; Chong *et al.*, 2014; Grönroos *et al.*, 2017; Mariscal *et al.*, 2016; Xiong *et al.*, 2016; Lian *et al.*, 2016; Wang *et al.*, 2008; Maacha *et al.*, 2016; Vandsemb *et al.*, 2016; Hollander *et al.*, 2016; Nakayama *et al.*, 2016; Zhang *et al.*, 2015; Yeh *et al.*, 2016; Yeh *et al.*, 2015; Zhou *et al.*, 2014). In fact, PRL-3 knockout mice exposed to procarcinogenic and inflammatory agents presented a reduction in colon tumor development (Zimmerman *et al.*, 2013), which raises the question of whether PRL-3 is an actual oncogene.

Epithelial to mesenchymal transition (EMT) is an extremely complex cell remodeling process critical during development and organogenesis where an epithelial cell loses its characteristic polarity and acquires migratory and invasive capabilities. In an adult organism, the cell plasticity conferred by EMT is the first step required for tumor metastasis (Diepenbruck and Christofori, 2016). PRL-3 may promote EMT as one of its oncogenic features in a phosphoinositide 3-kinase (PI3K)-dependent manner, as was shown in DLD-1 human colorectal cancer cells (Wang *et al.*, 2007). PI3K is a classical oncogene involved in PIP phosphorylation, mainly converting phosphatidylinositol (4,5)–bisphosphate ($PI(4,5)P_2$) to phosphatidylinositol (3,4,5)–triphosphate ($PI(3,4,5)P_3$) in the plasma membrane (see also section *1.3.5.*). $PI(3,4,5)P_3$ acts as a key second messenger in a broad range of cellular programs like cell migration, survival, and growth. Due to this, sustained $PI(3,4,5)P_3$ signaling is strictly associated with tumorigenesis (Yuan and Cantley, 2008), and a strong negative feedback loop driven by PTEN is required to ensure that this phospholipid is only transiently available at the cell surface (Carracedo and Pandolfi, 2008). Interestingly, elevated PRL-3 levels correlate with a reduction in PTEN (Wang *et al.*, 2007). Additionally, through PI3K, PRL-3 downregulates epithelial markers like E-cadherin, β_3 integrin, and γ-catenin (Wang *et al.*, 2007; Liu *et al.*, 2009; Zhao *et al.*, 2008), and up-regulates mesenchymal markers like fibronectin and Snail (Wang *et al.*, 2007).

PRL-3 overexpression also provokes the activation of another classical oncogene, the protein tyrosine kinase Src (Liang *et al.*, 2007). Src is involved in several cellular processes such as differentiation, motility, and adhesion, and its aberrant activation has been related with many human cancer types (Roskoski, 2004). PRL-3 mediates Src activation leading to constant phosphorylation of downstream targets of Src, such as ERK1/2. Moreover, PRL-3 itself is a Src substrate and a positive feedback loop may exist (Liang *et al.*, 2007; Fiordalisi *et al.*, 2013). Taking into consideration the drastic morphological and molecular changes that are needed for EMT and cell migration and invasion, PRL-3 might be affecting multiple signaling

pathways that have yet to be fully elucidated.

1.3.5. PRL-3 substrate candidates

Identification of PRL-3 substrates that correlate with the clinical and cellular phenotype observed upon PRL-3 overexpression remains the most challenging unsolved question in the field (Ríos *et al.*, 2014; Fahs *et al.*, 2016). During the last decade several substrates have been postulated for PRL-3, although the link between their dephosphorylation and cellular impact has not been strong enough to directly link them with the PRL-3 overexpression-caused cellular phenotypes. These potential substrates are $PI(4,5)P_2$, β_1 integrin, ezrin, keratin 8, nucleolin, stathmin, and elongation factor 2 (EF2), focal adhesion kinase (FAK) and sodium-hydrogen exchanger regulatory factor 1 (NHERF1)(McParland *et al.*, 2011; Orsatti *et al.*, 2009; Peng *et al.*, 2006; Mizuuchi *et al.*, 2009; Ping Zheng *et al.*, 2010; Semba *et al.*, 2010; Tian *et al.*, 2012; Peng *et al.*, 2009). However, of these only $PI(4,5)P_2$, β_1 integrin, and ezrin have been confirmed to be directly dephosphorylated by PRL-3, while a correlation between PRL-3 overexpression and reduced phosphorylation of the other proposed substrates has been shown and an indirect effect cannot be excluded. Moreover, recently PRL-3 was shown to also function as a pseudophosphatase given that the PRL-3 active site serves to interact with the magnesium transporters CNNM3 and CNNM4 without dephosphorylating them (Zhang *et al.*, 2017; Funato *et al.*, 2014). Substrates relevant to this study are discussed in the following:

- **$PI(4,5)P_2$:** PIPs are phosphorylated derivatives of the lipid phosphatidylinositol (PI). Reversible phosphorylation at positions 3, 4, and 5 position of the inositol ring generates seven interconvertible species (Fig. 4A) (Di-Paolo and De Camilli, 2006; Le-Roy and Wrana, 2005; Saarikangas *et al.*, 2010; Shewan *et al.*, 2011). All seven PIPs are minor components of eukaryotic cell membranes but are critical for several fundamental biological processes (Balla, 2013; Di-Paolo and De Camilli, 2006; Saarikangas *et al.*, 2010). Indeed, abnormal PI metabolism is related to many human diseases such as cancer, diabetes, and autoimmune disorders (Bunney and Katan, 2010; Balla, 2013; Majerus and York, 2009). Each PIP is spatially restricted in cellular membranous compartments (Fig. 4B). They can be rapidly interconverted from one species to another by lipid kinases and phosphatases, and the cleavage of the inositol head group by phosphoinositide-

specific phospholipase C enzymes (PLCs) serve to propagate and amplify signaling. PI(4,5)P_2 participates in virtually every event that occurs at the cell surface, including endo- and exocytosis, ion channel-mediated transport, cytokinesis, cell shape, motility, polarity, and adhesion, by modulation of its own levels and by its compartmentalization within the plasma membrane (McLaughlin *et al.*, 2002). Recently, it was described that PRL-3 can dephosphorylate PI(4,5)P_2 *in vitro* (McParland *et al.*, 2011), but the biological consequences of this activity and *in vivo* confirmation remain unaddressed.

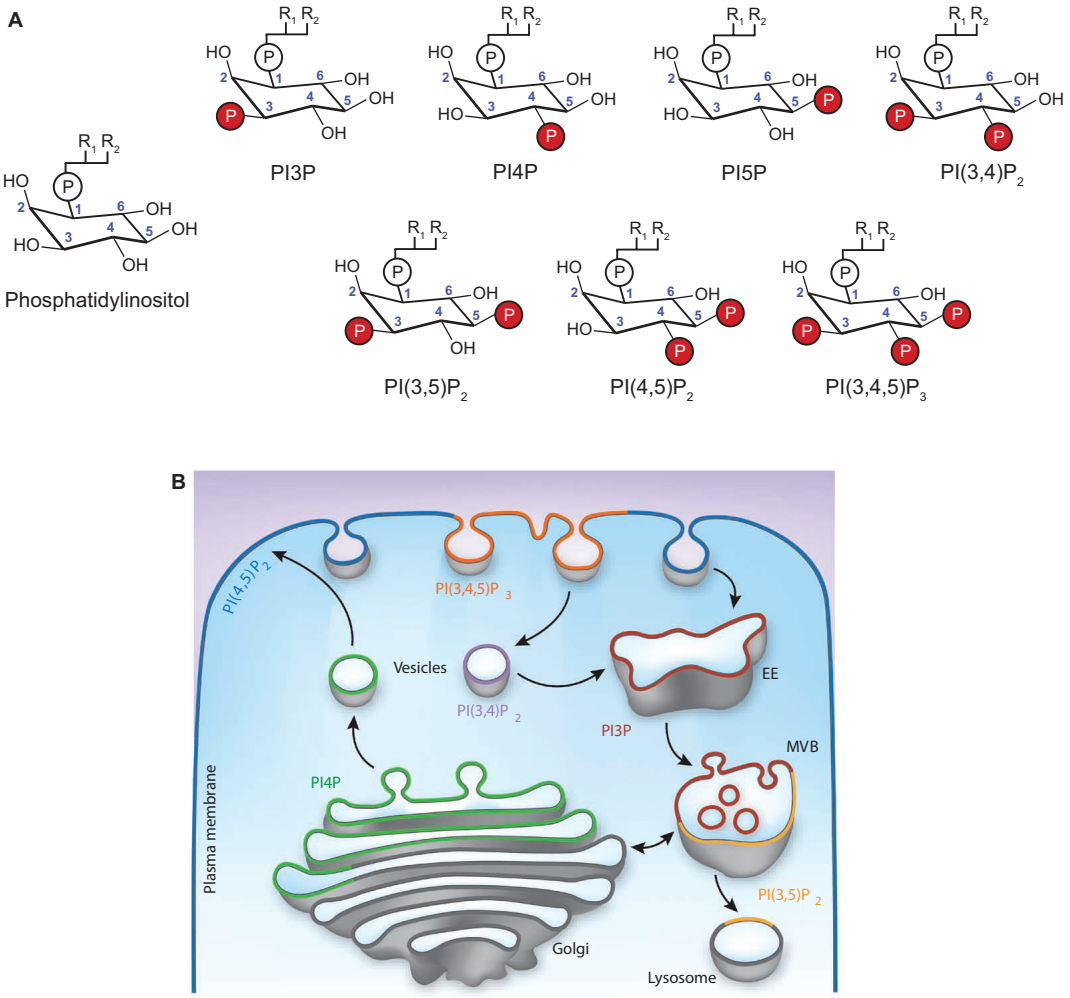

Figure 4. *Phosphatidylinositol phosphate structures and subcellular localization.* ***A*** *Phosphatidylinositol molecules are formed by a fatty acid backbone attached to an inositol ring thought a phosphate. Positions 3, 4 and 5 can be phosphorylated in any combination giving rise to 7 species. R_1 and R_2 = aliphatic chains.* ***B*** *Each phosphoinositide localizes to specific membranous compartments also contributing to its identity. EE = early endosome. MVB = multi-vesicle body. Adapted by permission from MacMillan Publishers LTD: Nature Chemical Biology (Kutateladze), copyright (2010).*

- **β_1 integrin:** Integrins are transmembrane proteins that mediate cell-cell and cell-extracellular matrix interactions. They are always found as heterodimers that contain an α and β subunit, but only the β subunits can be phosphorylated in the cytosolic region (Takada *et al.*, 2007; Shattil *et al.*, 2010). PRL-3 is an integrin-associated protein with preference for α1 and β1 integrin (Peng *et al.*, 2009; Peng *et al.*, 2006; Tian *et al.*, 2012). Furthermore, PRL-3 is able to dephosphorylate β1 integrin at pTyr783 (Tian *et al.*, 2012), but its biological significance remains unknown.

- **Ezrin:** Belonging to the Ezrin/Radixin/Moesin (ERM) family, Ezrin works as molecular scaffold between actin filaments and the plasma membrane. Tyr and/or Thr residue phosphorylation and PI(4,5)P_2 binding are both required for the exposure of the actin binding sites (Neisch and Fehon, 2011). Therefore, since PRL-3 can dephosphorylate Ezrin at pThr567 (Forte *et al.*, 2008), it might counteract Ezrin opening and activation. However, this effect was not confirmed in other experimental conditions, suggesting that this finding could be cell-type specific (Mizuuchi *et al.*, 2009).

1.4. Cell polarity and epithelial architecture maintenance

1.4.1. Structure of mammalian epithelia

Epithelial tissues contain a single sheet of clasped epithelial cells providing an impermeable barrier between two interfaces and are prone to forming cysts or tubules. In cysts the single layer of epithelial cells surrounds a central hollow lumen leading to a spherical shape, whereas in tubules this shape is elongated and cylindrical. Normally, in epithelial organs such as lung, mammary glands, or kidney, a combination of both structures can be found, forming a network of branching tubules that terminate in cysts (Brien *et al.*, 2002). Each cell taking part in an epithelial sheet is polarized, showing three types of plasma membrane domains that are morphologically and chemically different: a) an apical membrane that faces inward toward the lumen, b) a basal membrane that interacts with the extracellular matrix (ECM) through integrin and non-integrin receptors and, c) a lateral surface that establishes tight junctions, desmosomes, and adherens junctions with neighboring cells

to ensure tissue impermeability (St Johnston and Ahringer, 2010; Brien *et al.*, 2002; Roignot *et al.*, 2013; McCaffrey and Macara, 2009; Datta *et al.*, 2011). The heterogeneous distribution of both proteins and lipids across the plasma membrane creates a clear apico-basal polarity. The epithelium also provides some consistency and continuity to the tissue through a thick cortical belt of actin linked to the apical surface through ERM proteins. In the lateral membrane, members of the cadherin family bridge the adjacent plasma membranes of neighboring cells, forming desmosomes and adherens junctions that carry out adhesive functions (Baum and Georgiou, 2011). Tight junctions are located in the interphase between apical and lateral membranes and prevent membrane component diffusion between both domains (Matter and Balda, 2003).

1.4.2. Protein and lipid compartmentalization

As previously mentioned, epithelial cell polarity is defined as a heterogeneous distribution of different proteins and lipids throughout the cell. This compartmentalization is achieved through the cooperative contribution of different cellular machineries that take charge of protein and lipid segregation: the partitioning defective and atypical protein kinase (Par3/Par6/aPKC) complex, PIP asymmetric distribution, and polarized membrane-trafficking pathways.

- **The Par3/Par6/aPKC polarity complex:** This complex is a set of evolutionarily conserved proteins coupled to the junction structures (St Johnston and Ahringer, 2010). aPKC (isoforms ιPKC and ζPKC) is a serine/threonine protein kinase, and Par3 and Par6 are PDZ domain-containing scaffold proteins between the kinase and the tight junction. All three form a complex established by direct interactions subjected to different levels of regulation. Par6/aPKC recruitment is driven by cell division control protein 42 (Cdc42), which when activated binds to Par6 leading to aPKC activation. On the other hand, Par3 is recruited through the interaction of adhesion complex proteins and junctional adhesion proteins. Then, the active Par6-aPKC complex is recruited at the tight junction site through an association with Par3. The asymmetric localization of the complex promotes tight junction maturation and thereby contributes to protein and lipid segregation between apical and lateral membranes (Suzuki and Ohno, 2006; Aranda *et al.*, 2008). In addition, Par3 also recruits the Ras-related C3

botulinum toxin substrate (Rac) to the tight junction site and exchanges it with T-cell lymphoma invasion and metastasis 1 (TIAM1), which is required for the apical recruitment of PTEN and is necessary to induce PI asymmetry at the cell surface (Feng *et al.*, 2008; Chen and Macara, 2005).

- **Phosphatidylinositol phosphates:** Asymmetric PIP distribution across the plasma membrane is fundamental for apical and basolateral membrane identity determination (Shewan *et al.*, 2011). PI3K activation is a necessary part of the signaling pathways required for functional differentiation of epithelial cells (Laprise *et al.*, 2002). As a consequence, PI(3,4,5)P_3 levels in polarized epithelial cells are increased compared to non-polarized cells. However, its presence is restricted to the basolateral domain due the aforementioned apical recruitment of PTEN, which acts as a barrier by converting PI(3,4,5)P_3 to PI(4,5)P_2 and therefore prevents PI(3,4,5)P_3 diffusion in the apical domain (Fig. 5) (Comer and Parent, 2007; Datta *et al.*, 2011; Martin-Belmonte *et al.*, 2007). As a result, PI(4,5)P_2 is enriched at the apical surface, even though it can appear throughout the plasma membrane (Martin-Belmonte *et al.*, 2007; Gassama-Diagne *et al.*, 2006). This characteristic PIP distribution along the cell surface is crucial for the establishment and maintenance of cell polarity, and is achieved by the asymmetric recruitment of PIP-specific lipid-binding proteins, although the identity of these targets is still unknown.

- **Polarized membrane traffic:** In order to maintain each membrane domain protein and lipid identity, the uptake, transport, and cell surface delivery of a each kind must be vectorial and regulated (Apodaca *et al.*, 2012). On one hand, sorting signals present in the cytoplasmic cargo, transmembrane domain, or extracellular domain decoded by the corresponding transport machinery are required to ensure proper delivery to the correct membrane (Mellman and Nelson, 2008). While basolateral membrane proteins contain cytoplasmic domains like YXXØ-like or dileucine (LL/IL) motifs (Gonzalez and Rodriguez-Boulan, 2009), apical sorting determinants are more varied. Attachment to the membrane by a glycosylphosphatdylinositol anchor, extracellular glycosylation, Bin/ Amphiphysin/Rvs (BAR) domain-containing proteins, and belonging to lipid rafts are an example for apical sorting (Weisz and Rodriguez-Boulan, 2009; Mattila *et al.*, 2012; Stechly *et al.*, 2009; Mishra *et al.*, 2010; Dudek *et al.*, 2010). On the other hand, the membrane-trafficking network within the cell must also be polarized (Fig. 5). During protein biosynthesis, proteins are trafficked from the

endoplasmic reticulum to the Golgi apparatus, and distinct carriers for apical or basolateral membrane cargoes exist, although the specific carrier types are still unknown (Jacob and Naim, 2001; Farr *et al.*, 2009). Moreover, cell surface delivery from the Golgi apparatus can be direct or indirect through Ras-related in brain (Rab)8a and Rab11a GTPase-positive recycling endosomes (Ang *et al.*, 2004; Cramm-Behrens *et al.*, 2008), through Rab4 endosomes exclusively for apical transport (Cramm-Behrens *et al.*, 2008), or through Rab10-positive common recycling endosomes (CRE). Within the CRE, endosomes coming from the Golgi apparatus are mixed with apical or basolateral early endosomes coming from the plasma membrane (Bucci *et al.*, 1994). Again, cargoes need to be sorted from CRE according to their destination (Wang *et al.*, 2000; Babbey *et al.*, 2006; Henry and Sheff, 2008).

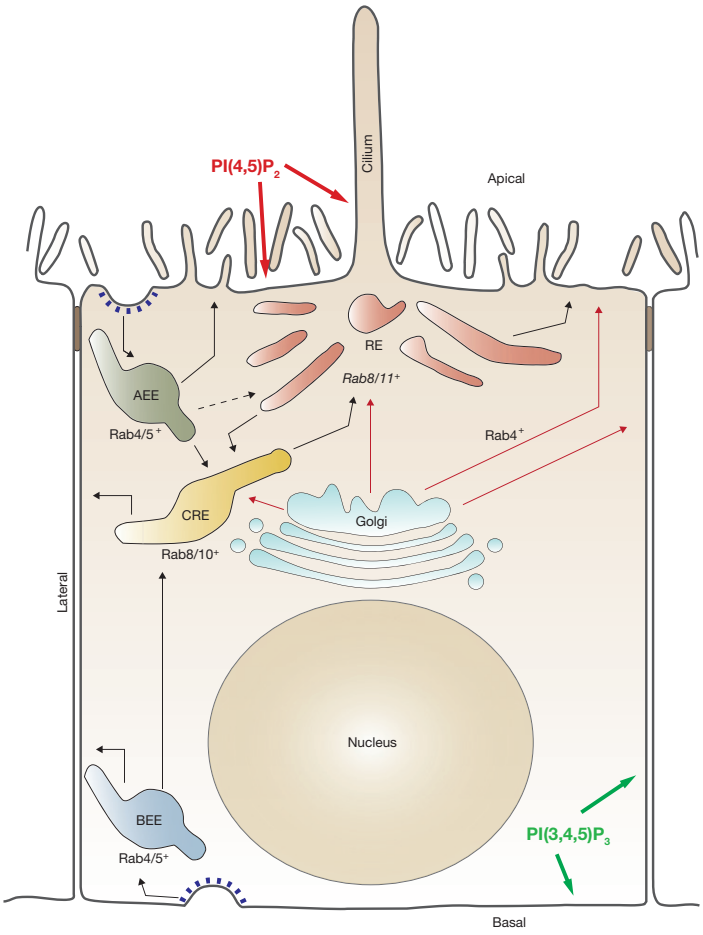

Figure 5. *Membrane-trafficking pathways in epithelial cells. Proteins, lipids, and fluids are internalized from the apical and basal membrane domain into apical (AEE) or basal (BEE) early endosomes, respectively. Then, they can either be recycled to the same membrane domain or transported to the common recycling endosome (CRE) where they mix with newly synthesized proteins coming from the Golgi apparatus. Consequently, they are trafficked to the recycling endosome (RE) or directly to the membrane. Newly synthesized proteins present in the Golgi*

apparatus can be transported to the destination membrane domain directly, through RE or CRE. $PI(4,5)P_2$ and $PI(3,4,5)P_3$ lipids are compartmentalized in the apical and lateral-basal membrane, respectively. Adapted by permission from MacMillan Publishers LTD: Nature Cell Biology (Apodaca et al.), copyright (2012).

The cytoskeleton also contributes in membrane transport directed by several proteins of the kinesin family. For example, Kifc3, Kif5B, and Kif17 are all involved in apical cargo transport (Noda *et al.*, 2001; Jaulin and Kreitzer, 2010; Jaulin *et al.*, 2007). Finally, vesicle fusion to the plasma membrane mediated by *N*-ethylmaleimide-sensitive factor attachment receptors associated with target membranes (t-SNAREs) proteins are also different according to the destination domain. Whereas syntaxin-1,-2, and -3 are involved in apical membrane fusion, syntaxin-4 localizes exclusively to the basolateral surface (Sharma *et al.*, 2006; Torkko *et al.*, 2008).

1.4.3. Three-dimensional epithelial cell model: a tool to study epithelial architecture in health and disease

In order to study molecular, cellular, and morphological mechanisms related with epithelial cells, canonical two-dimensional (2D) cell culture is not the best model to use since it does not recapitulate the physiologically distinctive features of epithelial cells *in vivo*. Indeed, epithelial cells grown in 2D are not polarized, are flat, and do not establish strong cell-cell interactions. Epithelial cells require external stimulation in order to differentiate and organize into an epithelial monolayer fed from an ECM microenvironment. Due to these limitations in 2D culture, efforts in the last two decades have been focused on the development of an artificial environment that resembles *in vivo* conditions.

Currently, Madin-Darby canine kidney (MDCK) epithelial cells and human Michigan Cancer Foundation 10A (MCF10A) breast cancer cells are extensively used to study epithelial cells in three dimensional (3D) culture (Apodaca, 2010; Debnath *et al.*, 2003; Bryant *et al.*, 2010; Bryant *et al.*, 2014; Gálvez-Santisteban *et al.*, 2012; Qu *et al.*, 2015; Rodríguez-Fraticelli *et al.*, 2015; Schlüter and Margolis, 2009; Jaffe *et al.*, 2008). In the presence of the 3D matrix, both cell lines are able to form spherical structures, named cysts or acini depending on the epithelial cell origin (Debnath and Brugge, 2005). MDCK cysts are described as a single layer of polarized epithelial cells surrounding a central hollow fluid-filled lumen. In these conditions, the apical domain

delineates the central lumen, while the basal membrane faces outside establishing protein interactions with the ECM, mimicking the epithelial architecture described in *1.4.1.* (Schlüter and Margolis, 2009). The plasticity of this 3D epithelial model also allows cellular and molecular biology tool applications such as protein knockdown, cDNA overexpression, and live-cell imaging, and being crowned as a powerful system to examine the molecular and cellular aspects of epithelial morphogenesis and related diseases (Debnath and Brugge, 2005; Brien *et al.*, 2002).

Notably, this 3D epithelial model has been extensively used since their development, not only to understand molecular mechanisms beyond lumen formation and maintenance but also in tumor promotion and development. Indeed, loss of polarity, luminal filling, epithelial architecture disruption, escape from apoptosis, and invasive behavior are considered key steps during epithelial organ tumorigenesis, all of which can be studied using these 3D models (Burstein *et al.*, 2004; Jaffe *et al.*, 2008; Debnath and Brugge, 2005; Leung and Brugge, 2012).

1.4.4. De Novo lumen formation

During development, tubular structures can develop either by a mechanical deformation by major morphogenetic movements of a pre-existing epithelial sheet, or by the programmed conversion of mesenchymal cells into epithelial cells and generation of a central lumen *de novo* through a complex molecular transformation known as mesenchymal-epithelial transition (MET), the opposite process to EMT (see also section *1.3.4.*) (Lubarsky and Krasnow, 2003). Within this second alternative, two mechanisms for *de novo* lumen generation have been determined: cavitation and hollowing (Bryant and Mostov, 2008; Datta *et al.*, 2011). For lumen generation by cavitation, a minimal critical cell mass is required. The inner cell population that is not in contact with the ECM suffers selective apoptosis, while the outer layer of cells progressively differentiates into polarized epithelial cells (Fig. 6). This process was observed in MCF10A 3D cysts mimicking mammary gland development, which have also been proven to be formed by the same mechanism (Debnath *et al.*, 2002; Mailleux *et al.*, 2007; Humphreys *et al.*, 1996).

For lumen generation through hollowing, which is of relevance to this study, polarization is generated from the very first epithelial cell division where the apical membrane domain separates and is coupled to polarized exocytosis, followed by fluid

and ion efflux in order to facilitate lumen growth and filling. As a result, a small lumen is initially formed in the center of the system that will grow as the cells continue to divide (Fig. 6). This mechanism has been proven in 3D MDCK cystogenesis, as well as during zebrafish gut development (Apodaca *et al.*, 2012; Bagnat *et al.*, 2007; Bryant and Mostov, 2008; Datta *et al.*, 2011).

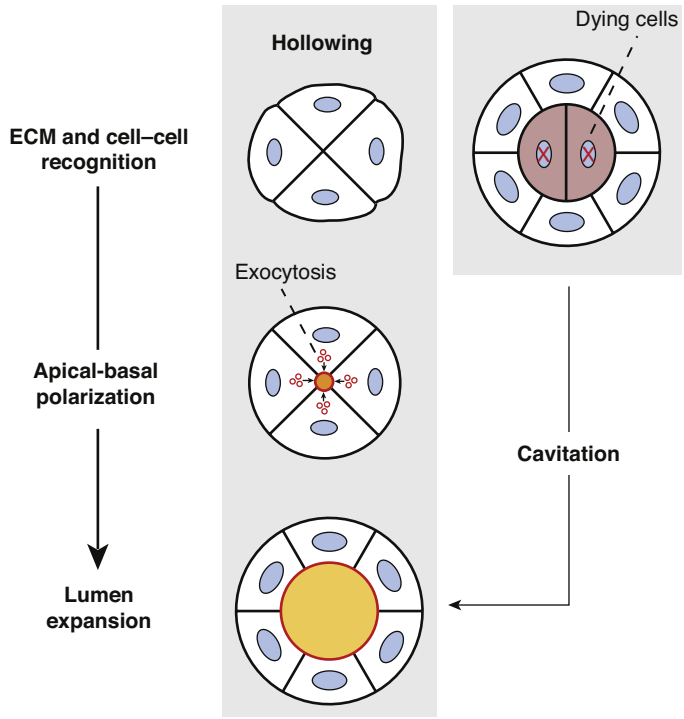

Figure 6. *Hollowing and cavitation mechanisms for de novo lumenogenesis. Polarization is generated from the very first epithelial cell division by* ***hollowing****. Then, the small lumen opened in the center of the system continually grows with ongoing cell divisions. However, lumenogenesis by* ***cavitation*** *requires a minimal critical cell mass before the inner cell population (not in contact with the ECM) suffers selective apoptosis, while the outer layer of cells differentiates into polarized epithelial cells. Adapted from Current Biology, 21, Datta, A., Bryant, DM. and Mostov KE, "Molecular regulation of lumen morphogenesis", R127, Copyright (2011), with permission from Elsevier.*

In MDCK cysts, *de novo* lumen formation requires for the originally non-polarized cells to receive initial external inputs to provide spatial coordinates in order to establish the direction of lumenogenesis and to induce apico-basal polarization (Schlu *et al.*, 2009). The initial signal comes from laminins and collagen IV present at the ECM that set an axis to orient the lumen position upon physical interaction with cellular β1 integrin (Treyer and Müsch, 2013; Cohen *et al.*, 2004; Datta *et al.*, 2011). Thereafter, primordial intercellular junctions (not tight junctions) are formed via a

multitude of adhesion molecules, like cadherins, in the cell-cell contact region, which establishes the second spatial cue (Datta *et al.*, 2011). After the polarity axis is set, the next step is the specification of the "apical membrane initiation site" (AMIS), a specialized membrane domain situated in the core region of the cell-cell contact zone and surrounded by the primordial junctions where apical determinants are transiently enriched by vectorial membrane-trafficking (Apodaca, 2010; Bryant *et al.*, 2010). The establishment of this region by selective delivery of apical determinant-containing vesicles (named polarized exocytosis) is the determining step to specify the lumen position since the lumen will subsequently open in this precise place delineated by the newly formed tight junctions (Wang *et al.*, 2014; D. Li *et al.*, 2014; Apodaca *et al.*, 2012; Schlüter *et al.*, 2009). The lumen will then start to form during the first cytokinesis around the midbody, the structure created within the intercellular bridge during cytokinesis (Fig. 7) (Steigemann and Gerlich, 2009; D'Avino and Capalbo, 2016; Overeem *et al.*, 2015; Schlüter and Margolis, 2009).

During AMIS specification at the two-cell stage, several apical signaling molecules, like the podocalyxin precursor (Podxl)-NHERF-1-Ezrin complex that is essential for apico-basal polarization, are not properly compartmentalized yet and are found diffused throughout the plasma membrane or at the basal surface (Bryant *et al.*, 2014). After this point, transcytosis of these apical components from the basolateral membrane to the forming luminal domain rapidly occurs, relying on the Rab11a-Rab8 guanine nucleotide exchange factor (Rabin8a)-Rab8a cascade. Apical cargo is taken up from the basolateral surface into FIP5/Rab11a positive vesicles. Then, Rab8a is recruited into those vesicles through Rabin8, which is able to control motor proteins, such as myosin-5B, for apical domain approach (Apodaca *et al.*, 2012; Bryant *et al.*, 2010; Dongying Li *et al.*, 2014). Finally, the hetero-octameric exocyst complex mediates apical cargo release into the target membrane creating and enhancing the AMIS. Moreover, this exocyst complex also localizes the Par3-aPKC complex and the Cdc42 activator Cdc42-GEF Tuba to the AMIS, which both contribute to this initial stage of lumenogenesis (Zuo *et al.*, 2009; Apodaca, 2010; Bryant *et al.*, 2010).

When AMIS is completely established, lumen maturation proceeds with Par3 and exocyst subunits Sec8 and Sec10 relocalization to the tight junction regions before the lumen physically opens (Bryant *et al.*, 2010). Par3 displacement drives the heterogeneous distribution of PTEN towards the tight junction border by physical interaction, leading to the exclusion of $PI(3,4,5)P_3$ from the apical membrane (see also section *1.4.2.*).

Finally, the last step of *de novo* lumen generation is the actual opening of the lumen. This stage is controlled by apical recruitment and activation of channels, pumps, and anti-adhesive proteins in charge of facilitating cell-cell membrane repulsion (Bryant and Mostov, 2008). These anti-adhesive proteins carry highly negatively charged groups, such as glycosyl and/or sialyl moieties, in their extracellular domains to accomplish their function by electrostatic repulsion (Meder *et al.*, 2005). This feature may explain why glycosylation in the extracellular domain is a cargo signal for apical delivery as previously described.

1.4.5. Lumen growth and maintenance in MDCK cysts

Since the apico-basal polarity axis in epithelial cells surrounding a lumen formed by the hollowing mechanism is already established from the first cell division, lumen growth is driven by continual division of the integrant epithelial cells. Normally, when cells in culture undergo mitosis, they reduce their contact with the substratum and neighboring cells to a minimum, and start to form a round shape. However, this behavior in epithelial cell would lead to the loss of polarity during cell division and subsequent problems in the restoration of the polarity axis. For that reason, all lateral, but not basal, junctions are kept during this process to ensure the maintenance of the polarity throughout the whole epithelium (Jinguji and Ishikawa, 1992; Baker and Garrod, 1993). Despite this, mitosis entails a big morphological change driven by the actomyosin contractile ring in charge of membrane fission at the end of the cell division, so partial rearrangement of these junctions is necessary for completion of the process (Morais-de-Sá and Sunkel, 2013; Ragkousi and Gibson, 2014). Like in the first cell division prior to the lumen opening, the AMIS is always recruited at the midbody and surrounds it during cell cytokinesis. This structure is then accompanied by apical machinery components able to develop a new lumen by themselves, so it must be delivered directly into the apical membrane in order to keep a single lumen, as well as to provide more apical components to the apical domain (Jaffe *et al.*, 2008; Dongying Li *et al.*, 2014; Morais-de-Sá and Sunkel, 2013; Overeem *et al.*, 2015; Schlüter *et al.*, 2009; Apodaca *et al.*, 2012). Then, cell-cell junction rearrangements required during cell division must be coordinated with the mitotic process to ensure the apical release of the midbody after abscission. While tight junctions are kept in the interphase between the apical and lateral membrane to avoid temporary loss of epithelium impermeability, E-cadherin that is normally distributed

in desmosomes and adherens junctions all along the lateral membrane is enriched close to the tight junctions before the actomyosin contractile ring is formed (Gloerich *et al.*, 2017; Ragkousi and Gibson, 2014).

In this scenario, midbody remnants seem to play a role after abscission, even if it is just as a scaffold for the AMIS. Indeed, it has been suggested that these remnants could participate in non-cytokinetic functions, such as cell fate determination and cell polarity specification (Chun-Ting Chen *et al.*, 2013; Kuo *et al.*, 2011; Morais-de-Sá and Sunkel, 2013). In fly notum and chick spinal cord, post-mitotic midbodies of neurons were found at polarized/apical domains, giving rise to the idea that post-mitotic midbodies might specify neuronal polarity (Pollarolo *et al.*, 2011; Chun-Ting Chen *et al.*, 2013). In *Drosophila* follicular epithelium, apical midbody localization provides a positional cue critical for the formation of the apico-basal axis of the tissue, as confirmed by disruption of the epithelial architecture in the case of the ectopic localization of the midbody (Morais-de-Sá and Sunkel, 2013). Finally, in transgenic mice expressing the GFP labeled midbody remnant marker mitotic kinesin-like protein (MKLP1), midbody remnants seem to mark the apical membrane of the embryonic neuroepithelium and adult intestinal crypts (Maliga *et al.*, 2013). Altogether, these findings suggest that midbodies have a role after cytokinesis, overturning the idea that they are just mitotic leftover that must be degraded.

The apical positioning of the midbody together with the AMIS is achieved by a two-step process (Jaffe *et al.*, 2008). First, the mitotic spindle must be oriented parallel to the basal membrane and perpendicular to the apico-basal membrane during metaphase. This alignment is achieved by its anchoring to the lateral membrane through astral microtubules. The assembly is controlled by a protein complex formed by guanine nucleotide-binding protein α i (Gαi), leu-gly-asn repeat protein (LGN), and the nuclear mitotic apparatus protein (NuMA) in a Par3/aPKC and E-Cadherin-dependent manner (Fig. 7) (Zhen Zheng *et al.*, 2010; Hao *et al.*, 2010; den Elzen *et al.*, 2009; Gloerich *et al.*, 2017). Loss of spindle orientation in polarized epithelial cells leads to midbody mispositioning (Fig. 7) and therefore to epithelial architecture disruption (Jillian C Pease and Tirnauer, 2011; Noatynska *et al.*, 2012; Fleming *et al.*, 2009; Jaffe *et al.*, 2008; Overeem *et al.*, 2015; Shahbazi and Perez-Moreno, 2015).

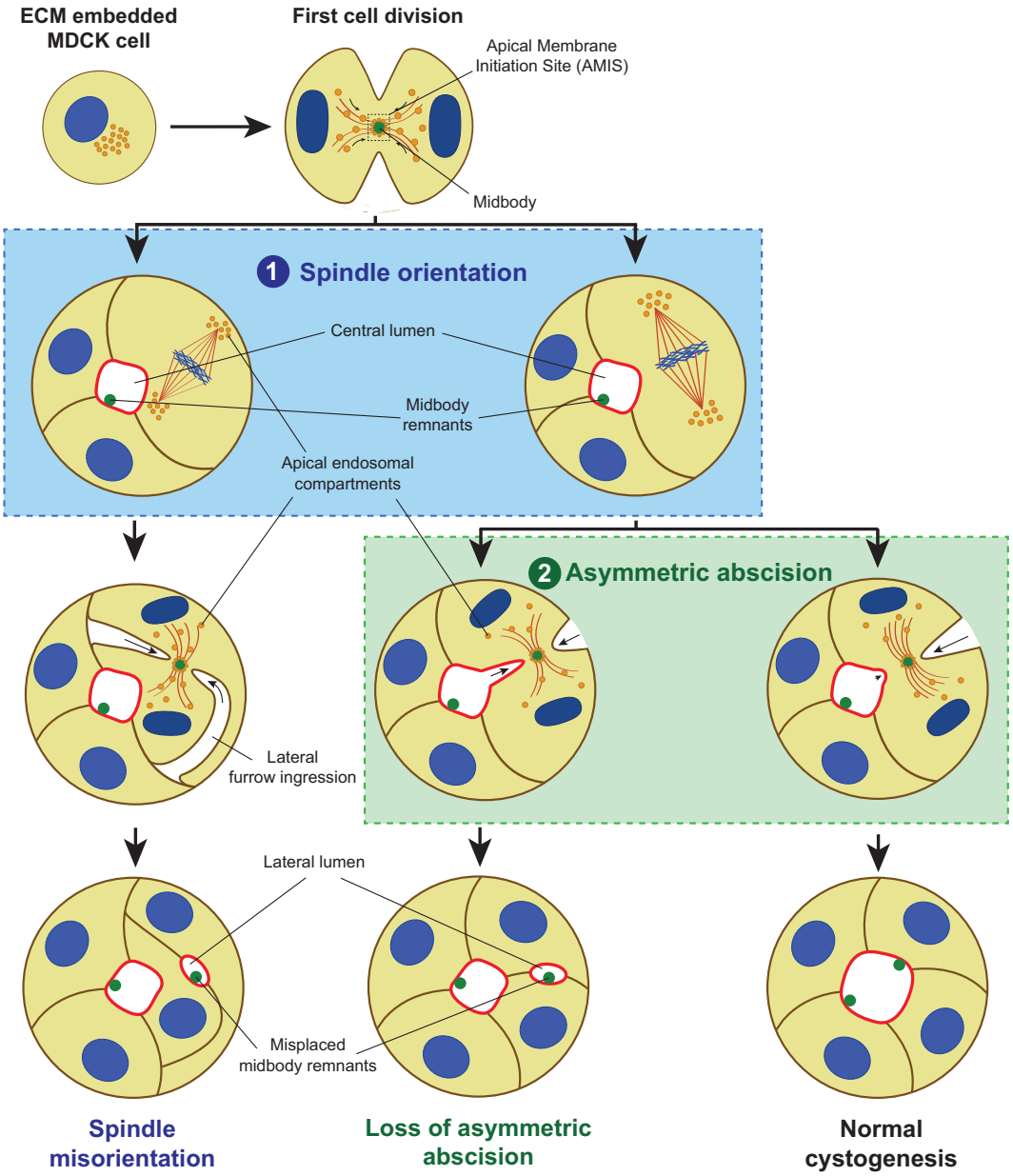

Figure 7. *Mechanisms for ectopic lumen formation through post-mitotic midbody mispositioning. At the early cystogenesis stage, apical components containing vesicles are recruited around the midbody during the first cell division forming the AMIS, which will turn into a lumen after abscission. In subsequent cell divisions, to ensure the single lumen maintenance, the midbody is delivered to the apical membrane with a planar orientation of the mitotic spindle to the apical-basal axis (1) followed by asymmetric furrow ingression (2). Loss of mitotic spindle orientation or loss of asymmetric furrow ingression may affect the apical positioning of the midbody leading to ectopic lumen development. Apical membrane = light red; basolateral membrane = brown; γ-tubulin = dark red; nuclei and chromosomes = blue; midbody and midbody remnants = green; apical endosomal compartment = orange.*

The second step in apical midbody positioning occurs when chromosomes move to the distal spindle poles during anaphase, and a cleavage furrow starts to be formed.

The progression of this furrow is driven by the actomyosin contractile ring, a transient structure located inside the plasma membrane at the location of the cleavage furrow. The mechanical tension applied from the contractile ring would be, theoretically, the same throughout the cleavage furrow if membrane composition is homogeneous, ending in a symmetric abscission (Mendes Pinto *et al.*, 2013). However, a differential junctional protein composition along the apico-basal axis in polarized cells leads to an asymmetric cell division that pushes the cytokinetic bridge to the apical membrane, facilitating delivery of the midbody to this membrane domain (Fig. 7) (Jaffe *et al.*, 2008). Unfortunately, the mechanism controlling this process is not well understood. Septins and anillin have been implicated in asymmetric cell division in *C. elegans*, but no further information has been added to this discovery (Maddox *et al.*, 2007). Since loss of asymmetric abscission could inherently lead to an inappropriate midbody positioning (Fig. 7), epithelial architecture disruption is a plausible hypothetical scenario that would also potentially promote tumor formation (Jaffe *et al.*, 2008; Overeem *et al.*, 2015; Schlüter *et al.*, 2009).

1.5. Cellular cytokinesis

Cytokinesis is the last step of mitosis where the cytosolic content of a single cell is divided into two. The cellular process begins with the assembly and narrowing of an equatorial contractile ring. Close to completion, the central region of the mitotic spindle is reorganized into a midbody that, from the center of the intracellular bridge, is in charge of direct abscission by action of the endosomal sorting complexes required for transport (ESCRT-III) proteins. The present section dissects the molecular mechanism of each cytokinetic step (Green *et al.*, 2012).

1.5.1. Establishing the place of cytokinesis

During anaphase, homologous chromosomes are separated and the spindle midzone is assembled between them. This structure consists of parallel microtubules with minus ends pointing to the poles and plus ends aggregated with the plus ends of the oppositely oriented microtubules, forming a narrow overlapped region called the

central spindle (Euteneuer and McIntosh, 1980; Glotzer, 2009). The formation of this region requires microtubule cross-linker protein regulator of cytokinesis (PRC1), kinesin (KIF4), and MKLP1 (Glotzer, 2009). This process is regulated by polo-like kinase (Plk1), the chromosomal passenger complex (CPC) formed by the kinase AuroraB and three additional regulatory subunits, and the centralspindlin, a protein complex formed by MKLP1, kinesin-6, and two molecules of CYK-4, a GTPase activating protein (GAP) that also recruits epithelial cell transforming protein (Ect2) to the central spindle (Fig. 8A) (Carmena *et al.*, 2009; Ruchaud *et al.*, 2007; Glotzer, 2009; Pavicic-Kaltenbrunner *et al.*, 2007). Several of these complexes might play a key role in promotion of the contracting ring assembly, but how the signal reaches the cortex from the central spindle remains unknown (Carmena *et al.*, 2009; Barr and Gruneberg, 2007).

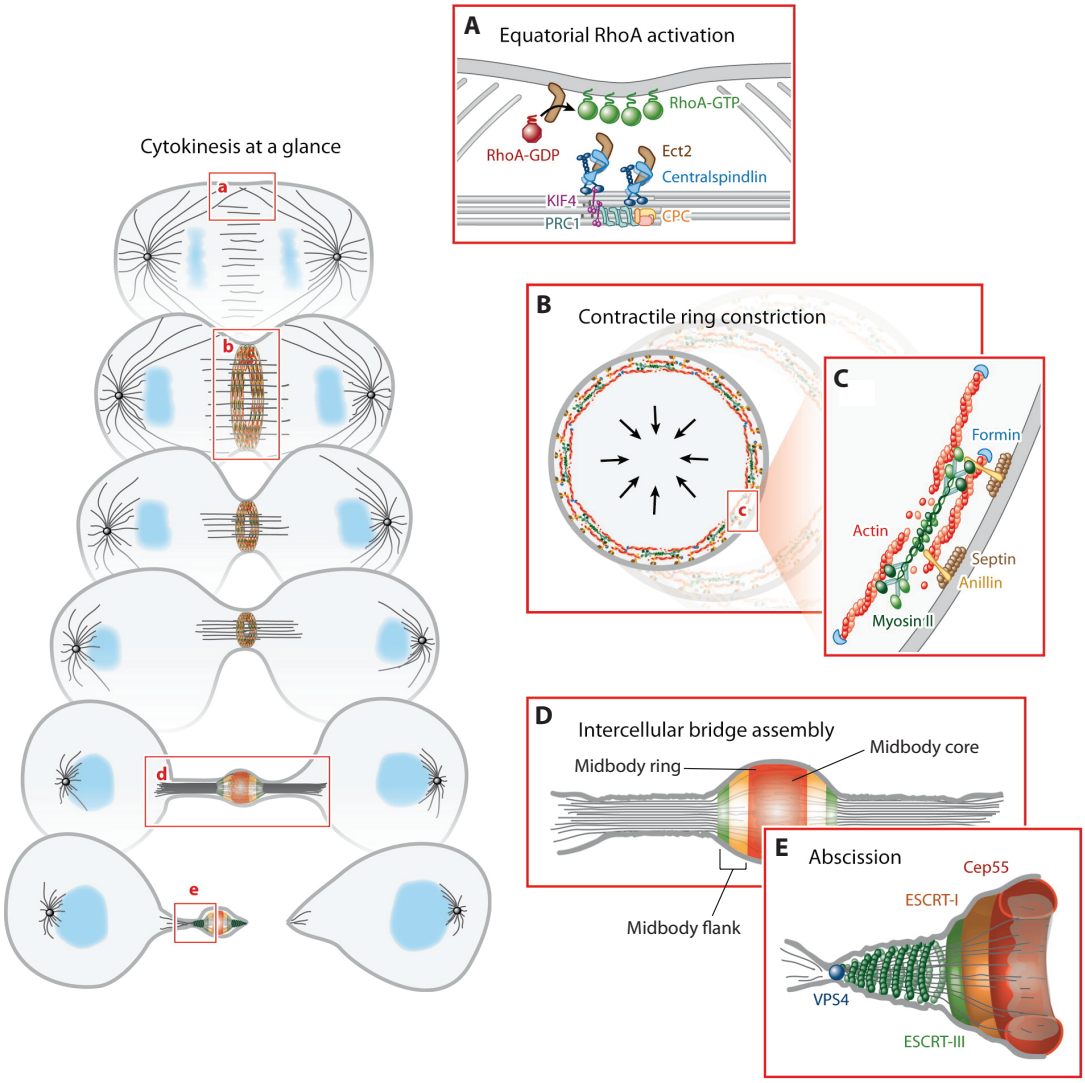

Figure 8. *Animal cell cytokinetic stages.* ***A*** *Signaling from the anaphase spindle and cortex generate an equatorial zone of active RhoA.* ***B,C*** *Active RhoA induces actomyosin contractile ring*

assembly, which changes cell shape by constriction. ***D*** *The midbody is formed in the matured midzone upon ring constriction. It has 3 regions: core, ring, and flanks.* ***E*** *For the final membrane abscission, ESCRT-III complex is recruited at the midbody sides, generating two daughter cells. Adapted by permission from Annual Reviews: Annual Review od Cell and Developmental Biology(Green et al.), copyright (2012).*

Meanwhile, active RhoA is accumulated in a narrow equatorial zone promoting the recruitment of contracting ring proteins and delineating the site of contractile ring assembly (Piekny *et al.*, 2005; Bement *et al.*, 2006). The particular distribution of active RhoA is not only driven by central spindle components, but also by the distal asters formed around the centrosomes that corral active RhoA, preventing it from spreading out from the cellular equator (Fig. 8A) (von Dassow, 2009).

1.5.2. Actomyosin contractile ring

After equatorial cortex zone specification, the contractile ring is assembled. It is composed of a thin layer of filamentous proteins cross-linked around the cellular equator beneath the cell surface (Cao and Wang, 1990). The ring is composed by myosin II and actin filaments that are the mechanical components of the complex; septins that bind to the membrane; and anillin that serves as a scaffold of the other three (Fig. 8B,C) (Eggert *et al.*, 2006; D'Avino, 2009; Piekny and Maddox, 2010). It also contains actin nucleation, polymerization, disassembly, capping, and cross-linking proteins that regulate ring formation and constriction by disassembly (Wu and Pollard, 2005; Eggert *et al.*, 2006).

1.5.3. Cell abscission

As the ring closes, the midzone is remodeled, forming the midbody in the center of the intracellular bridge. The presence of the spindle microtubules trapped in this bridge by the midbody inhibits the final membrane pinch by the actomyosin contractile ring. Therefore, the ring must be replaced by a ESCRT-III protein network that, together with midbody microtubule disassembly, will bring about abscission that is driven by spansin (Guizetti and Gerlich, 2012; Caballe and Martin-Serrano, 2011; Connell *et al.*, 2009). During midbody packing, three distinctive regions can be observed (Fig. 8D): the midbody core containing the microtubule

overlap region, KIF4, and PRC1; the midbody ring formed together with the leftovers of the contractile ring including centralspindlin, Ect2, anillin (to anchor the midbody to the plasma membrane), RhoA, Arf6, and centrosomal protein (Cep55); and the midbody flank, which includes AuroraB and MKLP2 (Hu *et al.*, 2012).

At both sides of the formed midbody, the ESCRT-III protein complex, consisting of seven core proteins called charged multivesicular body proteins (CHMPs), five regulatory proteins, and 2 vacuolar protein sorting-associated (VSP4) in charge of polymer disassembly (Morita, 2012), drives the abscission of membrane necks by spiral polymerization upon Cep55-mediated recruitment (Fig. 8E) (Carlton *et al.*, 2012). Before physical separation takes place, cells must pass through a cytokinetic checkpoint regulated by kinases Plk1, AuroraB, and Unc-51-like kinase 3 (ULK3) in order to control lagging chromosomes, tension forces at the midbody, or nuclear pore defects. Abscission timing is dictated by the efficiency of this checkup where all three kinases must be inactivated in order to proceed. Plk1 phosphorylates Cep55 preventing its recruitment to the midbody, but when Plk1 is degraded during mitotic exit, Cep55 is then transported to the cytokinetic bridge scaffolding ESCRT-III complex (Bastos and Barr, 2010; Carlton and Martin-Serrano, 2007; Morita, 2012; Johnson *et al.*, 2013). Aurora B, present in the midbody flank, prevents premature abscission by phosphorylation of ESCRT-III component CHMP4C, essential for ESCRT-III polymerization (Carlton *et al.*, 2012), while ULK3 works downstream of AuroraB, phosphorylating IST1, a VSP4 ESCRT-III subunit, preventing complex disassembly (Caballe, Dawn M Wenzel, *et al.*, 2015).

Together with the midbody and the ESCRT-III complex, membrane trafficking of furrow assembly-promoting proteins and membrane remodeling in the intracellular bridge are essential for the successful abscission (Neto *et al.*, 2011). Membrane remodeling is driven by selective endocytosis and exocytosis and the main endocytic pathway related with this process is clathrin-dependent endocytosis (Warner *et al.*, 2006). Membrane remodeling increases $PI(4,5)P_2$ presence at the intercellular bridge where it organizes cytoskeletal elements necessary for the late steps of cytokinesis (Echard, 2008).

1.6. Clathrin-dependent endocytosis

In eukaryotic cells, very few molecules can passively enter and exit the cell across the plasma membrane unaided by proteins. Adenosine triphosphate (ATP)-powered pumps, channel proteins, and transporters are embedded in the phospholipidic bilayer to support ion flux and small molecule uptake. However, these cellular tools are not able to facilitate the transport of larger macromolecules and particles. In order to accomplish this, these materials are engulfed by an area of the plasma membrane, which then buds inside the cell and forms a vesicle containing the ingested components in a process called endocytosis. There are many different endocytic pathways already known, with more being discovered as research in the field continues. The most common and best described ones are reviewed by Doherty and McMahon (Doherty and McMahon, 2009). In the present section, I will focus on the molecular mechanisms behind clathrin-dependent endocytosis (CDE), the first endocytic pathway described in the literature and the one most commonly used by eukaryotic cells, where cargo is packaged into vesicles with the aid of a clathrin coat.

1.6.1. CDE stages

CDE is crucial for signal transduction, neurotransmission, regulation of many plasma membrane activities, cytokinesis, and nutrient uptake into the cell. These clathrin-coated vesicles can be found in several membranous cellular compartments. However, the term CDE is only applied to vesicles formed from the plasma membrane (McMahon and Boucrot, 2011). In this context, clathrin-coated vesicle formation proceeds through five morphologically different stages.

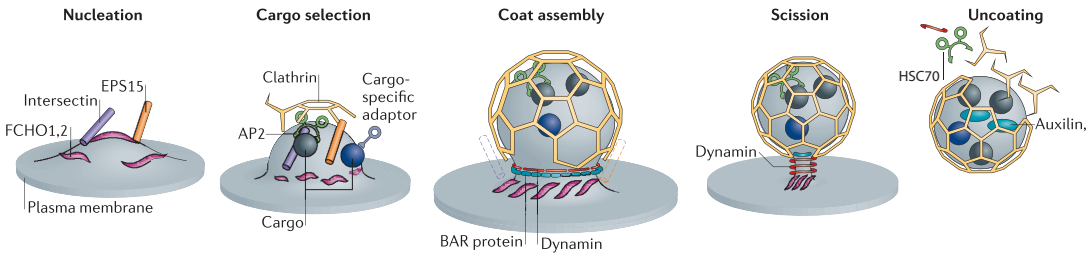

Figure 9. *Clathrin-dependent endocytosis stages.* ***Nucleation*** *CCP formation is initiated by AP2 recruitment to PI(4,5)P_2-rich zones of the plasma membrane after recruitment of EPS15, intersectins, and FCHO proteins.* ***Cargo selection*** *μ-subunit and σ-subunit of AP2 interact with specific cargo directly or through cargo-specific adaptors.* ***Coat assembly*** *Clathrin is recruited to AP2-rich zones where it polymerizes into hexagons and pentagons forming a spherical*

coat. ***Scission*** *Dynamin polymerizes at the neck of the forming vesicle, inducing membrane scission.* ***Uncoating*** *Auxilin recruits HSC70 for clathrin coat disassembly, which makes clathrin available for another round of CDE. Adapted by permission from MacMillan Publishers LTD: Nature Reviews Molecular Cell Biology (McMahon and Boucrot), copyright (2011).*

1.6.1.1. Nucleation

Historically, the initiation of the clathrin-coated pit (CCP) was thought to be boosted by the recruitment of adaptor protein 2 (AP2) to the plasma membrane through its binding to $PI(4,5)P_2$ and to endocytic motifs contained in the cytoplasmic tails of the cargo (McMahon and Boucrot, 2011; Höning *et al.*, 2005; Collins *et al.*, 2002). Nevertheless, recent investigations have unveiled that a putative nucleation module is assembled prior to AP2 recruitment, marking the site of clathrin recruitment and vesicle budding. This module is formed by FCH domain only (FCHO) proteins, intersectins, and epithelial growth factor receptor (EGFR) pathway substrate (EPS15), and it is recruited to the plasma membrane through $PI(4,5)P_2$ interaction (Fig. 9). The F-BAR domain of FCHO proteins can only bind to membranes with very low curvature, but its membrane-bending activity starts to generate a slight curvature necessary for procedure progression (Stimpson *et al.*, 2009; Henne *et al.*, 2010).

1.6.1.2. Cargo selection

As previously mentioned, the proteins of the putative nucleation module are in charge of recruiting AP2 to the plasma membrane in order to mediate cargo selection in collaboration with other cargo-specific adaptors and clathrin polymerization (Fig. 9). Due to its specific interaction with $PI(4,5)P_2$, AP2 is exclusively acting in the plasma membrane, while similar adaptor proteins work in CCP formation from other membranous compartments (Robinson, 2004). AP2 is the most abundant protein component in CDE after clathrin and acts as a major hub of interaction during CCP maturation, making it one of the key components of the endocytic pathway (Blondeau *et al.*, 2004). Together with AP2, a broad range of accessory adaptor proteins are required for specific cargo selection. For example, Dishevelled interacts with Frizzled (Yu *et al.*, 2007), stonin 2 binds to synaptojanin (Haucke and De Camilli, 1999), Numb recruits Notch (Giebel and Wodarz, 2012), and β-arrestin sequesters G protein-coupled receptors (GPCR) (Shukla *et al.*, 2014). Whichever is the case, the accessory adaptor always binds to the core AP2 (Edeling *et al.*, 2006). Also, FCHO proteins

contain a ligand-binding domain, meaning cargo selection might start as early as CCP nucleation (Henne *et al.*, 2010). Moreover, the AP180 amino-terminal (ANTH) and epsin N-terminal homology (ENTH) domains, which are membrane-binding and membrane-bending proteins, respectively, are also able to address cargo selection (Ford *et al.*, 2001; Ford *et al.*, 2002). It has been recently postulated that all of the proteins listed here and others involved in cargo selection are also curvature effectors in order to ensure that curvature is generated independently of the nature of the cargo (McMahon and Boucrot, 2011).

1.6.1.3. Clathrin coat assembly

After cargo has been selected and bound to AP2, around 100 soluble clathrin triskelia per vesicle are recruited from the cytosol to aid in coat formation in a combination of hexagonal and pentagonal arrays (Fig. 9) (McMahon and Boucrot, 2011). As a consequence of clathrin polymerization, the pit curvature is stabilized and some adaptor proteins, like epsin and EPS15, are displaced to the edge of the pit where they function more effectively (Hinrichsen *et al.*, 2006). Traditionally, it has been assumed that vesicle curvature is given by clathrin polymerization. However, clathrin binds to the flexible domains of AP2, AP180, and epsin, suggesting that the bending strength that clathrin imparts is not enough and that other curvature effectors are necessary to force vesicle bending (McMahon and Boucrot, 2011).

1.6.1.4. Vesicle scission

Prior to the complete scission of the clathrin-coated vesicle, a high negative curvature neck must be formed to close the gap left by the internalized section of membrane. This mechanochemical process is driven by dynamin (Kosaka and Ikeda, 1983), which is recruited to this particular region by BAR domain-containing proteins, such as endophilin, amphiphysin, and sorting nexin (SNX9), that bind to high curvature membranes, like in the neck of budding vesicles, through a Pro-rich domain that interacts directly with the SRC homology (SH3) domains of these proteins (Ferguson *et al.*, 2009). Dynamin polymerizes around the neck and undergoes a conformational change upon guanosine triphosphate (GTP) hydrolysis, leading to membrane fission (Fig. 9) (Sweitzer and Hinshaw, 1998).

1.6.1.5. Vesicle uncoating

Once the vesicle is detached from the plasma membrane, the clathrin machinery must be disassembled and returned back into the cytosol to be reused for another round of CCP formation and to allow endosome fusion with other vesicles (McMahon and Boucrot, 2011). Clathrin-coat disassembly is driven by the ATPase heat shock cognate (HSC70) and its cofactor, auxilin (Fig. 9). After the clathrin-coated vesicle buds, auxilin is recruited to the ankles and terminal domains of clathrin triskelia. Subsequently, HSC70 is recruited by auxilin towards the foot of the tripod formed by clathrin where the uncoating reaction starts (Schlossman *et al.*, 1984; Ungewickell *et al.*, 1995). According to *in vitro* studies, one auxilin and three or less HSC70 proteins per triskelia are required to achieve the maximum disassembly rate (Böcking *et al.*, 2011). It has been predicted that this uncoating process can only occur due to the fact that the clathrin-coated sphere is not complete. Indeed, when vesicle scission takes place, the clathrin-coating does not proceed over the zone where the neck was present, leaving a gap where disassembly can easily be initiated (McMahon and Boucrot, 2011). Together with HSC70 and auxilin, changes in the PI composition of the clathrin-coated vesicle are necessary for clathrin disassembly. $PI(4,5)P_2$ phosphatase synaptojanin mediates this process, but whether $PI(4,5)P_2$ dephosphorylation facilitates auxilin recruitment or activates any other mechanisms remains unknown (Cremona *et al.*, 1999).

1.6.2. PI conversion during CDE

Together with clathrin and AP2, $PI(4,5)P_2$ is a key hub in CDE. Its initial presence is as essential as the subsequently regulated dephosphorylation to other PIP species across the clathrin-coated vesicle. CCP nucleation is highly dependent on the general abundance of $PI(4,5)P_2$ in the plasma membrane since numerous endocytic adaptor proteins required for CCP initiation, like AP2, recognize this phospholipid (Fig. 10). $PI(4,5)P_2$ is synthesized in the plasma membrane from PI4P by type I phosphatidylinositol phosphate 5'-kinases (PIP5K) α, β, and γ, and CCP nucleation depends on their activity since enhanced $PI(4,5)P_2$ synthesis leads to an increase of CCP events (Balla, 2013; Antonescu *et al.*, 2011).

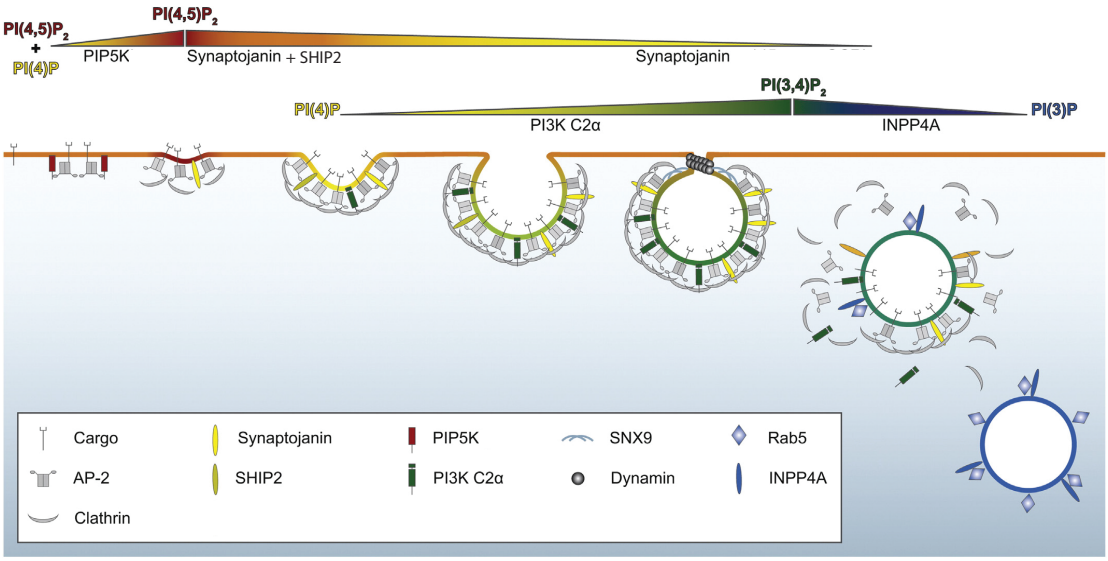

Figure 10. *PI conversion along clathrin-coated vesicle formation. PI(4,5)P_2 enrichment (red) is required for FCHO and AP2 recruitment to the plasma membrane during CDE nucleation, and it is generated by PIP5K. CCP maturation is driven by progressive lipid conversion from PI(4,5)P_2 to PI(3,4)P_2 (green). First, synaptojanin and SHIP2 dephosphorylate PI(4,5)P_2 to form PI4P (yellow) and then, PI3K C2a phosphorylates it, forming PI(3,4)P_2 in order to facilitate recruitment of SNX9. After vesicle scission, PI(3,4)P_2 (green) might be dephosphorylated to form PI3P (blue) by INPP4A/B. Adapted from BBA-Molecular and Cell Biology of Lipids, 1851(6), Posor, Y., Eichhorn-Grünig, M. and Haucke, V., "Phosphoinositides in endocytosis", p 799, Copyright (2015), with permission from Elsevier.*

During CCP maturation, 5-phosphatase synaptojanin-p170 (Snj1) and SH2 domain containing inositol 5-phosphatase (SHIP2) are recruited to the core of the CCP (Antonescu *et al.*, 2011; Nakatsu *et al.*, 2010). At this stage of the procedure, the dependence of clathrin coat stability on PI(4,5)P_2 associated adaptor proteins may be reduced, meaning that PI(4,5)P_2 presence in this plasma membrane region is not essential and can be readily converted to PI4P by the 5-phosphatases (Fig. 10) (Posor *et al.*, 2015; Antonescu *et al.*, 2011). Then, PI3K C2α is recruited to the CCP in a clathrin-dependent manner to enable PI4P conversion to PI(3,4)P_2 (Fig. 10) (Hammond *et al.*, 2012; Nakatsu *et al.*, 2010) . PI(3,4)P_2 production allows SNX9 recruitment and facilitates the transition of an open shallow CCP to an Ω–shaped structure, both needed for vesicle scission (Posor *et al.*, 2013). Moreover, as was previously mentioned, this postulated switch from PI(4,5)P_2 to PI(3,4)P_2 might also facilitate clathrin-coated vesicle uncoating by recruitment of HSC70 and auxilin (Cremona *et al.*, 1999).

1.6.3. Clathrin-coated pits and plaques

Although CDE has been explained in the CCP formation context, in eukaryotic cells two different ways of clathrin-mediated uptake exist. The aforementioned "canonical" pathway is where the coated pit leads to a curved clathrin lattice that deforms the underlying membrane, giving rise to the coated vesicles. However, clathrin-coated plaques are formed by a large extended clathrin lattice formed almost exclusively by hexagonal arrays, leading to low curvature budding endocytosis. Therefore, while pits are small and rapidly internalized (less than 2-3 min), plaques are much larger and the internalization slows down (several minutes). Presence of pits, plaques, or both together on the cell surface depends on the role of the membrane domain. For example, in Henrietta Lacks (HeLa) or Swiss albino mouse embryo tissue (Swiss 3T3) cells, the long-lived coated plaques are at the adherent surface in contact with the culture dish, whereas most, if not all, the clathrin-coated vesicles formed at the free surface are pits (Saffarian *et al.*, 2009).

2. Project objectives

Aberrant protein expression of the dual specificity phosphatase PRL-3 is involved in the development of cancer progression and metastasis. Interestingly, while its expression has been observed in a variety of cancer cells and tissues, it is barely found in healthy human adult tissue. Clinical and cell culture studies have revealed that PRL-3 overexpression leads to the activation of several oncogenic signaling pathways involved in cell proliferation, migration, invasion, and EMT. While enhanced cell growth can be explained by PRL-3's interaction with CNNMs, the exact molecular mechanisms behind the other phenotypes remain obscure due to the lack of PRL-3 substrates.

Since PRL-3 has been predominantly linked to cancers of epithelial origin, the group of Dr. Köhn has focused their studies on the dissection of the role of PRL-3 in epithelial cells leading to a cancer-related phenotype in 3D MDCK cyst model. Therefore, the challenging main goal of my thesis was to discover putative PRL-3 substrates in an organotypic 3D cell culture model in order to shed light into the mechanisms by which PRL-3 promotes epithelium-derived cancer. In chapter 3, entitled **"The role of PRL-3 in epithelial architecture"**, a phosphoproteomics approach was envisioned in an epithelial 3D cell culture model to elucidate PRL-3 substrates, followed by restricting the substrate searching window to the cellular context of PRL-3 action, defined through a fluorescent microscopy study of MDCK cystogenesis that was started previously by Dr. Giulia Varsano in the Köhn group.

The pursuit of PRL-3 substrates was followed in a non-protein context in chapter 4, entitled **"The role of PRL-3 in clathrin-dependent endocytosis"**. Previously, our lab has published that PRL-3 has $PI(4,5)P_2$ phosphatase activity *in vitro*. My goal was to further corroborate this finding *in vivo* and to search for a cellular function for this novel PRL-3 activity. Since $PI(4,5)P_2$ homeostasis is necessary for CDE and PRL-3 is internalized through this specific endocytic pathway, I focused my research on this context.

3. The role of PRL-3 in epithelial architecture

PRL-3 accelerates cytokinesis timing, altering the post-mitotic midbody position during epithelial development and maintenance

3.1. Results

Aberrant pathological PRL-3 mRNA and protein expression has been found throughout several cancer types, but according to the cell type origin, most are epithelial cancer (Rios *et al.*, 2013; Al-Aidaroos and Zeng, 2010; Guzińska-Ustymowicz and Pryczynicz, 2011; Bessette *et al.*, 2008; Rouleau *et al.*, 2006). However, the effect of high PRL-3 expression on epithelia development and maintenance has never been studied, neither at the cellular nor tissue level. In order to examine these effects, the stable overexpression of PRL-3 in MDCK cell cysts, an extensively used epithelial cell model (Debnath and Brugge, 2005; Schlüter and Margolis, 2009; Bryant *et al.*, 2010; Apodaca, 2010; Bryant *et al.*, 2014; Gálvez-Santisteban *et al.*, 2012; Rodríguez-Fraticelli *et al.*, 2015), was previously established in the Köhn laboratory. Embedded in a gelatinous extracellular protein mixture, single MDCK cells are able to develop spherical cysts containing a single hollow lumen in the center surrounded by a monolayer of polarized cells facing the apical membrane to the lumen and the basal membrane to the extracellular matrix (Schlüter and Margolis, 2009). Since actin is enriched below the apical membrane, it is used as an apical marker as well as to delineate the lumen of the cyst (Fig. 11A). In this model, the Köhn group demonstrated that the overexpression of the wild type (WT) version of PRL-3 fused to GFP frequently led to the abnormal formation of multiple lumens within a cyst (Fig. 11B,D), a phenotype related with cancer progression through epithelia architecture disruption (Debnath and Brugge, 2005; Hao *et al.*, 2010; Jaffe *et al.*, 2008; Schlüter *et al.*, 2009). This defect depends on PRL-3 phosphatase activity because the stable overexpression of the catalytically inactive GFP-fused mutant of PRL-3 (GFP-PRL-3 C104S) in MDCK cysts did not show a different phenotype compared to the parental phenotype (Fig. 11C,D).

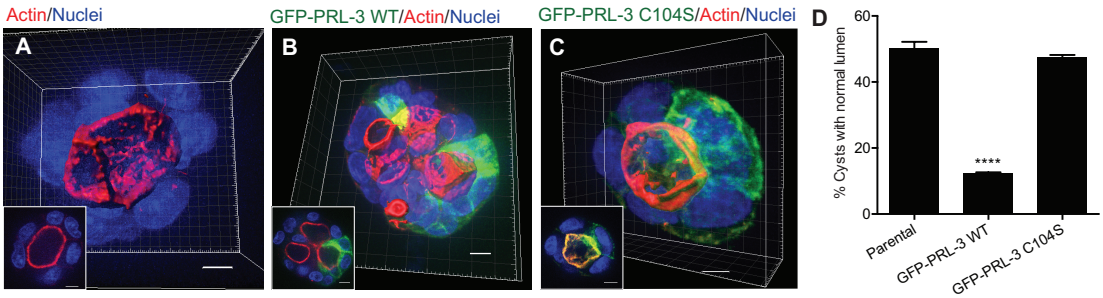

Figure 11. *PRL-3 WT overexpression in MDCK 3D-cysts led to ectopic lumen formation.* ***A-C*** *3D reconstruction of 72 hr parental (**A**), GFP-PRL-3 WT (**B**), or GFP-PRL-3 C104S (**C**) overexpressing MDCK cysts. Representative 2D plane from the selected cysts is shown in the bottom left corner. Scale bars, 5 µm.* ***D*** *Amount of MDCK cysts with a single lumen at 72 hr. Mean ± SEM of three independent experiments. n=300. Adapted by permission from Company of Biologists LTD: JCS (Lujan et al.), copyright (2016).*

3.1.1. PRL-3 down-regulation is needed in healthy epithelial cells

For a deeper phenotypic characterization, the levels of GFP-PRL-3 (WT and C014S) in MDCK stable cell lines, which are a pool of GFP positive clones, were first analyzed to ensure that the findings were due to a difference in protein expression. The PRL-3 protein is tightly regulated in cells (Myung Suk Choi *et al.*, 2011; Xing *et al.*, 2016) leading to heterogeneous cell-to-cell PRL-3 expression levels, in which sometimes expression is even completely lost. Therefore, repetitive FACS selection of GFP positive cells was carried out to maintain a population that was as homogeneous as possible. Due to their innate heterogeneity, PRL-3 protein levels were analyzed by flow cytometry, a single cell analysis method. Figure 12 illustrates this heterogeneity and shows that GFP-PRL-3 C104S expression was higher overall than the WT version, suggesting that the phenotype described in MDCK cysts was due in fact to the phosphatase activity of PRL-3.

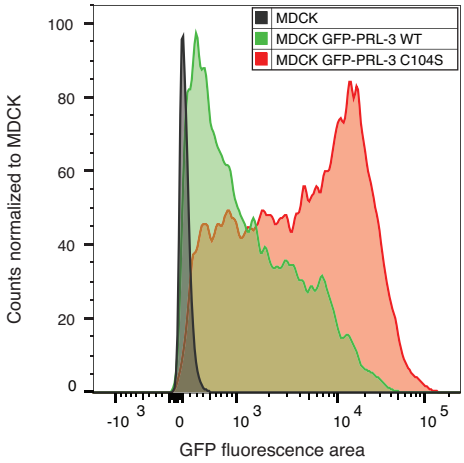

Figure 12. *Population distribution of GFP-fused PRL-3 WT or C104S content in MDCK cells measured by flow cytometry. Black: MDCK; green: MDCK GFP-PRL-3 WT; red: MDCK GFP-PRL-3 C104S. The experiment was done in triplicate. n=2x10⁵ cells/replicate. Adapted by permission from Company of Biologists LTD: JCS (Lujan et al.), copyright (2016).*

In order to discard the notion that this phenotype is cell type specific, PRL-3 overexpression was also carried out in Caco-2 cells, another widely used epithelial cell model (Jaffe *et al.*, 2008; Ivanov *et al.*, 2008; Townley *et al.*, 2012). In contact with extracellular matrix, Caco-2 cells also develop into spherical single-centered lumen-containing cysts like MDCK (Fig. 13A). As expected, the stable overexpression of GFP-PRL-3 WT in Caco-2 cysts also disrupted the parental phenotype by multiple lumen formation (Fig. 13B,D) and the catalytically inactive mutant (PRL-3 C104S) showed a phenotype comparable to the control (Fig. 13C,D), supporting the idea that the effect of PRL-3 on epithelia architecture is not cell type specific.

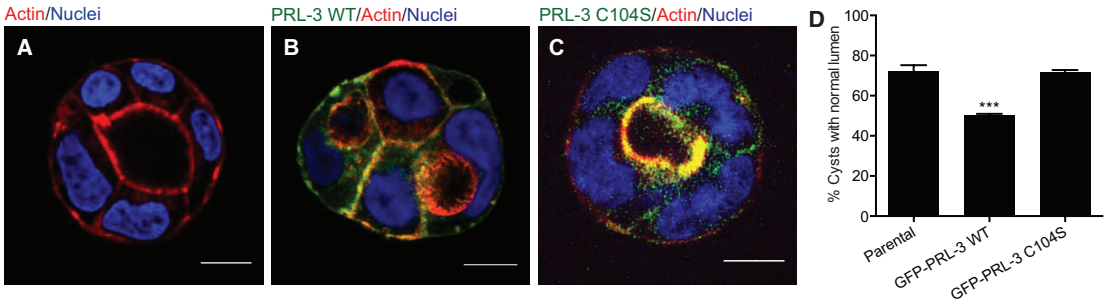

Figure 13. *PRL-3 WT overexpression in Caco-2 cysts also led to ectopic lumen formation.* ***A-C*** *Confocal images of 72 hr parental (**A**), GFP-PRL-3 WT (**B**) or GFP-PRL-3 C104S (**C**) overexpressing Caco-2 cysts. Scale bars, 10 µm.* ***D*** *Amount of Caco-2 cysts with a single lumen at 72 hr. n=300. Mean ± SEM of three independent experiments. Adapted by permission from Company of Biologists LTD: JCS (Lujan et al.), copyright (2016).*

To further study the effect of the phosphatase activity of PRL-3 in MDCK cysts, PRL-3 activity was modulated by mutation. In the Köhn group, it has been recently found that mutation of the glutamic acid of the PRL-3 catalytic site (PRL-3 E50R) increases its phosphatase activity against un-natural substrates (DiFMUP) and *in vitro* characterized substrates like $PI(4,5)P_2$ (B. Hoeger, M. Köhn, unpublished data). The stable overexpression of GFP-PRL-3 E50R in MDCK cysts did not show any difference compared to PRL-3 WT (Fig. 14A,B), suggesting that the aggressiveness of the phenotype does not depend on PRL-3 activity. Moreover, in order to ascertain if the phenotype was specific for PRL-3 or common for all PRLs since they are all related to cancer but have different outcomes and prognoses (Rios *et al.*, 2013), GFP-PRL-1 WT was transiently electroporated into MDCK cysts. Figure 14C,D shows that transfection with PRL-1 also leads to the multiple lumen phenotype of MDCK cysts but to a lesser extent compared to the PRL-3 WT, demonstrating that although

both of them show a similar phenotype, the degree of architectural disruption may be due to difference in substrate specificity (Rios *et al.*, 2013; McParland *et al.*, 2011).

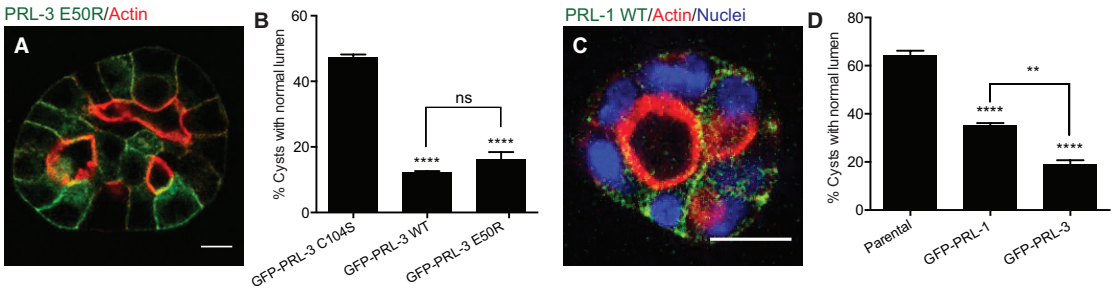

Figure 14. *PRL-3 E50R and PRL-1 WT overexpression in MDCK cysts also led to ectopic lumen formation.* ***A,C*** *Confocal images of 72 hr GFP-PRL-3 E50R (**A**) or GFP-PRL-1 WT (**C**) overexpressing MDCK cysts. Scale bars, 10 µm.* ***B,D*** *Amount of MDCK cysts with a single lumen at 72 hr. n=300. Mean ± SEM of three independent experiments.* ***C*** *and* ***D*** *are adapted by permission from Company of Biologists LTD: JCS (Lujan et al.), copyright (2016).*

Consistent with the normal phenotype shown upon PRL-3 C104S overexpression in both MDCK and Caco-2 cysts, the multiple lumen phenotype observed for PRL-3 WT overexpressing cysts can be rescued in a concentration-dependent manner when treated with a cell-permeable selective PRL inhibitor, Analog 3 (Hoeger *et al.*, 2014) (Fig. 15A,B). Consequently, parental and GFP-PRL-3 C104S overexpressing Caco-2 cysts do not show any change in the number of single lumen-containing cysts upon Analog 3 treatment (Fig. 15B). Nevertheless, MDCK cysts and cysts overexpressing GFP-PRL-3 C104S treated with Analog 3 slightly increased the proportion of normal cysts (Fig. 15A). This behavior could be due to the presence of endogenous PRL-3 in MDCK cells, but also to endogenous PRL-1 or PRL-2 since I have previously demonstrated that PRL-1 overexpression also gives rise to a similar phenotype, and Analog 3 inhibits all PRLs (Hoeger *et al.*, 2014).

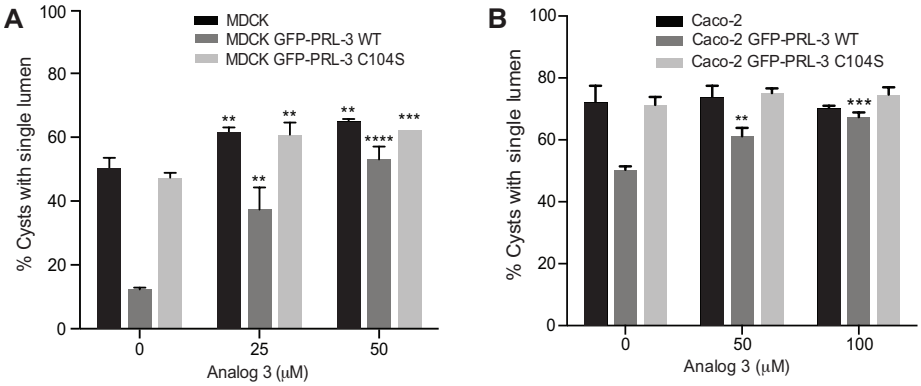

Figure 15. *Multiple-lumen phenotype of MDCK cysts upon PRL-3 WT overexpression in MDCK cysts can be reverted with PRL inhibitor Analog 3. Graphs represent the amount of cysts*

*with a single lumen in 72 hr MDCK (**A**) or Caco-2 (**B**) cysts or cysts stably expressing GFP-PRL-3 WT or GFP-PRL-3 C104S. Cells were treated with Analog 3 or DMSO as a control. n = 300. Mean ± SEM of three independent experiments. Adapted by permission from Company of Biologists LTD: JCS (Lujan et al.), copyright (2016).*

In order to clarify this finding, a considerable number of unsuccessful attempts were conducted to detect endogenous PRL-3 WT in MDCK and Caco-2 cells by Western blot (WB), using the Michigan Cancer Foundation breast cancer (MCF-7) and the *Homo sapiens* colon colorectal carcinoma (HCT116) cell lines as positive controls (data not shown) (Geiger *et al.*, 2012; Wang *et al.*, 2010; Xing *et al.*, 2016). Additionally, several specific PRL-3 antibodies from different sources were used, but all failed. To increase the sensitivity of the assay, different approaches were taken including loading up to 400 µg of total cell protein per sample; pre-treating cells with MG-132, a proteasome inhibitor, to avoid protein degradation; or immunoprecipitating PRL-3 from whole cell lysates. Unfortunately, it was not possible to detect endogenous PRL-3 using any of these methods. Moreover, most of the antibodies applied were not selective enough and membrane blots showed extra bands in the region where PRL-3 was expected to be found. Since PRL-3 lipidation can affect its migration in sodium dodecyl sulfate polyacrylamide gel electrophoresis (SDS-PAGE), the expected molecular weight in the blotted membrane might not correspond to the real one. Therefore, since the band detected in the region near the molecular weight of PRL-3 cannot be directly discarded as unspecific binding of the antibody, PRL-3 knockdown was done in MCF-7 and HCT116 cells to study the origin of those bands. Silencing efficiency was confirmed by reverse transcription polymerase chain reaction (RT-PCR), but the same band appeared in both control and PRL-3 knockdown cells, showing that the resulting bands were, indeed, due to antibody unspecificity. Sections *5.3.7.* and *5.3.8.* contain a deeper explanation of the different approaches to detect endogenous PRL-3 by WB.

Since endogenous PRL-3 detection was not possible by WB, a deep mass-spectrometric (MS) analysis, used to detect proteins with low expression levels, was carried out in MDCK cells overexpressing human GFP-PRL-3 WT and GFP-PRL-3 C104S as internal human PRL-3 controls in collaboration with Marco Hennrich from the group of Dr. Anne-Claude Gavin (Structural and Computational Biology Unit, EMBL Heidelberg). The overexpressed human version of PRL-3 was detected, confirming that the analysis worked properly, but endogenous dog PRL-3 was not detected. Interestingly, peptides corresponding to dog PRL-1 and PRL-2 were also

detected, though no distinction could be made between them due to a high sequence consensus for both proteins. These results suggest that the slight increase in single lumen-containing cyst percentage of parental and GFP-PRL-3 C104S overexpressing MDCK cysts under Analog 3 treatment might be due to endogenous PRL-1 and/or PRL-2, confirming that other PRLs are able to exert the observed phenotype on MDCK cystogenesis.

Although deep MS did not detect endogenous PRL-3, undetectable levels of the phosphatase may still be present, which could affect lumen formation. Therefore, PRL-3 was knocked down by small interfering RNA (siRNA) in MDCK and Caco-2 cysts and knockdown efficiency was confirmed by RT-PCR (Fig. 16). No difference in the proportion of single lumen-containing cysts was observed after PRL-3 knockdown compared to control, indicating the absence of PRL-3 in both epithelial cell systems and suggesting that PRL-3 might not be needed for cell polarity.

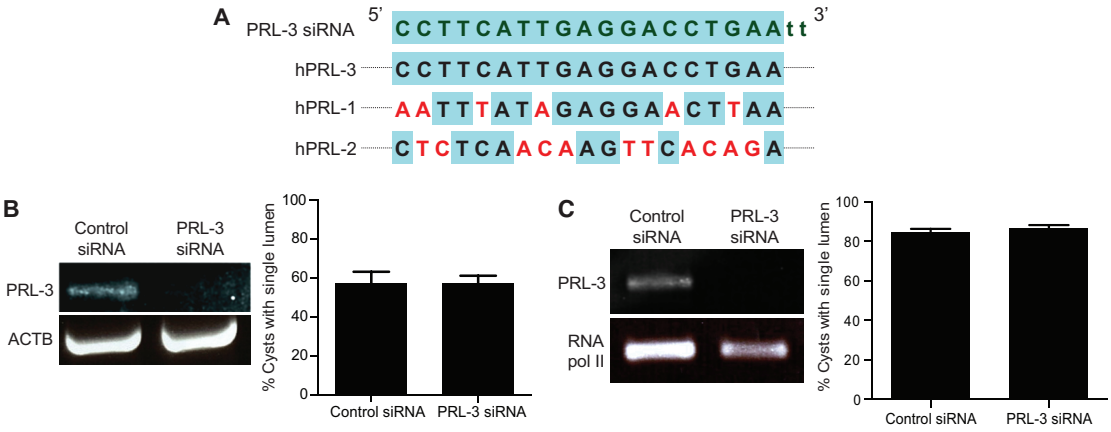

Figure 16. *MDCK and Caco-2 cells do not contain endogenous PRL-3.* ***A*** *DNA multiple alignment of sense PRL-3 siRNA sequence with human PRL-1, -2 and -3. Several mismatches with PRL-1 and -2 make unspecific knockdown unlikely.* ***B*** *Proportion of single lumen MDCK cysts electroporated with control or PRL-3 siRNA after 48 hr. PRL-3 mRNA content was measured by one-step RT-PCR using ACTB mRNA as loading control.* ***C*** *Proportion of single lumen Caco-2 cysts transfected with control or PRL-3 siRNA after 48 hr. PRL-3 mRNA content was measured by one-step RT-PCR using RNA pol II mRNA as control.* ***B,C*** *n=300. Mean ± SEM of three independent experiments. Adapted by permission from Company of Biologists LTD: JCS (Lujan et al.), copyright (2016).*

It is remarkable that, during the development of the previous experiments, PRL-3 mRNA was always measurable by RT-PCR (Fig. 16A,B), but no protein level was detected. This observation was already made in several cell lines where PRL-3 mRNA is widely expressed, but only a few of them contained detectable levels of the

translated protein (Rubio and Köhn, 2016; Wang *et al.*, 2010). Since this particular phenotype can be achieved through either translation inhibition (Wang *et al.*, 2010) or by oppressive protein degradation (Xing *et al.*, 2016; Myung Suk Choi *et al.*, 2011), PRL-3 mRNA translation was studied by polysome fractionation (Chassé *et al.*, 2016; Spangenberg *et al.*, 2013) in MDCK cells overexpressing human GFP-PRL-3 WT as an internal control. This approach allows the separation of untranslated free mRNA from translated mRNA, which is bound to several ribosomes (polysome), by sucrose gradient centrifugation (Fig. 17A). After sample division and mRNA extraction, the levels of *hPTP4A3* (human PRL-3), *dPTP4A3* (dog PRL-3), and *Renilla* (loading control) mRNA in each fraction were measured by RT-PCR.

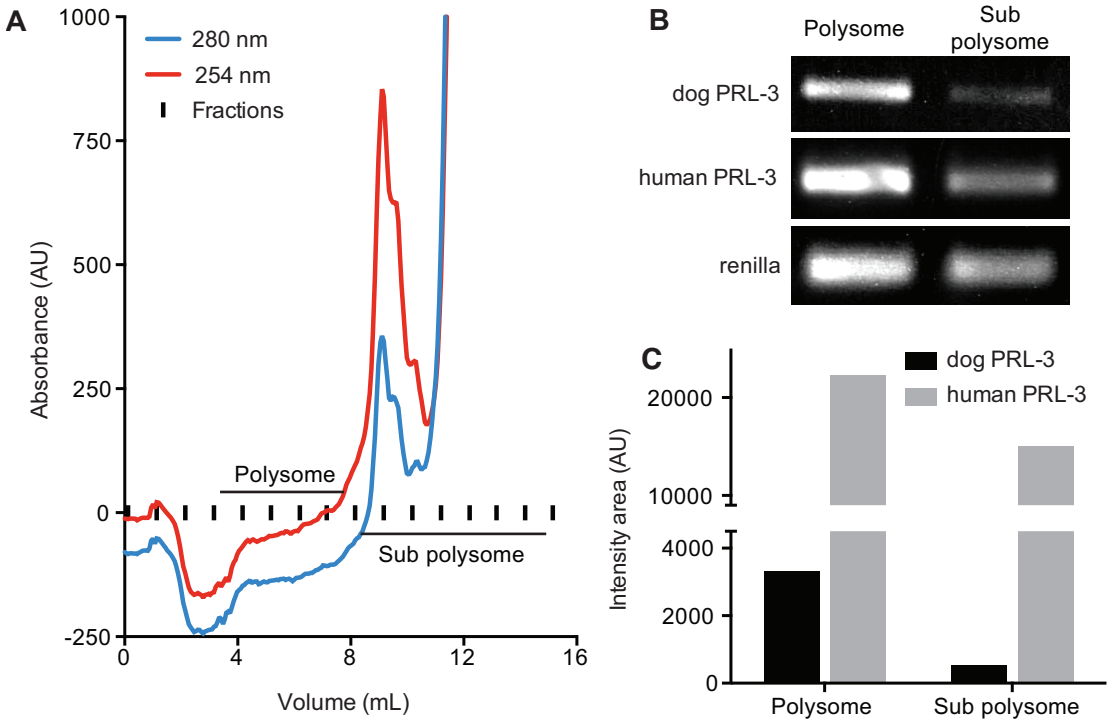

Figure 17. *Endogenous PRL-3 mRNA is translated in MDCK cells.* ***A*** *MDCK polysome fractionation: protein absorption detection from MDCK cell lysate solved by gradient centrifugation and collected in 1 mL fractions.* ***B*** *Extracted mRNA was assayed by one-step RT-PCR using Renilla mRNA as an extraction and loading control.* ***C*** *mRNA intensity quantification from the bands plotted in* ***B****. Adapted by permission from Company of Biologists LTD: JCS (Lujan et al.), copyright (2016).*

As expected, *hPTP4A3* was translated and the difference between translated and free mRNA was less than 25% (Fig. 17B,C). However, *dPTP4A3* was also translated (Fig. 17B,C) and the amount of polysome bound mRNA was 6 times bigger than free mRNA, implying that dPRL-3 is constantly translated in MDCK cells. This result

suggests that PRL-3 protein down-regulation might be driven by protein degradation. In this scenario, the equilibrium between translation and degradation is shifted towards translation for hPRL-3 and degradation for dPRL-3. This dynamic equilibrium is highly regulated and even small differences between two cells from the same cell population can result in dramatic changes in protein expression level and may explain the heterogeneity in MDCK GFP-PRL-3 (WT or C104S) stable cell lines (Fig. 12).

Since PRL-3 protein is undetectable in both MDCK and Caco-2 cells, it is not possible to study the endogenous effect of PRL-3 on cell polarity using these established epithelial cell models. Indeed, there is no epithelial cell line available at this time that develops into these hollow round-shaped cysts containing detectable levels of PRL-3 protein. Therefore, we used MCF-7 breast cancer cells, the only epithelial cell line that expresses the PRL-3 protein and is able to form 3D polarized structures (Geiger *et al.*, 2012; Wang *et al.*, 2010). Unlike MDCK cysts, MCF-7 cells develop into 3D tubular branched structures containing single or multiple actin positive lumens in the branch ends when in contact with the extracellular matrix (Fig. 18A) (Lee *et al.*, 2007; do Amaral *et al.*, 2011). To study the effect of endogenous PRL-3 in these MCF-7 structures, the phosphatase was first inhibited by treating the cells with Analog 3. Figure 18B shows that when cells were treated with the PRL inhibitor, the proportion of single lumen-containing branch ends increased in a concentration-dependent manner.

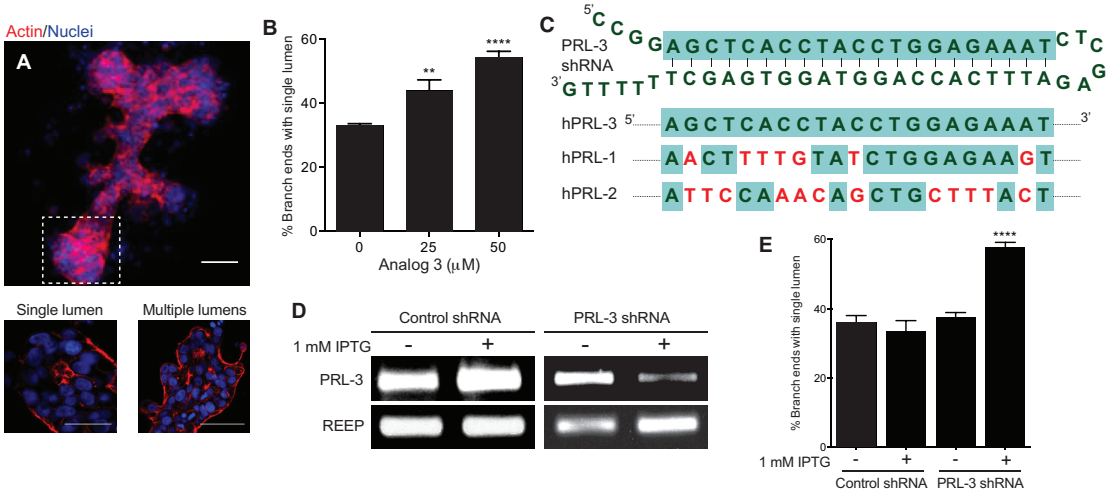

Figure 18. *Endogenous PRL-3 is responsible for the multiple lumen-containing branch ends in MCF-7 3D structures.* ***A*** *3D reconstruction of 15 days grown MCF-7 structure. The dashed square highlights a branch end that can present a single lumen (bottom left) or multiple lumens (bottom right). Scale bars; 100 μm (up), 50 μm (down).* ***B*** *Proportion of branch ends with single lumen in MFC-7 3D structures. Cells were treated with Analog 3 or DMSO (control) for*

15 days. ***C*** *DNA multiple alignment of the sense region of PRL-3 shRNA sequence with human PRL-1, -2 and -3.* ***D*** *Uninduced or induced PRL-3 knockdown with 1 mM IPTG in control cells or PRL-3 shRNA MCF-7 cells over 4 days. PRL-3 mRNA was assayed by one-step RT-PCR using REEP as a control.* ***E*** *Proportion of branch ends with a single lumen in 3D structures of MCF-7 stably expressing IPTG inducible control or PRL-3 shRNA. Cells were untreated or treated with 1 mM IPTG for 15 days.* ***B,E*** *n=300. Mean ± SEM of three independent experiments. Adapted by permission from Company of Biologists LTD: JCS (Lujan et al.), copyright (2016).*

In order to corroborate this result, PRL-3 was also knocked down. However, since these structures need over 14 days for lumen opening, transient siRNA transfection was not viable. Therefore, a stable isopropyl β-D-1 thiogalacto-pyranoside (IPTG) inducible PRL-3 short hairpin RNA (shRNA) (Fig. 18C) MCF-7 cell line was made to maintain PRL-3 knockdown during structural development (Fig. 18D). Upon PRL-3 silencing, the phenotype was comparable to the Analog 3 treatment (Fig. 18B,E) supporting the previous findings, and together suggesting a pathophysiological role of PRL-3 in epithelia-containing organs.

Besides disruptions in epithelial architecture, enhanced cell proliferation and invasion are other cancer hallmarks that can be studied in these epithelial cell models, in order to fully understand the effect of PRL-3 in this context. To examine invasiveness, parental, GFP-PRL-3 WT, and GFP-PRL-3 C104S overexpressing MDCK cysts were cultured in Matrigel-Collagen I (1:1) to allow cell invasion from the cyst towards the gelatinous matrix (Kwon *et al.*, 2011). While parental and GFP-PRL-3-C104S expressing MDCK cyst did not show invasive behavior, MDCK GFP-PRL-3 WT cysts presented a tubular invasive phenotype (Fig. 19A-D). Regarding proliferation, the size of parental, GFP-PRL-3 WT, and GFP-PRL-3 C104S overexpressing MDCK cysts was measured at 72 hr, but no difference in cyst size was detected (Fig. 19E), showing that PRL-3 overexpression is not related with aberrant cell proliferation in this epithelial system. However, this experiment revealed that the length of the apical-basal axis in MDCK GFP-PRL-3-C104S cysts increased, which lead to smaller lumens (Fig. 19F). This intermediate phenotype in MDCK cysts might be due to a substrate-trapping effect, as GFP-PRL-3-C104S can still bind its substrates but not dephosphorylate them.

Taken together, these results are a strong indication of an epithelial cancer-related phenotype driven by PRL-3, whose overexpression disrupts epithelial architecture and enhances cell invasion as its pathophysiological role. Since high levels of PRL-3 induce multiple lumen branch ends in MCF-7 3D cell structures, and other

epithelial models, like MDCK or Caco-2 3D, do not need the presence of PRL-3 to ensure their correct development, a low level or absence of PRL-3 would be needed in healthy epithelial tissue to guarantee the correct architecture.

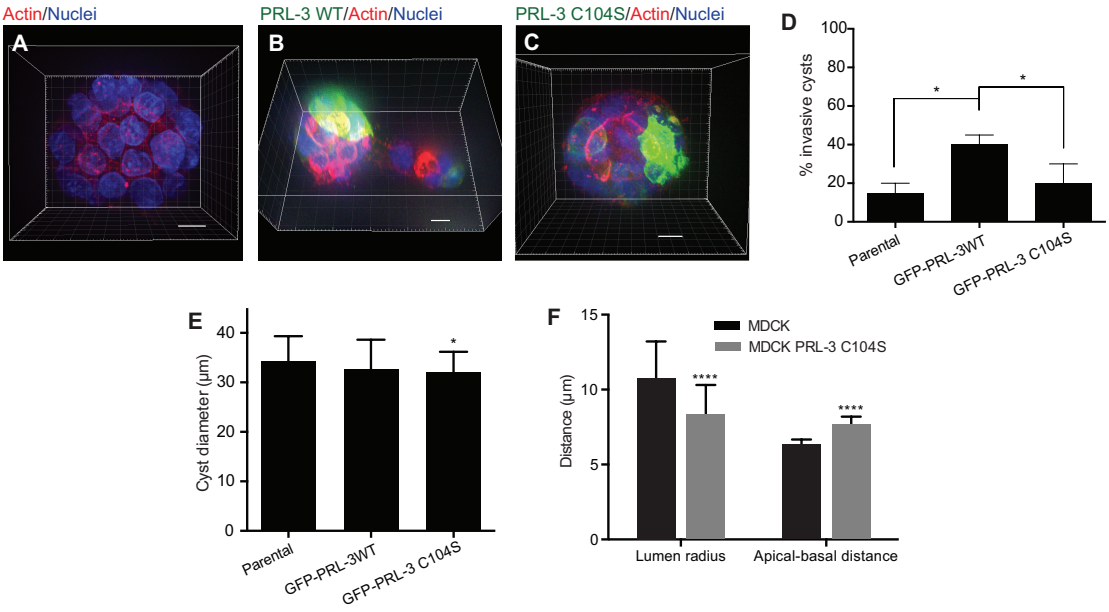

Figure 19. *PRL-3 overexpression induces invasiveness in MDCK cysts.* ***A-C*** *Invasion assay: Confocal images of 96 hr parental (**A**), GFP-PRL-3 WT (**B**), or GFP-PRL-3 C104S (**C**) overexpressing MDCK cysts seeded in Matrigel-Collagen I (1:1). Scale bars, 5 µm.* ***D*** *Proportion of invasive cysts 96 hr after seeding. n=60.* ***E*** *Diameter of parental, GFP-PRL-3 WT, and GFP-PRL-3 C104S MDCK cysts measured 72 hr after seeding. n=90.* ***F*** *Lumen radius and distance between apical and basal membranes measured in parental and GFP-PRL-3 C104S MDCK cysts measured 72 hr after seeding. n=90.* ***D-F*** *Mean ± SEM of three independent experiments. Adapted by permission from Company of Biologists LTD: JCS (Lujan et al.), copyright (2016).*

3.1.2. No substrate candidate was found by a phosphoproteomic approach in 3D MDCK cysts

Phosphatase substrate identification can be a really challenging task (Fahs *et al.*, 2016). This can be even more difficult for PRL-3 as a DSP that can potentially dephosphorylate almost any phosphorylated protein and non-protein substrate that is also related with cancer promotion, a pathology where several molecular and cellular pathways are involved. The range of possibilities is virtually incalculable, so a screening process would be required to identify the best candidates for further individual study. In order to keep it simple, we reduced the search to polarized

epithelial cells using the system previously described in order to link substrate candidates to the presented phenotype.

Hence, a phosphoproteomic approach was done in collaboration with Marco Hennrich, from the group of Dr. Anne-Claude Gavin (Structural and Computational Biology Unit, EMBL Heidelberg), by analyzing the phosphoproteome from 72 hr parental and GFP-PRL-3 C104S overexpressing MDCK cysts compared to MDCK GFP-PRL-3 WT MDCK cysts. Prior to MS phosphopeptide identification, the sample preparation protocol required some adjustment since the cysts are embedded in a matrix that contains high levels of extracellular proteins that must be discarded to avoid data masking by those proteins. Although dispase treatment is the most commonly used reagent for matrix dissociation (Chee and Pun, 2008), a gentle incubation with 0.25 % trypsin was enough to rid samples of the extracellular proteins (data not shown). After cellular protein extraction, a tryptic digestion of the protein content followed by phosphopeptide enrichment by TiO_2 chromatography was performed (see *Methods* section *5.3.10).*

After computational analysis of the data obtained, we looked for phosphopeptides enriched more than 1.5 fold in parental and GFP-PRL-3 C104S overexpressing MDCK cells in at least 2 out of 3 replicates since we are investigating for direct substrates of the phosphatase. From the list obtained in the assay, only 4 hits were reliable according to the data filters used:

- N'-A**pSpS**LNVLNVGGK-C' from kinesin light chain-1 (KLC1). Single phosphorylation might be in either serine residue with a higher probability at S(3) and it is the most reliable hit obtained from the experiment. KLC1 belongs to the kinesin holoenzyme, an ATP-dependent motor enzyme for cargo transport along microtubules in a plus-ended direction. KLC1 functions by binding directly to the cargo, while the heavy chains are the motor proteins bound to the microtubule (Fig. 20A) (Hirokawa *et al.*, 2009). Kinesins are able to move vesicles, so they are involved in the dynamics of Golgi apparatus, endoplasmic reticulum, and secretory vesicles (Woźniak and Allan, 2006; Hirokawa *et al.*, 2009) where PRL-3 has been found (Qi Zeng *et al.*, 2000), so it is spatially likely that they can interact. Moreover, membrane-trafficking pathways have been found critical for epithelial cell polarity (Apodaca *et al.*, 2012), so perturbations in KLC1 might be involved in this process.

- N'-GI**pS**PIVFDR-C' from YTH domain-containing protein 1 (YTHDC1). It is a nuclear alternative splicing regulator that binds specifically to RNAs that contain N6-methyladenosine (m6A), a modifier that plays a role in mRNA splicing efficiency (Xu *et al.*, 2014). Moreover, YTHDC1 is also present in the cytoplasm promoting ribosome loading of its target mRNA (Wang *et al.*, 2015). Since YTHDC1 cell localization does not correlate with PRL-3 membranous environment, it was discarded as a direct substrate candidate.

- N'-EL**pS**N**pS**PPREN**pS**FGSPLEFR-C' from serine/arginine repetitive matrix protein 2 (SRRM2). This peptide has up to 3 phosphorylation sites and several phosphorylation states have been detected, but drawing absolute conclusions with so many possible perturbations is difficult. SRRM2 is a spliceosome-associated factor involved in pre-mRNA splicing, sustaining precise genome stability and chromosome segregation (Zanini *et al.*, 2017). Its exclusive presence in the nucleus suggests that the direct interaction with PRL-3 is unlikely. Therefore, SRRM2 was also discarded as a potential PRL-3 substrate.

- N'-LTFDSSF**pS**PNTGK-C' from voltage-dependent anion channel 1 (VDAC1). Although it contains 3 possible phosphorylation sites, the highest probability is at position S(8). VDAC1 is the most abundant VDAC protein located in the outer mitochondrial membrane for the exchange of metabolites between the cytosol and the mitochondria. Its interaction with B-cell lymphoma 2 (Bcl-2) proteins and other anti-apoptotic proteins also confers a function in mitochondrial-mediated apoptosis (Shoshan-Barmatz and Ben-Hail, 2012). Besides its well-described role in mitochondria, it has been more recently found in the plasma membrane where, due to the characteristic voltage of that membrane, it remains in the closed state and only scaffold functions have been described for this localization so far (De Pinto *et al.*, 2010). Therefore, although it could interact with PRL-3 in the plasma membrane, it might not be the reason of the multiple lumen-containing cyst phenotype.

Out of these 4 reliable hits, KLC1 was the only protein that, due to its functions, characteristics, and cell localization, would fit as a PRL-3 substrate candidate in the phenotype observed in an epithelial context. KLC1 consists of two domains: an α-

helical coiled-coil heptad repeat domain in charge of interacting with the heavy chain and a C-terminal domain formed by six tetratricopeptide domains (TPR) thought to mediate cargo interactions followed by a variable sequence that leads to 19 different isoforms and infers cargo selectivity (Fig. 20A) (Woźniak and Allan, 2006; McCart *et al.*, 2003). Furthermore, this selectivity is tightly regulated by protein phosphorylation in the cargo-binding domain and it has been an aim of study for the last several years (Vagnoni *et al.*, 2011; Morfini *et al.*, 2002). As expected, the KLC1 down-regulated phosphosite detected in 3D MDCK GFP-PRL-3 WT cysts compared to parental and GFP-PRL-3 C104S overexpressing MDCK cysts belongs to the cargo-binding domain, suggesting that PRL-3 might be regulating vesicle transport by KLC1 dephosphorylation. Moreover, the intron that contains the phosphosite is only present in 4 isoforms named I, J, M, and N (Fig. 20B).

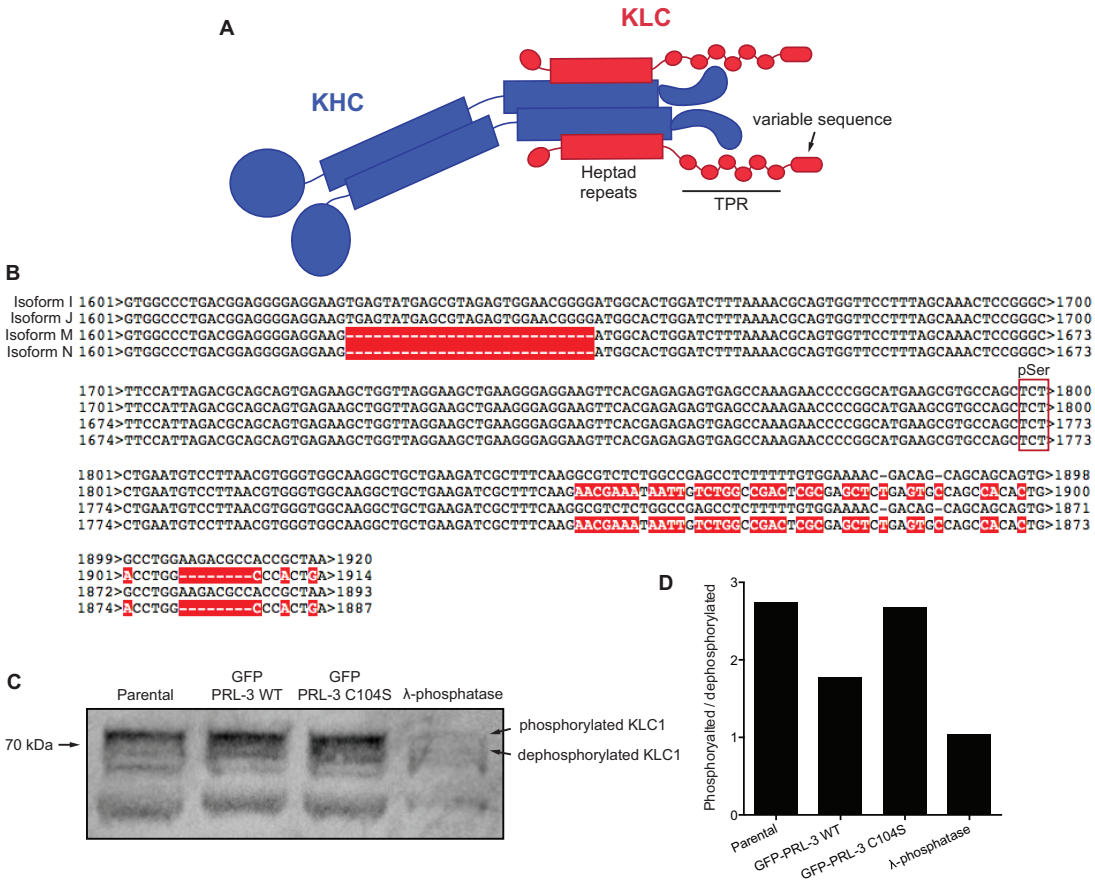

Figure 20. *PRL-3 overexpression induces KLC1 dephosphorylation in MDCK cysts.* ***A*** *Schematic representation of a kinesis heterotetramer. Kinesin heavy chain (KHC) contains the motor domain that binds to microtubule. KLC binds to KHC through the heptad repeat domain and to the cargo with the variable sequence.* ***B*** *Alignment of the variable sequence at the C-terminus of the 4 isoforms that contain the candidate pSer (highlighted) to be dephosphorylated by PRL-3.* ***C*** *Western Blot of the λ-phosphatase assay in parental MDCK cells or MDCK stably overexpressing GFP-PRL-3 WT or GFP-PRL-3 C104S cells. Anti-KLC1 was used as*

primary antibody. ***D*** *Relative protein quantification from the bands plotted in* ***C*** *as a ratio between phosphorylated and non-phosphorylated KLC1.*

In order to assess KLC1 dephosphorylation by PRL-3, WB was carried out in 2D parental, GFP-PRL-3 WT, and GFP-PRL-3 C104S overexpressing MDCK cysts using a KLC1 antibody to detect the phosphorylation status by run shift in SDS-PAGE. In order to distinguish between different isoforms or phosphorylation status, MDCK cell lysates were treated with λ-phosphatase, a promiscuous phosphatase that removes all phosphates from the proteome (Vernia *et al.*, 2009). Consequently, those bands that disappear upon λ-phosphatase incubation correspond to the phosphorylated version of the isoform that appears right below it, as observed in the two upper bands (Fig. 20C). Both band intensities were measured for every sample showing that PRL-3 WT was leading to a decrease of phosphorylation of that particular isoform as well as λ-phosphatase (Fig. 20C,D), confirming the results found by phosphoproteomics. This approach was also used in Caco-2 cells expressing GFP-PRL-3 WT, but there was no dephosphorylation visible in this epithelial model (data not shown), suggesting that KLC1 might be a specific substrate in dog cells or that the intron that contains the target phosphoserine (pS) is more abundant in dog than in human cells. Indeed, the only dog isoform annotated in the Uniprot database contains the target phosphosite.

Since the phosphoproteomic approach cannot distinguish between direct substrates and downstream effects (Fahs *et al.*, 2016), additional biochemical assays are necessary. Therefore, to study if KLC1 is a direct substrate of PRL-3, an *in vitro* dephosphorylation assay of the peptide containing the KLC1 target pS was performed. The peptide was rationally designed placing the pS in the middle flanked by 5 and 6 amino acids on its N- and C-termini, respectively (N'-MKRAS**pS**LNVLNV-C'). In order to investigate if the peptide was dephosphorylated by PRL-3, an Enzcheck assay was carried out. Different concentrations of the peptide were incubated with 6 μM of *E. Coli* purified human PRL-3 and the free phosphate resulting from the dephosphorylation was measured by a coupled reaction driven by nucleoside phosphorylase (PNP) that incorporates the free phosphate to 2-amino-6-mercapto-7-methylpurine riboside (MESG). The reaction is followed by absorption spectroscopy since the product obtained absorbs at 360nm (Webb, 1992). Unfortunately, PRL-3 did not dephosphorylate the KLC1 peptide suggesting that KLC1 dephosphorylation might actually be a downstream effect of PRL-3 overexpression in MDCK 3D cysts (Fig. 21A). As a positive control, 100 μM of lipid

$PI(4,5)P_2$ diC_8 was used (McParland *et al.*, 2011). Alternatively, both serines may have to be phosphorylated for the peptide to become a substrate, resembling the high density of negative charges found in $PI(4,5)P_2$.

In order to confirm this result, Biomol® Green, another free phosphate reporter, was used to overcome the incompatibilities with the Enzcheck approach. It is a 1-step end point phosphatase measurement method, which is a modification of the classic Malachite green reagent (Martin *et al.*, 1985). In this case, slight dephosphorylation was detected (Fig. 21B) but was not significant.

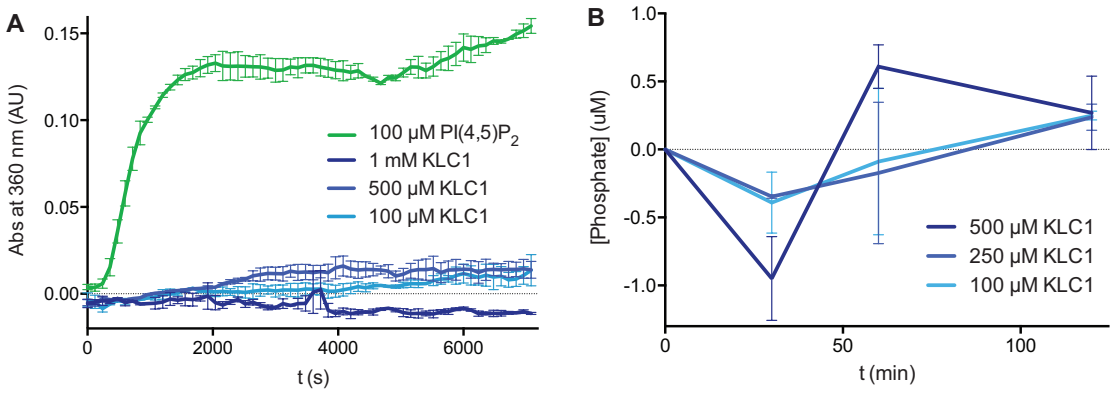

Figure 21. *PRL-3 does not dephosphorylate KLC1 in vitro.* ***A*** *Enzcheck assay performed with 6 µM purified human PRL-3 and different concentrations of pSer-containing KLC1 peptide. Mean ± SEM of three replicates.* ***B*** *Biomol® Green assayed at 3 different time points of 6 µM purified human PRL-3 incubation with different concentrations of pSer-containing KLC1 peptide. Mean ± SEM of two replicates.*

The negative results obtained from the *in vitro* kinetic assay with the target pS-containing peptide might be due to the requirement of the protein's tertiary structure for efficient recognition and dephosphorylation by PRL-3. Therefore, the *in vitro* interaction between KLC-1 and PRL-3 was studied to distinguish both possible scenarios. With this purpose, parental, GFP-PRL-3 WT, and GFP-PRL-3 C104S overexpressing MDCK cells were lysed and a co-immunoprecipitation using anti-GFP nanobodies coupled to beads was conducted. In this experiment, the catalytically inactive mutant was used as a substrate-trapping control to enhance assay sensitivity, stabilizing the interaction between KLC1 and PRL-3 (Fahs *et al.*, 2016). However, no interaction was detected by WB (Fig. 22A).

Since there may be a weak interaction with the KLC1 and it might be limited to certain cellular stages, the method used to detect it may not be sensitive enough. Therefore, in order to increase the chance of detecting an interaction, co-localization

was promoted by lysing cells that were synchronized in cytokinesis since PRL-3 and KLC1 localization is enriched in the cytokinetic bridge (Fig. 34A,B) (Ai and Skop, 2009). Unfortunately, no interaction was detected between KLC1 and PRL-3 WT nor KLC1 and PRL-3 C104S (Fig. 22B). Lastly, as an additional confirmation of the results, protein interactions and complexes were cross-linked with 1% of paraformaldehyde (PFA) in MDCK cell lysates overexpressing GFP-PRL-3 WT, or GFP-PRL-3 C104S, or with no overexpression (Kluger and Alagic, 2004; Fahs *et al.*, 2016). As expected, these results further confirmed that KLC1 is not interacting with PRL-3 (Fig. 22C), strongly suggesting that KLC1 dephosphorylation might be a downstream effect of PRL-3 overexpression in MDCK 3D cysts.

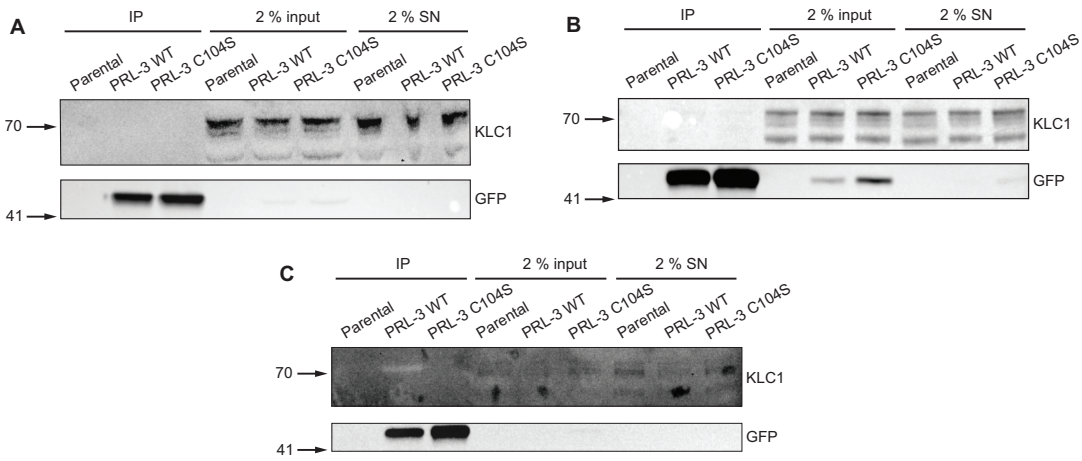

Figure 22. *PRL-3 does not physically interact with KLC1 in MDCK cells. Western Blot of GFP immunoprecipitation (IP) in untreated (**A**), synchronized in cytokinesis (**B**), or cross-linked with PFA (**C**) parental MDCK cells or MDCK cells stably overexpressing GFP-PRL-3 WT or GFP-PRL-3 C104S. Anti-KLC1 and anti-GFP were used as primary antibodies. GFP pull-down efficiency analyzed by GFP presence in the raw cell lysate (input) and after IP (SN) is also shown.*

Although KLC1 does not seem to be a PRL-3 substrate, variation of its phosphorylation status as a result of upstream effects can originate from different localizations within the polarized MDCK cells. In parental MDCK 3D cysts, KLC1 accumulated between the apical membrane and the nucleus (Fig. 23A) as expected since vesicle traffic toward the apical membrane is increased (Ai and Skop, 2009). Upon GFP-PRL-3 WT overexpression, KLC1 preserved its characteristic localization and, moreover, it did not seem to co-localize with PRL-3 (Fig. 23B,C).

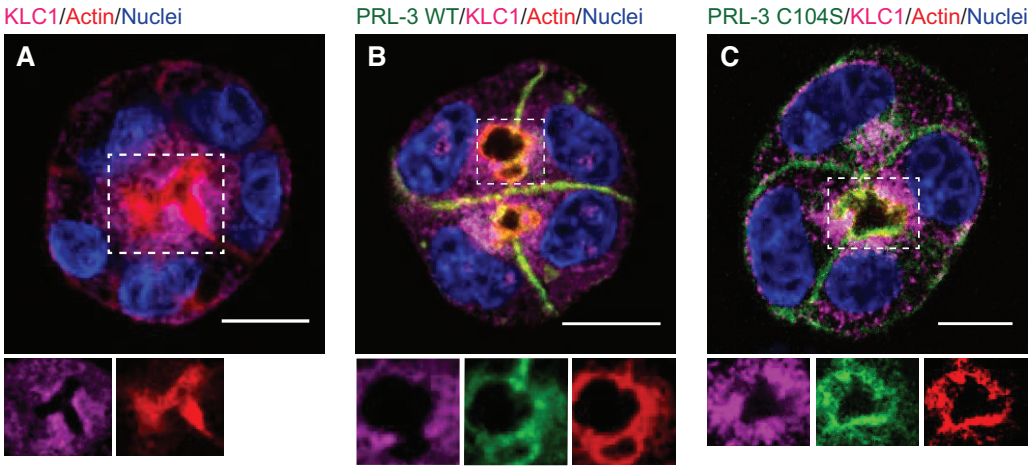

Figure 23. *PRL-3 WT does not co-localize with KLC1 in MDCK cysts. Confocal images of 48 hr parental (**A**), GFP-PRL-3 WT (**B**), or GFP-PRL-3 C104S (**C**) overexpressing MDCK cysts stained with KLC1 antibody (magenta). Bottom: higher magnification images of the indicated regions showing KLC1 (left), PRL-3 (middle), and actin (right). Scale bars, 10 µm.*

Taken together, these results suggest that KLC1 dephosphorylation in PRL-3 WT overexpressing MDCK cysts might be a downstream effect of aberrant phosphatase expression and might not be related with KLC1 cellular localization. However, the target phosphosite of KLC1 is only present in 4 out of 19 human isoforms. Therefore, a deeper study of each isolated tagged isoform could give a better picture of the effect of PRL-3 on the protein. Relative abundance of each isoform in cells is unknown, so the possibility that these 4 isoforms are not being abundant must be taken into consideration when an antibody that recognize all isoforms is used, as it is the case (Figs. 20C,D, 22A-C, 23A-C). Therefore, since the results obtained so far are not solid enough to rule out KLC1 as a direct substrate, further experiments should be performed in this direction.

Besides the four hits from the phosphoproteomic assay previously mentioned, another 282 phosphopeptides (Appendix, Table1) were found to be up- or down-regulated upon GFP-PRL-3 WT overexpression in MDCK cysts in 1 out of 3 replicates. One of these hits was plakophilin-4 (PKP4) with 3 down-regulated pS-containing phosphopeptides. PKP4 is an established binding partner in desmosomes and adherens junctions, both key for epithelia impermeability and epithelial cell polarity maintenance (Hofmann *et al.*, 2009; Desai *et al.*, 2009). Moreover, PKP4 activity is related with Ras homolog family member A (RhoA), much like PRL-3 (Ming *et al.*, 2009). Therefore, PKP4 was assessed for its potential as a PRL-3 substrate.

First, to confirm the result obtained by phosphoproteomics, PKP4 dephosphorylation by PRL-3 was analyzed on 2D MDCK cell lysate by adding different concentrations of *E. Coli* purified human PRL-3. Since there is no antibody available that selectively recognizes any of the PKP4 pS candidates, PKP4 was isolated by immunoprecipitation and incubated with PRL-3. Its phosphorylation status was measured by WB with a total anti-pS antibody. Surprisingly, in these conditions PKP4 was not phosphorylated (Fig. 24A) suggesting that it might only be phosphorylated in polarized cells. Repeating this experiment with polarized MDCK cell lysate requires a difficult technical set up. Due to this technical limitation, it was decided to assess whether PKP4 is a direct PRL-3 substrate beforehand by an *in vitro* dephosphorylation assay.

Similar to the approach taken for KLC1, 3 peptides containing the pSer candidates in the middle of the sequence were purchased: PL1 → N'-GQVGSS**pS**PKRSG-C'; PL2 → N'-GQDLR**pS**AVSPDL-C'; and PL3 → N'-DLRSAV**pS**PDLHI-C'. The phosphatase activity of 6 µM of *E. Coli* purified human PRL-3 against each peptide was monitored by Enzcheck assay, and 100 µM of lipid PI(4,5)P_2 diC_8 was used as a positive control to test the intrinsic phosphatase activity of PRL-3. The results showed that PRL-3 was not able to dephosphorylate any of the proposed peptides (Fig. 24B), indicating that PKP4 is not a direct PRL-3 substrate. The absence of activity could be due to the lack of the tertiary protein structure of PKP4, and although it cannot be completely discarded as a potential substrate, no deeper investigations were pursued at this time.

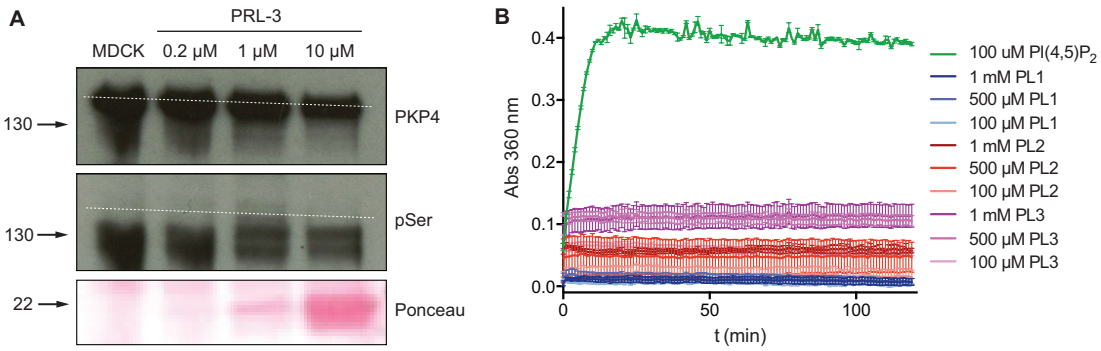

Figure 24. *PRL-3 WT does not dephosphorylate PKP4 in vitro.* ***A*** *Western Blot from PKP4 isolated from non MDCK cells and incubated with different concentrations of purified human PRL-3 (Ponceau staining). Dashed white lines mark the position of PKP4 that is not phosphorylated in non-polarized MDCK cells.* ***B*** *Enzcheck assay performed with 6 µM purified human PRL-3 and different concentrations of pSer-containing PKP4 peptides. Mean ± SEM of three replicates.*

Another member of the plakophilin family, plakophilin-2 (PKP2), was also found as a protein-protein interaction candidate in a glutathione S-transferase (GST)-PRL-3 WT pull down in human embryonic kidney (Hek293) cells carried out previously by Dr. Giulia Varsano in the Köhn lab. Since PKP2 is also a component of the desmosome (Kirchner *et al.*, 2012), it would be interesting to see if this interaction might explain the multiple lumen-containing MDCK cyst phenotype upon PRL-3 overexpression. As a first approach, the interaction detected in the large screening was assessed by PKP2 co-immunoprecipitation with GFP-PRL-3 in MDCK cells using GFP nanobodies coupled to beads. Besides GFP-PRL-3 WT, GFP-PRL-3 C104S was used to stabilize the interaction due to its substrate-trapping effect. GFP-PRL-3 E50R was also utilized to determine if an increase of the phosphatase activity would lead to any change in PKP2. Based on the results seen in Figure 25A, PKP2 was discarded as an interaction partner with PRL-3.

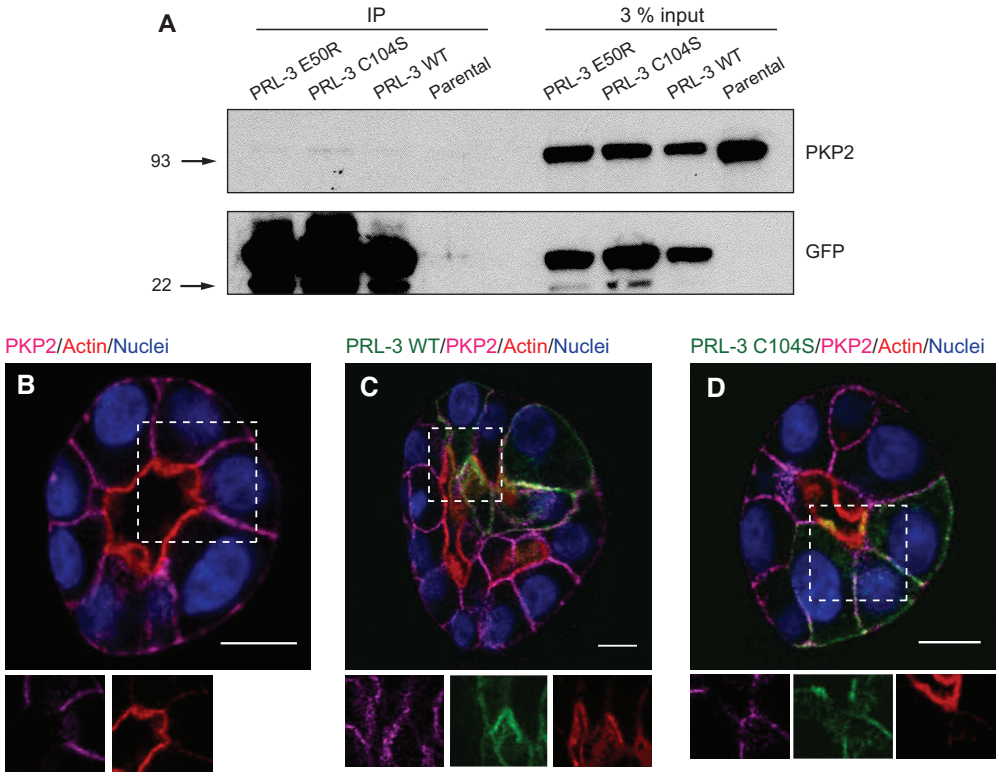

Figure 25. *PRL-3 WT does not interact with PKP2.* ***A*** *Western Blot of GFP immunoprecipitation (IP) from parental MDCK cells or MDCK stably overexpressing GFP-PRL-3 (WT, C104S, or E50R) cells. Anti-PKP2 and anti-GFP were used as primary antibodies. GFP pull-down efficiency is shown comparing GFP levels in IP and input.* ***B-D*** *Confocal images of 96 hr parental (**A**), GFP-PRL-3 WT (**B**), or GFP-PRL-3 C104S (**C**) overexpressing MDCK cysts stained with a PKP4 antibody (magenta). Bottom: higher magnification images of the indicated regions showing PKP2 (left), PRL-3 (middle), actin (right). Scale bars, 10 µm.*

To remove any doubt, PKP2 localization was analyzed in 96 hr parental, GFP-PRL-3 WT, and GFP-PRL-3 C104S overexpressing MDCK cysts fixed and stained with a PKP2 antibody. PKP2 is enriched in the lateral membrane in parental MDCK cysts (Fig. 25B) and this pattern does not change upon GFP-PRL-3 WT or GFP-PRL-3 C104S overexpression (Fig. 25C,D). Additionally, PKP2 was not enriched where PRL-3 was concentrated (Fig. 25C,D). Altogether, these results suggest that PKP2 is not a PRL-3 interacting protein.

In conclusion, the unsuccessful results obtained from the phosphoproteomic assay forced us to approach our PRL-3 substrate research in MDCK 3D cysts from another angle. Instead of looking for a substrate that could explain the phenotype first, we decided to undertake a deeper cellular study into the physical phenotype in order to decipher the original cellular process affected by PRL-3. The elucidation of this process would narrow our scope and simplify the search for PRL-3 substrates.

3.1.3. PRL-3 induces fully polarized ectopic lumens from incorrectly localized AMIS

The apical-basal cell polarity is established in MDCK cysts right after the first cell division, when the membranes that are in cell-cell contact acquire a clear apical identity in the center, and lateral identity between the apical and the basal membrane (Apodaca *et al.*, 2012; Bryant *et al.*, 2010; Apodaca, 2010). In order to find the cellular origin of the multiple lumen MDCK cyst phenotype, the cystogenesis process was studied in the reverse direction from how it naturally occurs. First, the resulting ectopic lumens that arose upon PRL-3 WT overexpression were analyzed to describe if they were still fully polarized.

Well-defined tight junctions are formed during lumen opening, so we investigated the localization of these tight junctions in the ectopic lumens from PRL-3 WT cysts. As a tight junction marker, the ZO-1 antibody, was used in 72 hr parental, GFP-PRL-3 WT, and GFP-PRL-3 C104S overexpressing MDCK cysts. Tight junctions were found localized to the boundary between the apical and lateral membrane flanking the central lumen in parental and GFP-PRL-3 C104S MDCK cysts (Fig. 26 A,C,D) as previously reported (Bryant *et al.*, 2010; Martin-Belmonte *et al.*, 2007). PRL-3-induced ectopic lumens were also surrounded by tight junctions (Fig. 26 B,D). Three dimensional reconstruction analysis of 660 cysts revealed that

these ectopic lumens seem to arise between lateral membranes and may be shared by two or more cells. Moreover, the architecture of these lumens can stay symmetric between cells like the central lumen in parental MDCK cysts, or show an invasive behavior towards one of the cells still flanked by tight junctions (Fig. 26 B,E).

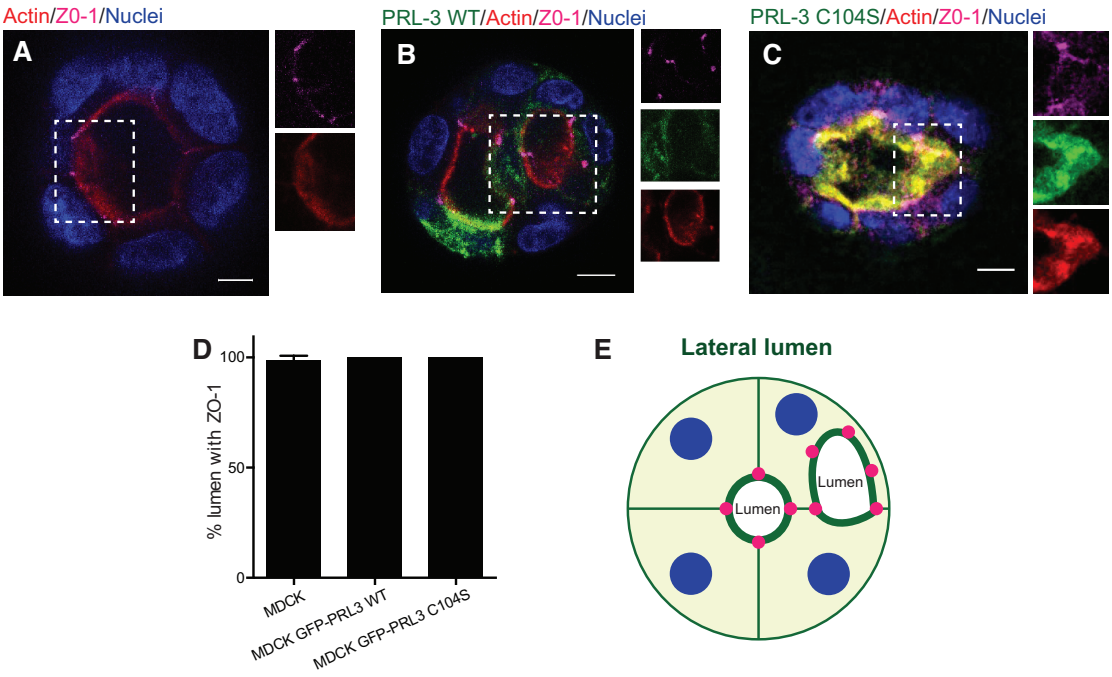

Figure 26. *The appearance of ectopic lumens upon PRL-3 WT overexpression maintain intact tight junctions in MDCK cysts.* ***A-C*** *Confocal images of 72 hr parental (**A**), GFP-PRL-3 WT (**B**), or GFP-PRL-3 C104S (**C**) overexpressing MDCK cysts stained with a ZO-1 antibody (magenta). Right: higher magnification images of the indicated regions showing ZO-1 (up), actin (middle), PRL-3 (down). Scale bars, 10 μm.* ***D*** *The proportion of cysts with ZO-1 staining in the lumen. n=90. Mean ± SEM of three independent experiments.* ***E*** *Schematic representation of MDCK cells overexpressing PRL-3 WT presenting an asymmetric invasive ectopic lumen flanked with ZO-1 (magenta dots). Adapted by permission from Company of Biologists LTD: JCS (Lujan et al.), copyright (2016).*

Tight junction and actin staining together suggest that ectopic lumens are still fully polarized, but more apical membrane markers should be tested. Indeed, three PRL-3 substrate candidates, PI(4,5)P_2 (McParland *et al.*, 2011), Ezrin (Forte *et al.*, 2008), and Na^+/H^+ exchanger regulatory factor 1 (NHERF1) (Fang *et al.*, 2015), are especially interesting since they are known to be decisive in cell polarity (Martin-Belmonte *et al.*, 2007; Fang *et al.*, 2015) by delineating the apical membrane, suggesting a potential involvement in the mechanism by which PRL-3 causes the multiple lumen phenotype.

Heterogeneous distribution of $PI(4,5)P_2$ and $PI(3,4,5)P_3$ in the apical and lateral/basal membranes of polarized cells, respectively, is crucial for polarity maintenance that is achieved by the polarized distribution of PTEN (Martin-Belmonte *et al.*, 2007; Thapa and Anderson, 2012; Leslie *et al.*, 2008). The presence of a $PI(4,5)P_2$ phosphatase candidate like PRL-3 could potentially impair its characteristic membrane distribution. Therefore, $PI(4,5)P_2$ presence in the apical membrane of 72 hr parental, pmKATE2-PRL-3 WT, and pmKATE2-PRL-3 C104S overexpressing MDCK cysts was analyzed by confocal microscopy. These cell lines also expressed the GFP tagged version of the Pleckstrin homology domain of phospholipase Cδ (GFP-PH-PLCδ), a cytosolic tagged domain that binds selectively to $PI(4,5)P_2$. Consequently, PH-PLCδ translocates from the cytosol to $PI(4,5)P_2$ containing membranes, and therefore, can be used as a reporter of $PI(4,5)P_2$ concentration in the apical membrane. As expected, $PI(4,5)P_2$ was qualitatively present at the apical membrane in all three parental, pmKATE2-PRL-3 WT, and pmKATE2-PRL-3 C104S overexpressing MDCK cysts (Fig. 27A-D). However, no decrease of $PI(4,5)P_2$ levels, as measured by GFP-PH-PLCδ fluorescence intensity ratio between apical membrane and the rest of the cell, was detected (Fig. 27D).

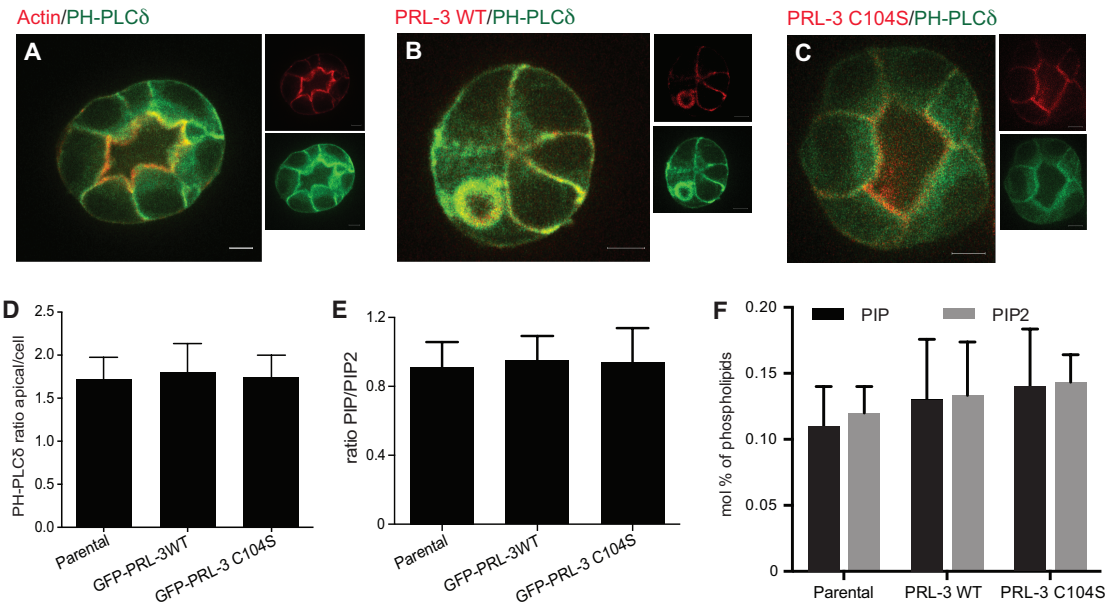

Figure 27. *PRL-3 WT overexpression does not decrease $PI(4,5)P_2$ levels in the apical domain of MDCK cysts.* ***A-C*** *Confocal images of 72 hr parental (**A**), pmKATE2-PRL-3 WT + GFP-PH-PLCδ (**B**), or pmKATE2-PRL-3 + C104S GFP-PH-PLCδ (**C**) overexpressing MDCK cysts. Right: separate channels showing actin or PRL-3 (WT or C104S) (up) and PH-PLCδ (down). Scale bars, 10 μm.* ***D*** *$PI(4,5)P_2$ dephosphorylation in the apical membrane measured as the fluorescence intensity ratio between apical and cytosolic membranes plus the basal GFP-PH-PLCδ in parental, pmKATE2-PRL-3 WT, and pmKATE2-PRL-3 C104S*

overexpressing MDCK cysts. n=90. ***E,F*** *Quantitative lipid MS in MDCK cysts or cysts stably expressing GFP-PRL-3 WT or GFP-PRL-3 C104S analyzed 5 days after seeding. The ratio between total phosphatidylinositol phosphates (PIP) and PIP2 is quantified (****E****) or given as an independent percentage compared to total phospholipids (****F****).* ***D-F*** *Mean ± SEM of three independent experiments. Adapted by permission from Company of Biologists LTD: JCS (Lujan et al.), copyright (2016).*

In order to corroborate this result, the overall phosphatidylinositol biphosphates (PIP_2) content in MDCK cysts was measured by quantitative MS in collaboration with Dr. Britta Brügger (Heidelberg University Biochemistry Center–BZH, Heidelberg, Germany). Since all three PIP_2 species have equal molecular weight, they are indistinguishable by MS and the result reflects the sum of all three. No difference was detected between GFP-PRL-3 WT overexpressing MDCK cysts compared to the controls (Fig. 27E,F). In light of these results, PRL-3 is apparently not dephosphorylating $PI(4,5)P_2$ in the polarized cell context. However, $PI(4,5)P_2$ homeostasis is highly regulated at the cell surface (Czech, 2000) and a fast turnover cannot be detected by the current techniques used or any other approach developed so far. Therefore, we cannot fully discount our current hypothesis since, when PRL-1 is overexpressed, which cannot dephosphorylate $PI(4,5)P_2$ (Jin-Peng Sun *et al.*, 2007; Rios *et al.*, 2013), we observed a similar but weaker phenotype compared to PRL-3 overexpression (Fig. 14D). Nevertheless, the specific localization of $PI(4,5)P_2$ agrees with the conclusion that the overall cell polarity is not disturbed.

In 2008, Forte et al. observed that PRL-3 overexpression leads to ezrin dephosphorylation on residue T(567), but no direct dephosphorylation has been described yet (Forte *et al.*, 2008). Ezrin is a member of the Ezrin/Radixin/Moesin (ERM) family that functions as a linker between the plasma membrane and F-actin upon T(567) phosphorylation (Zhu *et al.*, 2010). Since cytoskeleton assembly below the apical membrane on epithelial polarized cells is crucial for polarity establishment and maintenance, ezrin dephosphorylation in the apical membrane would disturb the cell polarity. Therefore, 72 hr parental, GFP-PRL-3 WT, and GFP-PRL-3 C104S overexpressing MDCK cysts were fixed and stained against both ezrin and pERM, which can detect phosphorylation of Ezrin T(567), Radixin T(564), and Moesin T(558) but was still used considering that MDCK cells express mainly ezrin (Wakayama *et al.*, 2011). Ezrin was shown in the apical membrane partially co-localizing with GFP-PRL-3 WT and GFP-PRL-3 C104S (Fig. 28A-D), confirming that cell polarity was undisturbed. However, compared to ezrin, pERM co-localized less with PRL-3 WT and PRL-3 C104S (Fig. 28D). A lesser co-localization of PRL-3

WT with the phosphorylated form of ezrin would suggest that some dephosphorylation might be occurring, but a similar tendency with PRL-3 C104S was also observed, discounting this hypothesis. In agreement with these results, the fluorescence intensity ratio measurement between pERM and ezrin showed no difference when GFP-PRL-3 WT was overexpressed compared to the parental and the GFP-PRL-3 C104S expressing MDCK cysts (Fig. 28E).

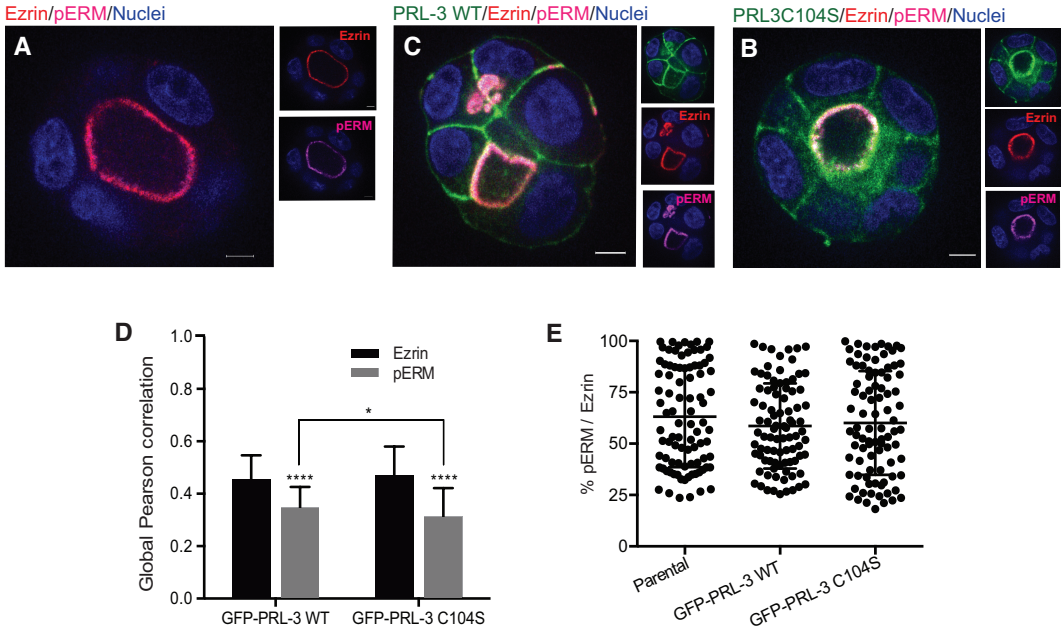

Figure 28. *PRL-3 WT does not dephosphorylate apical ezrin in MDCK cysts.* ***A-C*** *Confocal images of 72 hr parental (**A**), GFP-PRL-3 WT (**B**), or GFP-PRL-3 C104S (**C**) overexpressing MDCK cysts stained with ezrin and pERM antibodies. Right: separate channels showing PRL-3 (up), ezrin (middle), pERM (down). Scale bars, 10 µm.* ***D*** *Global Pearson correlation measured to study co-localization between PRL-3 WT or PRL-3 C104S, and ezrin or pERM.* ***E*** *Ezrin dephosphorylation measured by the fluorescence intensity ratio between pERM and ezrin in parental, GFP-PRL-3 WT, and GFP-PRL-3 C104S MDCK cysts.* ***D,E*** *n=90. Mean ± SEM of three independent experiments. Adapted by permission from Company of Biologists LTD: JCS (Lujan et al.), copyright (2016).*

The last apical marker examined was NHERF1, an adaptor protein that links several ion transporters with cellular receptors and other proteins. NHERF1 shifts from the apical membrane to the cytosol upon serine dephosphorylation, which has been related with cancer (Mangia *et al.*, 2012), and it was recently proposed as a PRL-3 substrate (Fang *et al.*, 2015). Therefore, we tried to confirm NHERF1 dephosphorylation upon PRL-3 overexpression in MDCK cells. With a specific NHERF1 antibody, the protein was immunoprecipitated from parental, GFP-PRL-3 WT, and GFP-PRL-3 C104S 2D MDCK cell lysates. Its pSer status was analyzed by

WB with a total pSer antibody. However, the isolated NHERF1 were not phosphorylated, suggesting that it might already be dephosphorylated in 2D MDCK cells (Fig. 29A). Moreover, NHERF1 immunoprecipitation did not pull down overexpressed PRL-3 WT nor PRL-3 C104S implying that no interaction takes place between both proteins (Fig. 29A). These results suggest that NHERF1 might only be phosphorylated in 3D MDCK cysts. However, NHERF1 immunoprecipitation in 3D MDCK total cell lysates is not a feasible approach due to the amounts of cells required for the biochemical technique, which is very difficult to reach in 3D polarized cell culture. For that reason, and since NHERF1 plasma membrane or cytosol localization depends on its phosphorylation status, NHERF1 localization was checked in 72 hr fixed parental, GFP-PRL-3 WT, and GFP-PRL-3 C104S MDCK cysts. GFP-PRL-3 WT overexpressing MDCK cysts showed exclusive NHERF1 plasma membrane localization as expected in parental and GFP-PRL-3 C104S MDCK cysts (Fig. 29B-D), postulating that NHERF1 might not be dephosphorylated by PRL-3 in this system, and corroborating once more that the polarity is not disturbed.

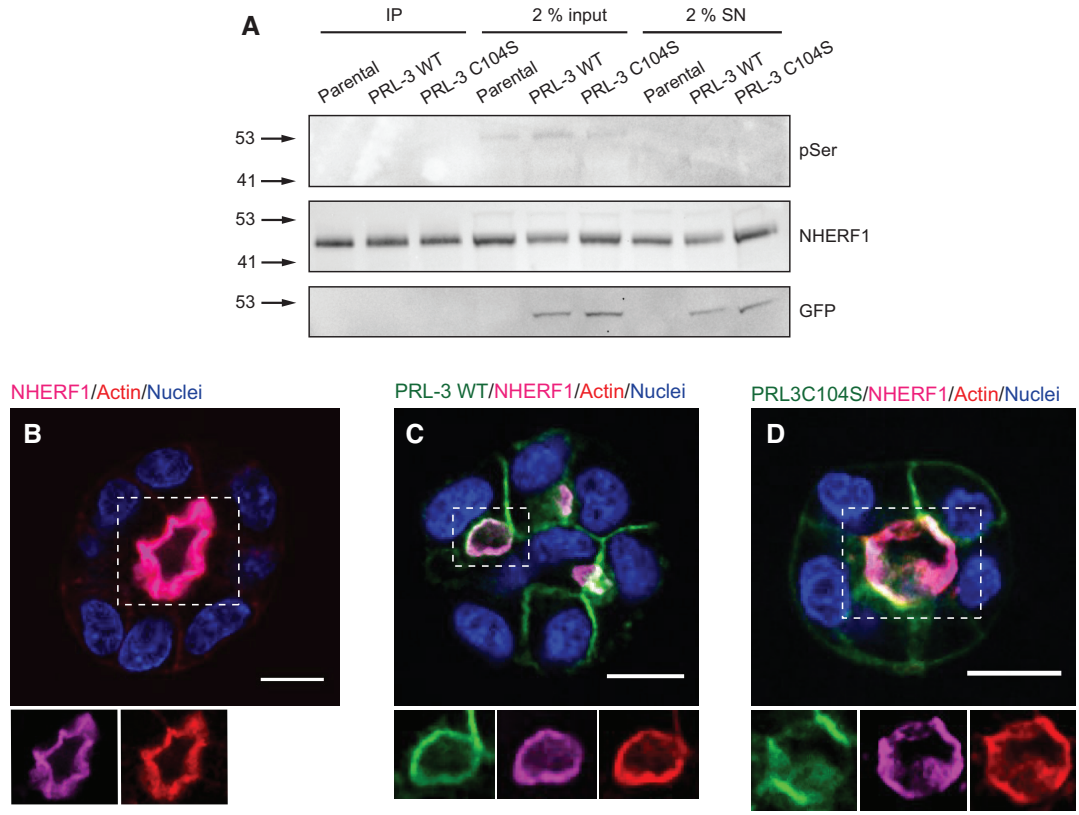

Figure 29. *PRL-3 WT co-localizes with NHERF1 in MDCK cysts but relocalization of NHERF1 through dephosphorylation was not detected, and neither was phosphorylation of NHERF1 in the WB from 2D MDCK cell culture.* ***A*** *Western Blot of NHERF1*

immunoprecipitation (IP) from parental MDCK cells or MDCK stably overexpressing GFP-PRL-3 WT or GFP-PRL-3 C104S cells. Anti-NHERF1, anti-pSer and anti-GFP were used as primary antibodies. NHERF1 pull-down efficiency analyzing NHERF1 presence in the raw cell lysate (input) and after IP (SN) is also shown. ***B-D*** *Confocal images of 72 hr parental (**B**), GFP-PRL-3 WT (**C**), or GFP-PRL-3 C104S (**D**) overexpressing MDCK cysts stained with NHERF1 antibody. Bottom: separate channels of the highlighted regions showing PRL-3 (left), NHERF1 (middle), actin (right). Scale bars, 10 μm.*

So far, these results indicate that PRL-3 does not disturb the lumen identity and, consequently, the cell polarity *per se*. Therefore, we hypothesized that aberrant PRL-3 expression might lead to lumen mispositioning instead. We then focused our studies in AMIS specification, an earlier step in lumenogenesis that precedes the lumen opening (Bryant *et al.*, 2010; Apodaca, 2010). As was postulated, in 48 hr parental and PRL-3 C104S MDCK cysts, that the AMIS, marked by the exocyst complex component Sec8, was recruited at both sides of cell-cell contacts in the center of the cysts marking the position of the future opened lumen (Fig. 30A,C,D) (citation). In PRL-3 WT overexpressing cysts, Sec8 stained AMIS is misplaced from the center of the cyst to the lateral membrane (Fig. 30B,D,E). In MDCK cysts, the delivery of apical determinants to the AMIS requires polarized vesicular trafficking (Bryant *et al.*, 2010). In light of this, we tested the hypothesis that PRL-3 overexpression could redirect vesicle trafficking to PRL-3-induced ectopic lumens. Figure 30F-H shows that exocytic vesicles, labeled with BODIPY-Tr-Ceramide (Van der Sluijs *et al.*, 1990), were indeed delivered to nascent PRL-3-induced lateral lumens. These results indicate that the AMIS is properly formed but mislocalized, what will give rise to an ectopic lumen opening.

In conclusion, these results indicate that PRL-3 disrupts proper lumen positioning at the center of the cyst rather than completely abolishing cell polarity. Therefore, PRL-3 seems to intervene at an earlier step in lumenogenesis.

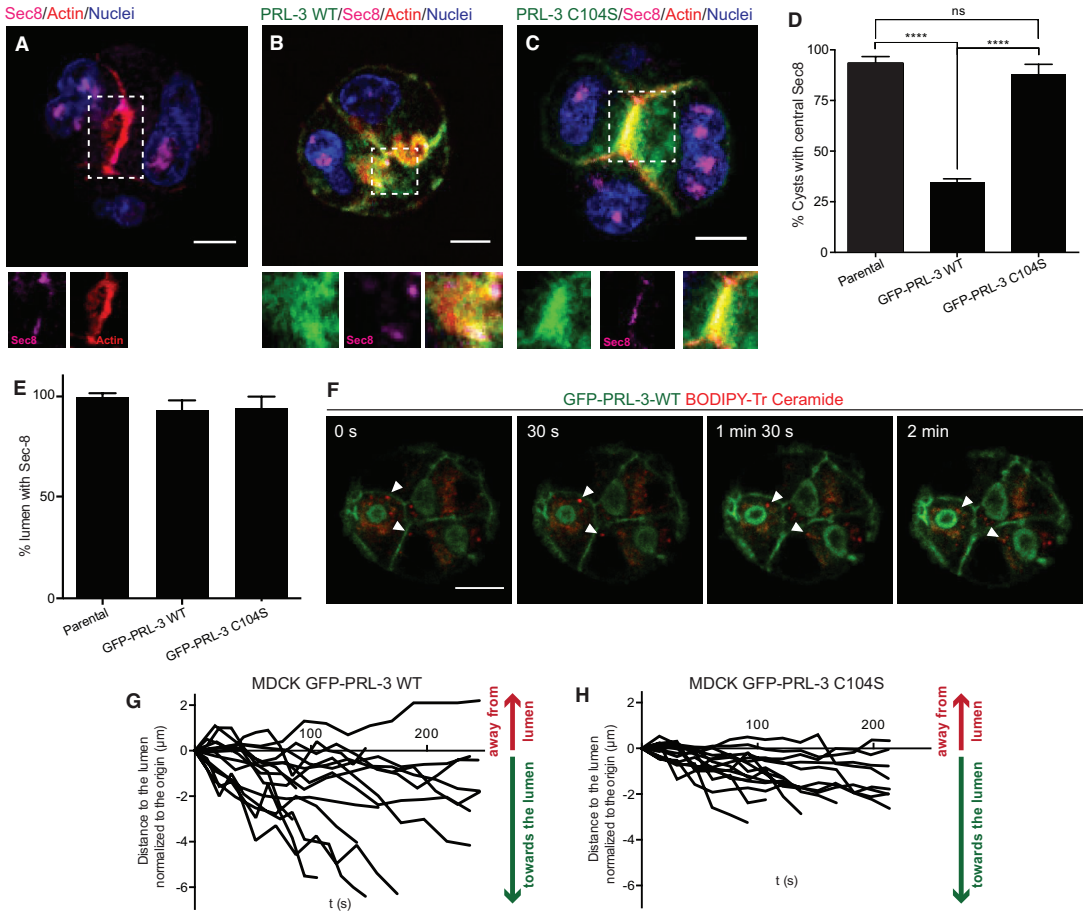

Figure 30. *AMIS is correctly formed but mispositioned prior to formation of ectopic lumens in PRL-3 WT overexpressing MDCK cysts.* ***A-C*** *Confocal images of 48 hr parental (**A**), GFP-PRL-3 WT (**B**), or GFP-PRL-3 C104S (**C**) overexpressing MDCK cysts stained with Sec8 antibody. Bottom: separate channels of the highlighted regions showing PRL-3 (left), Sec8 (middle), actin, or merge (right). Scale bars, 10 µm.* ***D*** *The proportion of cysts with central Sec8 staining and* ***E*** *The proportion of cysts with Sec8 staining in the nascent lumen. Mean ± SEM of three independent experiments. n=90.* ***F*** *Selected pictures of time-lapse live-cell imaging of 48 hr GFP-PRL-3 WT MDCK cysts showing vesicle trafficking (arrowheads) to ectopic AMIS. Scale bars, 10 µm.* ***G,H*** *Fluorescent BODIPY-TR ceramide stained vesicles tracked during time towards a nascent lumen when GFP-PRL-3 WT (**G**) or GFP-PRL-3 C104S (**H**) are overexpressed. The displacement of the vesicle is measured relative to the starting distance from the vesicle to the middle of the lumen. Negative values indicate vesicles approaching the lumen, while positive values indicate that vesicles move away from the lumen. n=15 of three independent experiments.* ***A-E*** *are adapted by permission from Company of Biologists LTD: JCS (Lujan et al.), copyright (2016).*

3.1.4. PRL-3 alters the midbody apical localization affecting lumen positioning

It has been recently reported that the AMIS is formed by the vesicular transport of apical components towards the midbody during and at the site of cytokinesis (D. Li *et al.*, 2014; Jaffe *et al.*, 2008). Consequently, the apical membrane is positioned by the midbody during and right after cytokinesis (Jaffe *et al.*, 2008; Overeem *et al.*, 2015; Schlüter *et al.*, 2009).

In order to determine the positions of midbodies in PRL-3 WT overexpressing MDCK cysts, different midbody markers were examined before the lumen was open (48 hr), including mitotic kinesin-like protein 1 (MKLP1), centrosomal protein 55 (Cep55), AuroraB, and γ-tubulin. In parental and GFP-PRL-3 C104S MDCK cysts, all markers stained spotty structures attached to the apical membrane that will form the central lumen (Fig. 31A,C,D, E,F), confirming that the post-mitotical midbody remains right after cell division in the apical membrane, instead of being internalized and degraded. This staining was also found in the ectopic lumens formed when GFP-PRL-3 WT is overexpressed in MDCK cysts (Fig. 31B,D,G,H). Cep55 is not exclusively found in the midbody, but rather can also be found in other subcellular structures like the centrosome (Martinez-Garay *et al.*, 2006). Additionally, the MKLP1 antibody showed high background fluorescence. Therefore, Cep55 and MKLP1 co-localization was only quantified in apical spotty structures to guarantee that they were post-mitotical midbodies (Fig. 31A-C,I).

Midbody remnant position was then distinguished between central (apical) or lateral retention in both MDCK and Caco-2 cysts overexpressing GFP-PRL-3 WT or GFP-PRL-3 C104S. The aberrant expression of PRL-3 WT led to the incorrect lateral localization of about 30-50% of post-mitotic midbody remnants compared to the central localization in parental and GFP-PRL-3 C104S MDCK cysts (Fig. 31J,K). To better understand the positioning of the midbody toward the apical membrane over time, we next carried out live cell-imaging experiments in PRL-3 C104S and PRL-3 WT overexpressing MDCK cysts using YFP-MKLP1 as a midbody reporter. At the two-cell stage, the post-mitotic midbody was maintained at the center in PRL-3 C104S MDCK cysts (Fig. 31M), whereas PRL-3 WT altered its position from the central to the lateral membrane. Subsequently, the AMIS is formed around the midbody at that position (Fig. 31L). These results are in line with our observation that ectopic lumens arise from the AMIS positioned at the lateral membrane (Fig. 30D,E).

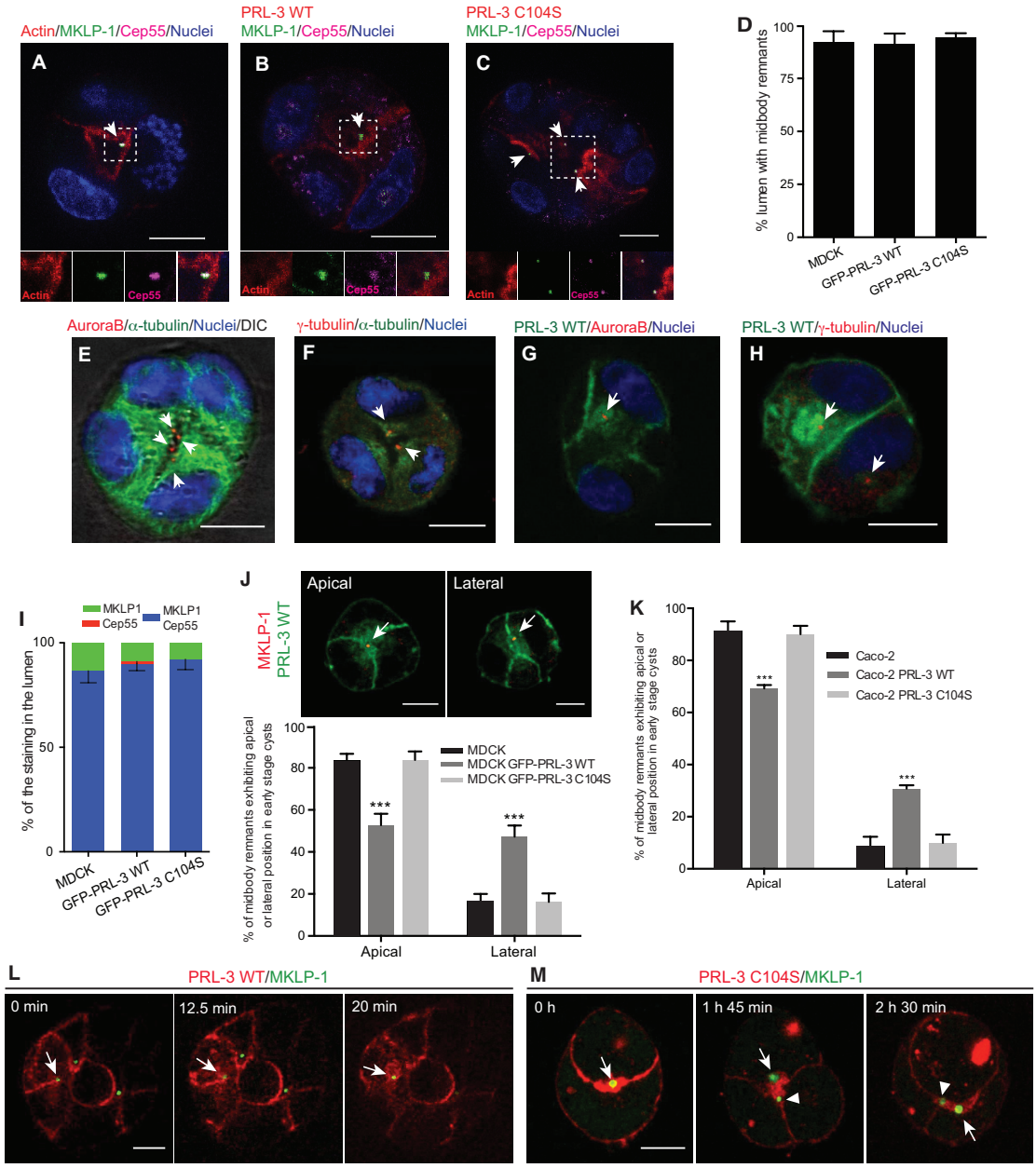

Figure 31. *PRL-3 activity alters the position of the post-mitotic midbody.* ***A-C*** *Confocal images of 48 hr (nascent lumen) parental (**A**), GFP-PRL-3 WT (**B**), or GFP-PRL-3 C104S (**C**) overexpressing MDCK cysts stained with MKLP1 and Cep55 antibody. Bottom: separate channels of the highlighted regions showing actin (left), MKLP1 (middle left), Cep55 (middle right), actin, or merge (right). Scale bars, 10 μm.* ***D*** *The proportion of cysts with lumen containing midbodies. n=300.* ***F-H*** *Representative images of parental MDCK cysts (**E,F**) or MDCK cysts overexpressing GFP-PRL-3 WT (**G,H**) at 48 hr after plating stained with antibodies against midbody remnant proteins: AuroraB (**E,G**), γ-tubulin (**F,H**). Cysts in **E** and **F** were additionally stained with a-tubulin to visualize microtubules. Arrows indicate midbody remnants marking the lumen position. Scale bars, 10 μm.* ***I*** *The proportion of staining in the lumen that contains MKLP1 and Cep55 as a measure for co-localization. n=300.* ***J,K*** *Midbody remnants (MKLP1) in 48 hr cysts expressing GFP-PRL-3 WT. Arrows indicate midbody remnants with central (apical) (left) or lateral (right) localization. Proportion of midbody remnants presenting central (apical) or lateral localization in MDCK (**J**) or Caco-2 (**K**) cysts and cysts stably expressing GFP-PRL-3 WT and GFP-PRL-3 C104S were*

analyzed 48 hr after seeding. n=90. ***L,M*** *Selected points of live-cell imaging of 45 hr cysts transiently co-expressing either pmKATE2-PRL-3 WT (**L**) or C104S (**M**), and YFP-MKLP1. Arrow in **L** indicates a midbody remnant that gets retained at the lateral plasma membrane with subsequent ectopic lumen formation. Representative results of three biological replicates are shown. Arrow in **I** highlights the first midbody remnant; the arrowhead highlights the midbody remnant coming from the second cytokinesis. Scale bars, 10 µm.* ***D,I,J,K*** *Mean ± SEM of three independent experiments. Adapted by permission from Company of Biologists LTD: JCS (Lujan et al.), copyright (2016).*

It has been postulated that post-mitotic midbodies can participate in functions unrelated to cytokinesis, but the fate of the midbody after cytokinesis remains unknown in this MDCK cyst model (Chun-Ting Chen *et al.*, 2013; Kuo *et al.*, 2011; Pollarolo *et al.*, 2011; Morais-de-Sá and Sunkel, 2013). Indeed, the first midbody (arrow) in Figure 31M stayed over time at the apical membrane after subsequent cell divisions. For that reason, we determined if the midbody remnants resulting from several cell divisions during cyst development were accumulated at the edge of the lumen or internalized and degraded. To accomplish this, parental, GFP-PRL-3 WT, and GFP-PRL-3 C104S MDCK 72 hr fixed cysts were stained with MKLP1 and Cep55 midbody markers. As previously described in proliferative epithelial surfaces in mice (Maliga *et al.*, 2013), midbody remnants persisted through cell division, delineating the edge of the central and ectopic lumens when PRL-3 was overexpressed (Fig. 32A-E). This result suggests that midbodies could play a role in cell polarity and lumen maintenance since they persist long after cell division instead of being internalized or degraded.

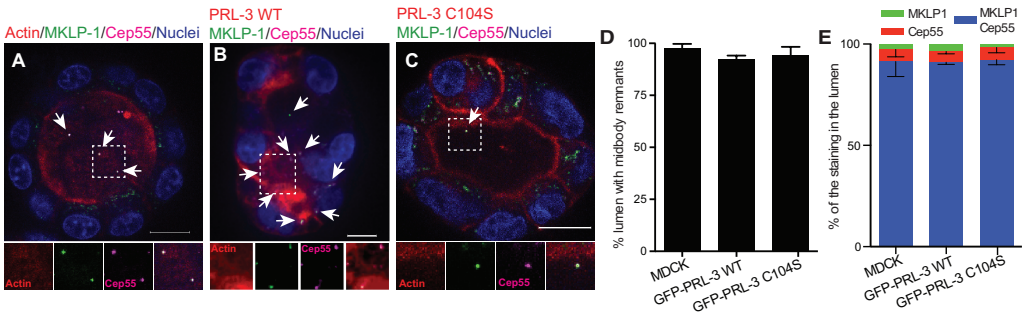

Figure 32. *Post-mitotic midbodies remain during cell division delineating the edge of the open lumen.* ***A-C*** *Confocal images of 72 hr (open lumen) parental (**A**), GFP-PRL-3 WT (**B**), or GFP-PRL-3 C104S (**C**) overexpressing MDCK cysts stained with the MKLP1 and Cep55 antibodies. Bottom: separate channels of the highlighted regions showing actin (left), MKLP1 (middle left), Cep55 (middle right), actin, or merge (right). Scale bars, 10 µm.* ***D*** *The proportion of cysts with lumen containing midbodies and **I** the proportion of staining in the lumen that contains both MKLP1 and Cep55. Mean ± SEM of three independent experiments. n=300. Adapted by permission from Company of Biologists LTD: JCS (Lujan et al.), copyright (2016).*

Taken together, these findings show that midbody remnants are positioned on the apical membrane after cytokinesis instead of being degraded, and suggest that the multiple lumen phenotype driven by PRL-3 is through midbody mislocalization during or after cell division. Moreover, it was demonstrated that these midbody remnants stay long after cell division, accumulating in the lumen, indicating a post-mitotic role for this protein complex.

3.1.5. PRL-3 alters the midbody remnant apical position by shortening cytokinesis timing

Midbody apical positioning in MDCK cysts is achieved by the perpendicular orientation of the mitotic spindle during metaphase followed by an asymmetric abscission, which ensures the positioning of the midbody to the apical membrane. The disruption of any of those processes lead to lateral retention of the midbody and, consequently, the appearance of an ectopic lumen (Jaffe *et al.*, 2008; Bryant *et al.*, 2010; D. Li *et al.*, 2014; Schlüter *et al.*, 2009; Overeem *et al.*, 2015). Indeed, loss of a planar orientation of the mitotic spindle has been largely studied, due to its implication in carcinoma formation (J. C. Pease and Tirnauer, 2011; Noatynska *et al.*, 2012). Knockdown of tumor suppressors Par3 or Cdc42 disrupts spindle orientation in MDCK cysts, leading to the multiple lumen phenotype seen in PRL-3 overexpression (Hao *et al.*, 2010; Jaffe *et al.*, 2008). Therefore, we examined if aberrant GFP-PRL-3 WT expression would affect mitotic spindle orientation. Mitotic spindles were stained with γ-tubulin and Hoechst, and measured at late metaphase as previously described in 48 hr parental, GFP-PRL-3 WT, and GFP-PRL-3 C104S overexpressing MDCK fixed cysts (Jaffe *et al.*, 2008; Hao *et al.*, 2010; Wei *et al.*, 2012; Zhen Zheng *et al.*, 2010; Rodriguez-Fraticelli *et al.*, 2010). Upon GFP-PRL-3 WT overexpression, mitotic spindle orientation was undisturbed compared to parental and GFP-PRL-3 C104S MDCK cysts (Fig. 33A), signifying that PRL-3 might be altering the asymmetric abscission, which would also theoretically lead to failure of the apical delivery of the midbody. Unlike mitotic spindle misorientation, this explanation is currently only theoretical speculation (Jaffe *et al.*, 2008; Overeem *et al.*, 2015).

In order to investigate this hypothesis, furrow ingression was stained with anillin, a actomyosin-based contractile ring scaffold protein (Piekny and Glotzer, 2008), in fixed 72 hr MDCK cysts, and measured as previously described (Liu *et al.*, 2012).

GFP-PRL-3 WT overexpression in MDCK cysts did not disrupt asymmetric abscission when compared to parental and GFP-PRL-3-C104S overexpressing MDCK cysts (Fig. 33B). Consequently, PRL-3 must be affecting midbody positioning by a novel alternative mechanism.

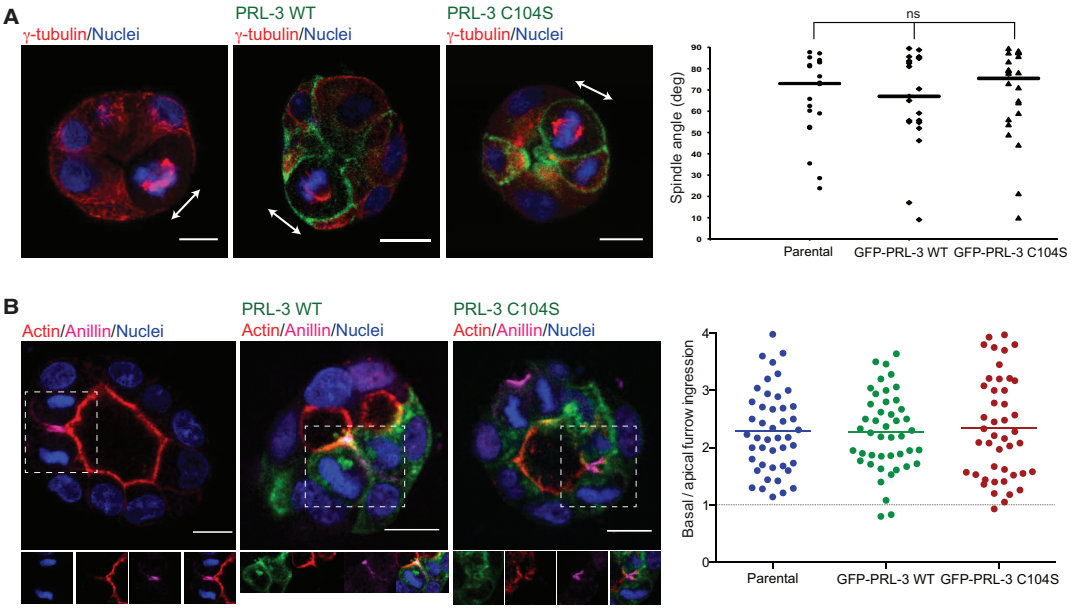

Figure 33. *PRL-3 overexpression leads to midbody lateral retention in MDCK cysts in a mitotic spindle and asymmetric cleavage furrow ingression-independent manner.* ***A*** *Confocal images of 72 hr parental (left), GFP-PRL-3 WT (middle), or GFP-PRL-3 C104S (right) overexpressing MDCK cysts stained with a γ-tubulin antibody. Arrows indicate the orientation of the mitotic spindles. Spindle angle was analyzed and plotted (graph). Deg=degree. n=15* ***B*** *Confocal images of 72 hr parental (left), GFP-PRL-3 WT (middle), or GFP-PRL-3 C104S (right) overexpressing MDCK cysts stained with an anillin (cleavage furrow) antibody. Bottom: separate channels of the highlighted cell in division showing nuclei or PRL-3 (left), actin (middle left), anillin (middle right), and merge (right). Asymmetry was measured as described in Methods section 5.3.5 and plotted (graph). Symmetric abscission=1. n=45. Scale bars, 10 μm.* ***A,B*** *Each result was plotted and the black lines represent the median (****A****) or mean (****B****) of three independent experiments. Adapted by permission from Company of Biologists LTD: JCS (Lujan et al.), copyright (2016).*

During cell division, PRL-3 WT and PRL-3 C104S were always (n=30) recruited to the cytokinetic bridge (Fig. 34A,B), suggesting that it might play a role during the last step of mitosis. Since an effect of PRL-3 in cytokinesis has never been addressed before, we decided to see if PRL-3 overexpression in MDCK cyst would affect it. Chromosome segregation prior to cell abscission is detected by AuroraB, which is then activated by phosphorylation. In turn, it phosphorylates MKLP1 blocking cleavage furrow regression (Steigemann *et al.*, 2009). The AuroraB inhibitor ZM447439 prevents MKLP1 phosphorylation leading to furrow regression and,

consequently, to cell tetraploidization (Ikezoe *et al.*, 2007; Steigemann *et al.*, 2009). Therefore, in order to study if PRL-3 might prevent MKLP1 phosphorylation abscission leading to tetraploid MDCK cells, ploidy was analyzed by flow cytometry quantification of incorporated Hoechst 33342 DNA staining. As anticipated, ZM447439-treated MDCK cells showed increased tetraploid cell population compared to the non-treated 2D MDCK cells (Fig. 34 C,D). However, tetraploidization when GFP-PRL-3 WT was overexpressed was comparable to non-treated parental and GFP-PRL-3 C104S MDCK cells (Fig. 34C-F). These results confirm that PRL-3 does not prevent cell abscission.

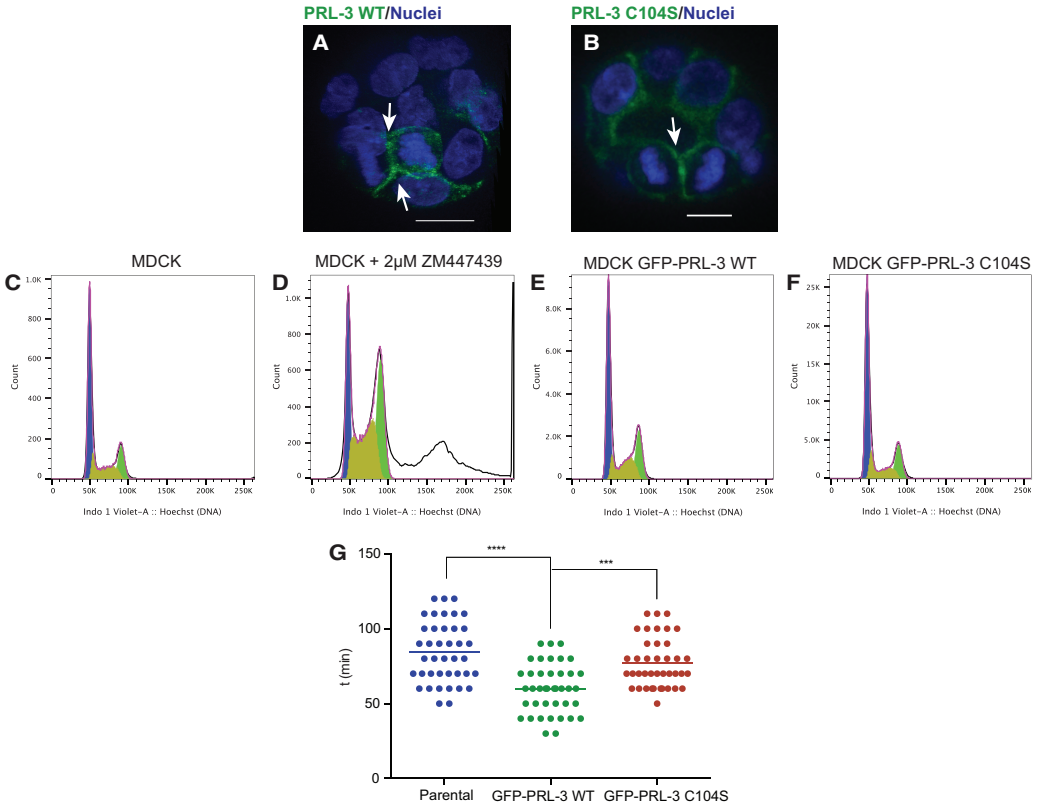

Figure 34. *PRL-3 accelerates cytokinetic timing.* ***A,B*** *Confocal images of 48 hr GFP-PRL-3 WT (left) or GFP-PRL-3 C104S (right) overexpressing MDCK cysts. Arrows indicate the position of the cytokinetic bridge.* ***C-F*** *Cell cycle analysis. MDCK cells (****C****), MDCK cells treated with 2 μM of ZM447439 (AuroraB inhibitor) over 48 hr (****D****), and MDCK cells stably expressing GFP-PRL-3 WT (****E****) or GFP-PRL-3 C104S (****F****) stained with Hoechst 3342 prior to analysis by flow cytometry. Blue: G0/G1; Ocher: S phase; Green: G2; White: tretraploid cell.* ***G*** *Abscission time is measured in parental, GFP-PRL-3 WT, or GFP-PRL-3 C104S overexpressing MDCK cells transfected with AuroraB to track cytokinesis over time. n=50. Each result was plotted and the black line represents the mean of three independent experiments. Adapted by permission from Company of Biologists LTD: JCS (Lujan et al.), copyright (2016).*

After eliminating the possibility of cytokinetic failure, we then examined the abscission time in 2D parental, GFP-PRL-3 WT, and GFP-PRL-3 C104S overexpressing MDCK cells, using AuroraB as a reporter to stain the cytokinetic bridge. Upon aberrant PRL-3 WT expression, MDCK cells showed faster abscission (Fig. 34G). This novel discovered phenotype of PRL-3 might unveil a new scenario where cell abscission takes place earlier than the apical positioning of the midbody which, in turn, would lead to the described multiple lumen phenotype in this epithelial cell model. Moreover, this discovery also narrows our focus for future studies to find PRL-3 substrates that would explain the molecular mechanism behind the proposed phenotype.

3.2. Discussion

Understanding how epithelial cells establish and maintain the axis of polarity is fundamental for our comprehension of how epithelial tissue organizes and how its deregulation may lead to tumor formation. During *de novo* lumenogenesis, apical lumen formation was proposed to be initiated by transport of apical components to the AMIS during cytokinesis, and that endosomes move along central spindle microtubules to fuse with the cleavage furrow plasma membrane around the midbody, which would finally generate an apical lumen (Dongying Li *et al.*, 2014). In the present study, I confirm this hypothesis by showing the dependence of the establishment of the lumen on the correct position of the midbody remnants and through my finding that the midbody is an apical landmark. In addition, I oberserved that the midbody is maintained in the following division at the edge of the lumen, proposing that it could be needed to keep the apical specification. It was previously shown that the resolution of the membrane connection between two daughter cells, during abscission, requires targeting and fusion of exocyst vesicles with the intracellular-bridge plasma membrane. Several subunits of the exocyst complex, including Sec8 as seen in our data, localized to the midbody during abscission (Gromley *et al.*, 2005) and were suggested to tether apical exocytic carriers to the AMIS (Bryant *et al.*, 2010). This selective co-localization of key tethering factors of the exocyst complex at the midbody during abscission could be the link between midbody remnants and apical membrane as well as AMIS specification.

PRL-3 does not appear to play a physiological role in lumen formation, but is found overexpressed in many epithelial cancers, and data points into the direction of PRL-3 being an oncogene (Rios *et al.*, 2013; Zimmerman *et al.*, 2013). Accordingly, we found that the overexpression of PRL-3 in a non-cancerous background (MDCK cysts) causes invasiveness and detrimental disorganization of epithelial structures, both fundamental events in tumor progression (McCaffrey and Macara, 2011). Unfortunately, the exact molecular mechanism could not be illuminated since PRL-3 substrates where not found in this context due to the failure in the determination of a direct substrate through the phosphoproteomic approach in 3D MDCK cell culture. Thus far, protein and non-protein substrates have been suggested, but none is established (Rios et al., 2013). Indeed, the identification of PRL-3 substrates has remained extremely challenging since its discovery over a decade ago (Al-Aidaroos and Zeng, 2010; Rios *et al.*, 2013). In the context of lumen formation, the suggested

PRL-3 substrates $PI(4,5)P_2$ and Ezrin are interesting candidates as they are known determinants of cellular polarity (Martin-Belmonte *et al.*, 2007). Nevertheless, we did not observe significant changes in the phosphorylation status of $PI(4,5)P_2$ and Ezrin when overexpressing PRL-3. Rapid changes of tightly controlled phosphorylation levels like in the cleavage furrow during abscission, may however be difficult to detect in this 3D system also because synchronization is not possible, and it will take the development of elaborate, sensitive methods to make progress in this area. Moreover, protein-protein interaction between PRL-3 and its partners like ancient conserved domain protein/cyclin M (CNNM) proteins should be taken into consideration.

Midbody positioning at the apical surface was postulated to be achieved through the combination of planar mitotic spindle orientation followed by asymmetric cleavage furrow ingression (Jaffe *et al.*, 2008; Morais-de-Sá and Sunkel, 2013; Bryant *et al.*, 2010) (Fig. 35). While mitotic spindle orientation has been extensively studied and polarity proteins like Par3 or Cdc42 have been described as key participants of the process (Fig. 35), loss of cytokinetic asymmetry in a spindle-independent manner still remains as a theoretical model (Fig. 35) (Jaffe *et al.*, 2008; Hao *et al.*, 2010; Dionne *et al.*, 2015). However, I show that PRL-3 leads to midbody mispositioning independently of a mitotic spindle-misorientation or asymmetric abscission. Indeed, I found that PRL-3 accelerates cytokinesis timing. This result lead us to suggest that prevention of the apical positioning of the midbody, and subsequent abscission in the lateral membrane, could be also triggered by faster cytokinesis (Fig. 35), as midbody positioning happens exactly during cytokinesis. Therefore, in the present study, for the first time, I provide evidence for a third model where cytokinesis timing plays the pivotal role in apical midbody positioning. However, since following the apical or lateral positioning of the midbody by life-cell imaging in the 3D cysts is technically challenging and the technologies available does not allows that yet, it cannot be discarded an alternative mechanism where, upon PRL-3 overexpression, the midbody reaches the apical membrane after cytokinesis and then it is pushed back to the lateral membrane by the action of PRL-3 although this is an unlikely scenario.

The molecular mechanisms underlying the abscission timing in epithelial cells, including a cytokinetic checkpoint, remains obscure due to its complexity (Green *et al.*, 2012; Carlton *et al.*, 2012; Steigemann *et al.*, 2009). One possible scenario relies on the regulation of the abscission checkpoint since cytokinesis timing seems to be dependent on checkpoint efficiency and it is a process governed by three kinases that must be counteracted in order to proceed. Therefore, PRL-3 could act downstream of

AuroraB causing a failure in abscission delay, like counteracting ULK3 or preventing Plk1 retention of Cep55 (Bastos and Barr, 2010; Carlton *et al.*, 2012; Caballe, Dawn M. Wenzel, *et al.*, 2015). However, although here I demonstrate that PRL-3 localizes to the site of cytokinesis, it is unclear if its involvement is direct or indirect.

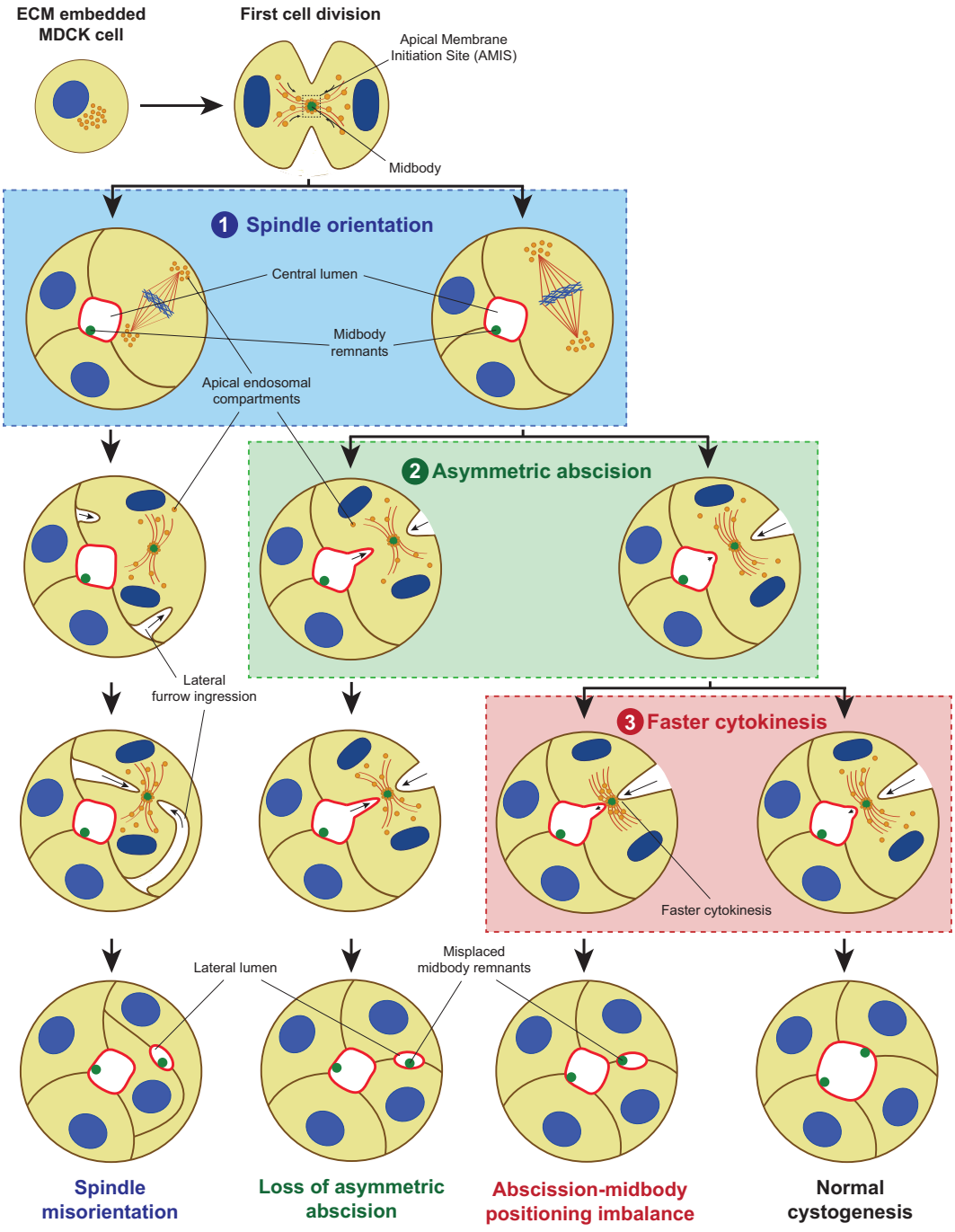

Figure 35. *Reviewed mechanisms for ectopic lumen formation through post-mitotic midbody mispositioning. After lumen opening, to ensure the single lumen maintenance the midbody is delivered to the apical membrane by a planar orientation of the mitotic spindle to the apical-basal axis (1) followed by asymmetric furrow ingression (2). Loss of mitotic spindle orientation or loss*

of asymmetric furrow ingression may affect the apical positioning of the midbody leading to ectopic lumen development. Furthermore, here we postulate a novel mechanism where faster abscission before the midbody reaches its luminal position (3) might also lead to lateral retention of the midbody, leading to the same multiple lumen phenotype. Apical membrane = light red; basolateral membrane = brown; γ-tubulin = dark red; nuclei and chromosomes = blue; midbody and midbody remnants = green; apical endosomal compartment = orange.

In conclusion, I propose a novel mechanism for the loss of epithelial organization in cancer involving cytokinesis timing that could cause the misplacement of midbody remnants as an alternative model to the already postulated ones: loss of spindle orientation and disruption of asymmetric abscission. Moreover, I identify PRL-3 as an enzyme that triggers epithelial architecture disruption through this alternative process.

4. The Role of PRL-3 in clathrin-dependent endocytosis

PRL-3 enhances clathrin-dependent endocytosis by PI(4,5)P_2 dephosphorylation

4.1. Results

Tumor metastasis is the second cause of death and responsible of nearly 90% of cancer-related deceases (Spano *et al.*, 2012) but is still poorly understood. Metastasis is a multi-step process where the migration and plasticity of the cancer cell is required. Cell migration is a complex cellular process where several molecular pathways are involved and interconnected (Polacheck *et al.*, 2013). Due to the complexity of this process and because of the absence of reliable substrate candidates (Rios *et al.*, 2013), deciphering how the cancer-promoting PRL-3 may affect tumor cell migration remains challenging. However, two recent theories that can be interconnected have gained attention in the field. One postulates that PRL-3-induced migration involves direct interaction with β1 integrin (Foy *et al.*, 2017; Krndija *et al.*, 2012; Peng *et al.*, 2006; Peng *et al.*, 2009), while Krndija *et al.* revealed that PRL-3 alters cell migration through enhanced recycling of matrix receptors. In the second scenario, Krndija and co-workers showed that PRL-3 enhances α5 integrins (heterodimer partner of β1 integrin) recycling from the Golgi apparatus to the plasma membrane activating the class I ADP-rybosylation factor (Arf1), a small GTPase associated with the Golgi apparatus that regulates vesicle trafficking (Krndija *et al.*, 2012; D'Souza-Schorey and Chavrier, 2006). Indeed, PRL-3 contains a MXXE Golgi-targeting motif (Honda *et al.*, 2005) required for its interaction with Arf-1, and its deletion is sufficient to disrupt the PRL-3 migration phenotype (Krndija *et al.*, 2012). Also, PRL-3 is mainly found in the plasma membrane as well as in the Golgi apparatus and in early and recycling endosomes (Qi Zeng *et al.*, 2000; Krndija *et al.*, 2012). Despite recycling rate increment, the overall surface α5 integrin concentration was unaffected upon PRL-3 overexpression (Krndija *et al.*, 2012), suggesting that α5 integrin uptake compensation might occur. Membrane trafficking pathways that take up or recycle integrins are essential for cell migration and any disturbance in integrin signaling or trafficking might contribute to cell invasion and migration during cancer metastasis (Paul *et al.*, 2015; Caswell *et al.*, 2008). In addition, turnover of PI(4,5)P_2 is required for clathrin-mediated endocytosis, and PRL-3 was previously reported to have phosphatase activity against PI(4,5)P_2 (McParland et al., 2011). For that reason, the aim of the

second part of the present project was to focus on the study of PRL-3 internalization and if PRL-3 actively participates in the endocytosis route where it is involved.

4.1.1. PRL-3 is taken up from the plasma membrane by clathrin-dependent endocytosis

PRL-3's presence in early endosomes (EE) suggests that it must be internalized through a membrane-bound endocytic pathway (Jovic *et al.*, 2010) making the involvement of other membrane free routes unlikely, like through guanosine nucleotide dissociation factor (GDI)-like solubilizing factors (Chandra *et al.*, 2012; DerMardirossian and Bokoch, 2005) or by lipid hydrolysis (Martin *et al.*, 2011; Lin and Conibear, 2015). Before being trafficked to the EE, a portion of the plasma membrane is pinched off as an endosome (Mayor and Pagano, 2007). In the last years, several mechanisms to form those mentioned endosomes have been described (Mayor and Pagano, 2007; McMahon and Boucrot, 2011) and each cargo is exclusively selected by one or few of those pathways to be internalized (Traub, 2009). For example, the transferrin receptor is an archetypical cargo for CDE (Le Roy and Wrana, 2005), whereas the uptake of α5 integrin from focal adhesions (FAs), while canonically associated with CDE (Chao and Kunz, 2009), has been recently linked also to macropinocytosis and syndecan-4 mediated caveolar endocytosis (Paul *et al.*, 2015). Both examples were used as reporters in the study of Krndija *et al.* on recycling enhancement by PRL-3. The experiments were realized on Henrietta Lacks (HeLa) cells, where levels of caveolin (cav-1) are very low (Skretting *et al.*, 1999). Therefore, proteins that can choose between clathrin and calveolar endocytosis prefer CDE if there is low expression of cav-1 (Singh *et al.*, 2003). That limits α5 integrin to CDE or macropinocytosis but, since this second route is dependent on platelet-derived growth factor (PDGF) activation (Paul *et al.*, 2015), it might rather be exclusively endocytosed by CDE in untreated HeLa cells. Then, it is likely that, if PRL-3 participates in both transferrin and α5 integrin recycling routes, the phosphatase might be internalized through the same common endocytic pathway, CDE. Therefore, confirming this hypothesis became the first step in our approach.

In order to determine how PRL-3 is taken up from the plasma membrane, its internalization in HeLa cells transiently overexpressing GFP-PRL-3 WT was followed by confocal microscopy upon treatment with different endocytosis pathway selective

inhibitors. Unfortunately, there is no CDE inhibitor that could guarantee the exclusive inhibition of this pathway without altering others (Dutta and Donaldson, 2012; Harper *et al.*, 2013). For that reason, inhibitors of other pathways were used to discard alternative candidate routes. In order to discern if PRL-3 internalization was sensitive to the applied inhibitors, PRL-3 translocation to the cytosol was forced since, in normal conditions, PRL-3 is predominantly in the plasma membrane and an increment of the phosphatase in this region would be hard to measure. For this purpose, GFP-PRL-3 WT overexpressing HeLa cells were also treated with brefeldin A (BFA), an Arf protein inhibitor (Helms and Rothman, 1992) that leads to reversible disassembly of the Golgi apparatus preventing protein export from the Golgi to the cell surface (Krndija *et al.*, 2012; Helms and Rothman, 1992; SG *et al.*, 1992). Therefore, if the PRL-3 endocytosis pathway is not sensitive to the inhibitor used, it will accumulate in the cytosol upon BFA treatment since it can still get internalized but not recycled back to the plasma membrane. However, if the inhibitor is affecting PRL-3 uptake, the phosphatase will be retained in the cell surface since it cannot be endocytosed.

Initially, HeLa GFP-PRL-3 WT cells were treated with 100 µM dynasore, a selective dynamin1, dynamin2 and mitochondrial dynamin-1-like protein (Dnp1) GTPase activity inhibitor (Macia *et al.*, 2006). Among endocytic pathways, only CDE and caveolar internalization require dynamin for the endosome fission step, so these are the only ones sensitive to dynasore treatment. Confocal pictures every 30 min were acquired during 90 min of dynasore pre-treated HeLa GFP-PRL-3 WT cells after being treated with 20 µM BFA. PRL-3 internalization was measured by quantifying the GFP fluorescent intensity ratio between the plasma membrane and the cytosol (Fig. 36A-E). As expected, PRL-3 was accumulated in the cytosol when cells were treated only with BFA, while in DMSO or dynasore treated cells, the phosphatase remained in the cell surface (Fig. 36A-C,E). However, when HeLa GFP-PRL-3WT cells were treated with both BFA and dynasore, PRL-3 still remained in the plasma membrane (Fig. 36D,E), demonstrating that PRL-3 internalization is sensitive to dynamin inhibition and suggesting that it may be internalized either by CDE or caveolar endocytosis.

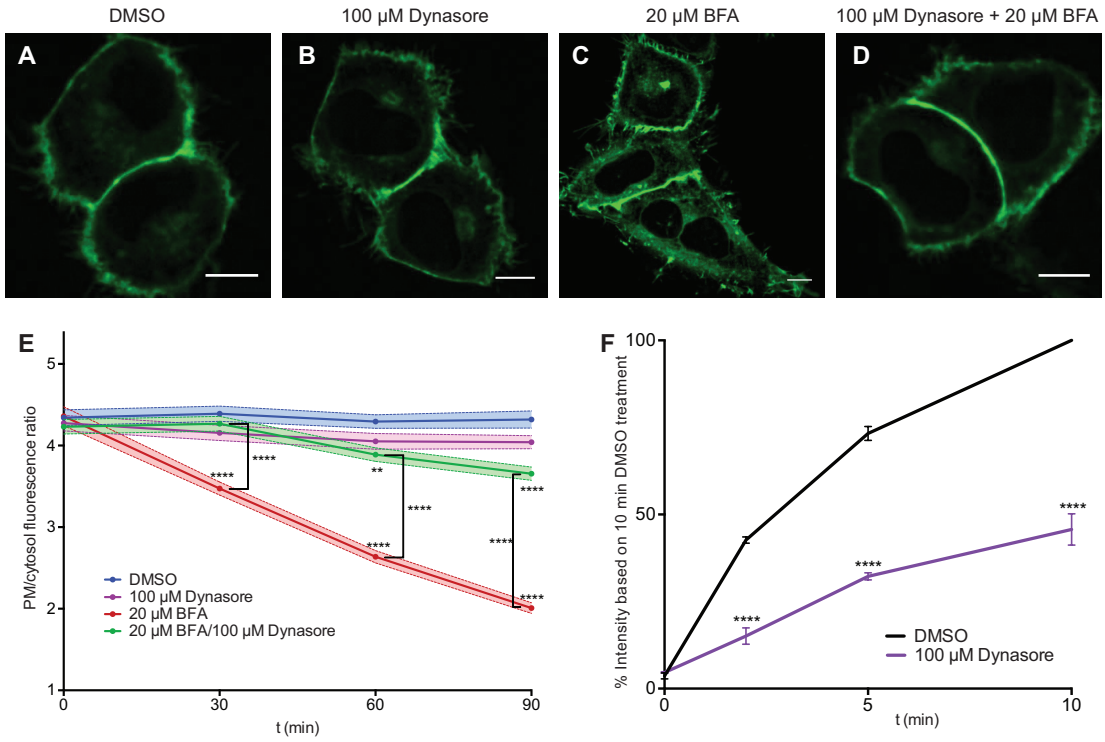

Figure 36. *PRL-3 is internalized in a dynamin-dependent manner in HeLa cells.* ***A-D*** *Confocal images of life HeLa cells transiently expressing GFP-PRL-3 WT after 90 min treatment with DMSO (**A**), 100 µM dynasore (**B**), 20 µM BFA (**C**) or 100 µM dynasore + 20 µM BFA (**D**). Scale bar = 10 µm.* ***E*** *Fluorescence intensity ratio of GFP signal between plasma membrane (PM) and cytosol in GFP-PRL-3 WT HeLa cells treated as in* ***A-D*** *measured by confocal microscopy every 30 min during 90 min after treatment. n = 90 cells. Mean ± SEM of three independent experiments.* ***F*** *Alexa Fluor® 633 transferrin incorporation by HeLa cells treated with dimethyl sulfoxide (DMSO) or 100 µM dynasore measured by flow cytometry at different time points. n = 60.000 cells. Median ± SEM of three independent experiments.*

When cells were treated with both inhibitors, there was a mild internalization after 60 min suggesting that either PRL-3 can be internalized through another dynamin-independent pathway in a lesser extend or that the dynasore inhibition was not 100% efficient. In order to elucidate which scenario was taking place and also to confirm that dynasore was inhibiting dynamin at that dose and treatment time frame, CDE inhibition was measured performing a transferrin uptake assay by flow cytometry. HeLa cells were treated for 1 hour with DMSO or 100 µM dynasore and then incubated at 37 °C with Alexa Fluor® 633 nm tagged transferrin to let it get endocytosed through CDE. Internalization was stopped by cooling the cells, and the remaining tagged transferrin associated with the plasma membrane was removed with an acidic buffer. Endocytosed transferrin was measured by flow cytometry and the median fluorescent intensity was represented in Fig. 36F. The result shows that 1

hour treatment with 100 µM dynasore led to approximately 60% inhibition of CDE in HeLa cells suggesting that the mild internalization observed when HeLa GFP-PRL-3WT cells were treated with both, BFA and dynasore, was due to residual dynamin activity.

To discern if PRL-3 was internalized by CDE or by caveolar endocytosis, HeLa cells transiently overexpressing GFP-PRL-3 WT were treated with 25 µg/mL nystatin, an antifungal antibiotic that sequesters cholesterol, which is a lipid required in the plasma membrane for caveolae clustering. Thus, nystatin treatment inhibits caveolar endocytosis (Singh *et al.*, 2003; Rothberg *et al.*, 1990; Rothberg *et al.*, 1992; Bolard, 1986). Before testing its effect on PRL-3 internalization, caveolar endocytosis inhibition efficiency was tested measuring the lactosylceramide (LacCer), a sphingolipid exclusively internalized by caveolar endocytosis (Singh *et al.*, 2003), uptake rate by flow cytometry. Similar to the transferrin uptake assay, BODIPY® FL C_5 tagged LacCer was incubated at 37 °C with HeLa cells pre-treated for 1 hour with DMSO or 25 µg/mL nystatin. Internalization was also stopped by cooling down the sample, and the remaining LacCer bound to the cell surface was cleared out with 5% defatted bovine serum albumin (DF-BSA) containing media. Internalized tagged LacCer was quantified by flow cytometry, showing that 1 hour treatment with 25 µg/mL nystatin inhibited more than 60% of calveolar endocytosis in HeLa cells (Fig. 37A). Although the inhibitory efficiency does not reach 100%, it should be sufficient to detect an effect in PRL-3 internalization, as was estimated when treated with dynasore (Fig. 36F). A higher concentration of nystatin might be toxic for HeLa cells and unpredictable side effects could interfere in the experimental read out.

Then, as done upon dynasore treatment (Fig. 36A-E), HeLa GFP-PRL-3 WT cells were pre-treated for 1 hour with 25 µg/mL nystatin and PRL-3 internalization was followed by confocal microscopy during 90 min after BFA treatment. As expected, PRL-3 remained in the plasma membrane in HeLa cells treated with DMSO or only nystatin (Fig. 37B,C,F), while recycling inhibition by BFA forced PRL-3 translocation to the cytosol (Fig. 37D,F). When cells were treated with both, BFA and nystatin, PRL-3 was then internalized like with BFA only treatment (Fig. 37E,F) demonstrating that PRL-3 endocytosis is not sensitive to cholesterol arresting by nystatin.

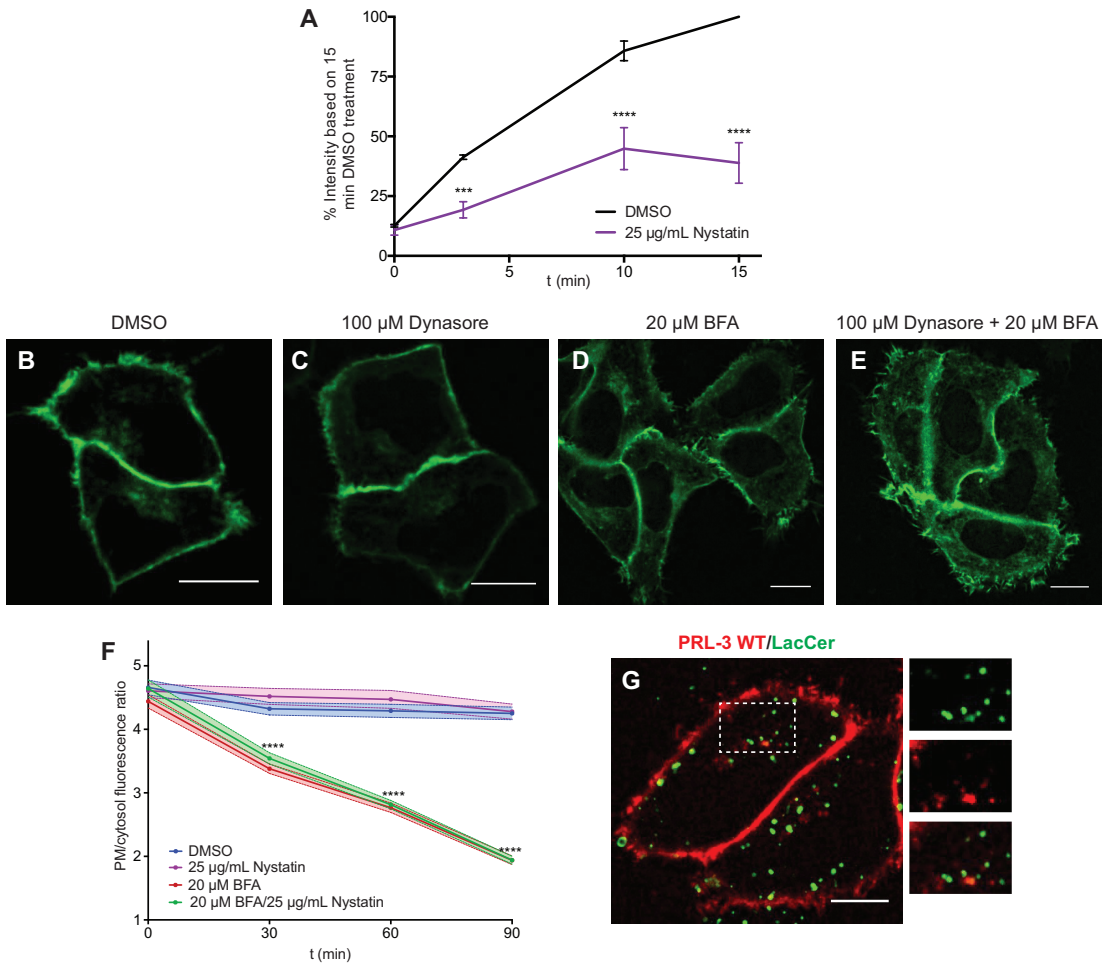

Figure 37. *PRL-3 is internalized through clathrin-dependent endocytosis in HeLa cells.* ***A*** *BODIPY® FL C_5 LacCer incorporation by HeLa cells treated with DMSO or 25 µg/mL nystatin measured by flow cytometry at different time points. n = 60.000 cells. Median ± SEM of three independent experiments.* ***B-E*** *Confocal images of life HeLa cells transiently expressing GFP-PRL-3 WT after 90 min treatment with DMSO (**B**), 25 µg/mL nystatin (**C**), 20 µM BFA (**D**) or 25 µg/mL nystatin + 20 µM BFA (**E**). Scale bar = 10 µm.* ***F*** *Fluorescence intensity ratio of GFP signal between plasma membrane (PM) and cytosol in GFP-PRL-3 WT HeLa cells treated as in **B-E** measured by confocal microscopy every 30 min during 90 min after treatment. n = 90 cells. Mean ± SEM of three independent experiments.* ***G*** *Confocal image of a pmKATE2-PRL-3 WT HeLa cell with BODIPY® FL C_5 LacCer incorporated for 15 min. Right: higher magnification of selected region showing separated channels: LacCer (up), PRL-3 WT (middle) and merge (down). Scale bar = 10 µm.*

This result implies that PRL-3 must be internalized by CDE, but to further corroborate the obtained result I performed a co-localization assay between pmKATE2-PRL-3 WT and BODIPY® FL C_5-LacCer in fixed HeLa cells. From 64 cells analyzed, 32±10% of LacCer-containing endosomes were positive for PRL-3 while 44±8% of PRL-3-containing endosomes were positive for LacCer (Fig. 37G). This low percentage agrees with the conclusion that PRL-3 might not be internalized

through calveolar endocytosis. Regardless the mode of entry, internalized cargoes are usually delivered to the early endosome where different routes of internalization converge (Grant and Donaldson, 2009). This fact can explain that, even if PRL-3 and LacCer are not internalized through the same pathway, they still co-localize in one third of the analyzed endosomes, which might correspond to endosomes formed downstream. The settings of this assay do not distinguish between different kinds of endosomes within the cell.

Finally, to further confirm that PRL-3 is internalized through CDE, a similar co-localization assay was realized with Alexa Fluor® 633 nm transferrin, a canonical CDE cargo (Le Roy and Wrana, 2005). From 67 cells quantified, 86±6% of transferrin-containing endosomes were positive for PRL-3 while 74±7% of PRL-3-containing endosomes were positive for transferrin (Fig. 38). The lower co-localization percentage of transferrin positive PRL-3-containing endosomes may be due to that, at the moment of transferrin incorporation, some PRL-3 was already taken up or being recycled and those endosomes remained unstained with transferrin.

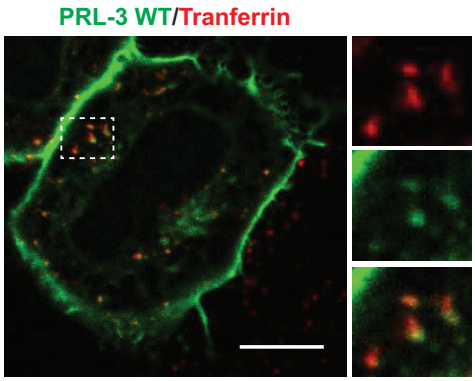

Figure 38. *PRL-3 is internalized through CDE in HeLa cells. Confocal image of a GFP-PRL-3 WT HeLa cell with Alexa Fluor® 633 transferrin incorporated for 15 min. Right: higher magnification of selected region showing separated channels: Transferrin (up), PRL-3 WT (middle) and merge (down). Scale bar = 10 µm.*

The use of selective endocytosis inhibitors together with co-localization assays in HeLa cells demonstrate that PRL-3 gets internalized through CDE in this cell system, a cellular process where regulated dephosphorylation of proteins and lipids is required for the proper endosome formation.

4.1.2. PRL-3 enhances CDE by the stabilization of productive clathrin coated pits (CCPs)

Cell migration speed is dictated by the flux of integrins through the endocytic pathway rather than by their levels on the cell surface. Therefore, CDE of integrins in

FAs (mainly α5β1 integrin) regulates the ability of cancer cells to migrate and invade (Paul *et al.*, 2015; Polo *et al.*, 2004). Indeed, several modulators of CDE have been related with integrin internalization and adhesion disassembly, and therefore, with cell migration (Paul *et al.*, 2015). For example, clathrin adaptor disabled homolog (Dab2) deletion inhibits cell migration (Paul *et al.*, 2015; Teckchandani *et al.*, 2009), Arf6 GTPase activating protein (GAP) and ankyrin repeat and PH domain (ARAP2) are required for α5β1 integrin internalization (Paul *et al.*, 2015; Pei Wen Chen *et al.*, 2013; Campa and Randazzo, 2008), and the Arf5/Arf6 guanine nucleotide exchange factor (GEF) brefeldin A-resistant Arf (BRAG2) binds to clathrin and adaptor protein (AP2) and activates Arf5 to promote internalization of integrins in cancer cells (Paul *et al.*, 2015; Sakurai *et al.*, 2011; Moravec *et al.*, 2012). Therefore, since PRL-3 is internalized through CDE and its overexpression is related with oncogenically enhanced cell migration and invasion, we analyzed the effect of PRL-3 on CDE.

As a first approach, CDE rate variation in HeLa cells upon PRL-3 overexpression was investigated measuring the transferrin internalization rate since it is incorporated exclusively by CDE (Le Roy and Wrana, 2005). As displayed before, in order to study the dynasore inhibitory effect, the CDE rate was measured at different incubation times of HeLa cells with Alexa Fluor® 633 transferrin at 37 °C. Transferrin incorporation was stopped at 4°C and the remaining transferrin bound to the cell surface was removed by acidic rinsing. Then, internalized transferrin was quantified by flow cytometry. In order to include an internal parental control, HeLa cells were transiently transfected with GFP-PRL-3 WT to obtain a mixed population of parental (GFP negative) and GFP-PRL-3 WT overexpressing (GFP positive) HeLa cells easy to sort and analyze independently by flow cytometry.

As hypothesized, PRL-3 WT overexpression enhanced transferrin uptake, which corresponds to an increment of the CDE rate (Fig. 39). To elucidate if this observed phenotype depends on the phosphatase activity of PRL-3, the catalytic inactive mutant of the phosphatase (GFP-PRL-3 C104S) was transiently overexpressed in HeLa cells. PRL-3 C104S did not affect the CDE rate (Fig. 39) suggesting that CDE enhancement was due to the phosphatase activity of PRL-3. This result was confirmed in HeLa cells transiently transfected with GFP-PRL-3 WT pre-treated during 1 hour with the PRL inhibitor analog 3 (Hoeger *et al.*, 2014), which rescued the phenotype. On the other hand, an increase of the intrinsic phosphatase activity of PRL-3 by a mutation close to the active site (GFP-PRL-3 E50R) led to a decrease of the CDE rate (Fig. 39), suggesting that the observed

phenotype depends on the particular low activity of PRL-3.

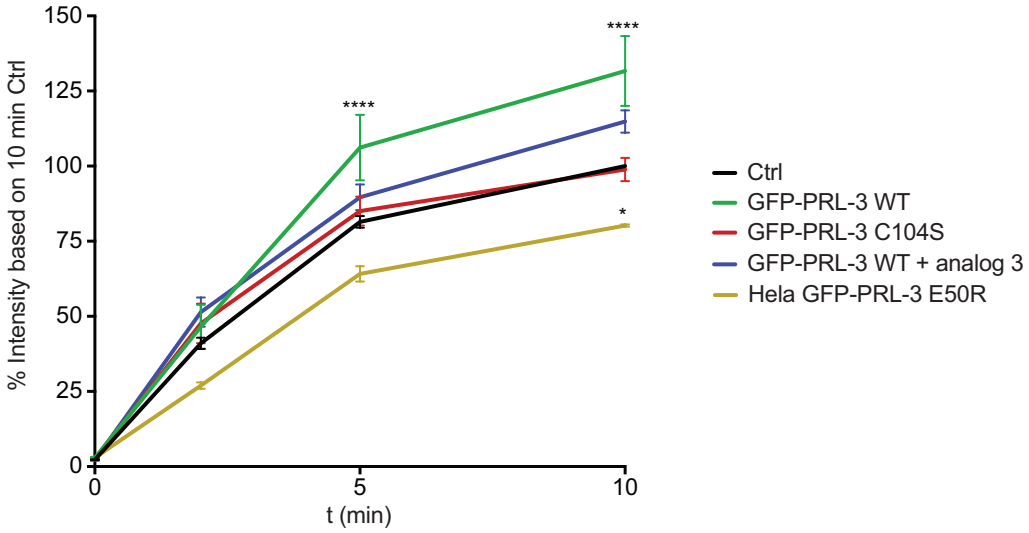

Figure 39. *PRL-3 enhances CDE in HeLa cells. Alexa Fluor® 633 transferrin incorporation by HeLa cells (Ctrl) (black) and HeLa cells transiently overexpressing GFP-PRL-3 WT untreated (green) or treated with 50 µM analog 3 (blue), GFP-PRL-3 C104S (red) or GFP-PRL-3 E50R (ocher) measured by flow cytometry at different time points. n = 30.000 cells. Median ± SEM of three independent experiments.*

To further corroborate that the increment of the CDE rate observed upon PRL-3 WT overexpression is not due to a side effect of protein aberrant overexpression, these results were confirmed by knocking down PRL-3. However, as in many other cell lines, endogenous PRL-3 protein level in HeLa cells is undetectable (Nagaraj *et al.*, 2011). Therefore, the experiment was performed in cells where PRL-3 endogenous expression was already reported: the colorectal carcinoma HCT116 (Xing *et al.*, 2016) and the breast cancer MCF-7 (Geiger *et al.*, 2012; Wang *et al.*, 2010) cell lines. PRL-3 was knocked down in HCT116 by siRNA transient transfection (Fig. 16A) 48 hours prior to the transferrin uptake assay. After the experiment was performed, remaining cell sample was used to confirm by RT-PCR that PRL-3 was efficiently silenced (Fig. 40A). Fig. 40B confirms that PRL-3 enhanced CDE since its deletion led to a decrease of transferrin uptake as a reporter of CDE rate decay. These results were also corroborated in MCF-7 cells. However, transient PRL-3 knockdown efficiency was too low (data not shown) to perform a transferrin uptake assay since it cannot discriminate between transfected and untransfected cells. Therefore, an IPTG inducible PRL-3 shRNA MCF-7 cell line was used (Figs 18C, 40C) for homogeneous PRL-3 silencing. Moreover, an IPTG inducible Ctrl shRNA MCF-7 was used to discard off-target or IPTG disturbance in the assay. shRNA expression was induced during 4 days before carrying out the

transferrin uptake assay to ensure PRL-3 protein deletion. As expected, PRL-3 silencing led also to decreased CDE rate in MCF-7 cells (Fig. 40D,E). These results not only confirm that PRL-3 phosphatase activity intervenes in CDE, but also shows that the phenotype described in HeLa cells is not cell type specific.

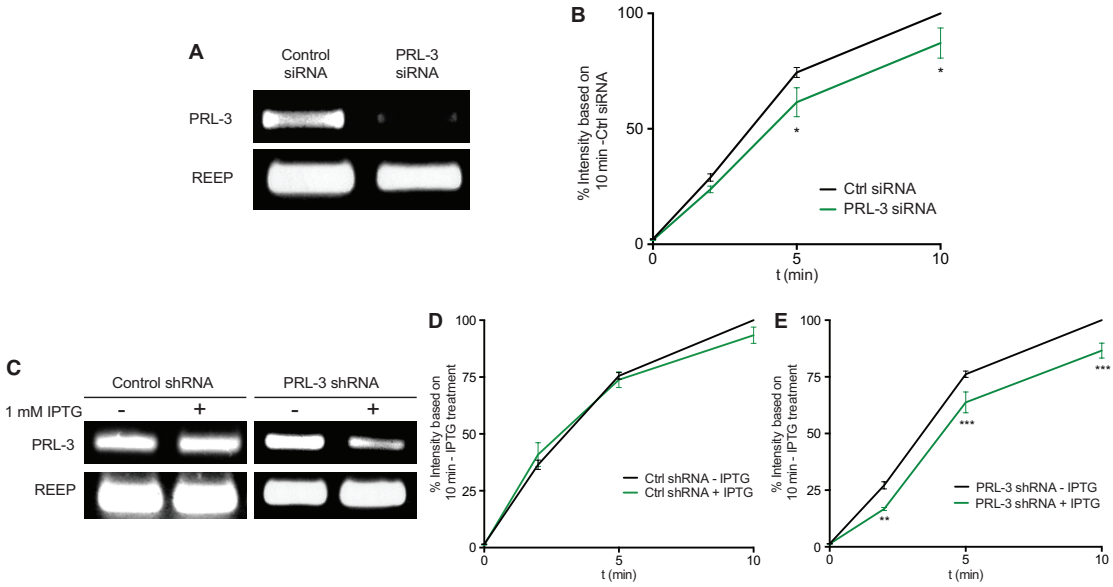

Figure 40. *Endogenous PRL-3 enhances CDE in HCT116 and MCF-7 cells.* ***A*** *PRL-3 mRNA content in HCT116 cells transiently transfected with Ctrl or PRL-3 siRNA was measured by one-step RT-PCR using REEP mRNA as loading control.* ***B*** *Alexa Fluor® 633 transferrin incorporation in HCT116 cells transiently transfected with Ctrl or PRL-3 siRNA measured by flow cytometry at different time points.* ***C*** *Uninduced or induced PRL-3 knockdown with 1 mM IPTG in control or PRL-3 shRNA MCF-7 cells during 4 days. PRL-3 mRNA was assayed by one-step RT-PCR using REEP as a control.* ***D,E*** *Alexa Fluor® 633 transferrin incorporation in IPTG uninduced or induced control (****D****) or PRL-3 (****E****) shRNA MCF-7 measured by flow cytometry at different time points.* ***B,D,E*** *n = 60.000 cells. Median ± SEM of three independent experiments.*

After describing that PRL-3 alters CDE, we investigated the origin of this phenotype. In order to form a clathrin-coated vesicle, the fist step is the recruitment of clathrin and adaptor proteins to the plasma membrane in a process named nucleation. This clathrin-coated pit (CCP) formed in the inner leaflet of the plasma membrane goes through a process of maturation where different proteins and lipids play a role in a hierarchical and tightly regulated manner. Finally, the vesicle is cleaved from the cell surface through dynamin-dependent fission (explained in detail in the *Introduction*) (Loerke *et al.*, 2009; Doherty and McMahon, 2009; Loerke *et al.*, 2011; Kirchhausen *et al.*, 2014). However, CCP maturation is gated by an endocytic checkpoint and the progression through this point is dependent on the CCP stability

given by concentration of cargo receptors, dynamin, AP2 adaptors, and probably also by other still unknown factors that CCPs must sequentially recruit along maturation to prevent coat disassembly. This quality control leads to the abortion of half of the nascent CCPs (Loerke *et al.*, 2009; Antonescu *et al.*, 2011).

Therefore, an increment of CCP density on the plasma membrane, a faster maturation of the pit or a higher percentage of productive CCPs would lead to a faster CDE. All these parameters can be quantified by total internal reflection fluorescence (TIRF) microscopy of fluorescently tagged clathrin overexpressing cells. Using this technique, we can visualize only the cell plasma membrane in contact with the glass surface where they are cultured on (Fish, 2009; Mattheyses *et al.*, 2010). Then, clathrin nucleation and disassembly or vesicle fission can be monitored (Antonescu *et al.*, 2011) in presence or absence of PRL-3 WT in order to understand the effect of PRL-3 overexpression on CCP dynamics. With that purpose, I transiently transfected mEmerald-clathrin light chain B (CLTB) together with pmKATE2-CaaX or pmKATE2-PRL-3 (WT, C104S or E50R) in HeLa cells. The first striking fact shown by TIRF is that PRL-3 is not enriched in the CCP (Fig. 41A), which is a more characteristic feature known for CCP related kinases than from phosphatases.

Regarding CCPs analysis, overexpression of pmKATE2-PRL-3 WT, but not PRL-3 C104S or PRL-3 E50R, resulted in an increase of the proportion of productive CCPs compared to the pmKATE2-CaaX control cell line (Fig. 41B), consistent with the phenotype observed in the CDE rate. This effect was also attenuated when cells were treated with PRL inhibitor, analog 3 (Fig. 41B). These results suggest that PRL-3 might contribute to achieving CCP stability, increasing the chances of passing through the endocytic checkpoint. Upon PRL-3 WT overexpression, lifetime of both, abortive and progressive CCPs, are slightly increased (Fig. 41C,D) indicating that the phosphatase might also be interfering with the assembly and maturation of the CCP. Inhibition of PRL-3 WT with analog 3 abolishes its effect on the abortive CCP lifetime but not on the productive, while the catalytically inactive mutant shows a phenotype that is similar to the one of the pmKATE2-CaaX control cell line (Fig. 41C,D), confirming that the effect depends on PRL-3 activity. Here, PRL-3 E50R also increased the productive CCPs lifetime (Fig. 41D) while it did not affect the number of CPPs (Fig. 41B), suggesting that PRL-3's effect on CCP maturation does not dependent on its phosphatase strength, and that the small increase in lifetime does not have an impact on the increase in the

number of productive CCPs. Finally, CCP initiation density was also analyzed. Overexpression of PRL-3 WT did not modify CCP initiation density, indicating that the phosphatase is not affecting CCP nucleation (Fig. 41E). However, when its phosphatase activity was increased (PRL-3 E50R), the amount of nucleated CCPs dramatically decreased (Fig. 41E). This is consistent with the effect exhibited on CDE rate and suggests a link to its increased phosphatase activity, which decreases the amount of PI(4,5)P_2 to a level that is below the one required for efficient nucleation.

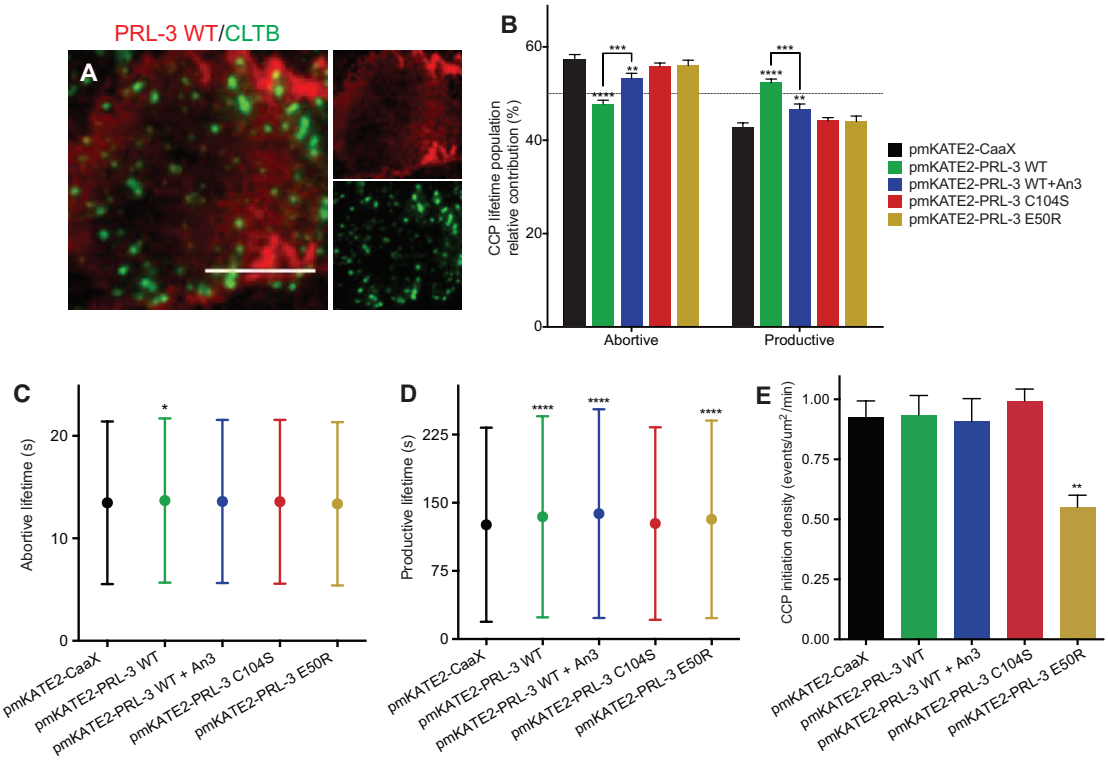

Figure 41. *PRL-3 stabilizes CCP in HeLa cells.* ***A*** *TIRF microscopy picture showing the plasma membrane of a HeLa cell overexpressing pmKATE2-PRL-3 WT (red) and mEmerald-CLTB (green). Right: separated channels of PRL-3 WT (up) and CLTB (down). Scale bar = 10 µm.* ***B-E*** *Graph representation of percentage of CCPs with a lifetime of less (abortive) or more (productive) than 30s (**B**), average lifetime of abortive (**C**) or productive (**D**) CCPs; and CCP events initiation density (**E**) in HeLa cells transiently overexpressing pmKATE2-CaaX (69 cells, 75017 endosomes) (black), pmKATE2-PRL-3 WT untreated (70 cells, 37827 endosomes) (green) or treated with 50 µM analog 3 (61 cells, 51282 endosomes) (blue), pmKATE2-PRL-3 C104S (96 cells, 82399 endosomes) (red) or pmKATE2-PRL-3 E50R (86 cells, 42968 endosomes) (ocher). Dashed line in **B** represent 50%. Mean ± SEM (**B,E**) or standard deviation (**C,D**) of three independent experiments.*

These results were corroborated by PRL-3 knockdown in HCT116 and in inducible PRL-3 shRNA MCF-7 cells by siRNA transient transfection or IPTG induction, respectively (FIG. 42A,B) to confirm that the effect observed was not due

to an overexpression artifact. As expected, knockdown of PRL-3 in both, HCT116 and MCF-7 cells, resulted in the decrease in the proportion of the productive CCPs (Fig. 42C,D) and also the decreased lifetime of abortive and productive CCPs (Fig. 42E-H), confirming its positive effect in CCP stabilization and its slightly negative influence in CCP assembly and maturation. In MCF-7 cells, IPTG treatment to induce control shRNA expression also slightly affected abortive CCP lifetime (Fig. 42G) probably as a side effect of the compound treatment. Also uninduced PRL-3 shRNA MCF-7 presented increased productive lifetime compared to uninduced PRL-3 shRNA MCF-7 (Fig. 42H) probably also as a side effect of the different shRNA genome integration that led to two different cell lines with different characteristics. Knockdown of PRL-3 did not alter CCP initiation density in HCT116 (Fig. 42I) but it did in MCF-7 (Fig. 42J), where a decrease of the density of events was observed upon PRL-3 knockdown. This diverting result suggests that PRL-3 might affect CCP nucleation in some cell lines, possibly depending on the present amount of $PI(4,5)P_2$ in the cells.

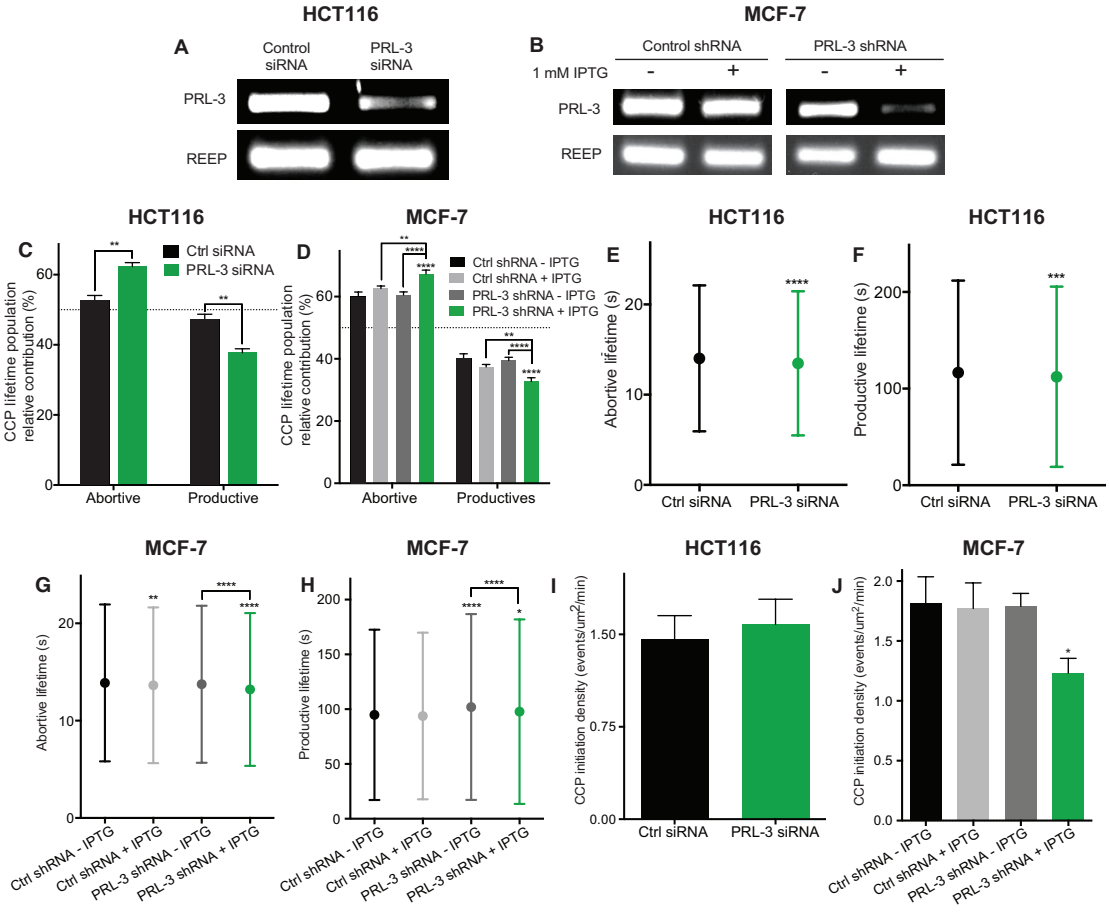

Figure 42. *PRL-3 stabilizes CCP in HCT116 and MCF-7 cells.* ***A*** *PRL-3 mRNA content in HCT116 cells transiently transfected with Ctrl or PRL-3 siRNA was measured by one-step*

RT-PCR using REEP mRNA as loading control. ***B*** *Uninduced or induced PRL-3 knockdown with 1 mM IPTG in control or PRL-3 shRNA MCF-7 cells during 4 days. PRL-3 mRNA was assayed by one-step RT-PCR using REEP as a control.* ***C-J*** *Graph representation of percentage of CCPs with a lifetime of less (abortive) or more (productive) than 30s (**C,D**), average lifetime of abortive (**E,G**) or productive (**F,H**) CCPs and CCP events initiation density (**I,J**) in HCT116 cells (**C,E,F,I**) transiently transfected with ctrl siRNA (73 cells, 19396 endosomes) (black) or PRL-3 siRNA (80 cells, 28823 endosomes) (green) or in IPTG uninduced or induced control shRNA (uninduced: 49 cells, 49244 endosomes; induced: 45 cells, 47876 endosomes) or PRL-3 shRNA (uninduced: 45 cells, 56786 endosomes; induced: 47 cells, 33249 endosomes) MCF-7 cells (**D,G,H,J**). Dashed line in **C,D** represent 50%. Mean ± SEM (**C,D,I,J**) or standard deviation (**E-H**) of three independent experiments.*

Taken together, CCP dynamics analysis upon presence or absence of PRL-3 confirms that the phosphatase actively participates in this process, stabilizing the CCP formation and slightly extending pit assembly and maturation. However, its action to increase the formation of productive CCPs seems to override its negative effect on pit assembly and maturation, since the overall outcome is an increase in the CDE rate.

4.1.3. PRL-3 dephosphorylates PI(4,5)P_2 *in vivo*

From the stages of clathrin nucleation until vesicle scission and uncoating, CDE is tightly regulated by protein and lipid kinases and phosphatases (McPherson *et al.*, 2013). For example, presence of lipid PI(4,5)P_2 in the bulk plasma membrane is essential for CCP initiation to recruit several PI(4,5)P_2-binding domain-containing adaptor proteins, like AP2 (Höning *et al.*, 2005), which are required for clathrin nucleation in the cell surface. Then, its turnover by 5'-dephosphorylation occurs within the CCP for its maturation and vesicle formation (detailed explained in the *Introduction*) (Antonescu *et al.*, 2011). Indeed, knockout of PI(4,5)P_2 kinases and phosphatases like phosphatidylinositol phosphate 5'-kinase (PIP5Kγ), the major PIP5K isoform in neurons, or synaptojanin (Snj1) in neuronal cells inhibit clathrin-mediated recycling of synaptic vesicles (Wenk *et al.*, 2001; Cremona *et al.*, 1999; Harris *et al.*, 2000). Recently, it has been demonstrated that PRL-3 is able to dephosphorylate PI(4,5)P_2 (McParland *et al.*, 2011) *in vitro*. This finding suggests that the phosphatase might be altering CDE through PI(4,5)P_2 level modulation within the CCP.

In order to address this hypothesis, I set out to corroborate the *in vitro* PI(4,5)P_2 phosphatase activity of PRL-3. However, the techniques available to determine lipid

dephosphorylation in cells are not as selective and sensitive than for protein phosphorylation detection (Fahs *et al.*, 2016). Moreover, $PI(4,5)P_2$ homeostasis in the cell surface is tightly regulated by several kinases and phosphatase and it is subject to a rapid continuous turnover (Czech, 2000). For that reason, detection of *in vivo* $PI(4,5)P_2$ dephosphorylation by a weak phosphatase like PRL-3 is a challenging task. In fact, several unsuccessful attempts have been carried out before setting up a reliable technique sensitive enough to detect it. Previously in Dr. Köhn's laboratory, thin layer chromatography (TLC) was realized extracting phosphatidylinositol phosphates (PIPs) ^{32}P labeled from parental and PRL-3 (WT and C104S) stably overexpressing Hek293 cells but no difference in $PI(4,5)P_2$ level was detected (data not shown).

Then, total PIP_2 level from cell extract was measured by quantitative MS lipidomics, which is more sensitive and quantitative than TLC. The experiment was performed in collaboration with Dr. Britta Brügger's laboratory (Heidelberg University Biochemistry Center – BZH, Heidelberg, Germany). In previous collaborations between the laboratories of Dr. Köhn and Dr. Brügger they tried to corroborate the *in vitro* $PI(4,5)P_2$ dephosphorylation in PRL-3 stably overexpressing Hek293 cells. However, the PIP_2 level was not significantly different between Flag-PRL-3 WT Hek293 and parental or Flag-PRL-3 C104S overexpressing Hek293 cells (data not shown). Therefore, I tried to repeat the set experiment in HeLa cells, where the CDE-related phenotype was observed. Acidic/neutral lipid extraction was realized in parental HeLa cells and HeLa cells transiently transfected with GFP-PRL-3 WT, GFP-PRL-3 C104S (catalytic inactive mutant), GFP-PRL-3 E50R (hyperactive mutant), GFP-PRL-1 WT (no PIP phosphatase activity) or type IV 5'-phosphatase (5-ptase) (positive control (Varnai *et al.*, 2006)) prior to MS measurement. Unfortunately, the results of this experiment were not analyzable since the controls used did not show the predicted PIP_2 level (Fig. 43). Overexpression of the known $PI(4,5)P_2$ phosphatase 5-ptase did not decrease the PIP_2 levels while the overexpression of the negative control GFP-PRL-3 C104S showed a dramatic increase in PIP2 levels, although the high variability led to no statistically relevant differences among the samples (Fig. 43).

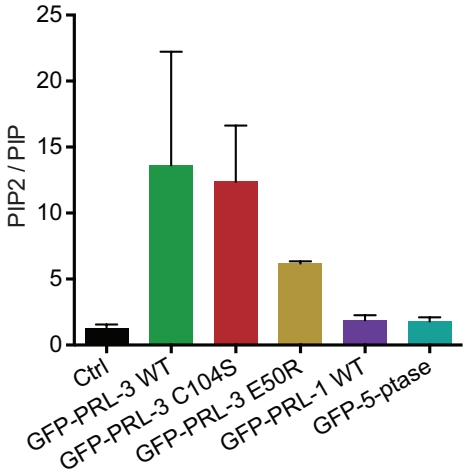

Figure 43. *No PI(4,5)P_2 dephosphorylation by PRL-3 was detected in HeLa cells by quantitative MS lipidomics. Acidic and neutral lipids were purified from HeLa cells (Ctrl) (black) and HeLa cells transiently overexpressing GFP-PRL-3 WT (green), GFP-PRL-3 C104S (red), GFP-PRL-3 E50R (ocher), GFP-PRL-1 WT (purple) and GFP-5-ptase (dark aquamarine) and total PIP and PIP2 were measured by quantitative MS lipidomics and the ratio was plotted. Median ± SEM of three technical replicates.*

This unpredictable result can be due to technical problems or masked by the PI(4,5)P_2 present in the nucleus (Mellman *et al.*, 2008; Bunce *et al.*, 2006). Theoretically, none of the proteins are able to dephosphorylate nuclear lipids since they exclusively localize in the cytosol and cell surface. However, downstream effects due to the overexpression of these particular proteins in HeLa cells may occur and the variation of total PI(4,5)P_2 level in the cell becomes uncertain. For that reason, the experiment was repeated after nuclear extraction from HeLa cells. To set it up, I removed the nuclei from the HeLa cell sample. However, although the nuclei were successfully cleared out, PIP_2 was undetectable (data not shown), probably due to the removal of PI(4,5)P_2 nuclear fraction leaving only the cell surface-bound PIP_2, which might be not enough material to be detected by MS lipidomics.

The common factor of the previous techniques is that the lipid quantification was done mixing together a pool of cells and measuring the total PI(4,5)P_2 present in the sample. However, small variations from cell to cell cannot be detected, which decreases the sensitivity of the methods. Therefore, single cell measurement techniques would theoretically increase the changes to detect a PI(4,5)P_2 level decrease upon PRL-3 WT overexpression.

To this end, initially immunofluorescence was tested with a specific PI(4,5)P_2 antibody in HeLa cells. Several fixation and permeabilization methods were tried out since the integrity of the plasma membrane is crucial for fluorescence measurement reliability. Nevertheless, none of the combinations tested led to plasma membrane staining in HeLa cells as previously shown in human osteosarcoma SaOS-2 cells (Ozkucur *et al.*, 2011). Instead, the PI(4,5)P_2 antibody was detecting only the nuclear

fraction of the lipid or, depending on the applied treatment, also a portion of a cytosolic PI(4,5)P_2 fraction (Fig. 44). This behavior suggests that either the PI(4,5)P_2 nuclear fraction is much higher than the cell surface one, so that the fluorescence intensity in the nucleus is masking the signal from the plasma membrane, or the cell surface was compromised during the immunofluorescence procedure. Therefore, in our hands PI(4,5)P_2 staining with antibodies is not a plausible technique in HeLa cells to determine a decrease of the given lipid in the plasma membrane.

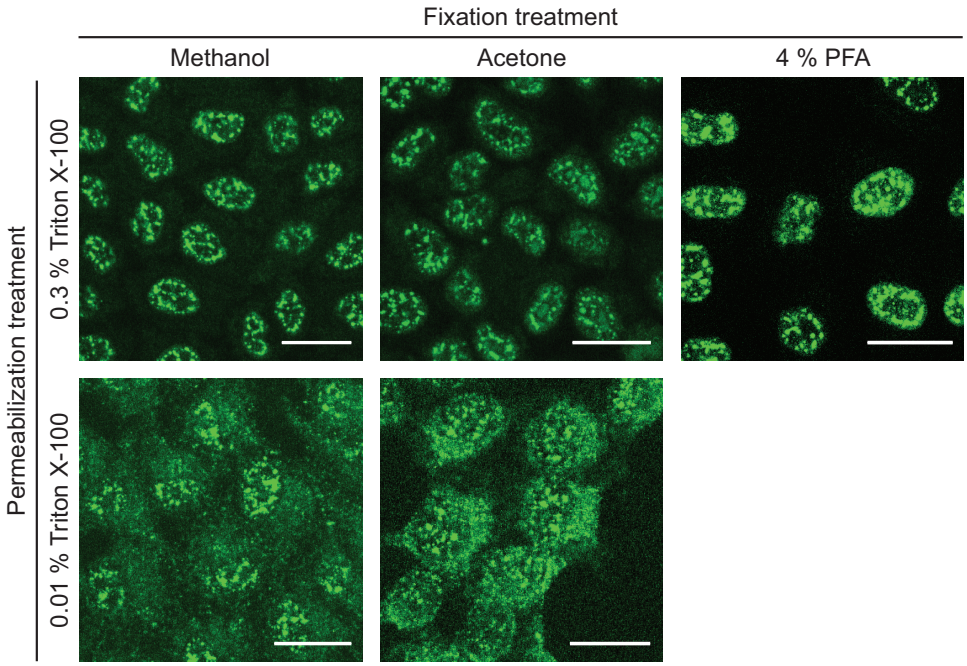

Figure 44. *PI(4,5)P_2 antibodies does not stain plasma membrane PI(4,5)P_2 in HeLa cells. Confocal microscopy picture of HeLa cells fixed and permeabilized with different treatments for PI(4,5)P_2 immunofluorescence. Scale bar = 25 µm.*

Keeping the idea of single cell PI(4,5)P_2 measurement, the GFP-tagged PH domain of PLCδ (GFP-PH PLCδ), that selectively binds to PI(4,5)P_2 (Balla *et al.*, 2009) used in the previous chapter as a reporter of this lipid in the apical membrane of MDCK cysts, was transiently overexpressed in HeLa cells together with the pmKATE2 tagged CaaX motif (negative control), 5-ptase (positive control), PRL-3 WT, PRL-3 C104S (catalyticaly inactive mutant) and PRL-3 E50R (hyperactive mutant used to increase PI(4,5)P_2 dephosphorylation activity to increase the chances of detection) to determine PI(4,5)P_2 levels in the cell surface. A similar technique based on the same principle has been recently used to determine phosphatidylinositol 3-phosphate (PI3P) levels (Ketel *et al.*, 2016). The PH domain PLCδ is a cytosolic

domain that only binds to the plasma membrane in presence of $PI(4,5)P_2$. Since this lipid is frequently found in the cell surface in normal conditions, PH-PLCδ will be recruited to the plasma membrane (Fig. 45A). However, if 5-ptase is overexpressed and $PI(4,5)P_2$ is dephosphorylated, the PH domain cannot be retained in the cell surface and is released to the cytosol (Fig. 45E). Another advantage of this method is that the PH domain cannot cross the nuclear pore, avoiding nuclear $PI(4,5)P_2$ detection that could mask the result (Fig. 45A-E). Then, quantifying the GFP fluorescence intensity ratio between the plasma membrane and the cytosol is a direct indicator of $PI(4,5)P_2$ presence in the cell membrane: the lower the ratio is, the less $PI(4,5)P_2$ remains in the plasma membrane.

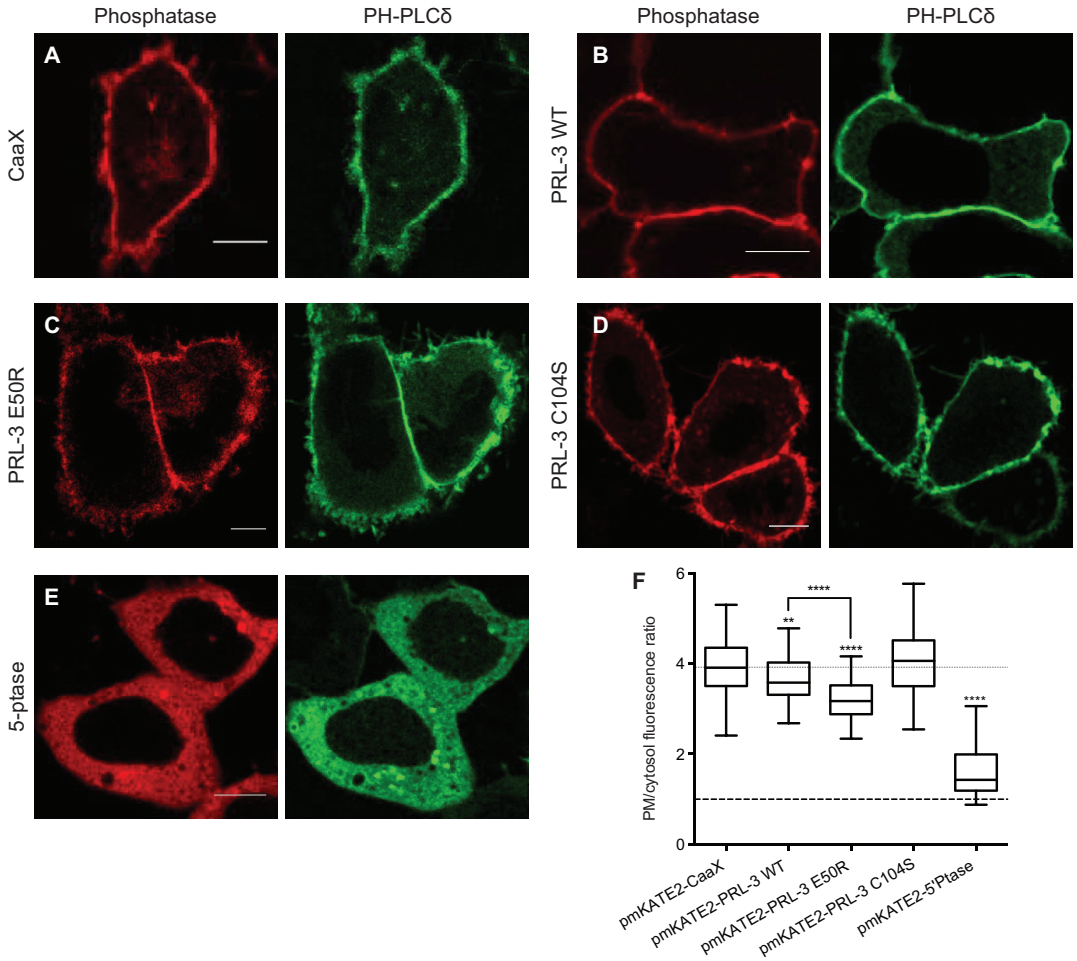

Figure 45. *PRL-3 dephosphorylates $PI(4,5)P_2$ in HeLa cells.* ***A-E*** *Confocal microscopy picture of life HeLa cells transiently overexpressing GFP-PH-PLCδ and pmKATE2-CaaX (**A**), pmKATE2-PRL-3 WT (**B**), pmKATE2-PRL-3 E50R (**C**), pmKATE2-PRL-3 C104S (**D**) or pmKATE2-5-ptase (**E**). Scale bar = 5 µm.* ***F*** *Box and whisker chart representing GFP-PH-PLCδ fluorescence intensity ratio between plasma membrane (PM) and cytosol in* ***A-E*** *samples. Thick dashed line at ratio 1 represent total $PI(4,5)P_2$ dephosphorylation at the plasma membrane. Thin dotted line at ratio 3.9 represents $PI(4,5)P_2$ level in HeLa cells in normal conditions. n = 105 cells. Three independent experiments.*

Despite being statistically significant, PI(4,5)P_2 decrease upon PRL-3 WT overexpression was quite low and visually not obvious, so further methodology modifications were carried out. First, human bone osteosarcoma epithelial (U2OS) and Hek293 cell lines were used to test if the plasma membrane/cytosol ratio was higher in normal conditions in order to have a bigger working frame. Hek293 are rather small cells and the cytosol area pictured by confocal microscopy was not big enough to rely on the result. Moreover, the plasma membrane/cytosol ratio was lower than in HeLa cells (data not shown). On the other hand, U2OS cells are bigger than HeLa cells but they are very flat, so there is no clear plane where the plasma membrane is perpendicular to the confocal plane, and drawing a sharp picture of the cell surface is not possible. Instead, the U2OS plasma membrane is almost parallel to the pictured plane and it is seen as a fuzzy area that cannot be used for this kind of quantifications.

As it was aforementioned, one of the handicaps for PI(4,5)P_2 dephosphorylation detection inside the cell is that its homeostasis is highly regulated by several distinct kinases and phosphatases (Czech, 2000). Therefore, as soon as the lipid is dephosphorylated by PRL-3, it may be easily phosphorylated again by a neighbor kinase avoiding its detection by any technique. This might be the reason why, upon PRL-3 overexpression in HeLa cells, the decrease of PI(4,5)P_2 levels is rather small. In order to corroborate our hypothesis, phosphatidylinositol (PI) kinases were inhibited to avoid new PI(4,5)P_2 formation with wortmannin, a potent, covalent and irreversible phosphatidylinositol 3-kinase (PI3K) inhibitor that can also inhibit several PI4K and PI5K in the µM range (Standaert *et al.*, 1995; McNamara and Degterev, 2011; Xie *et al.*, 1999; Liu *et al.*, 2001). pmKATE2-PRL-3 WT and GFP-PH PLCδ transiently co-transfected in HeLa cells were treated with 50 µM wortmannin 1 hour before confocal microscopy pictures were taken. Compared to wortmannin treated parental HeLa cells, PRL-3 WT overexpression led to 35% decrease of PI(4,5)P_2 level compared to the 7% difference when untreated (Fig. 46). As expected, pmKATE2-PRL-3 E50R dephosphorylates even more PI(4,5)P_2 than PRL-3 WT, and the catalytic inactive mutant overexpression (pmKATE2-PRL-3 C104S) did not modify the level of the lipid, whereas overexpression of pmKATE2-5-ptase abolished all PI(4,5)P_2 from the cell surface when treated with wortmannin (Fig. 46). Moreover, also pmKATE2-PRL-1 WT, which does not show *in vitro* PI(4,5)P_2 phosphatase activity (Rios *et al.*, 2013), was co-transfected with GFP-PH PLCδ in HeLa cells and treated with 50 µM wortmannin during 60 min. Here, the PI(4,5)P_2 levels were

comparable to parental and pmKATE2-PRL-3 C104S overexpressing HeLa cells (Fig. 46), confirming that PRL-1 cannot dephosphorylate this phospholipid.

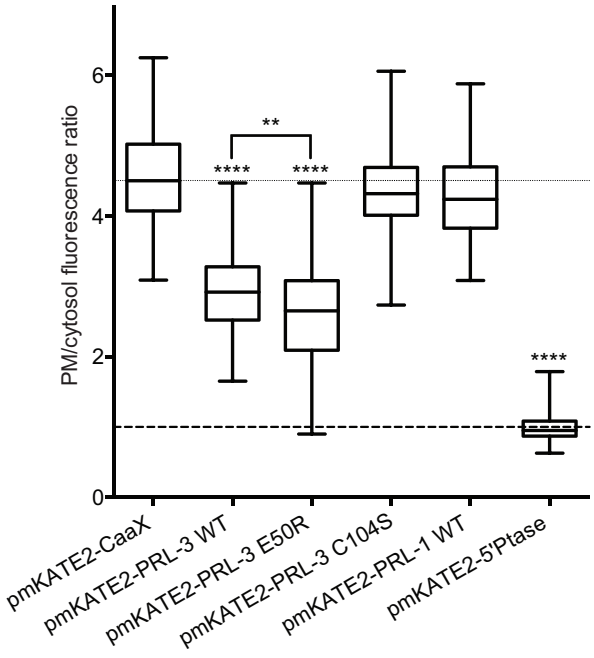

Figure 46. *PRL-3 dephosphorylates PI(4,5)P_2 in HeLa cells. Box and whisker chart representing GFP-PH-PLCδ fluorescence intensity ratio between plasma membrane (PM) and cytosol in HeLa cells transiently overexpressing GFP-PH-PLCδ and pmKATE2-CaaX, pmKATE2-PRL-3 WT, pmKATE2-PRL-3 E50R, pmKATE2-PRL-3 C104S or pmKATE2-5-ptase and treated with 50 μM wortmannin during 1 hour prior to image acquisition. Thick dashed line at ratio 1 represents total PI(4,5)P_2 dephosphorylation at the plasma membrane. Thin dotted line at ratio 4.5 represents PI(4,5)P_2 level in HeLa cells in normal conditions. n = 105 cells. Three independent experiments.*

After setting up a suitable methodology to determine small variations of PI(4,5)P_2 in the cellular plasma membrane, I use it to corroborate that not only aberrant PRL-3 expression but also endogenous levels of the protein are able to dephosphorylate PI(4,5)P_2. Therefore, variation of the phospholipid was measured upon PRL-3 knockdown in MCF-7 and HCT116, which contain endogenous PRL-3 protein levels (Fig. 47A,B). As predicted, PRL-3 knockdown in HCT116 cells transiently expressing GFP-PH PLCδ treated with 50 μM wortmannin during 60 min showed an increase of PI(4,5)P_2 in the plasma membrane compared to control (Fig. 47C). The same result was observed when PRL-3 silencing was induced in the IPTG inducible PRL-3 shRNA MCF-7 cell line compared to non induced and to IPTG induced and uninduced Ctrl shRNA MCF-7 (Fig. 47D).

The extensive use of different cell lines with overexpression and knockdown of a PI(4,5)P_2 phosphatase, together with the use of several positive and negative controls, demonstrate that the new microscopy method to determine PI(4,5)P_2 content in live cells is robust and trustable, and it has been imperative to corroborate that PRL-3 dephosphorylates PI(4,5)P_2 also *in vivo*. Moreover, the new quantitative use of PIPs binding domain enrich their already high applicability (Balla *et al.*, 2009).

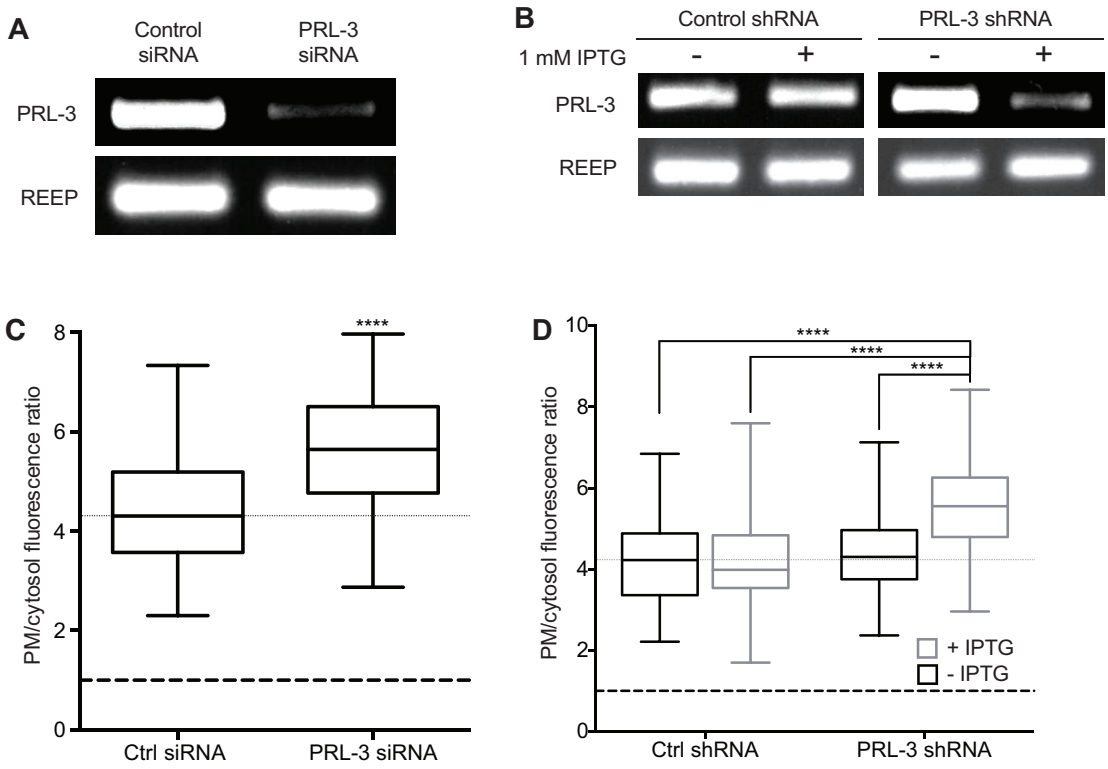

Figure 47. *PRL-3 dephosphorylates PI(4,5)P_2 in HCT116 and MCF-7 cells.* ***A*** *PRL-3 mRNA content in HCT116 cells transiently transfected with Ctrl or PRL-3 siRNA was measured by one-step RT-PCR using REEP mRNA as loading control.* ***B*** *Uninduced or induced PRL-3 knockdown with 1 mM IPTG in control or PRL-3 shRNA MCF-7 cells during 4 days. PRL-3 mRNA was assayed by one-step RT-PCR using REEP as a control.* ***C,D*** *Box and whisker chart representing GFP-PH-PLCδ fluorescence intensity ratio between plasma membrane (PM) and cytosol in HCT116 cells transiently transfected with ctrl siRNA or PRL-3 siRNA (**C**) or in IPTG uninduced or induced control or PRL-3 shRNA MCF-7 cells (**D**). Cells were treated with 50 µM wortmannin during 1 hour prior to image acquisition. Thick dashed line at ratio 1 represent total PI(4,5)P_2 dephosphorylation at the plasma membrane. Thin dotted line at ratio 4.3 (**C**) or 4.2 (**D**) represents PI(4,5)P_2 level in HCT116 or MCF-7 cells respectively in normal conditions. n = 105 cells. Three independent experiments.*

4.1.4. PRL-3's effect on CDE depends on PI(4,5)P_2 dephosphorylation.

GFP-PH PLCδ is a powerful quantitative tool that could be theoretically used to determine PI(4,5)P_2 dynamics during CCP initiation and maturation and to determine if PRL-3 modifies it, what would link the confirmed substrate with the given phenotype. Indeed, this approach has been applied to investigate PI(4,5)P_2 enrichment in larger structures than CCPs such as the cleavage furrow of *Drosophila* spermatocytes (Wong *et al.*, 2005) and the site of phagocytosis (Botelho *et al.*, 2000). However, either a single or even tandem PH domains to increase PI(4,5)P_2 affinity are

not able to detect the phospholipid within CCPs. PI(4,5)P_2 in CCPs is probably sequestered by its numerous binding proteins recruited during its formation and hence unavailable for its detection (Antonescu *et al.*, 2011). A similar PI(4,5)P_2-binding domain that is also involved in CDE, the AP180 N-terminal homology (ANTH) domain from Src-like adapter (Sla2), has been successfully used in yeast (Yidi Sun *et al.*, 2007), but not in mammalian cells (Antonescu *et al.*, 2011).

Therefore, since direct visualization of PI(4,5)P_2 in CCP context remains inaccessible, I indirectly investigated if PRL-3 was affecting CDE through PI(4,5)P_2 dephosphorylation by counteracting the action of the phosphatase with the overexpression of the corresponding kinase. Only if the substrate of a kinase is the product of a phosphatase the phenotype given by its partner can be rescued. Therefore, the rescue of the PRL-3 phenotype by a PIP kinase would strongly suggest that the hypothesis is correct. Although PI(4,5)P_2 has been postulated as a PRL-3 substrate, the position that is hydrolyzed remains unknown (McParland *et al.*, 2011). However, since phosphatidylinositol 4-phosphate (PI4P) functions as a precursor pool of PI(4,5)P_2 in the plasma membrane and it is also formed and required during CCP maturation (Schmid and Mettlen, 2013; Dickson *et al.*, 2014; Antonescu *et al.*, 2011), it is likely that PRL-3 might be dephosphorylating the 5' position. Therefore, phosphatidylinositol 4-phosphate 5-kinase type I (PIP5K) was used to rescue PRL-3 phenotype on CDE. Among the 3 existing isoforms of PIP5K (α, β and γ), the β isoform is located in endomembranes and γ is more predominantly present in neurons, while α is present in the cell surface and it has been already related to CDE (Schramp *et al.*, 2015; Anderson *et al.*, 1999; Brown and Auger, 2011). Therefore, PIP5Kα is the isoform that was used for the assays.

First, PI(4,5)P_2 content in untreated HeLa cells overexpressing blue fluorescent protein (BFP)-tagged PIP5Kα was measured with PI(4,5)P_2 reporter GFP-PH PLCδ. As predicted, the PIP kinase overexpression increased the amount of PI(4,5)P_2 in the cell surface (Fig. 48). BFP-PIP5Kα was also co-transfected with pmKATE2 PRL-3 WT what partially counteracted the PI(4,5)P_2 production given by the kinase (Fig. 48) corroborating that PRL-3 is a PI(4,5)P_2 phosphatase. As a positive control of this PI(4,5)P_2 production rescue, the PIP kinase was co-transfected with pmKATE2-5-ptase, a proven PI(4,5)P_2 phosphatase, also decreasing the phospholipid content in the plasma membrane (Fig. 48). However, PRL-3 was unable to completely rescue a PI(4,5)P_2 content comparable to parental HeLa while 5-ptase was even stronger than the kinase leading to a slight drop of PI(4,5)P_2 levels in comparison with the parental

control. This difference confirms that PRL-3 is not a strong phosphatase (Rios *et al.*, 2013; McParland *et al.*, 2011) since cannot completely counteract the kinase effect, a fact that must be taken into consideration in future experiments.

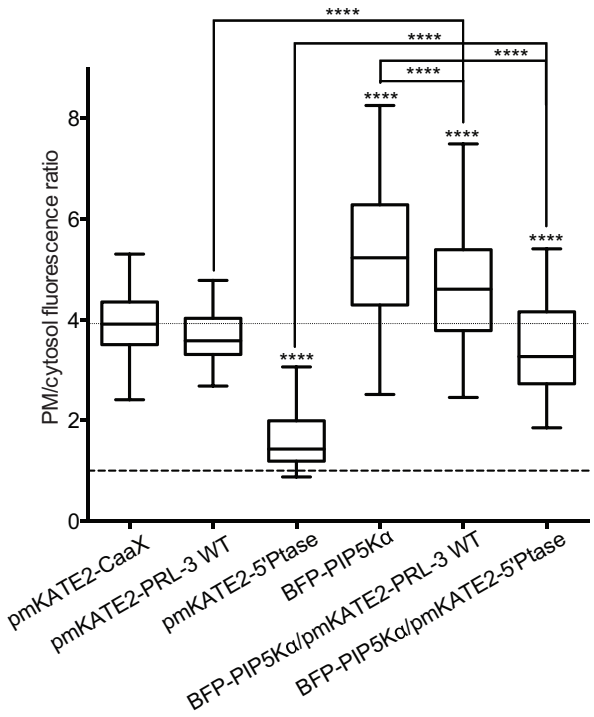

Figure 48. *PIP5Ka overexpression increases PI(4,5)P_2 levels in HeLa cells. Box and whisker chart representing GFP-PH-PLCδ fluorescence intensity ratio between plasma membrane (PM) and cytosol in HeLa cells transiently overexpressing GFP-PH-PLCδ and pmKATE2-CaaX, pmKATE2-PRL-3 WT, pmKATE2-5-ptase, BFP-PIP5Ka, BFP-PIP5Ka + pmKATE2-PRL-3 WT and BFP-PIP5Ka + pmKATE2-5-ptase. Thick dashed line at ratio 1 represent total PI(4,5)P_2 dephosphorylation at the plasma membrane. Thin dotted line at ratio 3.9 represents PI(4,5)P_2 level in HeLa cells in normal conditions. n = 105 cells. Three independent experiments.*

After confirming that PIP5Kα is able to counteract PI(4,5)P_2 depletion upon PRL-3 overexpression, I used the kinase as a tool to examine if it would also rescue the PRL-3 phenotype on CDE. Moreover, PRL-1 WT, which does not show PI(4,5)P_2 phosphatase activity (Rios *et al.*, 2013), was used as a negative control and the known PI(4,5)P_2 phosphatase, 5-ptase, as a positive control. Hence CCP dynamics were again measured in mEmerald-CLTB transiently overexpressing HeLa cells by TIRF microscopy. The results are shown in Fig. 49.

PRL-1 WT transient overexpression in mEmerald-CLTB HeLa cells showed a productive CCPs proportion, abortive CCPs lifetime and CCPs initiation density comparable to parental HeLa cells (Fig. 49A,C,E), supporting that PRL-3 might be affecting CDE by PI(4,5)P_2 dephosphorylation. However, the lifetime of productive CCPs increased (Fig. 49D) suggesting that PRL-1 overexpression might slightly affect CCP maturation through another pathway. Since this action of PRL-3 seemed to counteract the increase in the formation of productive CCPs (chapter 4.1.2.), it is possible that this effect is caused by a common mechanism of PRL-1 and PRL-3, and not by PRL-3 dephosphorylating PI(4,5)P_2.

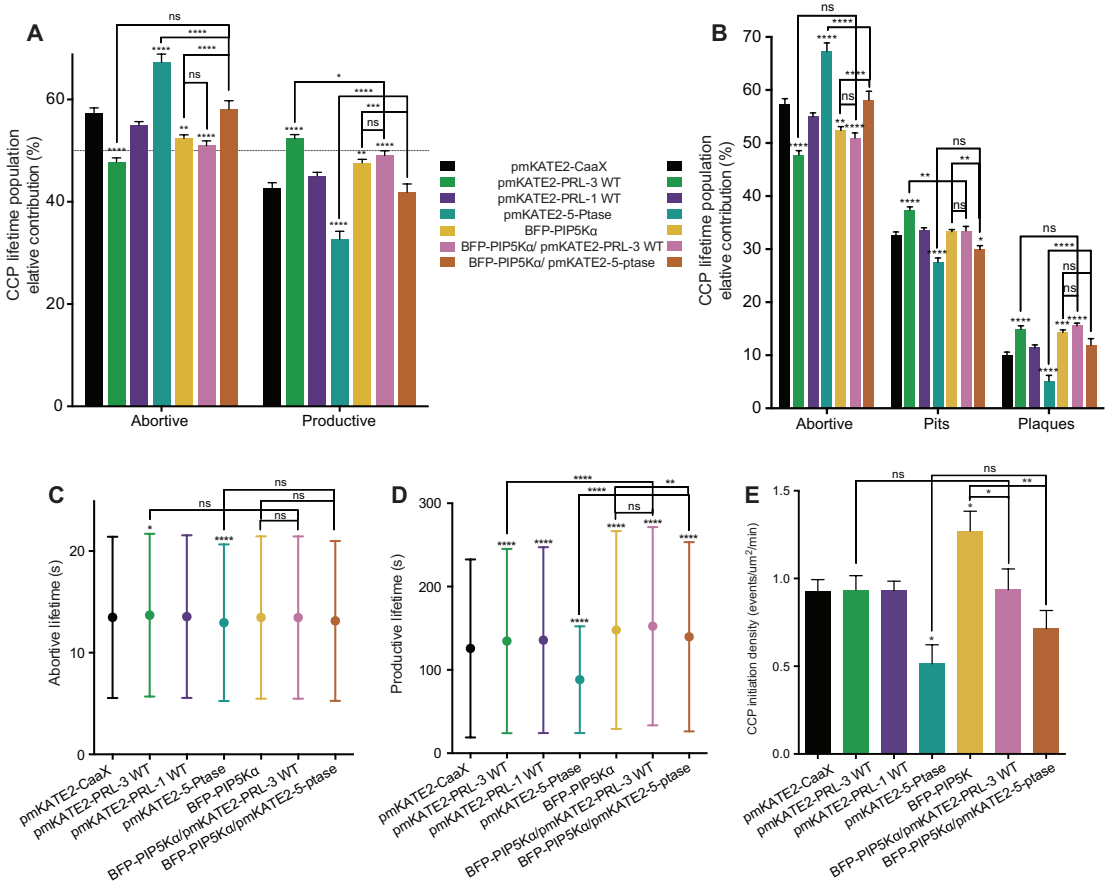

Figure 49. *PRL-3 stabilizes CCP through PI(4,5)P₂ dephosphorylation in HeLa cells. Graph representation of percentage of CCPs with a lifetime of less (abortive) or more (productive) than 30s (**A**), percentage of CCPs with a lifetime of less than 30s (abortive), between 30s and 180s (pits) and more than 180s (plaques) (**B**), average lifetime of abortive (**C**) or productive (**D**) CCPs and CCP events initiation density (**E**) in HeLa cells transiently overexpressing pmKATE2-CaaX (69 cells, 75017 endosomes) (black), pmKATE2-PRL-3 WT (70 cells, 37827 endosomes) (green), pmKATE2-PRL-1 WT (72 cells, 56204 endosomes) (purple), pmKATE2-5-ptase (68 cells, 25075 endosomes) (aquamarine), BFP-PIP5Ka (34 cells, 18326 endosomes) (orange), BFP-PIP5Ka + pmKATE2-PRL-3 WT (32 cells, 12210 endosomes) (pink) or BFP-PIP5Ka + pmKATE2-5-ptase (29 cells, 9475 endosomes) (brown). Dashed line in **A** represent 50%. Mean ± SEM (**A,B,E**) or standard deviation (**C,D**) of three independent experiments.*

On the other hand, despite both being PI(4,5)P_2 phosphatases, 5-ptase and PRL-3 showed a different effect on CCP dynamics. While PRL-3 was stabilizing the pit increasing the amount of productive CCPs, although its assembly and maturation was slowed down, PI(4,5)P_2 ablation by 5-ptase overexpression dramatically reduced the proportion of productive CCPs, the lifetime of abortive and productive CCPs, and also resulted in less initial CCP events (Fig. 49A,C-E). Overexpression of a strong phosphatase like the 5-ptase is an extreme scenario were PI(4,5)P_2 is almost not present anymore. Since its presence in the bulk plasma membrane is required for CCP nucleation, results observed in CCP density upon 5-ptase overexpression are consistent with this idea whereas PRL-3 overexpression, a weaker PI(4,5)P_2

phosphatase, does not exert the same phenotype. This is also the case when comparing the PRL-3 phenotype with other proven $PI(4,5)P_2$ phosphatases like Sjn1 (Antonescu *et al.*, 2011; Nakatsu *et al.*, 2010). Since $PI(4,5)P_2$ dephosphorylation in the core of the pit is necessary for CCP maturation, shorter lifetimes upon 5-ptase overexpression is also expected. However, $PI(4,5)P_2$ dephosphorylation also leads to coating destabilization, so if the dephosphorylation is too fast, the CCP may not be stable enough to go through the endocytic checkpoint. This is in agreement with my finding that the abortive CCP proportion is increasing when 5-ptase is present. These findings are also in agreement with the intermediate phenotype observed upon PRL-3 E50R overexpression in HeLa cells (Fig. 41B-E). The higher phosphatase activity of the mutant compared to WT is able to dephosphorylate enough $PI(4,5)P_2$ from the bulk plasma membrane to decrease the CCP event density but it is not as potent as 5-ptase to destabilize the clathrin coat affecting the abortive/productive relative contribution or lifetimes. Therefore, differences to the PRL-3 WT phenotype may be caused by the WT's weaker phosphatase activity and possibly also by a different phosphatase distribution within the CCP.

Consistently, an increase of $PI(4,5)P_2$ in the bulk plasma membrane reached upon PIP5Kα overexpression in HeLa cells facilitates clathrin nucleation as observed in the increase of the density of events (Fig. 49E), which was previously proven (Antonescu *et al.*, 2011). This $PI(4,5)P_2$ production increase also stabilizes the CCP during maturation reflected in a higher productive population, but also in a longer productive CCP lifetime (Fig. 49A,D) since CCP maturation, driven by $PI(4,5)P_2$ dephosphorylation, will require more time to clear out the lipid from the pit. To gain a deeper understanding of both phenotypes, the productive population was divided in pit and plaque subpopulations (see *Introduction*) (Saffarian *et al.*, 2009). Fig. 49B shows that PRL-3 overexpression increases both the pits and plaques proportion compared to parental HeLa cells, while PIP5Kα only modifies the plaques population. This result confirms that the increase of available $PI(4,5)P_2$ in the plasma membrane by PIP5Kα enables clathrin polymerization in larger areas in the cell surface (Antonescu *et al.*, 2011), what could potentially transform pits into plaques. On the other hand, as explained above PRL-3 dephosphorylation of $PI(4,5)P_2$ leads to an increase in the proportion of productives, both pits and plaques, and it likely acts through another mechanism to increase the lifetime of the productives.

When PRL-3 and PIP5Kα are both overexpressed in mEmerald-CLTB HeLa cells, then the observed phenotype is comparable to the one obtained through only

PIP5Kα overexpression (Fig. 49B-E), except for a reduction of CCP initiation which is comparable to that of parental HeLa cells. This difference in event initiation density can be explained by the fact that the presence of both together leads to lower $PI(4,5)P_2$ levels than only with the kinase (Fig. 48). These results demonstrate that the kinase can counteract the PRL-3 phenotype confirming that PRL-3 affects CDE through $PI(4,5)P_2$ dephosphorylation. Moreover, together with the phenotype exerted by PRL-3 E50R (Fig. 41B-E) where only the CCP density was affected, these finding suggests that the initial CCP nucleation is the most sensitive endocytosis stage to $PI(4,5)P_2$ levels.

When not considering the strength of the enzymatic activity, one could have expected that PRL-3 and PIP5Kα co-transfection would have led to a phenotype comparable to parental HeLa cells. As a proof of principle of the rescue experiment, the kinase was therefore also overexpressed with a known PI(4,5)P2 phosphatase, 5-ptase. In this scenario, the CCP dynamics were comparable to the parental HeLa cells (Fig. 49B-E) except for the lifetime of productive CCPs, which was increased. These results suggest that the difference between this result and the one shown when PRL-3 and PIP5Kα were co-overexpressed was due to the catalytic potency of PRL-3 and 5-ptase. While the strong phosphatase activity of 5-ptase could be counteracted by PIP5Kα, the kinase was stronger than PRL-3, exceeding the rescue towards the PIP5Kα overexpression phenotype.

In order to determine if the observed CCP dynamics phenotype rescue driven by the PI5P kinase over PRL-3 and 5-ptase overexpression had an impact on the CDE rate, a transferrin uptake assay was performed with the same conditions used in the previous experiments. GFP-PRL-1 WT overexpression in HeLa cells did not alter the transferrin uptake rate (Fig. 50A) suggesting that the slight effect observed in productive CPP lifetime is not strong enough to alter CDE rate, reinforcing the hypothesis that PRL-3 affects CDE by $PI(4,5)P_2$ dephosphorylation. When BFP-PIP5Kα was overexpressed, then the CDE rate was slowed down (Fig. 50B) as previously demonstrated by Antonescu *et al.*, since an increase in $PI(4,5)P_2$ levels may uncouple CCP nucleation and maturation (Antonescu *et al.*, 2011). Moreover, the increase of the plaques proportion might also affect CDE rate since they require longer time to get internalized (Saffarian *et al.*, 2009). On the other hand, strong reduction of $PI(4,5)P_2$ through GFP-5-ptase overexpression also led to a decrease in CDE rate (Fig. 50C), which is in agreement with the increase of abortive CCPs and the drop of CCP initiation. Finally, when BFP-PIP5Kα was co-transfected with GFP-

PRL-3 WT or GFP-5-ptase, the given phenotype was rescued in both cases (Fig. 50B,C), confirming that PRL-3 WT alters CDE through PI(4,5)P_2 dephosphorylation.

Taken together, after confirming that PRL-3 WT is a PI(4,5)P_2 phosphatase, here we show that the phenotype observed in CCP stabilization and CDE enhancement upon PRL-3 overexpression is due to this phosphoinositide activity. We prove it by counteracting the decrease of PI(4,5)P_2 within the CCP driven by PRL-3 with the overexpression of the appropriate kinase, PIP5Kα. The lack of effect of PRL-1 overexpression on CDE, which does not have PI(4,5)P_2 phosphatase activity, supports this finding. Interestingly, the overexpression of 5-ptase resulted in the opposite phenotype compared to PRL-3 WT. This dramatic difference can be explained by the different strengths in phosphatase activity, since the overexpression of the PRL-3 hyperactive mutant (PRL-3 E50R) led to an intermediate phenotype between PRL-3 WT and 5-ptase in agreement with the aforementioned results.

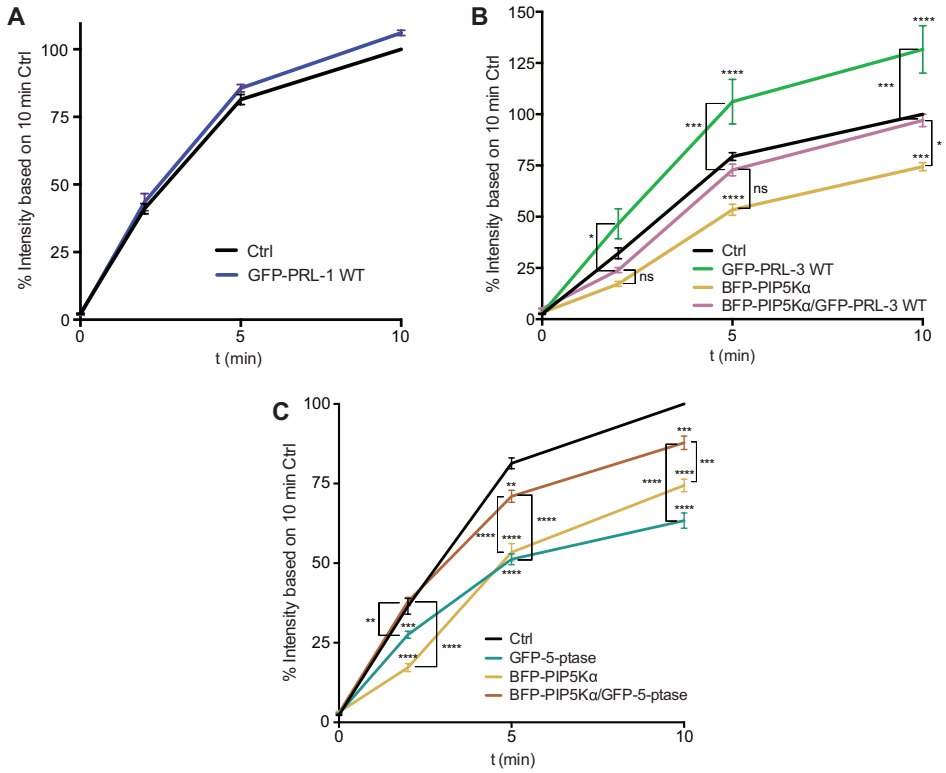

Figure 50. *PRL-3 enhances CDE through PI(4,5)P_2 dephosphorylation in HeLa cells. Alexa Fluor® 633 transferrin incorporation in HeLa cells (Ctrl) (black) and HeLa cells transiently overexpressing GFP-PRL-1 WT (purple) (**A**); GFP-PRL-3 WT (green), BFP-PIP5Ka (orange) or BFP-PIP5Ka + GFP-PRL-3 WT (pink) (**B**); or GFP-5-ptase (aquamarine), BFP-PIP5Ka (orange) or BFP-PIP5Ka + GFP-5-ptase (brown) (**C**) measured by flow cytometry at different time points. n = >2.000 cells/replicate. Mean ± SEM of ten (Ctrl), six (GFP-PRL-3 WT, BFP-PIP5Ka, GFP-5-ptase) and three (BFP-PIP5Ka + GFP-PRL-3 WT, BFP-PIP5Ka + GFP-5-ptase) independent experiments.*

4.1.5. PRL-3 spatial localization within the CCP region is crucial for pit stabilization.

The participation of $PI(4,5)P_2$ in the formation of a vesicle through CDE is spatially and temporally regulated (Antonescu *et al.*, 2011; Nakatsu *et al.*, 2010; Yidi Sun *et al.*, 2007; Posor *et al.*, 2015). For that reason, the activity of $PI(4,5)P_2$ kinases and phosphatases is also regulated in time and space. For example, while PIP5Kα is homogenously present in the plasma membrane to synthetize $PI(4,5)P_2$ in the bulk cell surface to enable CCP initiation, Snj1 is only recruited within the initiated pit to proceed along the maturation phase (Antonescu *et al.*, 2011). Therefore, a detailed investigation of PRL-3 localization during vesicle formation is required to understand its function in this process.

Unlike Sjn1 (Antonescu *et al.*, 2011), pmKATE2-PRL-3 WT overexpressed in HeLa cells is constantly present in the bulk plasma membrane, like PIP5Kα (Fig. 41A). However, when closely examining its distribution within the CCP, PRL-3 seems to redistribute to the periphery of the pit from the CCP nucleation until the vesicle is cleaved (Fig. 51A,B). Since $PI(4,5)P_2$ is only dephosphorylated inside the pit during CCP maturation, the theoretical distribution of the lipid within the pit must be similar to the one observed for PRL-3 (Fig. 10). In order to quantify this particular distribution for PRL-3, the Pearson correlation between pmKATE2-PRL-3 and mEmerald-CLTB was measured, showing that PRL-3 levels are reduced in the center of the CCP compared to prenylated pmKATE2 (pmKATE2-CaaX) (Fig. 51B,C). PRL-3 distribution within the CCP also depends on its $PI(4,5)P_2$ phosphatase activity because its inhibition with analog 3 (Hoeger *et al.*, 2014) in HeLa cells modified its distribution within the CCP. Also pmKATE2-PRL-3 C104S and pmKATE2 PRL-1 WT distribution was homogeneous compared to CLTB (Fig. 51B,C) confirming the hypothesis.

During CCP nucleation and maturation, several proteins that take part of this machinery are recruited by interaction with $PI(4,5)P_2$. Moreover, this phospholipid gets dephosphorylated during maturation. Combination of both features leaves the area with few available $PI(4,5)P_2$ molecules, and this is the reason why it is not possible to detect it with fluorescently tagged PLCδ (Antonescu *et al.*, 2011). Therefore, and based on its specific distribution around the CPPs, I hypothesized that PRL-3 might not only dephosphorylate $PI(4,5)P_2$, but also interact with the lipid probably through the *C*-terminal polybasic sequence that the phosphatase contains

adjacent to the lipidated cysteine. This sequence could potentially establish an electrostatic interaction with the negatively charged lipid.

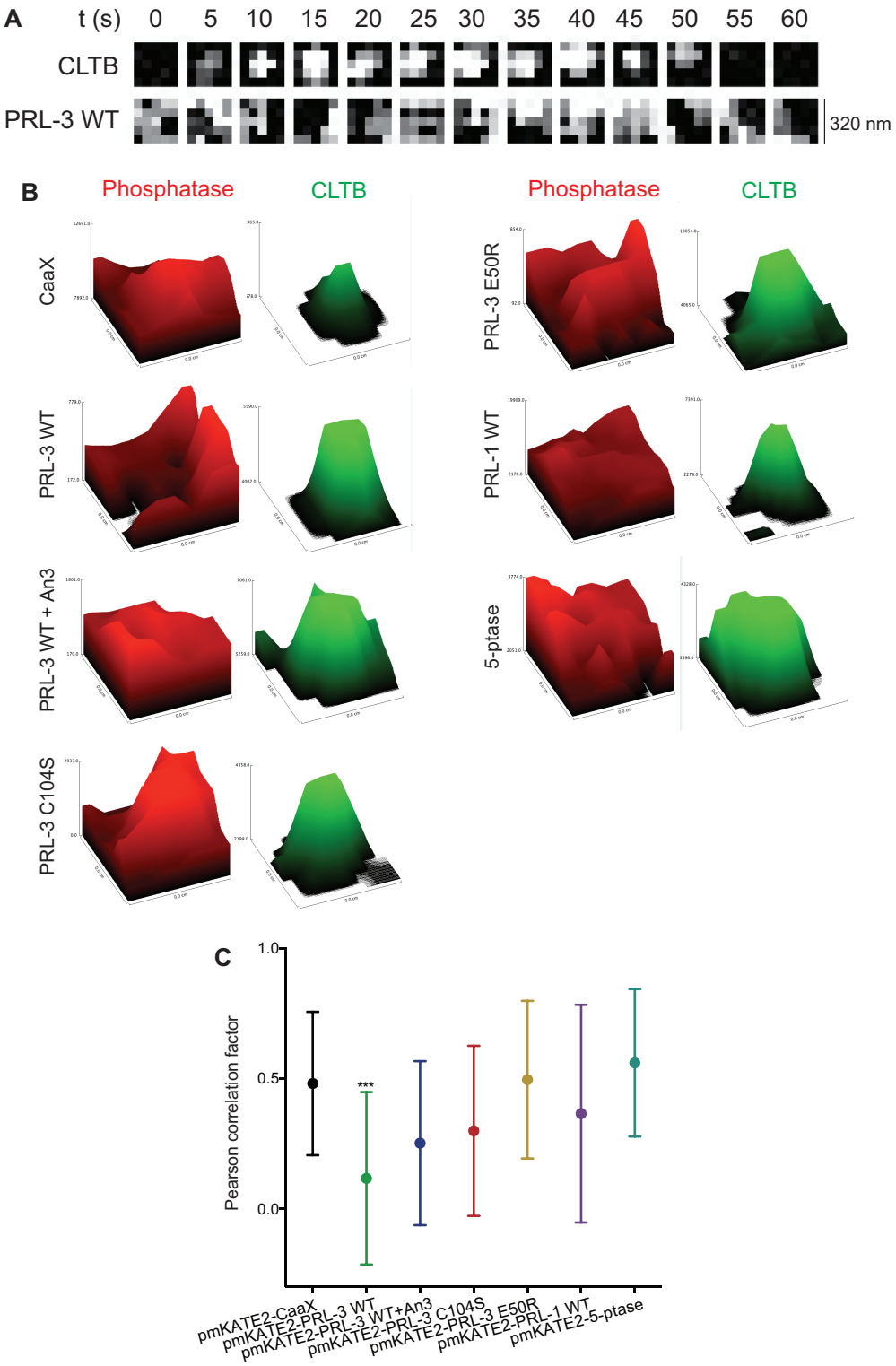

Figure 51. *PRL-3 WT is relocated to the periphery of the CCP during vesicle formation.* ***A*** *TIRF microscopy time-lapse taking pictures every 5 s following a single vesicle formation (CLTB) showing PRL-3 localization (PRL-3 WT) within the CCP area in HeLa cells*

transiently overexpressing mEmerald-CLTB and pmKATE2-PRL-3 WT. ***B*** *3D representation of fluorescence intensity (z) of CLTB and pmKATE2-CaaX, pmKATE2-PRL-3 WT untreated or treated with 50 µM analog 3, pmKATE2-PRL-3 C104S, pmKATE2-PRL-3 E50R, pmKATE2-PRL-1 WT or pmKATE2-5-ptase where a clathrin-coated vesicle is being formed (xy).* ***C*** *Pearson correlation between the CCP (CLTB) and the given phosphatase. The closer the value is to 1, the more phosphatase is found within the CCP. n = 30 cells. Mean ± standard deviation of three independent experiments.*

Indeed, it was previously mentioned that PRL-3 could bind to phosphoinositides similarly to PRL-1, through the polybasic sequence, but data was not shown (Sun *et al.*, 2007). Then, the lack of available $PI(4,5)P_2$ in the core of the pit would expel PRL-3 to a $PI(4,5)P_2$-richer region surrounding the pit, where it can freely dephosphorylate more $PI(4,5)P_2$. Theoretically, this process would form a ring around the pit where less $PI(4,5)P_2$ would be available, which could delimitate nucleation expansion and ensure pit maturation.

In order to prove this hypothesis, Dr. Pablo Rios, a colleague from Dr. Köhn's laboratory, realized an *in vitro* interaction assay between purified non-lipidated human PRL-3 and $PI(4,5)P_2$-containing liposomes to determine if they interact, using flow cytometry as readout. Indeed, PRL-3 WT interacts with $PI(4,5)P_2$-containing liposomes in a lipid-concentration dependent manner (Fig. 52A). This interaction was specific for $PI(4,5)P_2$ since it was stronger than with the other PIP species (Fig. 52B), where a residual interaction is observed, perhaps due to electrostatic unspecific interactions between the lipid phosphates and the polybasic sequence of PRL-3. As expected, this interaction depended on the polybasic sequence of PRL-3, since mutations of the positively charged amino acids to alanine (GFP-PRL-3 3A2) abolished the interaction (Fig. 52C). Moreover, the active site plays also a role in this interaction since the trapping-mutant (GFP-PRL-3 C104S) was a stronger binder. Given that PRL-3 interacts with $PI(4,5)P_2$, the lipid distribution over the plasma membrane could be driving PRL-3 localization toward regions where the lipid is enriched. Therefore, within a maturating CCP where $PI(4,5)P_2$ is being dephosphorylated and where the phosphatase must compete with other interacting proteins involved in clathrin-coated vesicle formation, the phosphatase might be redirected to regions richer in $PI(4,5)P_2$ like the ones surrounding the CCP.

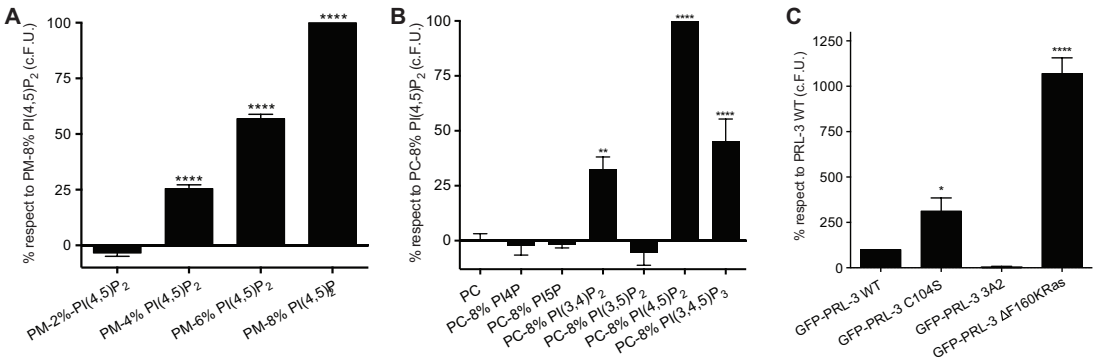

Figure 52. *PRL-3 specifically interacts with PI(4,5)P2 in vitro. The interaction between fluorophore-containing liposomes with different lipid composition and purified GFP-tagged phosphatase is measured by flow cytometry.* ***A*** *Interaction between GFP-PRL-3 WT and plasma membrane (PM)-like lipid composition liposomes containing increasing amounts of PI(4,5)P2. n = 4 samples.* ***B*** *Interaction between GFP-PRL-3 WT and phosphatidylcholine (PC) liposomes containing 8% of different PIP species. n = 8,3,8,6,6,8 and 8 samples respectively to the sample order in the chart.* ***C*** *Interaction between GFP-PRL-3 (WT, C104S, 3A2 and ΔF160 KRas) and PC liposomes containing 8% PI(4,5)P2. n = 6 samples. c.F.U. = corrected fluorescence units. Mean ± SEM of three independent experiments.*

If the proposed hypothetical scenario is correct, disruption of PRL-3 WT distribution within the CCP without altering its phosphatase activity should also affect CCP dynamics and, consequently, CDE rate. The polybasic sequence of PRL-3 is formed by 6 positively charged amino acids scattered throughout 11 amino acids. In order to make it stronger, the C-terminus was exchanged from amino acid 160 until the end with the same amount of amino acids corresponding to KRas (GFP-PRL-3 ΔF160 KRas), which contains 6 lysines in a row and can potentially interact more strongly with $PI(4,5)P_2$. To confirm this, the interaction between $PI(4,5)P_2$ and GFP-PRL-3 ΔF160 KRas was tested in liposomes. Fig. 52C shows that the hypothesis was correct with an binding increase of 10 times compared to PRL-3 WT. To ensure that the chimera was still active, its $PI(4,5)P_2$ phosphatase activity was tested *in vivo* in GFP-PH PLCδ overexpressing HeLa cells upon wortmannin treatment. As expected, the chimera was still active although the dephosphorylation efficiency was slightly lower compared to pmKATE2-PRL-3 WT (Fig. 53A).

Then, this chimera was overexpressed in mEmerald-CLTB HeLa cells to analyze CCP dynamics by TIRF microscopy. As expected, polybasic sequence exchange was sufficient to avoid being expelled to the surrounding area of the CCP (Fig. 53B). This differential distribution affected the phenotype exerted by PRL-3, since the chimera did neither vary the productive CCP proportion nor lifetime of productive CCP (Fig. 53C,E). However, it did increase the lifetime of abortive CCPs

and also decreased the CCP initiation (Fig. 53D,F) density meaning that the chimera is affecting CCP nucleation maybe inhibiting $PI(4,5)P_2$ spatial accumulation due to the strong interaction with the lipid, or, since it is not expelled, due to the dephosphorylation of $PI(4,5)P_2$. Finally, in order to test if this differential CCP dynamics pattern had an effect on the CDE rate, a transferrin uptake assay was performed in HeLa cells overexpressing GFP-PRL-3 ΔF160 KRas. As expected from the strong decrease of CCP initiation density, the overexpression of the chimera led to a decrease of CDE rate, confirming the proposed hypothesis (Fig. 53G). The different phenotype exerted by the chimera confirms that the characteristic localization of PRL-3 WT during CCP formation and maturation is crucial for the phenotype.

The results presented here strongly support the suggested scenario where the distribution of PRL-3 WT in the surrounding area of the CCP is crucial to stabilize the CCP, leading to an enhanced CDE rate. This distribution is driven by the specific interaction between the phosphatase polybasic sequence and $PI(4,5)P_2$. This interaction must be strong enough to enable the lipid to alter PRL-3 distribution on the plasma membrane but not too strong to compete with other $PI(4,5)_2$-interacting proteins required for CCP formation. Interestingly, overexpression of GFP-PRL-3 ΔF160 KRas leads to similar outcomes as overexpression of the E50R mutant, in which the activity is slightly (about 3fold) increased (B. Hoeger, M. Köhn, unpublished results) while the polybasic sequence is intact. Altogether, this suggests that the exact combination of the $PI(4,5)P_2$ affinity to the polybasic sequence and the low phosphatase activity is required for the effect on CDE, and that minor changes in either feature have a strong impact on the outcome in CDE.

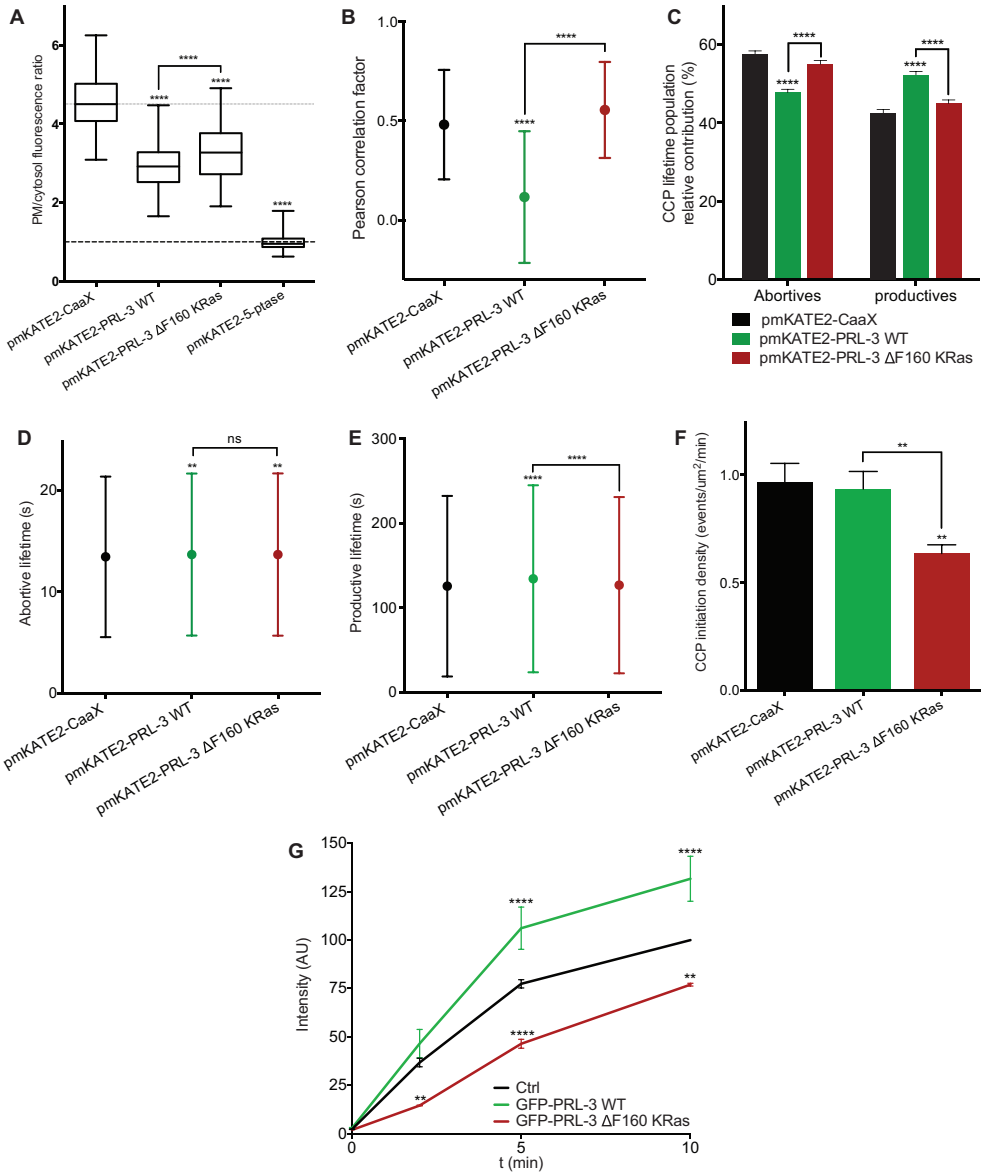

Figure 53. *PRL-3 localization within the CCP is driven by its interaction with PI(4,5)P₂ through the polybasic sequence.* ***A*** *Box and whisker chart representing GFP-PH-PLCδ fluorescence intensity ratio between plasma membrane (PM) and cytosol in HeLa cells transiently overexpressing GFP-PH-PLCδ and pmKATE2-CaaX, pmKATE2-PRL-3 WT or pmKATE2-PRL-3 ΔF160 KRas and treated with 50 μM wortmannin during 60 min prior to image acquisition. Thick dashed line at ratio 1 represent total PI(4,5)P₂ dephosphorylation at the plasma membrane. Thin dotted line at ratio 4.5 represents PI(4,5)P₂ level in HeLa cells in normal conditions. n = 105 cells. Three independent experiments.* ***B-F*** *Graph representation of Pearson correlation factor between the CCP (CLTB) and the given phosphatase (**B**), percentage of CCPs with a lifetime of less (abortive) or more (productive) than 30s (**C**), average lifetime of abortive (**D**) or productive (**E**) CCPs and CCP events initiation density (**F**) in HeLa cells transiently overexpressing pmKATE2-CaaX (69 cells, 75017 endosomes) (black), pmKATE2-PRL-3 WT (70 cells, 37827 endosomes) (green) or pmKATE2-PRL-3 ΔF160 KRas (43 cells, 42525 endosomes) (red). Mean ± SEM (**C,F**) or standard deviation (**B,D,E**) of three independent experiments.* ***G*** *Alexa Fluor® 633 transferrin incorporation in HeLa cells (Ctrl) (black) and HeLa cells transiently overexpressing GFP-PRL-3 WT (green) or GFP--PRL-3 ΔF160 KRas (red) n = 5.000 cells/replicate. Mean ± SEM of sixteen (Ctrl), six (GFP-PRL-3 WT) and three (GFP--PRL-3 ΔF160 KRas) independent experiments.*

4.2. Discussion

The molecular basis behind the carcinogenic behavior of the phosphatase PRL-3 has remained obscure since its discovery due to the lack of a solid substrate. The challenge of finding PRL-3 substrate(s) is mainly due to its low intrinsic phosphatase activity and the lack of approaches sensitive enough to detect that in the cell (Rios *et al.*, 2013; Fahs *et al.*, 2016). Indeed, PRL-3 has been recently proposed to act as a pseudophosphatase (Zhang *et al.*, 2017), but the $PI(4,5)P_2$ phosphatase activity observed in the present study is in disagreement with this hypothesis. In fact, given the multitude of pathways that PRL-3 has an effect on (Rios *et al.*, 2013), it is rather likely that both phosphatase and pseudophosphatase action contribute to the different phenotypes that PRL-3 causes.

PRL-3 expression causes several different cellular phenotypes such as enhancing cell growth, migration, and invasion, and disrupting epithelial architecture, depending on the cell types and experimental settings used. Of these diverse phenotypes, cell migration is an extremely complex process that requires an uncountable amount of molecular and cellular processes where scientific investigations could also unveil only the tip of iceberg (Polacheck *et al.*, 2013; Paul *et al.*, 2015; Friedl *et al.*, 2012; Petrie *et al.*, 2009; Webb and Horwitz, 2003). However, recent investigations agree that PRL-3 might be enhancing cell migration altering integrin clustering in the FA through direct interaction between integrins and PRL-3 (Foy *et al.*, 2017; Peng *et al.*, 2006; Peng *et al.*, 2009) and/or through integrin turnover (Krndija *et al.*, 2012; Chao and Kunz, 2009). While these two models can occur synergetically, in the present work I have focused in the second scenario. Recently, it was postulated that PRL-3 enhances integrin recycling without altering the concentration in the plasma membrane (Krndija *et al.*, 2012), showing enhanced exocytosis and suggesting enhanced uptake, probably through CDE (Chao and Kunz, 2009; Paul *et al.*, 2015). I aimed to prove this proposed involvement of PRL-3 in CDE.

Here, I show for the first time that PRL-3 is internalized from the plasma membrane selectively by CDE from where it goes to early endosomes, like it was previously observed (Qi Zeng *et al.*, 2000). Together with the recycling endosome pathway from the Golgi apparatus that was recently shown (Krndija *et al.*, 2012), now we have the larger picture of how PRL-3 localization in the plasma membrane and its turnover are achieved, although the pathway taken by the phosphatase from the early

endosomes back to the Golgi apparatus is still unknown. Further investigations in this regard would be helpful for rational drug design to disrupt the plasma membrane localization of PRL-3, which is crucial to exert its carcinogenic phenotype (Rios *et al.*, 2013; Foy *et al.*, 2017).

Moreover, PRL-3 is actively enhancing the CDE rate, which is consistent with the initial hypothesis where only a faster integrin uptake would explain that the integrin concentration in the plasma membrane can remain constant upon recycling enhancement (Krndija *et al.*, 2012). In the formation of a clathrin-coated vesicle, there are three master keys: clathrin, AP2 and $PI(4,5)P_2$ (McMahon and Boucrot, 2011; Posor *et al.*, 2015). Since $PI(4,5)P_2$ was proposed as an *in vitro* PRL-3 substrate (McParland *et al.*, 2011), I further investigated in this direction to understand how PRL-3 interferes with CDE. However, the available approaches to quantify cellular $PI(4,5)P_2$ levels were not sensitive enough and the variability among cells could not be taken into account, so the low activity of PRL-3 required the development of a more sensitive, quantitative and single cell-based approach to detect the small lipid variation exclusively in the plasma membrane. It was successfully achieved due to a specific $PI(4,5)P_2$ reporter (PH-PLCδ) that was fluorescently tagged and followed in live cells by confocal microscopy. Moreover, the sensitivity of the approach was improved by inhibiting the PI kinases with wortmannin to avoid $PI(4,5)P_2$ formation after being dephosphorylated by PRL-3. While I was able to corroborate that PRL-3 is a $PI(4,5)P_2$ phosphatase *in vivo* with this novel technique, it was not possible to use it to quantify $PI(4,5)P_2$ within the CCP due to protein-protein interaction competition with several members of the endocytic machinery (Antonescu *et al.*, 2011). I solved this obstacle by using a PI kinase (PIP5Kα) to rescue the PRL-3 phenotype in order to confirm that PRL-3 was indeed enhancing CDE by $PI(4,5)P_2$ dephosphorylation.

The study of CCP dynamics by TIRF microscopy upon PRL-3 WT was imperative to understand how PRL-3 affects the formation of the clathrin-coated vesicle (Antonescu *et al.*, 2011). PRL-3 overexpression facilitates pit stabilization slowing down the assembly and maturation process but ensuring that the pit that is being formed can progress through the endocytic checkpoint. This finding is in disagreement with the effect exerted by other $PI(4,5)P_2$ phosphatase like 5-ptase, Sjn1 or SHIP2 (Posor *et al.*, 2015; Antonescu *et al.*, 2011; Nakatsu *et al.*, 2010). $PI(4,5)P_2$ is required only for CCP nucleation as an anchor in the plasma membrane for the endocytic machinery. Then, $PI(4,5)P_2$ dephosphorylation must occur in the core of the pit during the maturation prior to vesicle scission. The aforementioned

phosphatases are recruited to the core of the pit during maturation to dephosphorylate $PI(4,5)P_2$, but the aberrant expression of any of them would destabilize the CCP leading to more abortive CCP (Antonescu *et al.*, 2011). Moreover, 5-ptase overexpression leads to less $PI(4,5)P_2$ available in the plasma membrane and, consequently, less CCP formed. The opposite behavior exerted by PRL-3 is due to two mayor differences between this phosphatase and all the others mentioned:

- **Low phosphatase activity:** here I corroborate that the intrinsic phosphatase activity of PRL-3 is much lower compared to other lipid phosphatase like 5-ptase, which explains why the deletion of $PI(4,5)P_2$ in the bulk plasma membrane by PRL-3 WT is not enough to affect CCP nucleation. In agreement with this, when the hyperactive PRL-3 mutant (PRL-3 E50R) was overexpressed, CCP initiation density decreased confirming that the observed phenotype on CCP nucleation was due to PRL-3's low intrinsic enzymatic activity.

- **Spatial localization within the CCP:** whereas Sjn1 or SHIP2 are recruited to the core of the CCP during pit assembly (Posor *et al.*, 2015; Antonescu *et al.*, 2011; Nakatsu *et al.*, 2010) and 5-ptase is also found within the CCP, PRL-3 gets concentrated in the surrounding area. This localization is driven by the specific interaction *C*-terminal polybasic sequence of the phosphatase with $PI(4,5)P_2$ and, if the strength of the mentioned interaction is modified (PRL-3 F160 KRas), PRL-3 looses the characteristic spatial pattern within the CCP also affecting the phenotype. This result proves that the PRL-3 accumulation in the boundary of the CCP is crucial for pit stabilization, and also that the interaction affinity of the PRL-3 polybasic sequence with $PI(4,5)P_2$ is the optimal one to provoke this localization.

Taken together, these observations show that the pathological function of PRL-3 cannot be explained only with the description of a substrate, but it also needs to be taken into account to which extent PRL-3 can dephosphorylate it in a concrete cellular context. PRL-3's biological behavior unveils the presence of a fine-tuned regulation of cellular processes like CDE, where small variations of the rate of phosphorylation or dephosphorylation and alterations in the location of the activity can lead to opposite consequences.

Cell migration is accomplished by the formation and disassembly of FA, and how fast this structures are recycled control the migratory speed (Nagano *et al.*, 2012). Krndija et al. demonstrated that PRL-3 enhances FA formation (Krndija *et al.*, 2012) while Foy et al. have recently proposed that PRL-3 interact with β1 integrin and the focal adhesion kinase (FAK) facilitating their dephosphorylation (Foy *et al.*, 2017). β1 integrin T788/T789 phosphorylation is essential for ECM interaction (Margadant *et al.*, 2011) and FAK Y397 dephosphorylation is necessary during integrin endocytosis (Nagano *et al.*, 2012). Dephosphorylation of both proteins would lead to a faster FA disassembly through microtubule-stimulated CDE (Ezratty *et al.*, 2009), which might be a possible scenario upon PRL-3 presence. In addition to these findings, here we demonstrate that PRL-3 accelerates CDE through $PI(4,5)P_2$ dephosphorylation, shedding light on the complex puzzle of FA dynamics regulation by PRL-3.

CDE is also required in the cleavage furrow probably for plasma membrane remodeling (Warner *et al.*, 2006) and $PI(4,5)P_2$ presence at the intercellular bridge is required for localizing cytoskeletal elements necessary for the late steps of cytokinesis (Echard, 2008). The present results open a new hypothetical scenario to be studied where PRL-3 might accelerate cytokinesis (see chapter *3*) through an enhanced CDE or by remodeling $PI(4,5)P_2$ within the intercellular bridge.

In conclusion, here I demonstrate that PRL-3 acts not solely as a pseudophosphatase since it can dephosphorylate $PI(4,5)P_2$ in cells. Moreover, I also found a function for this activity in CDE where its particular characteristics on binding and dephosphorylating $PI(4,5)P_2$ reinforce CCP stabilization, facilitating the successful completion of a clathrin-coated vesicle.

5. Conclusions and Outlook

In the presented study, I uncovered a new role for the cancer-promoting phosphatase PRL-3 in the productive enhancement of cellular cytokinesis timing. This new phenotype might be directly related with the epithelial architecture disruption driven by the phosphatase previously observed in Dr. Köhn's group. Mimicking PRL-3 clinical outcome in epithelial tumors, the phosphatase was overexpressed in 3D epithelial models leading to the generation of ectopic lumens, a consequence related to cancer formation (Debnath and Brugge, 2005; Hao *et al.*, 2010; Jaffe *et al.*, 2008; Schlüter *et al.*, 2009). Here, I deduced that these ectopic lumens arise from mispositioned midbodies after cell division. This phenotype was previously associated with tumor suppressors like Par3 and Cdc42, whose knockdown disrupts the planar orientation of the mitotic spindle in polarized epithelial cells leading to midbody retention in the lateral membrane (Hao *et al.*, 2010; Jaffe *et al.*, 2008). As an alternative, loss of asymmetric furrow ingression during cell abscission was also postulated as a theoretical scenario that would retain the midbody far from the apical membrane (Jaffe *et al.*, 2008). However, PRL-3 does neither interfere with spindle orientation nor with furrow ingression symmetry. Therefore, since the midbody is a structure derived from cell division, and spatial disturbance of cytokinesis leads to midbody mispositioning in the epithelial context, a temporal alteration of the abscission would likely infer also an alteration in the final position of the midbody. For that reason, the acceleration of cytokinesis timing by PRL-3 might be the cause of the ectopic lumen phenotype observed in 3D epithelial cysts.

Unfortunately, the lack of PRL-3 consolidated substrates together with the unsuccessful phosphoproteomics assays in the epithelial context carried out in the present study highlight not only the challenge of deciphering PRL-3 substrates *in vivo*, but also impede to elucidate the molecular mechanism behind the observed cellular phenotype. PRL-3 substrate candidates related with epithelial polarity like ezrin, $PI(4,5)P_2$ or NHERF1 where analyzed here and no change in the phosphorylation status or localization was observed. These conclusions were drawn upon observation of static fixed confocal pictures of the 3D cysts, so phosphorylation variation during dynamic processes like cell abscission were not possible to monitor due to physical and technical challenges impossible to solve with the state-of-art technology. Therefore, improvements in 3D cyst image acquisition would be required to further investigate the PRL-3 phenotype in this context and also to unequivocally prove that cytokinesis acceleration leads to midbody mispositioning. Moreover, a deeper study in the

cytokinesis process upon PRL-3 presence applying molecular biology techniques could unveil PRL-3 substrates.

As aforementioned, several protein substrates and one lipid substrate have been postulated for PRL-3. The suggested lipid is $PI(4,5)P_2$, which was shown to be dephosphorylated by PRL-3 *in vitro* (McParland *et al.*, 2011). In the present study, I have confirmed the phosphoinositide phosphatase activity of PRL-3 *in vivo* through the development of a sensitive, selective, quantitative single-cell approach taking advantage of the selective interaction between PH-PLCδ and $PI(4,5)P_2$. Thus, I disproved the current proposition that it acts solely as a pseudophosphatase (Zhang *et al.*, 2017). $PI(4,5)P_2$ plays a key role in several processes like inducing signal transduction in many signaling pathways, regulating the function of many membrane proteins and ion channels, or in cell polarity and endocytosis. Here, I focused the attention CDE since it is implicated in cell migration, which might explain how PRL-3 exerts this cancer-related phenotype (Balla, 2013; Antonescu *et al.*, 2011; Rios *et al.*, 2013). Enhanced CDE was shown to lead to faster turnover of integrins and focal adhesions (?, citation), and to contribute in this way to accelerating cell migration. Indeed, PRL-3 enhances the CDE rate through the stabilization of the CCP increasing the chances of succeeding in the final vesicle formation, although the time required for CCP nucleation and maturation is slightly longer. PRL-3 shows the opposite phenotype on CDE compared to other 5'-phosphatases like 5-ptase, SHIP2 or Snj1. However, while the aforementioned 5'-phosphatases are recruited to the core of the CCP to dephosphorylate $PI(4,5)P_2$, PRL-3 is enriched in the periphery of the pit probably delimitating and stabilizing the size of the pit. This particular spatial organization depends on its phosphatase activity together with the interaction between the polybasic sequence of the phosphatase and $PI(4,5)P_2$.

Although the presented study focuses on two different biological processes, it is possible that both are linked, and that $PI(4,5)P_2$ could be the substrate relevant for cytokinesis. Indeed, $PI(4,5)P_2$ is required in the intercellular bridge prior to the last step of cytokinesis to organize the cytoskeleton ensuring proper membrane abscission (Echard, 2008). Moreover, CDE and hence $PI(4,5)P_2$ is also required for plasma membrane remodeling in the cleavage furrow (Warner *et al.*, 2006). Therefore, as PRL-3 enhances CDE, the plasma membrane can be remodeled faster leading to a quicker membrane abscission. Unfortunately, this scenario could not be addressed with the techniques used here in the detection of $PI(4,5)P_2$ dephosphorylation in 3D cysts upon PRL-3 overexpression, as the lipid turnover dynamics are too fast and

spatio-temporally restricted to cell abscission. Therefore, although the general levels of $PI(4,5)P_2$ in 3D cyst was undisturbed in presence of PRL-3, the lipid cannot be discarded as the cause of cytokinesis acceleration and hence the origin of the ectopic lumens. Refinement of currently available techniques and potentially the study in 2D polarized or non-polarized systems could help to clarify this scenario.

6. Material and Methods

6.1. Materials and equipment

6.1.1. Chemicals and reagents

Analog 3 (PRL inhibitor) was purchased from Enamine (Z44389470). ZM447439 (AuroraB inhibitor), dynasore (dynamin inhibitor) and nystatin (cholesterol sequestering reagent) were obtained from Santa Cruz Biotechnology. Wortmannin (PI3K inhibitor), the microtubule polymerization inhibitor methyl-(5-[2-thienylcarbonyl]-1 H-benzimidazol-2-YL) carbamate (Nocodazole), paraformaldehyde (PFA), cyclohexamyde (CHX) (transcription inhibitor), MG132 (proteasome inhibitor) and rapamycin were acquired from Sigma–Aldrich, and RNase inhibitor RNasin® from Promega. Brefeldin A (BFA) was a kind gift from Dr. Jeroen Krijgsveld (Deutsches Krebsforschungszentrum (DKFZ), Heidelberg, Germany). BODIPY® FL C_5-Lactosylceramide (LacCer) complexed with bovin serum albumin (BSA) was obtained from ThermoFisher Scientifics. PI(4,5)P_2 diC_8, PI(4,5)P_2 17:0/20:4 and PI4P 17:0/20:4 were purchased from Avanti Polar Lipids. For stable cell clone selection, the antibiotics used were: G418 (Geneticin) purchased from ThermoFisher Scientifics, puromycin from Santa Cruz Biotechnology, and nourseothricin (NTC) from Jena Bioscience. For 3D cell culture, BD Matrigel™ basement membrane matrix growth factor reduced was purchased from BD Biosciences and 3-D culture Collagen I (rat tail) from Cultrex®. For transient mammalian transfection, FugeneHD was purchased from Roche, jetPRIME® from Polyplus transfection®, Amaxa SF Cell Line 4D Nucleofector from Lonza and Lipofectamine 200 and Lipofectamine LTX from Invitrogen. IPTG for shRNA induction was from Peqlab. Dynabeads® Protein G for immunoprecipitation was from ThermoFisher Scientifics. Rapigest SF surfactant was from Waters. For protein extraction, the protease inhibitor cocktail (cOmplete, EDTA free) and the phosphatase inhibitor cocktail (phoSTOP) were acquired from Roche. BluEye pre-stained protein marker was bought from Jena Biosciences. The EnzChek Phosphate assay kit was obtained from Life Technologies, and the BIOMOL® Green assay kit from Enzo Life Science. Mowiol® 4-88 mounting medium was purchased from Sigma-Aldrich.

6.1.2. Cell culture

MDCK cells were obtained from Dr. Fernando Martin-Belmonte laboratory (Centro de Biología Molecular Severo Ochoa (CBMSO), Madrid, Spain). MDCK GFP-PRL-3 WT, MDCK GFP-PRL-3 C104S, MDCK pmKATE2-PRL-3 WT GFP-PH PLCδ, MDCK pmKATE2-PRL-3 C104S GFP-PH PLCδ, Caco-2 GFP-PRL-3 WT, Caco-2 GFP-PRL-3 C104S stable cell lines were provided by Dr. Giulia Varsano (European Molecular Biology Laboratory (EMBL), Heidelberg, Germany). Caco-2 BBe, MCF-7, HeLa Kyoto, Hek293 and U2OS cell lines were available at EMBL. HCT116 cell line was purchased from ATCC. Every not yet listed stable cell line used in the present project was developed during the course of the investigation. Minimum Essential Medium (MEM) and Dulbecco's Modified Eagle's Medium (DMEM) culture medium were provided by the EMBL Media Kitchen. McCoy's 5A (Modified) medium, OptiMEM, fetal Bovine Serum (FBS) were purchased from Gibco. L-glutamine, Penecilin/Streptomycin and 0.5% trypsin was obtained from Sigma-Aldrich. BHI and Hemin were bought from Jena Bioscience. Standard cell culture dishes were acquired from Thermo Scientific, 35 mm glass bottom dishes (14 mm, No. 1.5) from MatTek Corporation, and 8-chambered glass bottom dishes from Nunc™ Lab-Tek™ (ThermoFisher Scientific). All cell lines were tested for mycoplasma contamination (Lonza MycoAlert; LT07-118).

6.1.3. DNA plasmids, siRNA, shRNA, molecular cloning and bacterial strains

Mammalian expression vectors pEGFP-PRL-3 WT, pEGFP-PRL-3 C104S, pEGFP-PRL-1 WT, pmKATE2-PRL-3 WT, pmKATE2-PRL-3 C104S and pEGFP-PH PLCδ were provided by Dr. G. Varsano, EMBL. pEGFP-PRL-1 WT and pEGFP-PRL-3 F160 KRas were supplied by Dr. Pablo Rios (EMBL, Heidelberg, Germany). mRFP-FKBP12-PRL-3 E50R ΔCaaX was provided by Dr. Birgit Höger (EMBL, Heidelberg, Germany). mEmerald-CLTB was obtained from Dr. Ori Avinoam (EMBL, Heidelberg, Germany). Finally, pEGFP-PRL-3 E50R, pmKATE2-PRL-3 E50R, pEGFP-5-ptase, pmKATE2-5-ptase, pmKATE2-PRL-1 WT, BFP-PIP5Kα and pmKATE2-PRL-3 F160 KRas were cloned during the development of the described project (see 6.2.5 and 6.2.8 in this section).

Synthetic double-stranded siRNA was obtained from Ambion (Life Technologies): Silencer Select Negative Control #1 siRNA and PRL-3 siRNA (sense 5'-CCUUCAUUGAGGACCUGAATT-3'). For inducible PRL-3 knock down in MCF-7 cells, a stable cell line was developed instead: MISSION 3X LacO Inducible Non-Target shRNA Control Plasmid DNA (Sigma-Aldrich, catalog no. SHC332) was used as a control shRNA and was provided by Dr. Amy Cooke, EMBL. For PRL-3 knock-down shRNA, sense 5'-CCGGAGCTCACCTACCTGGAGAAATCTCGAG ATTTCTCCAGGTAGGTGAGCTTTTTTG-3' extracted from MISSION shRNA Plasmid DNA was inserted in the IPTG inducible vector pLKO-puro-IPTG-3xLacO.

FastDigest restriction enzymes, T4 DNA ligase, Phusion HF DNA polymerase, dNTP mix, 6xDNA loading dye and GeneRuler 1kB DNA ladder were purchased from ThermoFisher Scientific. PCR primers were obtained from MWG Biotech, SYBR Safe DNA Gel Stain from Invitrogen, and agarose from Sigma-Aldrich. DNA was purified using QuickLyse Miniprep and HiSpeed Plasmid Maxi kits from QUIAGEN. DNA gel extraction kit and PCR purification kit were purchsed from QUIAGEN. Probes for DNA sequencing were sent to GATC Biotech. *E. coli* competent bacterial strains Top10 (prepared in-house) were use to amplify DNA plasmid content. RNA was extracted with RNeasy® purification kit and the RT-PCR with OneStep RT-PCR kit, both from QUIAGEN.

6.1.4. Peptides, proteins and antibodies

Phosphopeptides from KLC1 (Acetyl-GQVGSS-pS-PKRSG-NH_2) and PKP4 were synthetized by JPT Innovative Peptide Solutions. They were purified by high-performance liquid chromatography (HPLC) with a purity >90%. λ -phopshatase was bought from Santa Cruz Biotechnology, and lysyl endopeptidase (Lys-C) from Wako. Transferrin from human serum conjugated with Alexa Fluor® 633 was purchased from ThermoFisher Scientifics, and transferrin unconjugated from BD Bioscience.

Primary mouse antibodies used were: anti-Sec8 (1:100; Enzo Life Sciences; catalog no. ADI-VAM-SV016; clone 14G1; lot 08010910); anti-AuroraB (1:200; BD Transduction Laboratories; catalog no. 611082; clone 6/AIM-1); anti-PKP2 (1:100; MyBioSource; catalog no. MBS375114); anti-PKP4 (1:50; Progen; catalog no. 651166; clones 406.3.1/433.10.3/7.7.9); anti-γ-tubulin (1:100; Sigma-Aldrich; clone GTU-88); anti-pSer (1:2500; BD Transduction Laboratories; catalog no. 612546);

anti-PIP2 (1:100; Santa Cruz Biotechnology; catalog no. sc-53412; clone 2C11), anti-Ezrin (1:100; BD Transduction Laboratories, catalog no. 610602, lot 87352) and anti-Flag (1:100; Sigma-Aldrich; catalog no. F3040; clone M1). Primary rabbit antibodies used were: anti-MKLP1 (1:1000; Santa Cruz Biotechnology; catalog no. sc-867; clone N-19; lot I1614); anti-KLC1 (1:200; LifeSpan BioSciences; catalog no. LS-C334131; lot 61746); anti-α-tubulin (1:500; Millipore; catalog no. 04-1117; clone EP1332Y); anti-EBP50 (NHERF1) (1:1000; Abcam; catalog no. ab3452); anti-ZO-1 (1:200; Invitrogen; catalog no. 40-2200; clone TJP1) and anti-phospho-ERM (Ezrin (pT567)/Radixin (pT564)/Moesin (pT558)) (1:100; Abcam; catalog no. ab76247; clone EP2122Y; lot GR14705-13). Primary goat antibody used were: anti-Cep55 (1:100; Santa Cruz Biotechnology; catalog no. sc-162675; clone E-14; lot C0813) and anti-Anillin (1:25; Abcam; catalog no. ab5910; lot GR270489-1). GFP-Trap® nanobodies were from Chromotek and were used for immunoprecipitation of GFP-fused proteins. For PRL-3 detection, antibodies used were: anti-PRL-3 (1:200; mouse antibody; Santa Cruz Biotechnologies; catalog no. sc-130355; clone 318; lot F2111), anti-PRL-3 (1:1000; rabbit antibody; Sigma-Aldrich; catalog no. P0498; lot 104K4792) and anti-PTP4A3 (1:1000; rabbit antibody; Sigma-Aldrich; catalog no. SAB2101908; lot QC16627), but we did not observe a signal in Western Blot with any of them (data not shown). Alexa fluorophore-conjugated secondary antibodies (1:1000 for all secondary antibodies; Invitrogen) or rhodamine phalloidin (1:1000; Invitrogen; catalog no. R415; lot 1090018) and, for nuclei labeling, Hoechst 33342 (10 µg/mL; Sigma-Aldrich; catalog no. B2261), 4' ,6-Diamidine-2' -phenylindole (DAPI) (1 µg/mL; Roche, catalog no. 10236276001) and propidium iodide (PI) (1 µg/mL; Sigma-Aldrich; catalog no. P4170) were utilized.

6.1.5. Cell media and buffers

The composition of the buffers included in the commercial kits is not described here as their detailed composition is not disclosed by the companies.

- **Bacterial culture: LB medium**

  5 g/L yeast extract, 10 g/L tryptone, 5 g/L NaCl, pH 7.7, 1 g/L glucose; selection medium contained ampicillin (100 µg/mL) or kanamycin (50 µg/mL), depending on the plasmids used; culture plates were supplemented with 15 g/L agar and prepared by the EMBL Media Kitchen.

- **Bacterial culture: SOC medium**

  0.5 % (w/v) yeast extract, 2 % (w/v) tryptone, 10 mM NaCl, 2.5 mM KCl, 10 mM $MgCl_2$, 10 mM $MgSO_4$ and 20 mM glucose.

- **MDCK culture medium**

  MEM, 4.5 g/L glucose, 10% FBS, 100 U/mL penicillin and 100 µg/mL streptomycin and 2mM L-glutamine.

- **Caco-2 culture medium**

  DMEM, 4.5 g/L glucose, 10% FBS, 100 U/mL penicillin and 100 µg/mL streptomycin, 2mM L-glutamine and 0.01 mg/mL transferrin.

- **MCF-7 and Hek293 culture medium**

  DMEM, 4.5 g/L glucose, 10% FBS, 100 U/mL penicillin and 100 µg/mL streptomycin and 2mM L-glutamine.

- **HCT116 culture medium**

  McCoy's 5A (Modified), 4.5 g/L glucose, 10% FBS, 100 U/mL penicillin and 100 µg/mL streptomycin and 2mM L-glutamine.

- **HeLa and U2OS culture medium**

  DMEM, 1.5 g/L glucose, 10% (v/v) FBS, 100 U/mL penicillin and 100 µg/mL streptomycin and 2mM L-glutamine.

- **Serum-free medium (SFM)**

  Prepare it as any other culture media without 10% (v/v) FBS.

- **Phosphate-buffered saline (PBS)**

  137 mM NaCl, 2.7 mM KCl, 10 mM Na_2HPO_4 and 1.8 mM KH_2PO_4.

- **TAE buffer for agarose gel electroforesis**

  40 mM Tris-HCl, pH 8.0, 20 mM acetic acid and 1 mM ethylenediamine-tetracetic acid (EDTA).

- **Ripa lysis buffer for WB**

  125 mM Tris-HCl pH 7.5, 150 mM NaCl, 1 % (v/v) NP-40, 0.25 % (v/v) sodium deoxycholate, 1tablet/25mL cOmplete, EDTA free and 1pill/10mL PoshSTOP when required.

- **HNTG lysis buffer for WB**

  50 mM Hepes pH 7.5, 150 mM NaCl, 10 % (v/v) glycerol, 0.1 % (v/v) Triton X-100, 1 mM EDTA, 1 mM ethylene glycol-bis(β-aminoethyl ether)-N,N,N',N'-tetraacetic acid (EGTA), 1tablet/25mL cOmplete, EDTA free and 1pill/10mL PoshSTOP when required.

- **Reaction buffer (5x)**

  1 M Tris-HCl pH 7.5, 5 M NaCl, 10 % (v/v) Triton X-100 and 1M dithiothreitol (DTT).

- **λ-phosphatase lysis buffer**

  10 mM Tris-HCl pH 7.5, 150 mM NaCl, 0.5 % (v/v) NP-40 and 20 % (w/v) sacarose.

- **SDS sample buffer (4x)**

  250 mM Tris-HCl pH 6.8, 40 % (v/v) glycerol, 8 % (w/v) SDS, 4 % (w/v) β-mercaptoethanol, 50 mM EDTA and 0.05 % (w/v) bromophenol blue.

- **MOPS buffer for SDS-PAGE**

  50 mM (3-(N-morpholino) propanesulfonic acid) MOPS, 50 mM Tris-HCl, pH 7.7, 0.1 % (w/v) SDS and 1 mM EDTA.

- **Resolving gel solution**

  12 % (v/v) acrylamide, 375 mM Tris-HCl, pH 8.8, 0.1 % (w/v) SDS, 0.1 % (w/v) ammonium persulfate and 0.04 % (v/v) tetramethylethylenamine TEMED.

- **Stacking gel solution**

  5 % (v/v) acrylamide, 130 mM Tris-HCl, pH 6.8, 0.1 % (w/v) SDS, 0.1 % (w/v) ammonium persulfate and 0.1 % (v/v) TEMED.

- **WB transfer buffer**

  25 mM Tris-HCl, pH 8.3, 190 mM glycine, 0.1 % (w/v) SDS and 20 % (v/v) methanol.

- **Ponceau staining**

  0.2 % (w/v) Ponceau S and 5 % (v/v) glacial acetic acid.

- **Tris-buffered saline with Tween (TBS-T) for WB**
  20 mM Tris-HCl, pH 7.4, 150 mM NaCl and 0.05 % (v/v) Tween-20.

- **WB blocking solution**
  TBS-T with 5 % (w/v) BSA or milk powder depending on the antibody used, according to the manufacturer's instructions.

- **IF blocking solution**
  10% (w/v) FBS in PBS and 0.5 % (v/v) Triton X-100.

- **RSB buffer for polysome fractionation (2x)**
  200 mM Tris-HCl, pH 7.4, 20 mM NaCl, 3 mM $MgCl_2$ and 1pill/25mL cOmplete, EDTA free.

- **Polysome extraction buffer**
  100 mM Tris-HCl, pH 7.4, 10 mM NaCl, 1.5 mM $MgCl_2$, 1 % (v/v) Triton X-100, 2 % (v/v) Tween-20 and 1pill/25mL cOmplete, EDTA free.

- **Light and heavy sucrose solutions for polysome fractionation**
  10 mM Tris-HCl, pH 7.4, 75 mM KCl, 1.5 mM $MgCl_2$ and 20% (light) or 50 % (heavy) (w/v) sucrose.

- **Acidic buffer for transferrin uptake assay**
  0.1 M glycine, 150 mM NaCl, pH 3.

6.1.6. Equipment

Thermomixer from Eppendorf and MixingBlock from Bioer were used for different temperature incubation in 1.5 mL Eppendorf tubes. Centrifugation was carried out on Eppendorf 5415R, Eppendorf 5810 and Sorvall RC6 centrifuges and Beckman Coulter Optima L-100 XP ultracentrifuge with a SW40 rotor. DNA and RNA concentration was measured on a NanoDROP 1000 Spectrophotometer. PCR and RT-PCR were performed on a Primus25 from Peqlab. For agarose and protein gel electrophoresis, power was supplied by a LBK-EPS 500/400 power supply from Pharmacia. Pre-cast Nu-PAGE 4-12 % Bis-Tris SDS gels were from Life Technologies. Dry protein transfer for WB was performed on iBlot from Invitrogen

with a BioRad power supply and revealed on a BioRad imager ChemiDoc Touch. Cell electroporation was performed in 4D-Nucleofector Core Unit from Lonza.

Microscopes used for immunofluorescence assays visualization were: PerkinElmer Ultraview VoX containing AOTF for fast switching of laser lines and PerkinElmer Ultraview ERS spinning disk confocal microscope using a Plan-Apochromat 63x 1.4 NA objective, Olympus-ScanRcube5 microscope using a Plan-Apochromat 20x 0.7 NA objective and Olympus Cell^R multi-color TIRF microscope with an UAPON 100XOTIRF 1.49 NA objective. Microscopes were provided by the EMBL Advanced Light Microscopy Facility. Flow cytometry was performed on a BD LSR-Fortessa bench top analyser (BD Bioscience) that belongs to EMBL Flow Cytometry Core Facility. TECAN Infinite M1000 Pro multiwell plate readers was used to measure Enzcheck and BioMol® Green assays.

For mass spectrometry, an Agilent 1260 infinity HPLC was used with a Waters XBridge C_{18}; 3.5 µm. The Sep-Pak tC18 1cc 100 mg cartridge, the nanoAcquity UPLC system, the nanoAcquity Symmetry C18; 5 µm; 180 µm x 20 mm, the nanoAcquity BEH C18; 1.7 µm; 75 µm x 200 mm and the Pico-Tip Emitter 360 µm OD x 20 µm ID; 10 µm tip were from Waters. The LTQ Orbitrap Velos Pro was from ThermoFisher Scientifics. The QTRAP 5500 was from AB Sciex and was equipped with a Triversa Nanomate from Advion Biosciences.

6.1.7. Software

Graph representation and ANOVA statistical analysis were processed with GraphPad Prism 6.0 software whereas Mann-Whitney rank sum test was performed with XLSTAT (XLSTAT for Excel). Western blots were analyzed with Image Lab 5.2 software from BioRad. Microscope 2D pictures were processed and visualized using Fiji software (National Institute of Health). Microscope 3D reconstruction and TIRF time-lapses analysis were performed using Imaris software (Oxford Instruments). Spinning disc confocal microscopes were equipped with Volocity software (PerkinElmer) and TIRF microscope with Xcellence software (Olympus). Mass spectrometry raw data were processed with proteome discoverer (PD) software version 1.4.0.288 (Thermo Scientific) and LipidView from AB Sciex. Flow cytometry data were analyzed with FlowJo software.

6.2. General methods

6.2.1. Mammalian cell culture

All cells were grown at 37 °C in a humidified atmosphere containing 5 % CO_2. Each cell line was grown in his respective medium as specified in section *6.1.5.* De-attaching of cells was carried out with 1 mL trypsin solution per 10 cm culture dish (2 mL per 10 cm dish culture for MDCK) by incubation at 37 °C for 4 minutes, subsequent addition of growth medium and pelleting by centrifugation at 1000 RPM for 3 minutes. Pellet was resuspended in growth medium and part of the cells was re-seeded on a new culture dish.

6.2.2. Mammalian cell transfection and stable inducible expression

Transient transfection of mammalian cells with DNA plasmids was performed with FugeneHD transfection agent 24 hr after seeding cells for HeLa, Hek293, U2OS and HCT116. In the appropriate amount of OptiMEM, DNA plasmid was added (60 ng in 8-chambered glass bottom dish, 500 ng in a MatTek and 5 µg in a 10 cm dish culture) and then supplemented with Fugene HD (6 µL per 1 µg DNA). The mixture was incubated for 15 minutes at room temperature before adding to the sample containing fresh growth medium. Cells were transfected, at least, 16 hrs prior to assay.

DNA plasmid and siRNA incorporation in MDCK were performed by electroporation. $2x10^5$ cells are pelleted by centrifugation and resuspended in 20 µL Amaxa SF Cell Line 4D Nucleofector buffer. 0.4 µg DNA plasmid or 250 pmol siRNA were added to this cell suspension transferred to the electroporation device. After cell electroporation with program CA-152, 80 µL of RPMI medium was added to the cell mixture and incubated for 10 minutes at 37 °C. Finally, $2x10^4$ cells were seeded for 3D cyst development in an 8-chambered glass bottom dishes (see section *6.3.2.*). Cells were transfected maximum 72 hrs prior to assay.

siRNA transfection in Caco-2 cells was performed with jetPRIME® in 3.5 cm culture dish. 110 pmoles of siRNA are diluted in 200 µL of jetPRIME® buffer. Vortex 10 s and spin it down. Add 4 µL of jetPRIME® reagent, vortex 10 s, spin it down and incubate 10 minutes at room temperature before adding to the sample containing fresh growth medium. Cells were transfected maximum 72 hrs prior to assay.

siRNA transfection in HCT116 cells was performed with Lipofectamine 2000. $6x10^5$ HCT116 cells were seeded in a 3.5 cm culture dish with 2 mL of culture medium 24 hr prior transfection. In a 1.5 mL Eppendorf tube, 250 pmol of siRNA was diluted in 250 µL of OptiMEM. In another 1.5 mL Eppendorf tube, 10 µL of Lipofectamine 2000 was diluted in 250 µL of OptiMEM. Both separated mixtures were incubated for 5 minutes at room temperature. After that, Lipofectamine 2000-containing OptiMEM was added drop by drop over siRNA-containing OptiMEM and this new mixture was incubated at room temperature for 20 minutes before adding to the sample containing fresh growth medium. The experiments were performed 48 hrs post-transfection.

For shRNA stable expression in MCF-7 cells, cells were transfected with Lipofectamine LTX. $2x10^6$ MCF-7 cells are seeded in a 3.5 cm culture dish with 2 mL of culture medium 24 hr prior transfection. In a 1.5 mL Eppendorf tube, 2.5 µg of DNA plasmid was diluted in 500 µL of OptiMEM. Then, 7.5 µL of LTX reagent and 2.5 µL of Plus reagent was added to the transfection cocktail. Mixture was then incubated 25 minutes at room temperature before adding to the sample containing fresh growth medium. 48 hrs post-transfection, medium was replaced with fresh medium containing 1 µg/mL puromycin for positive clone selection. Puromycin containing medium was replaced every 2-3 days during 10 days to ensure that only positive clones stay alive. 4 different constructs were transfected: pLKO-puro-IPTG-3xLacO-Ctrl and 3 different PRL-3 shRNA containing pLKO-puro-IPTG-3xLacO plasmids (#1: 5'-CCGGCACCTTCATTGAGGACCTGAACTCGAGTTCAGGTCCTCAATGAAGGTGTTTTG-3'; #2: 5'-CC GGGCGTGTGTGTGAAGTGACCTACTCGAGTAGGTCACTTCACACACACGCTTTTT-3'; #3: 5'-CCGGAGCTCACCTACCTGGAGAAATCTCGAGATTTCTCCAGGTAGGTGAGCTTTTTTG-3'). Then, the polyclonal mixture was tested for PRL-3 knockdown efficiency upon 4 days induction with 1 mM IPTG containing medium during 4 days changing the medium with fresh one containing IPTG every 2 days. RNA extraction (see section *6.2.3.*) and RT-PCR (see section *6.2.4.*) were performed to check PRL-3 knockdown and only shRNA #3 was actually silencing PRL-3 mRNA production (data not shown). Thus, cells were plated individually in 96-wells dish for single clone expansion. When a considerable number of cells was reached, PRL-3 knockdown was induced in each clone upon IPTG treatment during 4 days and PRL-3 mRNA silencing is measured by RT-PCR (data not shown). The best candidate was then used for the experiments described in the present manuscript.

6.2.3. RNA extraction from mammalian cell sample

RNA content was extracted from different mammalian cell line samples using the RNeasy® purification kit and filtered tips to avoid RNA degradation by contaminant ribonucleases (RNases). Briefly, a full 3.5 cm culture dish was lysed with 350 µL RLT buffer at room temperature. Lysed cells were scraped with a sterile spatula, collected in a 1.5 Eppendorf tube and further homogenized by passing the lysate at least 5 times throught a blunt 20-gauge needle (0.9 mm diameter) fitted to an RNase-free syringe. 350 µL ethanol was added to the sample and homogenized by pipetting. The sample was the transferred to an RNeasy spin column and centrifuged at 10,000 RPM for 15 s at room temperature. The flow-through was discarded and the column was rinsed once with RW1 buffer and twice with RPE buffer. Finally, purified RNA was eluted with 50 µL RNase-free water in a 1.5 collection tube by centrifugation at 10,000 RPM for 1 minute at room temperature.

6.2.4. PCR and RT-PCR

PCR for insert amplification with addition of restriction sites was performed in 25 µL volume containing 30 ng DNA plasmid template, 0.2 µM forward and reverse primer (specific primers per plasmid are enlisted in sections *6.3.1.* and *6.4.1.*), 200 µM of each dNTP, 8 % DMSO, 0.5 µL Phusion DNA polymerase and 5 µL 5x HF Phusion buffer. The following cycling parameters were used: 95 °C for 2 minutes followed by 30 cycles of denaturing at 95 °C for 30 s, annealing at 56 °C for 45 s and extension at 72 °C with 40 s/kb. Final extension was performed at 72 °C for 5 minutes and DNA storage was at 4 °C. Then, PCR was directly purified or run into an agarose gel for its identification and subsequently extracted from the gel. Either process was performed with the PCR purification kit or the gel extraction kit, respectively, following the manufacturer's instruction.

PRL-3 mRNA cell content together with receptor expression-enhancing protein (REEP) as a housekeeping gene were measured by RT-PCR. After RNA extraction from cell sample (see section *6.2.3.*), RT-PCR was performed in 50 µL volume containing 250 ng RNA, 0.6 µM forward and reverse primer (PRL-3 fwd 5'-GGTGAGCTACAAACACATGCG-3'; PRL-3 rev 5'-TTCCACTACCTTGCCG GGC- 3'; REEP fwd 5'-TGCAGATGCCATCACTAAAGA- 3'; REEP rev 5'-CA TCAAGCTCCAGTA GGAAGGT- 3'), 400 µM of each dNTP, 2 µL QUIAGEN

OneStep RT-PCR Enzyme Mix and 10 µL 5x QUIAGEN OneStep RT-PCR buffer. The following cycling parameters were used: reverse transcription at 50 °C for 30 and the initial PCR activation at 95 °C for 15 minutes followed by 30 (PRL-3) or 28 (REEP) cycles of denaturing at 94 °C for 30 s, annealing at 57 °C (PRL-3) or 55 °C (REEP) for 30 s and extension at 72 °C for 1 minute. Final extension was performed at 72 °C for 10 minutes and DNA storage was at 4 °C.

6.2.5. DNA digestion with restriction enzymes

Plasmid or PCR product Restriction digestion with the respective restriction enzymes of interest was performed with FastDigest restriction enzymes. Briefly, 500 ng of PCR product or 1 µg of plasmid was incubated with 4 µL/µg of DNA of the respective restriction enzymes and the adequate buffer according to the manufacturer's instruction. Mix was incubated at 37 °C for 1 hr. Subsequently, DNA was directly purified or run into an agarose gel. DNA purification or gel extraction were performed with PCR purification kit or the gel extraction kit respectively following the manufacturer's instruction and immediately subjected to ligation.

6.2.6. DNA ligation for plasmid construction

Ligation of digested DNA fragments with digested vector was subsequently performed. The appropriate amount of digested insert and vector was prepared with a ratio of 1:5 respectively. 0.5 µL of T4 DNA ligase and buffer were added and the final mix was incubated for 15 minutes at 22 °C. Then, the products were combined and directly subjected to transformation into competent *E. coli* Top10 cells. A variable number of grown colonies were chosen depending on the amount obtained, the plasmid construct was purified using the MiniPrep DNA purification kit, and test digestion was realized applying the restriction enzymes used in the previous step. Insert incorporation was then evaluated by agarose gel electrophoresis and the sequence of positive clones were checked by DNA sequencing.

6.2.7. Agarose gel electrophoresis

1 % (w/v) (DNA cloning) or 2 % (w/v) (RT-PCR) agarose gels were prepared by adding the respective amount of agarose to TAE buffer. Additional boiling in a microwave is required for agarose complete dissolution. After cooling down the mixture SYBR Safe DNA gel stain was added and the mixture was poured into a gel chamber and left at room temperature for its polymerization. When required, DNA samples were mixed with appropriate amounts of 6x loading dye and loaded into the gel wells. To estimate DNA sample size, 5 µL GeneRuler 1kB DNA ladder was included in an extra well. Probes were separated at ≤120 V and illuminated in a UV illumination chamber.

6.2.8. Bacterial transformation for plasmid amplification

Bacterial cultures handling was performed with sterile equipment and in close proximity to a Bunsen flame. Total ligation mix was added to 100 µL homemade competent cells *E. coli* Top10 for transformation. After 30 minutes incubation on ice, bacteria were heat-shocked at 42 °C for 30 s and then kept on ice for 2 minutes more. Pre-warmed 250 µL SOC medium was added and the suspension was incubated at 37 °C on a thermomixer with 400 RPM shaking for 45 minutes. The suspension was plated on LB-agar plates containing the respective antibiotic to ensure that only the colonies containing the antibiotic-resistant plasmid will grow and incubated at 37 °C over-night. Grown colonies were picked for MiniPrep DNA extraction and sequencing.

6.2.9. DNA purification (MiniPrep/MaxiPrep)

DNA plasmid of interest was amplified on transformed *E. coli* Top10 cells. A small volume of bacteria were grown over-night in 5 mL (MiniPrep) or 250 mL (MaxiPrep) LB medium containing the corresponding resistant antibiotic and subjected to DNA extraction according to the manufacturer's instructions (QUIAGEN).

6.2.10. MS-based lipidomics for cellular phosphoinositide quantification (collaboration with the group of Dr. Britta Brügger, BZH)

Phosphoinositide quantification was performed as described previously (Haag *et al.*, 2012). Briefly, >1x10^6 cells were subjected to an acidic/neutral extraction on ice: Culture medium was aspirated, cells were rinsed three times with ice-cold PBS, 1.2 mL ice-cold 0.5 M TCA was added and incubated for 5 minutes and subsequently the lysate was scraped out with a sterile spatula. The cell lysate was centrifuged at maximum speed for 20 minutes at 4 °C and the supernatant discarded. The pellet was rinsed two times with 1 mL ice-cold 5 % (w/v) TCA containing 1 mM EDTA and centrifuged at maximum speed for 3 minutes at 4 °C. The resulting pellet was then lash frozen in liquid N_2. PI(4)P 17:0/20:4 and PI(4,5)P2 17:0/20:4 internal standards for quantification were added to TCA-washed cell pellets. Mass spectrometry was performed on a QTRAP 5500 equipped with a Triversa NanoMate. Phosphoinositides were measured by scanning for neutral losses of m/z 357 (PIP) and m/z 437 (PIP2) with collision energies of 25 eV and 35 eV, respectively. Mass spectra were evaluated with LipidView software. PIP and PIP2 amounts were normalized to total phospholipid, which was determined in neutral and acidic phase as described (Özbalci *et al.*, 2013).

6.2.11. Data analysis

Ordinary two-tailed one- or two-way ANOVA and Tukey's multiple comparision test were performed to study statistical significance except for CCP initiation density measurements that were analyzed with the Mann-Whitney rank sum test: (*) $p \leq 0.05$, (**) $p \leq 0.01$, (***) $p \leq 0.001$ and (****) $p \leq 0.0001$.

6.3. Methods applied in chapter 3

6.3.1. Plasmid cloning

Molecular cloning was performed as described in sections *6.2.4. – 6.2.9.* pEGFP and pmKATE2 versions of PRL-3 E50R were generated by EcoRI and BamHI restriction sites incorporation by PCR using pcDNA5/FRT/TO-3xFlaf-PRL-3 E50R (provided by Dr. Birgit Höger) as a template. The same PCR product was useful for both plasmid vectors since they share the same multiple cloning site. The primer pair used was: 5'-CGGAATTCTATGGCTCGGATGAACCGCC-3' and 5'-CGGGATC CTTACTACATAACGCAGCACCGGG-3'.

6.3.2. 3D cell culture in ECM (Matrigel™)

3D cell cyst formation was performed as previously described (Martin-Belmonte *et al.*, 2007). MDCK, Caco-2 or MCF-7 cells were trypsinized to a single cell suspension of $5x10^4$ cells/mL in its correspondent culture medium containing 2% (MDCK), 5% (Caco-2) or 10% (MCF-7) of BD Matrigel™. 250µL of cell suspension were then plated into 8-chambered glass bottom dishes, pre-coated with 100 µL of 10% BD Matrigel™ in serum-free MEM (MDCK), 10% BD Matrigel™ in serum-free DMEM (Caco-2) or 100% BD Matrigel™ (MCF-7). To study cell invasion in 3D cysts, MDCK were seeded as previously described but with a mix of BD Matrigel™-Collagen I (1:1) instead of only BD Matrigel™. In order to inhibit PRL-3, analog 3 (Enamine) was added to MDCK, Caco-2 and MCF-7 cysts and culture medium was replaced with fresh inhibitor every 2. Live cell images were recorded on the same microscope with stable monitored temperature of 37 °C and 5% CO_2 acquiring single plane every 3 minutes during 90 minutes in 3D MDCK YFP-MKLP-1 pmKATE2-PRL-3 WT and every 5 minutes during 14 hr in 3D MDCK YFP-MKLP-1 pmKATE2-PRL-3 C104S. For 3D cyst pictures, a confocal picture was taken every 1 µm and the subsequent digital reconstruction was performed with Imaris software.

6.3.3. Immunofluorescence staining

3D cyst immunolabelling was performed as previously described (Elia and Lippincott-Schwartz, 2009). Briefly, samples were rinsed twice with PBS and fixed

with 4 % (w/v) PFA for 30 minutes. Cell fixation was subsequently quenched with 0,1 M glycine in PBS for 20 minutes, permeabilized with 0.5 % (v/v) Triton X-100 in PBS for 10 minutes and IF blocking solution for 30 minutes. Samples were then incubated with primary antibodies in IF blocking solution at 4 °C over-night, followed by rinsing three times with PBS and incubation with Alexa fluorophore-conjugated secondary antibody (together with Hoechst and/or rhodamin phalloidin when required) for 1 hr at room temperature that was removed rinsing three times with PBS. Samples were stored in PBS at 4 °C for microscopy analysis.

6.3.4. Mitotic spindle angle measurement in 3D cysts

Mitotic spindle orientation was measured as previously described (Hao *et al.*, 2010; Jaffe *et al.*, 2008; Wei *et al.*, 2012; Zhen Zheng *et al.*, 2010; Rodriguez-Fraticelli *et al.*, 2010). Briefly, MDCK cyst were grown and fixed at 72 hr as described for immunofluorescence labeling (see section *6.3.3.*). Anti-γ-tubulin antibody and Hoechst were used to stain the mitotic spindle. Confocal images of cells in metaphase in the middle plane of the cyst were then taken. A line in the direction of the mitotic spindle was drawn using Fiji software. Another radial lane between the center of the cyst and the basal membrane was drawn crossing the first line. The small angle formed between both lines was quantified.

6.3.5. Cleavage furrow ingression measurement in 3D cysts

Cleavage furrow ingression symmetry during cell division was measured as previously described (Liu *et al.*, 2012). Briefly, MDCK cyst were grown and fixed at 72 hr as described for immunofluorescence labeling (see section *6.3.3.*). Anti-anillin antibody was used to stain the cleavage furrow together with rhodamine phalloidin and Hoechst. Confocal images of cells in cytokinesis were taken when the cleavage furrow was around 50% ingressed. A line tangent to the apical membrane and another to the basal membrane were drawn using Fiji software. The shortest distance between each line and the cleavage furrow were measured and the ratio between basal and apical membrane furrow ingression was plotted. A value of 1 represents symmetric abscission.

6.3.6. GFP-PRL-3 level in MDCK measured by flow cytometry

To quantify the heterogeneous intercellular GFP-PRL-3 WT and C104S protein level in stably expressing MDCK cell lines by flow cytometry, $3x10^6$ cell/sample were resuspended in 200 µL ice-cold PBS. GFP content of life 2 $x10^5$ cells was measured by flow cytometry in a LSR-Fortessa bench top analyzer. Life cell were gated using 1 µg/mL DAPI, a plasma membrane impermeable nuclei stain that can only be incorporated in dead cells.

6.3.7. Mammalian cell lysis, SDS-PAGE and Western Blot

Cell line of interest was cultured on a 10 cm culture dish and grown up to 90-95 % confluence. The following steps were carried out always on ice: Culture medium was aspirated, cells were rinsed with ice-cold PBS, lysed with 250 µL ice-cold Ripa lysis buffer and subsequently lysate was scraped out with a sterile spatula. Collected in a 1.5 mL Eppendorf tube, the cell lysate was passed through a blunt 20-gauge needle (0.9 mm diameter) fitted to a syringe and then incubated during 30 minutes. After incubation, the sample was centrifuged at maximum speed for 15 minutes at 4 °C. The supernatant was then collected and subjected to total protein determination concentration using Bradford reagent following the manufacturer's instructions. Equal amounts of boiled protein containing SDS sample buffer 4x were loaded onto SDS gels in a range of 30-400 µg protein/sample. Under 75 µg protein/sample, pre-casted Nu-PAGE 4-12 % Bis-Tris SDS gels were used. However, homemade 12% acrylamide gels were set for higher amount of protein loaded. glass sheets (20 cm x 20 cm) are clamped together leaving a gap of 0.75 mm with rubber stripes. Then, resolving gel solution is added leaving 2-3 cm gap at the upper part. After polymerization at room temperature, stacking gel solution is added together with the comb to generate the wells. Upon acrylamide polymerization, the comb can be then removed and the gel used for electrophoresis. Gels were blotted onto nitrocellulose membrane by dry transfer if the pre-casted gels or by wet transfer if homemade acrylamide gels were used instead. Then, the membrane was stained in Ponceau staining solution for 30 seconds to check that protein amount loaded was balanced and to discard running or transferring problems. De-staining was performed by consecutive washing steps with TBS-T. Blocking of membranes was performed for 45 minutes at room temperature in TBS-T containing 5 % (w/v) milk powder. After the

membrane is blocked, TBS-T containing 5 % (w/v) BSA and primary antibody was added and incubated rocking over-night at 4 °C. After 3 steps of washing with TBS-T, membrane was incubated with TBS-T containing 5 % (w/v) milk powder and the respective secondary antibody for 1 hr at room temperature, followed by another 3 steps of washing with TBS-T. Developing was performed by incubation with ECL+ detection reagents for 1 minute and imaging on a BioRad imager ChemiDoc Touch.

6.3.8. Protein immunoprecipitation (IP) in mammalian cell lysate

6.3.8.1. PRL-3 IP in MCF-7 cells

MCF-7 cells were cultured on a 10 cm culture dish and grown up to 90-95 % confluence. On ice: Culture medium was aspirated, cells were rinsed with ice-cold PBS, lysed with 450 µL ice-cold Ripa lysis buffer and subsequently lysate was scraped out with a sterile spatula. Collected in a 1.5 mL Eppendorf tube, the cell lysate was passed through a blunt 20-gauge needle (0.9 mm diameter) fitted to a syringe and then incubated during 30 minutes. After incubation, the sample was centrifuged at maximum speed for 15 minutes at 4 °C and 9 µL were taken as an "input" sample. 2 µL of anti-PRL-3 (Sigma-Aldrich; P-0498) was added to the collected supernatant and the incubation underwent over-night at 4 °C rocking on a wheel. 20 µL of Dynabeads® Protein G were washed three times with Ripa lysis buffer. Magnetic beads were then added to the sample and incubated for 2 hr at 4 °C rocking on a wheel. Once the beads are conjugated to the antibody, the complex is pulled down using a magnetic support. 9 µL of sample was taken as "supernatant" sample. Beads were washed three times with Ripa lysis buffer before adding 20 µL of SDS sample buffer 4x and boiling to detach PRL-3 from the beads. Samples were loaded on a pre-casted Nu-PAGE 4-12 % Bis-Tris SDS gels and proceeded as describe in section *6.3.7*.

6.3.8.2. NHERF1 IP in MDCK cells

Parental MDCK and MDCK stably overexpressing GFP-PRL-3 WT and GFP-PRL-3 C104S were cultured on a 10 cm culture dish and grown up to 90-95 % confluence. On ice: Culture medium was aspirated, cells were rinsed with ice-cold PBS, lysed with 450 µL ice-cold HNTG lysis and centrifuged at maximum speed for 15 minutes at 4 °C and 9 µL were taken as an "input" sample. 2 µL of anti-NHERF1

was added to the collected supernatant and the incubation underwent over-night at 4 °C rocking on a wheel. 25 µL of Dynabeads® Protein G were washed three times with Ripa lysis buffer. Magnetic beads were then added to the sample and incubated for 2 hr at 4 °C rocking on a wheel. Once the beads are conjugated to the antibody, the complex is pulled down using a magnetic support. 9 µL of sample was taken as "supernatant" sample. Beads were washed three times with HNTG lysis buffer before adding 20 µL of SDS sample buffer 4x and boiling to detach NHERF1 from the beads. Samples were loaded on a pre-casted Nu-PAGE 4-12 % Bis-Tris SDS gels and proceeded as describe in section *6.3.7.*

6.3.8.3. GFP-Trap® nanobodies co-IP in MDCK cells

Parental MDCK and MDCK stably overexpressing GFP-PRL-3 WT and GFP-PRL-3 C104S were cultured on a 10 cm culture dish and grown up to 90-95 % confluence. On ice: Culture medium was aspirated, cells were rinsed with ice-cold PBS, lysed with 300 µL ice-cold HNTG lysis buffer and subsequently lysate was scraped out with a sterile spatula. Collected in a 1.5 mL Eppendorf tube, the cell lysate was passed through a blunt 20-gauge needle (0.9 mm diameter) fitted to a syringe and then incubated during 30 minutes. After incubation, the sample was centrifuged at maximum speed for 15 minutes at 4 °C and 6 µL were taken as an "input" sample. 15 µL of GFP-Trap® nanobodies were washed three times with HNTG lysis buffer. Cell lysates were then added to the nanobodies and incubated for 2 hr at 4 °C rocking on a wheel. Once the GFP tagged proteins were conjugated to the nanobodies, the complex was pulled down by mild centrifugation at 800 RPM for 1 minute at 4 °C. 6 µL of sample was taken as "supernatant" sample. Beads were washed three times with HNTG lysis buffer before adding 10 µL of SDS sample buffer 4x and boiling to detach PRL-3 from the beads. Samples were loaded on a pre-casted Nu-PAGE 4-12 % Bis-Tris SDS gels and proceeded as describe in section *6.3.7.*

In order to perform the previously described assay in synchronized MDCK cells in cytokinesis, cells were treated with 0.2 µg/mL nocodazole for 16 hr at 37 °C in a humidified atmosphere containing 5 % CO_2. Then, culture media was replaced with nocodazole-free pre-warmed fresh culture media for 30 minutes to let the cell proceed from metaphase up to cytokinesis. Subsequently, HNTG lysis buffer was added and the protocol proceeds as previously described.

To further increase the chances of detecting PRL-3 substrate, interacting partners were cross-linked with PFA. For that, confluent cells were trypsinized as described in *6.2.1.* and resuspended in 1 % (w/v) PFA-containing PBS. Cross-linking was incubated for 7 minutes at room temperature followed by centrifugation at 1000 RPM for 3 minutes at room temperature. Cell lysis and co-IP was then continued as described.

6.3.8.4. PKP4 IP in MDCK and in vitro dephosphorylation with purified PRL-3

MDCK cells were cultured on a 10 cm culture dish and grown up to 90-95 % confluence. On ice: Culture medium was aspirated, cells were rinsed with ice-cold PBS, lysed with 500 µL ice-cold HNTG lysis buffer without PhosSTOP and subsequently lysate was scraped out with a sterile spatula and collected in a 1.5 mL Eppendorf tube. On the other hand, 20 µL of Dynabeads® Protein G were washed three times with HNTG lysis buffer and 100 µL of anti-PRL-3 (Sigma-Aldrich; P-0498) was added to the beads and the incubation underwent over-night at 4 °C rocking on a wheel. Antibody conjugated magnetic beads were then added to the cell lysate and incubated all together over-night at 4 °C rocking on a wheel. Once the protein-antibody-beads complex is established, it is pulled down using a magnetic support and washed three times with HNTG lysis and three more times with reaction buffer 1x. 20 µL of reaction buffer 1x containing purified human PRL-3 was then incubated with the beads for 1 hr at 37 °C before adding 6.7 µL of SDS sample buffer 4x and boiling to detach PKP4 from the beads. Samples were loaded on a pre-casted Nu-PAGE 4-12 % Bis-Tris SDS gels and proceeded as describe in section *6.3.7.*

6.3.9. MS-based PRL-detection in MDCK cells (collaboration with Dr. Marco L. Hennrich from Dr. Anne-Claude Gavin's group, EMBL)

6.3.9.1. *Cell lysis, protein digestion and peptide labeling*

$3x10^6$ MDCK cells and MDCK stably overexpressing GFP-PRL-3 WT and GFP-PRL-3 C104S cells from 3D culture were suspended in a buffer containing HEPES 200mM pH 7.8, 1 mg/mL Rapigest SF and cOmplete, EDTA-free. Cell lysate was subsequently heated for 5 minutes at 95 °C and sonicated for 20 minutes. Then, proteins were reduced with DTT and cysteine residues were carbamidomethylated with iodoacetamide followed by digestion with Lys-C for 4 hrs

at 37 °C followed by a tryptic digestion overnight at 37 °C. The resulting peptides were desalted and dimethyl labeled on Sep-Pak tC$_{18}$ 1cc 100 mg cartridges as described previously (Boersema *et al.*, 2009). The three samples were light, intermediate or heavy dimethyl labeled with either 4 % formaldehyde (CH_2O) (ThermoFisher Scientifics), deuterated formaldehyde (CD_2O) (Sigma-Aldrich) or heavy deuterated formaldehyde ($^{13}CH_2O$) (Isotec) in 50 mM Na_3PO_4 pH 7.5 buffer containing 0.6 M cyanoborohydride (Sigma-Aldrich) or cyanoborodeuterate (Sigma-Aldrich). The peptides were flushed for 10 minutes with labeling solution, washed with 0.6 % (v/v) acetic acid and eluted using 0.6 % (v/v) acetic acid in 80% (v/v) acetonitrile.

6.3.9.2. Peptide fractionation

The dimethyl labeled samples were evenly mixed and concentrated in a vacuum centrifuge. The sample pH was increased over pH 10 with 25 % (v/v) NH_3 in a final volume up to 50 µL. The sample was separated on an Agilent 1260 infinity HPLC system equipped with a Waters XBridge C18; 3.5 µm; 1 x 100 mm reversed phase column at a flow rate of 75 µL/min with 20 mM NH_4HCO_2 at pH 10 and 100 % (v/v) acetonitrile as buffers. 90 fractions were collected and concentrated under vacuum. Then, fractions were desalted and pooled into 18 pooled fractions. 16 of these were pooled by collecting one early, one middle, and one late eluting fraction and 2 were created by mixing a part of the earliest and latest fractions together.

6.3.9.3. NanoLC-MS/MS analysis

The 18 fractions were analyzed on a nanoAcquity UPLC system directly connected to an LTQ Orbitrap Velos Pro through a Proxeon nanospray source. The peptides were trapped on a nanoAcquity Symmetry C$_{18}$, 5 µm, 180 µm x 20 mm trapping column and further separated on a nanoAcquity BEH C$_{18}$, 1.7 µm, 75 µm x 200 mm analytical column. The mobile phases were 0.1 % (v/v) CH_2O_2 in water and 0.1 % (v/v) CH_2O_2 in acetonitrile. The applied three-step gradient had a range from 3 % to 40 % (v/v) acetonitrile in a flow rate of 300 nL/min. The eluent was directly introduced into the mass spectrometer via a Pico-Tip Emitter 360 µm OD x 20 µm ID; 10 µm tip. The capillary temperature was set to 300 °C and the applied spray voltage was 2.2 kV. The mass range of the full scan MS spectra was 300-1700 m/z. MS1 spectra were recorded in profile mode in the Orbitrap with a resolution of 30,000. Lock mass correction was used for internal calibration using a background ion

at m/z 446.12003. The 15 most abundant parent ions were subjected to fragmentation by CID setting normalized collision energy of 40. Charge state screening was enabled with only multiply charged ions being selected for fragmentation.

6.3.9.4. Data analysis

Raw data were processed with PD software. The MS2 spectra were filtered with a Top N peaks filter set to 6 with a 100 Da mass window. The resulting data was searched against the Uniprot dog database (26,106 sequences) and against a database consisting of the Uniprot human database and common contaminants (86,945). The search algorithm applied was Mascot version 2.2 (Matrix Science). The search parameters were 2 missed cleavages with trypsin as enzyme; a mass tolerance of 20 ppm for MS1 and 0.5 Da for MS2. As fixed modification, carbamidomethylation as a fixed modification for cys and oxidation on methionine were chosen. Phosphorylation on serine, threonine and tyrosine as variable modifications. A false discovery rate of 1 % was calculated by the percolator algorithm that is implemented in PD. Quantification was also done with PD with a mass precision set to 2 ppm and the quantification spectra of all peptides of any PRL isoform were checked manually.

6.3.10. MS-based phosphoproteomics in 3D MDCK cysts upon PRL-3 overexpression (collaboration with Dr. Marco L. Hennrich from Dr. Anne-Claude Gavin's group, EMBL)

$1x10^6$ 3D MDCK cysts and 3D MDCK stably overexpressing GFP-PRL-3 WT and GFP-PRL-3 C104S cysts were treated with 0.25 % (v/v) trypsin, centrifuged at 1000 RPM for 3 minutes at room temperature to remove the BD Matrigel™. Then, cells were lysed to extract the protein content that was digested and labeled as described in section *6.3.9.1.* After that, samples were enriched for phosphopeptides in a homemade TiO_2-packed column. The sample was washed with 6% TFA to remove unspecific binding and the elution was done under alkaline conditions using 25 % (v/v) NH_3 pH 10 solution. The elution was then immediately neutralized with 0.1 % (v/v) CH_2O_2 in water to prevent alkaline hydrolysis of the phosphoesters on serine and threonine. The elution and the flow through (corresponding to the none phosphorylated peptides) were analyzed on a nanoflow LC-MS/MS platform as described in section *6.3.9.3.* The data was analysed as explained in section *6.3.9.4.*

6.3.11. Cell proteome dephosphorylation by λ-phosphatase

MDCK cells were cultured on a 10 cm culture dish and grown up to 90-95 % confluence. On ice: Culture medium was aspirated, cells were rinsed with ice-cold PBS, lysed with 500 µL ice-cold λ-phosphatase lysis buffer and subsequently lysate was scraped out with a sterile spatula and collected in a 1.5 mL Eppendorf tube. Cell lysate was passed through a blunt 20-gauge needle (0.9 mm diameter) fitted to a syringe and centrifuged at maximum speed for 15 minutes at 4 °C. The supernatant was then collected and subjected to total protein determination concentration using Bradford reagent following the manufacturer's instructions. 15 µL of sample containing 2 µg/µL was then used for the assay. 2 µL λ –phosphatase buffer 10x, 2 µL $MnCl_2$ and 1 µL λ –phosphatase were added to the sample and incubated for 30 minutes at 37 °C. 6.7 µL of SDS sample buffer 4x were added to stop the reaction and loaded on a pre-casted Nu-PAGE 4-12 % Bis-Tris SDS gels and proceeded as describe in section *6.3.7.*

6.3.12. In vitro phosphatase activity assays

6.3.12.1. EnzChek Phosphatase Assay

Peptide dephosphorylation by PRL-3 was quantified using the EnzChek Phosphate Assay kit. The reaction was carried out in a total volume of 50 µL containing: 6 µM PRL-3, 100 µM – 1 mM peptide, 10 µL MESG (fluorogenic substrate), 0.8 µL PNP (conjugated enzyme), 10 mM DTT, kit buffer 20x and water. 100 µM $PI(4,5)P_2$ diC_8 was used as a positive control. Kinetics were followed measuring absorbance at 360 nm every 20 s at 37 °C for 2 hr.

6.3.12.2. BIOMOL® Green Assay

Peptide dephosphorylation by PRL-3 was also quantified using the BIOMOL® Green Assay kit as an end-point free phosphate quantification approach. The reaction was carried out in a total volume of 100 µL containing: 6 µM PRL-3, 100-500 µM peptide, 200 mM NaCl, 10 mM DTT and water. After given time points, the reaction carried at 37 °C was stopped adding 1 mL of the BIOMOL® Green reagent and incubated for 30 minutes at room temperature. 100 Then, fluorescence was measured at 620 nm. In order to quantify free phosphate concentration in each sample, a

phosphate titration was performed in the same buffer with a scale of serial dilutions of H_3PO_4 from 0 to 2 µM.

6.3.13. Polysome fractionation

6.3.13.1. Gradient preparation

Sucrose solution must be the maximum time possible on ice. Light sucrose solution was carefully added in a Polyallomer 14x95 mm (BeckmanCoulter) centrifuge tube up to the middle line. Heavy sucrose solution was loaded in a syringe with a long needle attached to fill the centrifuge tube from the bottom until the middle line. The tube was closed carefully to avoid bubbles, and the tube was placed in the sucrose mixer, which was set to generate a gradient from 20-50 %.

6.3.13.2. Sample preparation

MDCK GFP-PRL-3 WT cells were cultured on a 10 cm culture dish and grown up to 90-95 % confluence. Prior to cell lysis, live cells were treated with 100 µg/mL CHX for 30 minutes at 37 °C in a humidified atmosphere containing 5 % CO_2 to block transcription linking the ribosome to the transcribed mRNA. Working on ice, medium was aspirated, the cells were rinsed with ice-cold 100 µg/mL CHX-containing PBS, scraped out with a sterile spatula and centrifuged at 1200 RPM for 5 minutes at 4 °C. Cell pellet was resuspended in 175 µL RSB buffer 1x containing 0.5 % RNasin and 175 µL polysome extraction buffer was added to lyse the cells and incubated for 10 minutes. Samples were spinned for 10 s to pellet the nuclei and supernatant was centrifuged at maximum speed for 10 minutes at 4 °C. The supernatant was then collected and subjected to total protein determination concentration using Bradford reagent following the manufacturer's instructions. 2 mg protein was loaded on top of the sucrose gradient and the centrifuge tube was firmly closed and placed in the SW40Ti rotor. Samples were ultracentrifuged at 350,000 RPM for 2 hr and 39 minutes at 4 °C.

6.3.13.3. Fraction collection

1 mL sample fractions are collected in 1.5 Eppendorf tubes from the bottom of the tube using the pump of the ÄKTA protein purification system and an absorbance detector at 254 nm and 280 nm to determine in which fraction the polysomes are

contained. After that, all polysome fractions and all free mRNA fractions are pooled together for RNA extraction (see section *6.2.3.*) to perform an RT-PCR (see section *6.2.4.*) to analyze specific mRNA content in each pool. Renilla mRNA was added prior to RNA extraction as an internal standard.

6.3.14. Cell cycle analysis

MDCK cells were treated with 2 µM ZM447439 during 48 hr before the assay. Cell cycle analysis in treated and untreated MDCK by flow cytometry was performed as described previously (Schmid and Sakamoto, 2001). Briefly, MDCK cells were resuspended in MEM culture medium without phenol red to a final concentration of $2.6x10^6$ cells/mL. 30 µg/µL of Hoechst 33342 was added to the cell suspension and the incubation was carried out for 45 minutes at 37 °C. Finally, DNA content was measured by flow cytometry in the LSR-Fortessa bench top analyzer. Data was analyzed with FlowJo software.

6.3.15. Abscission timing measurement

Measurement of cytokinesis duration was carried out in 2D non-polarized MDCK cells. mCherry-AuroraB was electroporated to stain the cleavage furrow and cells were seeded on an 8-chambered glass bottom dish. Pictures were taken every 10 minutes during 24 hr in Olympus-ScanRcube5 microscope with an incubation chamber able to monitor the temperature at 37 °C in a humidified atmosphere containing 5 % CO_2. Time between cytokinetic bridge formation and complete abscission was quantified.

6.4. Methods applied in chapter 4

6.4.1. Plasmid cloning

Molecular cloning was performed as described in sections *6.2.4. – 6.2.9.* pEGFP and pmKATE2 versions of 5-ptase were generated by EcoRI and BamHI restriction

sites incorporation by PCR using mRFP-FKBP12-5-ptase ΔCaaX (provided by Dr. Giulia Varsano) as a template. The 5-ptase C'-terminal CaaX motif was also incorporated in the reverse primer. The same PCR product was useful for both plasmid vectors since they share the same multi restriction site. The primer pair used was: 5'-AATCGGAATTCAATGCCGTC-3' and 5'-CGGGATCCTCAAGAAAC GGAGCAGCTGGTGCTG-3'. pmKATE2-PRL-1 WT was subcloned from pEGFP-PRL-1 WT (provided by Dr. Pablo Rios) using the EcoRI and BamHI restriction sites included in the multiple cloning site of both vectors. mRFP-NES-FKBP12-PRL-3 E50R ΔCaaX was generated by HindIII and BamHI restriction sites incorporation by PCR using pmKATE2-PRL-3 E50R as a template. The CaaX motif was also removed in the PCR. The primer pair used was: 5'-ATCAAGC TTATGGCTCGGATGAACCGCC-3' and 5'-CGGGATCCCTACCGGGTCTTG TGCGTGT-3'. BFP-PIP5Kα was made by BglII and SalI restriction sites incorporation by PCR using pWZL-Neo-Myr-Flag- PIP5Kα (purchased from Addgene #20580) as a template. The primer pair used was: 5'-AGTAGA TCTATGGCGTCGGCTCCTCC-3' and 5'-TCAGTCGACTTAATGGGTGAA CTCTGACTCT-3'. pmKATE2-PRL-3 F160 KRas was subcloned from pEGFP-PRL-3 F160 KRas (provided by Dr. Pablo Rios) by digestion with EcoRI and BamHI restriction enzimes from pEGFP and transferred into pmKATE2 vector by ligation.

6.4.2. PRL-3 localization in HeLa cells followed by confocal microscopy

HeLa cells were cultured on a 10 cm culture dish and grown up to 100 % of confluence. Cells were trypsinized and diluted 1/100. 250 µL of diluted HeLa cells were then plated in 4 wells from an 8-chambered glass bottom dish. 24 hr after, cells were transfected with pEGFP-PRL-3 WT plasmid with FugeneHD (see section *6.2.2.*). 24 hr later, medium was replaced with 100 µL fresh HeLa culture medium without phenol red containing 100 µM dynasore, 25 µg/mL nystatin or the equivalent volume of DMSO depending on the sample condition. After 1 hr incubation, another 100 µL fresh HeLa culture medium without phenol red containing 100 µM dynasore, 25 µg/mL nystatin, 20 µM BFA, 20 µM BFA + 100 µM dynasore, 20 µM BFA + 25 µg/mL nystatin or the equivalent volume of DMSO depending on the sample condition were added. Immediately after adding it, several pictures were taken for each condition every 30 minutes during a 90 minutes period. PerkinElmer Ultraview

VoX microscope equipped with a Plan-Apochromat 63x 1.4 NA objective and an incubation chamber able to monitor the temperature at 37 °C in a humidified atmosphere containing 5 % CO_2 was used for the experiment.

To quantify GFP-PRL-3 WT translocation from the plasma membrane to the cytosol upon cell treatment, the ratio of GFP fluorescence intensity between both compartments was measured with Fiji software. Firstly, background subtraction (rolling ball radius = 25) and 1 pixel median filters were applied. Then, pixel intensity threshold was used to segment PM and cytosol independently. Finally, mean fluorescence intensity in each compartment was measured and the ratio was calculated.

6.4.3. Transferrin uptake assay by flow cytometry

HeLa, HCT116 or MCF-7 cells were seeded in 10 cm culture dish and phosphatase sequence-containing plasmid or PRL-3 siRNA were transfected or shRNA expression was induced according to section *6.2.2.* When the cell culture in the dish was grown up to 95-100 % confluence, culture media was aspirated and cells were rinsed twice with its corresponding pre-warmed SFM. 7 mL of SFM were then added to the cells and incubated for >30 minutes at 37 °C in a humidified atmosphere containing 5 % CO_2. SFM was aspirated, cells were rinsed with PBS and trypsinized with 1 mL 0.5 % (v/v) trypsin and collected in SFM as a single cell suspension that was split in 8 1.5 mL Eppendorf tubes. The following steps were carried out always on ice: Cells were centrifuged at 1000 RPM for 3 minutes at 4 °C, supernatant was discarded and pellet was resuspended in 100 µL ice-cold SFM containing Alexa Fluor® 633-transferrin. The mixture was incubated for 10 minutes at 4 °C prior to different incubation times at 37 °C to activate the endocytic machinery. Cells were centrifuged at 1000 RPM for 3 minutes at 4 °C, the supernatant was discarded, and the pellet rinsed once with 150 µL ice-cold SFM + once with 150 µL ice-cold PBS + twice with 150 µL ice-cold acidic buffer + once with 150 µL ice-cold PBS. Cells were finally resuspended in 200 µL ice-cold PBS with 1 µg/mL DAPI when only 1 fluorescently tagged protein was overexpressed or 1 µg/mL PI when 2 fluorescently tagged proteins were overexpressed. Samples were filtered with a 70 µm strainer and loaded into the proper cytometry tube. Internalized Alexa Fluor® 633-transferrin was quantified by flow cytometry in a LSR-Fortessa bench top analyzer and data was

analyzed with FlowJo software.

The same procedure was realized to see transferrin internalization by confocal microscopy directly on an 8-chambered glass bottom dish where no cell suspension is required.

6.4.4. LacCer uptake assay by flow cytometry

HeLa cells were cultured on a 10 cm culture dish and grown up to 95-100 % confluence. Culture medium was aspirated, cells were rinsed with PBS and trypsinized with 1 mL 0.5 % (v/v) trypsin and collected in 10 mM HEPES containing MEM culture medium (HMEM) as a single cell suspension that was splited in 8 1.5 mL Eppendorf tubes. The following steps were carried out always on ice: Cells were centrifuged at 1000 RPM for 3 minutes at 10 °C, supernatant was discarded and pellet was rinsed once with 150 µL ice-cold HMEM. Cells were resuspended in 50 µL ice-cold HMEM containing BODIPY® FL C_5-LacCer and the mixture was incubated for 30 minutes at 10 °C. Cells were centrifuged to discard free LacCer at 1000 RPM for 3 minutes at 4 °C and rinsed once with 150 µL ice-cold HMEM. Cells were resuspended in 100 µL ice-cold HMEM and incubated at 37 °C for different time points. Endocytosis was stopped cooling down the samples that were rinsed once with HMEM. Then, cells were resuspended in ice-cold 5% (w/v) defatted (DF)-BSA-containing HMEM, incubated for 10 minutes at 10 °C, centrifuged at 1000 RPM for 3 minutes at 10 °C and the supernatant was removed. This step was repeated 5 times. Cells were rinsed once more with ice-cold PBS prior to resuspend them in 200 µL ice-cold PBS with 1 µg/mL DAPI. Internalized BODIPY® FL C_5-LacCer was quantified by flow cytometry in the LSR-Fortessa bench top analyzer and data was analyzed with FlowJo software.

The same procedure was realized to see transferrin internalization by confocal microscopy directly on an 8-chambered glass bottom dish where no cell suspension is required.

6.4.5. TIRF acquisition

HeLa, HCT116 or MCF-7 cells were seeded in 35 mm MatTek and

phosphatase sequence-containing plasmid or PRL-3 siRNA were transfected or shRNA expression was induced according to section *6.2.2.* Moreover, 24 hr prior to TIRF microscopy picture acquisition, cells were transfected with mEmerald-CLTB as a reporter of CCPs. 24 hr after DNA transfection, 48 hr after siRNA transfection or 4 days after shRNA expression induction, pictures from the cellular plasma membrane in contact with the cover glass were recorded with an Olympus Cell^R multi-color TIRF microscope equipped with an UAPON 100XOTIRF 1.49 NA objective and an incubation chamber able to monitor the temperature at 37 °C in a humidified atmosphere containing 5 % CO_2. Pictures were taken every 5 s during 8 minutes and 20 s (100 time points). The parameter required for CCP analysis that can be extracted from these data is the CCP lifetime and it was quantified using the "particle tracking" plugin of Imaris software. Data was filtered according to: estimate XY diameter = 0.65 µm; quality = 500 a.u.; Brownian motion consideration with a maximum distance of 0.6 µm and a maximum gap size of 2 frames; track duration = 5-490 s and track intensity maximum mEmerald-CLTB > 4000 a.u.

CCP lifetimes were distributed between abortive (< 30 s) and productive (30-180 s) pits, as well as plaques (> 180 s). Percentages of CCPs in each population were represented as population distribution and the mean of each population was plotted ad CCP lifetime. Pearson correlation between CLTB and the phosphatase overexpressed was measured in a region of the area of plasma membrane in contact with the cover glass without any major shape artifacts that could lead to false correlation. Finally, the amount of CCPs formed was divided per cell surface area in contact with the cover glass and time to measure CCP density.

6.4.6. Microsomal fractionation for nuclei extraction in HeLa cells

HeLa cells were seeded in 24.5 x 24.5 cm squared culture plate and grown up to 90-95 % confluence. The following steps were carried out always on ice: Culture medium was aspirated, cells were rinsed twice with 10 mL ice-cold PBS, and harvested in 12 mL ice-cold PBS using a sterile spatula. Cells were pelleted by centrifugation at 500 g during 5 minutes at 4 °C and rinse one more time with 10 mL ice-cold PBS. Then, hypotonic lysis was carried out resuspending the cell pellet in 7.5 mL ice-cold 50 mM Tris pH 7.5 and incubating for 30 minutes at 4 °C. Cell swelling was checked under vertical microscope and extra incubation time was applied if

required. Plasma membrane of swollen cells was disrupted with a Dounce homogenizer. The amount of strokes required depends on the lysis efficiency that must be checked under microscope. Sample is finally centrifuged at 1000 g during 13 minutes at 4 °C to discard free nuclei and intact cells.

6.4.7. PI(4,5)P_2 detection with specific antibody (immunofluorescence)

HeLa cells seeded in an 8-chambered glass bottom dish were rinsed twice with PBS and different fixation and permeabilization condition were tested. For fixation cells were treated with: 4 % (w/v) PFA for 30 minutes, methanol for 5 minutes at -20 °C, or ice-cold acetone for 2 minutes. Then cells were permeabilized with either 0.3 or 0.05 % (v/v) Triton X-100 in PBS for 10 minutes. Then, immunofluorescence was finished as described in section *6.3.3*.

6.4.8. PI(4,5)P_2 detection with specific interacting PH-PLCδ by life-cell confocal microscopy

HeLa, HCT116 or MCF-7 cells were seeded in an 8-chambered glass bottom dish. pmKATE2 plasmid containing the sequence of the phosphatase of interest or PRL-3 siRNA were transfected or shRNA expression was induced together with GFP-PH PLCδ plasmid according to section *6.2.2*. 24 hrs after transfection, cells were mock treated or treated with 50 µM wortmannin added to fresh culture medium without phenol red. 1 hr after treatment, pictures are taken in a PerkinElmer Ultraview VoX microscope equipped with a Plan-Apochromat 63x 1.4 NA objective and an incubation chamber able to monitor the temperature at 37 °C in a humidified atmosphere containing 5 % CO_2.

To quantify GFP-PH PLCδ attachment to the plasma membrane, the ratio of GFP fluorescence intensity between both compartments was measured with Fiji software. Firstly, background subtraction (rolling ball radius = 50) and 1 pixel median filters were applied. Then, pixel intensity threshold was used to segment PM and cytosol independently. Finally, mean fluorescence intensity in each compartment was measured and ratio calculated.

7. Appendix

Gene Name	Ratio
CSTF1	0.012
PSAP	0.026
WDR74	0.041
FOLR2	0.043
UBR4	0.054
UBE2M	0.063
OTUB1	0.073
FTH1	0.074
PFKP	0.075
COG6	0.086
HDGF	0.092
CASP8	0.117
SUPV3L1	0.117
UFC1	0.117
COQ2	0.122
TPT1	0.124
SULT1A1	0.129
ETF1	0.144
SNX2	0.152
ANXA4	0.157
GRN	0.165
SNCG	0.170
PSIP1	0.172
UBAP2	0.172
DKC1	0.176
CLIC4	0.186
NACA	0.190
CASP10	0.194
TBRG4	0.197
PAFAH1B3	0.197
EIF3H	0.202
COPE	0.208
HPRT1	0.210
HYAL1	0.213
Cfa.23622	0.214
IPO5	0.222
STIP1	0.227
CMPK1	0.228
RBM5	0.230
CDK9	0.233
GLUL	0.234
LOC486100	0.236
LOC491969	0.239
GPI	0.241
CTTN	0.248
RRAGD	0.249
IFI30	0.251
CUL1	0.255
AKT1	0.256
PSME1	0.258
DCUN1D1	0.260
MCEE	0.265
CARHSP1	0.267
IL17RC	0.278
ANXA11	0.283
GLB1	0.285
HMGCL	0.285
KIAA0664	0.289
PGK1	0.290
FBP2	0.297
TPI1	0.304
FMO5	0.305
HPF1	0.310
PGD	0.313
RPS21	0.316
CLIC1	0.317
ANXA10	0.318
WARS	0.319
PGAM1	0.324
PRDX6	0.324
TALDO1	0.325
RNH1	0.325
CTSB	0.325
LNPEP	0.328
RPIA	0.328
PAFAH1B2	0.330
CYLD	0.331
SH3GL1	0.335
PXDN	0.337
CHCHD2	0.338
MAPK8	0.343
PTGES2	0.345
ARPC5L	0.348
TXN	0.350
OSTF1	0.351
BCAS2	0.361
DAK	0.364
ARHGDIA	0.367
ERAP1	0.368
SORL1	0.370
ZCCHC8	0.372
DYNLL1	0.374
ANP32A	0.375
DSTN	0.382
RRS1	0.389
CRYAB	0.392
APEX1C	0.394
CLIC2	0.398
MUT	0.400
DST	0.404
CTCF	0.405
SEC23A	0.408
THOP1	0.412
GOLT1B	0.413
CCBL1	0.424
NPEPPS	0.426
CA2	0.428
SEPHS1	0.428
ANXA7	0.429
LDHA	0.435
GNB2L1	0.438
NUP62	0.441
TPP1*	0.442
IPO7	0.454
UQCRH	0.457
MAN2B1	0.459
LIPA	0.466
ERC1	0.467
PNPO	0.473
GGCX	0.474
CTNNBL1	0.475
UPP1	0.477
PDHX	0.481
ADH5	0.484
CDC42	0.486
GPRC5C	0.486
UBE2H	0.486
COMMD2	0.489
TPP1*	0.491
NAGPA	0.493
FAAH	0.498
MBOAT7*	2.020
GNA13	2.026
TIMM50	2.039
RPL18A	2.056
GNA11	2.077
OCLN	2.080
GOLPH3	2.118
LONP1	2.119
ATP2A2	2.123
TOR1AIP1	2.137
SLC25A12	2.139
MKI67	2.149
CLPTM1L	2.152
P4HA1	2.152
RAB33B	2.160
TBL2	2.184
GNG12	2.198
CD47	2.206
HSD3B7	2.209
IK	2.224
LMNB2	2.227
COX7A2L*	2.228
GRAMD3	2.229
PYCR1	2.231
TRPA1	2.231
LMAN1	2.235
RPL6	2.240
CEBPZ	2.247
NDUFA2	2.249
SPTLC2	2.260
RAVER1	2.273
GLB1	2.280
DHRS7B	2.308

RAB18	2.331
UBE2C	2.346
FBL	2.361
SLC3A2	2.363
RBM14	2.370
SLC35F2	2.379
RBMX	2.463
ACOT13	2.468
PRKAR1A	2.473
MLEC*	2.475
NOP2	2.496
MCCC2	2.529
MYO18A	2.544
DAP3	2.569
NAT10	2.578
PRDX4	2.584
PREB	2.590
PYGB	2.685
MYO5B	2.696
NDUFS7	2.698
MRPS27	2.712
POLDIP2*	2.721
USP39	2.727
ERLIN1	2.729
TIMM17B	2.732
ATP6V1G1	2.771
SEC61A1	2.797
DNAJB1	2.805
MYO1D	2.853
MAGT1	2.853
DDX54	2.868
TMEM33	2.927
MYO19	2.938
NDUFS3	2.993
SLC2A1	3.034
ZMPSTE24	3.036
SLC38A10	3.101
RSU1	3.102
VDAC3	3.108
RBM12B	3.152
POLDIP2*	3.200
ESYT2	3.216
PARL	3.240
NDUFV1	3.242
EBP	3.256
CYP51A1	3.355
ERP44	3.372
REEP4	3.401
DDX21	3.402
ABCD3	3.432
TMEM120A	3.482
NDUFS2	3.544
FNBP4	3.552
SYVN1	3.628
WDR36	3.641
DNAJC11	3.645
DNAJC10	3.651
SSFA2	3.652
PRPSAP1	3.686
TMEM256	3.777
MLEC*	3.816
ATP13A1*	3.824
CYB5R1	3.847
PRKACB	3.883
AKAP1*	3.913
SQRDL	3.921
ZNF598	3.943
LSR	4.071
TECR	4.109
TMEM11	4.156
SMARCB1	4.159
OGT	4.184
VTA1	4.206
BMS1	4.319
TMEM48	4.336
ATAD3A	4.382
SIGMAR1	4.405
DHCR7	4.414
GGTLA4	4.449
SUPT16H	4.499
EBNA1BP2	4.542
DERL1*	4.565
SF3B6	4.582
PTCD3	4.608
PTPLAD1	4.703
DERL1*	4.724
VPS13C	4.731
DHCR24	4.772
AKAP1*	4.783
HINT2	4.806
MRPS34	4.821
SCD	4.882
AIP	5.031
LBR	5.049
MBOAT7*	5.130
BAG2	5.207
RPL7L1	5.265
GHITM	5.292
SRP54	5.320
RBM8A	5.612
ATP13A1*	5.859
COX7A2L*	6.017
YIF1A	6.141
MOGS	6.163
GTPBP4	6.359
MFSD10	6.379
JAGN1	6.383
LPCAT3	6.426
SKIV2L	6.642
GALNT2	6.808
ND5	6.984
PKP4	7.036
NUP205	7.105
RAB14	7.507
CDS2	7.631
GALK1	7.790
TPD52L2	7.829
SLC22A18	8.408
NKRF	10.247
EIF3K	10.685
LARP1	12.441
WDR46	12.648
SDHC	12.681
NFKB2	27.711
PDCD10	41.076
TMED5	100.000

Table 1. *Phosphorylated and dephosphorylated protein in 3D MDCK cysts upon PRL-3 WT overexpression. List of proteins obtained in the phosphoproteomic assay carried out in 3D MDCK cysts stably overexpressing GFP-PRL-3 WT compared to parental and GFP-PRL-3 C104S overexpressing MDCK cysts. Data was sorted according to the ratio between the phosphorylated protein in GFP-PRL-3 WT MDCK cysts and the phosphorylated protein in parental and GFP-PRL-3 C104S MDCK cysts. Dephosphosporylated proteins upon PRL-3 WT presence (red) have a ratio below 0.666 and proteins that showed an increment of their phosphorylation status upon PRL-3 overexpression (blue) have a ratio over 1.5. (*) Hits shown in 2 replicates. The experiment was performed in triplicate.*

8. References

Ai, E., Skop, A.R. (2009) Endosomal recycling regulation during cytokinesis. *Communicative and Integrative Biology*. **2**(5), 444–447.

Al-Aidaroos, A.Q.O., Zeng, Q. (2010) PRL-3 phosphatase and cancer metastasis. *Journal of cellular biochemistry*. **111**(5), 1087–98.

do Amaral, J.B., Rezende-Teixeira, P., Freitas, V.M., Machado-Santelli, G.M. (2011) MCF-7 cells as a three-dimensional model for the study of human breast cancer. *Tissue engineering. Part C, Methods*. **17**(11), 1097–107.

Anderson, R.A., Boronenkov, I. V., Doughman, S.D., Kunz, J., Loijens, J.C. (1999) Phosphatidylinositol phosphate kinases, a multifaceted family of signaling enzymes. *Journal of Biological Chemistry*. **274**(15), 9907–9910.

Ang, A.L., Taguchi, T., Francis, S., Fölsch, H., Murrells, L.J., Pypaert, M., Warren, G., Mellman, I. (2004) Recycling endosomes can serve as intermediates during transport from the Golgi to the plasma membrane of MDCK cells. *Journal of Cell Biology*. **167**(3), 531–543.

Antonescu, C.N., Aguet, F., Danuser, G., Schmid, S.L. (2011) Phosphatidylinositol-(4,5)-bisphosphate regulates clathrin-coated pit initiation, stabilization, and size. *Molecular biology of the cell*. **22**(14), 2588–600.

Apodaca, G. (2010) Opening ahead: early steps in lumen formation revealed. *Nature cell biology*. **12**(11), 1026–8.

Apodaca, G., Gallo, L.I., Bryant, D.M. (2012) Role of membrane traffic in the generation of epithelial cell asymmetry. *Nature Cell Biology*. **14**(12), 1235–1243.

Aranda, V., Nolan, M.E., Muthuswamy, S.K. (2008) Par complex in cancer: a regulator of normal cell polarity joins the dark side. *Oncogene*. **27**(55), 6878–87.

Babbey, C.M., Ahktar, N., Wang, E., Chih-Hsiung Chen, C., Grant, B.D., Dunn, K.W. (2006) Rab10 Regulates Membrane Transport through Early Endosomes of Polarized Madin-Darby Canine Kidney Cells. *Molecular Biology of the Cell*. **17**(7), 3156–3175.

Bagnat, M., Cheung, I.D., Mostov, K.E., Stainier, D.Y.R. (2007) Genetic control of single lumen formation in the zebrafish gut. *Nature cell biology*. **9**(8), 954–60.

Baker, J., Garrod, D. (1993) Epithelial cells retain junctions during mitosis. *Journal of cell science*. **104 (Pt 2**, 415–425.

Balla, T. (2013) Phosphoinositides: tiny lipids with giant impact on cell regulation. *Physiological reviews*. **93**(3), 1019–137.

Balla, T., Varnai, P., Ter (2009) Visualization of cellular phosphoinositide pools with GFP-fused protein-domains. *Current Protocols in Cell Biology*. (SUPPL. 42).

Barr, F.A., Gruneberg, U. (2007) Cytokinesis: Placing and Making the Final Cut. *Cell*. **131**(5), 847–860.

Basak, S., Jacobs, S.B.R., Krieg, A.J., Pathak, N., Zeng, Q., Kaldis, P., Giaccia, A.J., Attardi, L.D. (2008) The metastasis-associated gene Prl-3 is a p53 target involved in cell-cycle regulation. *Molecular Cell*. **30**(3), 303–314.

Bastos, R.N., Barr, F.A. (2010) Plk1 negatively regulates Cep55 recruitment to the midbody to ensure orderly abscission. *Journal of Cell Biology*. **191**(4), 751–760.

Baum, B., Georgiou, M. (2011) Dynamics of adherens junctions in epithelial establishment, maintenance, and remodeling. *The Journal of cell biology*. **192**(6), 907–917.

Bement, W.M., Miller, A.L., Von Dassow, G. (2006) Rho GTPase activity zones and transient contractile arrays. *BioEssays*. **28**(10), 983–993.

Bessette, D.C., Qiu, D., Pallen, C.J. (2008) PRL PTPs: Mediators and markers of cancer progression. *Cancer and Metastasis Reviews*. **27**(2), 231–252.

Blondeau, F., Ritter, B., Allaire, P.D., Wasiak, S., Girard, M., Hussain, N.K., Angers, A., Legendre-Guillemin, V., Roy, L., Boismenu, D., Kearney, R.E., Bell, A.W., Bergeron, J.J.M., McPherson, P.S. (2004) Tandem MS analysis of brain clathrin-coated vesicles reveals their critical involvement in synaptic vesicle recycling. *Proceedings of the National Academy of Sciences of the United States of America*. **101**(11), 3833–8.

Böcking, T., Aguet, F., Harrison, S.C., Kirchhausen, T. (2011) Single-molecule analysis of a molecular disassemblase reveals the mechanism of Hsc70-driven clathrin uncoating. *Nature structural & molecular biology*. **18**(3), 295–301.

Boersema, P.J., Raijmakers, R., Lemeer, S., Mohammed, S., Heck, A.J.R. (2009) Multiplex peptide stable isotope dimethyl labeling for quantitative proteomics. *Nature protocols*. **4**(4), 484–94.

Boivin, B., Tonks, N.K. (2010) Analysis of the redox regulation of protein tyrosine phosphatase superfamily members utilizing a cysteinyl-labeling assay. *Methods in enzymology*. **474**(10), 35–50.

Bolard, J. (1986) How do the polyene macrolide antibiotics affect the cellular membrane properties? *BBA - Reviews on Biomembranes*. **864**(3-4), 257–304.

Botelho, R.J., Teruel, M., Dierckman, R., Anderson, R., Wells, A., York, J.D., Meyer, T., Grinstein, S. (2000) Localized biphasic changes in phosphatidylinositol-4,5-bisphosphate at sites of phagocytosis. *Journal of Cell Biology*. **151**(7), 1353–1367.

Brautigan, D.L. (2013) Protein Ser/Thr phosphatases--the ugly ducklings of cell signalling. *The FEBS journal*. **280**(2), 324–45.

Brien, L.E.O., Zegers, M.M.P., Mostov, K.E. (2002) Building epithelial architecture: insights from three-dimensional culture models. *Nature Reviews Molecular Cell Biology*. **3**(July), 1–7.

Brown, J.R., Auger, K.R. (2011) Phylogenomics of phosphoinositide lipid kinases: perspectives on the evolution of second messenger signaling and drug discovery. *BMC Evolutionary Biology*. **11**(1), 4.

Bryant, D.M., Datta, A., Rodríguez-Fraticelli, A.E., Peränen, J., Martín-Belmonte, F., Mostov, K.E. (2010) A molecular network for de novo generation of the apical surface and lumen. *Nature cell biology*. **12**(11), 1035–45.

Bryant, D.M., Mostov, K.E. (2008) From cells to organs: building polarized tissue. *Nature reviews. Molecular cell biology*. **9**(11), 887–901.

Bryant, D.M., Roignot, J., Datta, A., Overeem, A.W., Kim, M., Yu, W., Peng, X., Eastburn, D.J., Ewald, A.J., Werb, Z., Mostov, K.E. (2014) A Molecular Switch for the Orientation of Epithelial Cell Polarization. *Developmental Cell*. **31**(2), 171–187.

Bucci, C., Wandinger-Ness, A., Lütcke, A., Chiariello, M., Bruni, C.B., Zerial, M. (1994) Rab5a is a common component of the apical and basolateral endocytic machinery in polarized epithelial cells. *Proceedings of the National Academy of Sciences of the United States of America*. **91**(11), 5061–5.

Bunce, M.W., Bergendahl, K., Anderson, R.A. (2006) Nuclear PI(4,5)P2: A new place for an old signal. *Biochimica et Biophysica Acta - Molecular and Cell Biology of Lipids*. **1761**(5-6), 560–569.

Bunney, T.D., Katan, M. (2010) Phosphoinositide signalling in cancer: beyond PI3K and PTEN. *Nature reviews. Cancer*. **10**(5), 342–52.

Burstein, H.J., Polyak, K., Wong, J.S., Lester, S.C., and Kaelin, C.M. (2004) Ductal Carcinoma in Situ of the Breast. *The New England Journal of Medicine*. (350), 1430–1441.

Caballe, A., Martin-Serrano, J. (2011) ESCRT machinery and cytokinesis: The road to daughter cell separation. *Traffic*. **12**(10), 1318–1326.

Caballe, A., Wenzel, D.M., Agromayor, M., Alam, S.L., Skalicky, J.J., Kloc, M., Carlton, J.G., Labrador, L., Sundquist, W.I., Martin-Serrano, J. (2015) ULK3 regulates cytokinetic abscission by phosphorylating ESCRT-III proteins. *eLife*. **4**, 1–70.

Campa, F., Randazzo, P.A. (2008) Arf GTPase-activating proteins and their potential role in cell migration and invasion. *Cell adhesion & migration*. **2**(4), 258–262.

Cao, L.G., Wang, Y.L. (1990) Mechanism of the formation of contractile ring in dividing cultured animal cells. I. Recruitment of preexisting actin filaments into the cleavage furrow. *Journal of Cell Biology*. **110**(4), 1089–1095.

Carlton, J.G., Caballe, A., Agromayor, M., Kloc, M., Martin-Serrano, J. (2012) ESCRT-III governs the Aurora B-mediated abscission checkpoint through CHMP4C. *Science (New York, N.Y.)*. **336**(6078), 220–5.

Carlton, J.G., Martin-Serrano, J. (2007) Parallels between cytokinesis and retroviral budding: a role for the ESCRT machinery. *Science (New York, N.Y.)*. **316**(5833), 1908–12.

Carmena, M., Ruchaud, S., Earnshaw, W.C., Building, M.S., Road, M. (2009) Making the Aurora glow: regulation of Aurora A and B kinase function by interacting proteins. *Current Opinion in Cell Biology*. **21**(6), 796–805.

Carracedo, A., Pandolfi, P.P. (2008) The PTEN-PI3K pathway: of feedbacks and cross-talks. *Oncogene*. **27**(41), 5527–5541.

Caswell, P.T., Chan, M., Lindsay, A.J., McCaffrey, M.W., Boettiger, D., Norman, J.C. (2008) Rab-coupling protein coordinates recycling of a5b1 integrin and EGFR1 to promote cell migration in 3D microenvironments. *Journal of Cell Biology*. **183**(1), 143–155.

Chandra, A., Grecco, H.E., Pisupati, V., Perera, D., Cassidy, L., Skoulidis, F., Ismail, S. a., Hedberg, C., Hanzal-Bayer, M., Venkitaraman, A.R., Wittinghofer, A., Bastiaens, P.I.H. (2012) The GDI-like solubilizing factor PDEδ sustains the spatial organization and signalling of Ras family proteins. *Nature Cell Biology*. **14**(2), 329–329.

Chao, W.T., Kunz, J. (2009) Focal adhesion disassembly requires clathrin-dependent endocytosis of integrins. *FEBS Letters*. **583**(8), 1337–1343.

Chassé, H., Boulben, S., Costache, V., Cormier, P., Morales, J. (2016) Analysis of translation using polysome profiling. *Nucleic acids research*. **45**(3), e15.

Chee, P.N., Pun, S.H. (2008) A perfusable 3D cell-matrix tissue culture chamber for in situ evaluation of nanoparticle vehicle penetration and transport. *Biotechnology and Bioengineering*. **99**(6), 1490–1501.

Chen, C.-T., Ettinger, A.W., Huttner, W.B., Doxsey, S.J. (2013) Resurrecting remnants: the lives of post-mitotic midbodies. *Trends in cell biology*. **23**(3), 118–28.

Chen, P.W., Jian, X., Yoon, H.Y., Randazzo, P.A. (2013) ARAP2 signals through arf6 and rac1 to control focal adhesion morphology. *Journal of Biological Chemistry*. **288**(8), 5849–5860.

Chen, X., Macara, I.G. (2005) Par-3 controls tight junction assembly through the Rac exchange factor Tiam1. *Nature cell biology*. **7**(3), 262–9.

Cheng, S.W., Tsai, H.W., Lin, Y.J., Cheng, P.N., Chang, Y.C., Yen, C.J., Huang, H.P., Chuang, Y.P., Chang, T.T., Lee, C.T., Chao, A., Chou, C.Y., Chan, S.H., Chow, N.H., Ho, C.L. (2013) Lin28B is an oncofetal circulating cancer stem cell-like marker associated with recurrence of hepatocellular carcinoma. *PLoS ONE*. **8**(11).

Choi, M.-S., Min, S.-H., Jung, H., Lee, J.D., Lee, T.H., Lee, H.K., Yoo, O.-J. (2011) The essential role of FKBP38 in regulating phosphatase of regenerating liver 3 (PRL-3) protein stability. *Biochemical and biophysical research communications*. **406**(2), 305–9.

Choi, M.S., Min, S.H., Jung, H., Lee, J.D., Lee, T.H., Lee, H.K., Yoo, O.J. (2011) The essential role of FKBP38 in regulating phosphatase of regenerating liver 3 (PRL-3) protein stability. *Biochemical and Biophysical Research Communications*. **406**(2), 305–309.

Chong, P.S.Y., Zhou, J., Cheong, L.L., Liu, S.C., Qian, J., Guo, T., Sze, S.K., Zeng, Q., Chng, W.J. (2014) LEO1 is regulated by PRL-3 and mediates its oncogenic properties in acute myelogenous leukemia. *Cancer Research*. **74**(11), 3043–3053.

Cohen, D., Rodriguez-Boulan, E., Müsch, A. (2004) Par-1 promotes a hepatic mode of apical protein trafficking in MDCK cells. *Proceedings of the National Academy of Sciences of the United States of America*. **101**(38), 13792–13797.

Cohen, P. (2002) The origins of protein phosphorylation. *Nature Cell Biology*. **4**, 127–130.

Collins, B.M., McCoy, A.J., Kent, H.M., Evans, P.R., Owen, D.J. (2002) Molecular architecture and functional model of the endocytic AP2 complex. *Cell*. **109**(4), 523–535.

Comer, F.I., Parent, C.A. (2007) Phosphoinositides specify polarity during epithelial organ development. *Cell*. **128**(2), 239–240.

Connell, J.W., Lindon, C., Luzio, J.P., Reid, E. (2009) Spastin couples microtubule severing to membrane traffic in completion of cytokinesis and secretion. *Traffic*. **10**(1), 42–56.

Cramm-Behrens, C.I., Dienst, M., Jacob, R. (2008) Apical cargo traverses endosomal compartments on the passage to the cell surface. *Traffic*. **9**(12), 2206–2220.

Cremona, O., Di Paolo, G., Wenk, M.R., Lüthi, A., Kim, W.T., Takei, K., Daniell, L., Nemoto, Y., Shears, S.B., Flavell, R.A., McCormick, D.A., De Camilli, P. (1999) Essential role of phosphoinositide metabolism in synaptic vesicle recycling. *Cell*. **99**(2), 179–188.

Czech, M.P. (2000) PIP2 and PIP3: complex roles at the cell surface. *Cell*. **100**(6), 603–606.

D'Avino, P.P. (2009) How to scaffold the contractile ring for a safe cytokinesis - lessons from Anillin-related proteins. *Journal of cell science*. **122**(Pt 8), 1071–9.

D'Avino, P.P., Capalbo, L. (2016) Regulation of midbody formation and function by mitotic kinases. *Seminars in Cell & Developmental Biology*. **53**, 57–63.

D'Souza-Schorey, C., Chavrier, P. (2006) ARF proteins: roles in membrane traffic and beyond. *Nature reviews. Molecular cell biology*. **7**(5), 347–358.

von Dassow, G. (2009) Concurrent cues for cytokinetic furrow induction in animal cells. *Trends in Cell Biology*. **19**(4), 165–173.

Datta, A., Bryant, D.M., Mostov, K.E. (2011) Molecular regulation of lumen morphogenesis. *Current biology : CB*. **21**(3), R126–36.

Debnath, J., Brugge, J.S. (2005) Modelling glandular epithelial cancers in three-dimensional cultures. *Nature reviews. Cancer*. **5**(9), 675–88.

Debnath, J., Mills, K.R., Collins, N.L., Reginato, M.J., Muthuswamy, S.K., Brugge, J.S. (2002) The role of apoptosis in creating and maintaining luminal space within normal and oncogene-expressing mammary acini. *Cell*. **111**(1), 29–40.

Debnath, J., Muthuswamy, S.K., Brugge, J.S. (2003) Morphogenesis and oncogenesis of MCF-10A mammary epithelial acini grown in three-dimensional basement membrane cultures. *Methods*. **30**(3), 256–268.

DerMardirossian, C., Bokoch, G.M. (2005) GDIs: Central regulatory molecules in Rho GTPase activation. *Trends in Cell Biology*. **15**(7), 356–363.

Desai, B. V., Harmon, R.M., Green, K.J. (2009) Desmosomes at a glance. *Journal of cell science*. **122**(24), 4401–4407.

Di-Paolo, G., De Camilli, P. (2006) Phosphoinositides in cell regulation and membrane dynamics. *Nature*. **443**(7112), 651–7.

Dickson, E.J., Jensen, J.B., Hille, B. (2014) Golgi and plasma membrane pools of PI(4)P contribute to plasma membrane PI(4,5)P2 and maintenance of KCNQ2/3 ion channel current. *Proc Natl Acad Sci U S A*. **111**(22), E2281–90.

Diepenbruck, M., Christofori, G. (2016) Epithelial-mesenchymal transition (EMT) and metastasis: Yes, no, maybe? *Current Opinion in Cell Biology*. **43**, 7–13.

Dionne, L.K., Wang, X.-J., Prekeris, R. (2015) Midbody: from cellular junk to regulator of cell polarity and cell fate. *Current opinion in cell biology*. **35**, 51–8.

Doherty, G.J., McMahon, H.T. (2009) Mechanisms of endocytosis. *Annual review of biochemistry*. **78**, 857–902.

Dong, Y., Zhang, L., Zhang, S., Bai, Y., Chen, H., Sun, X., Yong, W., Li, W., Colvin, S.C., Rhodes, S.J., Shou, W., Zhang, Z.-Y. (2012) Phosphatase of regenerating liver 2 (PRL2) is essential for placenta development by downregulating PTEN (phosphatase and tensin homologue deleted on chromosome 10) and activating Akt. *The Journal of Biological Chemistry*. **2**(Epub ahead of print), 11–15.

Duan, G., Li, X., Köhn, M. (2015) The human DEPhOsphorylation database DEPOD: a 2015 update. *Nucleic acids research*. **43**(Database issue), D531–5.

Dudek, S.M., Chiang, E.T., Camp, S.M., Guo, Y., Zhao, J., Brown, M.E., Singleton, P. a, Wang, L., Desai, A., Arce, F.T., Lal, R., Van Eyk, J.E., Imam, S.Z., Garcia, J.G.N. (2010) Clustering and Lateral Concentration of Raft Lipids by the MAL Protein. *Molecular biology of the cell*. **21**(22), 4042–4056.

Dumaual, C.M., Sandusky, G.E., Crowell, P.L., Randall, S.K. (2006) Cellular localization of PRL-1 and PRL-2 gene expression in normal adult human tissues. *The journal of histochemistry and cytochemistry : official journal of the Histochemistry Society*. **54**(12), 1401–12.

Dutta, D., Donaldson, J.G. (2012) Search for inhibitors of endocytosis: Intended specificity and unintended consequences. *Cellular logistics*. **2**(4), 203–208.

Echard, A. (2008) Membrane traffic and polarization of lipid domains during cytokinesis. *Biochem Soc Trans*. **36**(Pt 3), 395–399.

Edeling, M.A., Mishra, S.K., Keyel, P.A., Steinhauser, A.L., Collins, B.M., Roth, R., Heuser, J.E., Owen, D.J., Traub, L.M. (2006) Molecular switches involving the AP-2 β2 appendage regulate endocytic cargo selection and clathrin coat assembly. *Developmental Cell*. **10**(3), 329–342.

Eggert, U.S., Mitchison, T.J., Field, C.M. (2006) Animal cytokinesis: from parts list to mechanisms. *Annual review of biochemistry*. **75**, 543–566.

den Elzen, N., Buttery, C. V, Maddugoda, M.P., Ren, G., Yap, A.S. (2009) Cadherin Adhesion Receptors Orient the Mitotic Spindle during Symmetric Cell Division in Mammalian Epithelia. *Molecular Biology of the Cell*. **20**(16), 3740–3750.

Euteneuer, U., McIntosh, J.R. (1980) Polarity of midbody and phragmoplast microtubules. *Journal of Cell Biology*. **87**(2 I), 509–515.

Ezratty, E.J., Bertaux, C., Marcantonio, E.E., Gundersen, G.G. (2009) Clathrin mediates integrin endocytosis for focal adhesion disassembly in migrating cells. *Journal of Cell Biology*. **187**(5), 733–747.

Fahs, S., Lujan, P., Köhn, M. (2016) Approaches to study phosphatases. *ACS Chemical Biology*. **11**(11), 2944–2961.

Fang, X.-Y., Song, R., Chen, W., Yang, Y.-Y., Gu, Y.-H., Shu, Y.-Q., Wu, X.-D., Wu, X.-F., Sun, Y., Shen, Y., Xu, Q. (2015) PRL-3 Promotes the Malignant Progression of Melanoma via Triggering Dephosphorylation and Cytoplasmic Localization of NHERF1. *The Journal of investigative dermatology*. **135**(9), 1–10.

Farr, G.A., Hull, M., Mellman, I., Caplan, M.J. (2009) Membrane proteins follow multiple pathways to the basolateral cell surface in polarized epithelial cells. *Journal of Cell Biology*. **186**(2), 269–282.

Feng, W., Wu, H., Chan, L.-N., Zhang, M. (2008) Par-3-mediated junctional localization of the lipid phosphatase PTEN is required for cell polarity establishment. *The Journal of biological chemistry*. **283**(34), 23440–9.

Ferguson, S., Raimondi, A., Paradise, S., Shen, H., Mesaki, K., Ferguson, A., Destaing, O., Ko, K., Takasaki, J., Cremona, O., O' Toole, E., De Camilli, P. (2009) Coordinated actions of actin and BAR proteins upstream of dynamin at endocytic clathrin-coated pits. *Developmental Cell*. **17**(6), 811–822.

Fiordalisi, J.J., Dewar, B.J., Graves, L.M., Madigan, J.P., Cox, A.D. (2013) Src-mediated phosphorylation of the tyrosine phosphatase PRL-3 is required for PRL-3 promotion of Rho activation, motility and invasion. *PloS one*. **8**(5), e64309.

Fish, K.N. (2009) Total internal reflection fluorescence (TIRF) microscopy. *Current protocols in cytometry / editorial board, J. Paul Robinson, managing editor ... [et al.]*. **Chapter 12**(October), Unit12.18.

Fleming, E.S., Temchin, M., Wu, Q., Maggio-Price, L., Tirnauer, J.S. (2009) Spindle misorientation in tumors from APCmin/+ mice. *Molecular Carcinogenesis*. **48**(7), 592–598.

Ford, M.G.J., Mills, I.G., Peter, B.J., Vallis, Y., Praefcke, G.J.K., Evans, P.R., McMahon, H.T. (2002) Curvature of clathrin-coated pits driven by epsin. *Nature*. **419**(6905), 361–366.

Ford, M.G.J., Pearse, B., Higgins, M., Vallis, Y., Owen, D., Gibson, A., Hopkins, C., Evans, P., McMahon, H. (2001) Simultaneous binding of PtdIns(4,5)P2 and clathrin by AP180 in the nucleation of clathrin lattices on membranes. *Science*. **291**, 1051–1055.

Forte, E., Orsatti, L., Talamo, F., Barbato, G., De Francesco, R., Tomei, L. (2008) Ezrin is a specific and direct target of protein tyrosine phosphatase PRL-3. *Biochimica et biophysica acta*. **1783**(2), 334–44.

Foy, M., Anézo, O., Saule, S., Planque, N. (2017) PRL-3/PTP4A3 phosphatase regulates integrin β1 in adhesion structures during migration of human ocular melanoma cells. *Experimental Cell Research*. **353**, 88–99.

Friedl, P., Sahai, E., Weiss, S., Yamada, K.M. (2012) New dimensions in cell migration. *Nature Reviews Molecular Cell Biology*. **13**(11), 743–747.

Funato, Y., Yamazaki, D., Mizukami, S., Du, L., Kikuchi, K., Miki, H. (2014) Membrane protein CNNM4-dependent Mg2+ efflux suppresses tumor progression. *Journal of Clinical Investigation*. **124**(12), 5398–5410.

Gálvez-Santisteban, M., Rodriguez-Fraticelli, A.E., Bryant, D.M., Vergarajauregui, S., Yasuda, T., Bañón-Rodríguez, I., Bernascone, I., Datta, A., Spivak, N., Young, K., Slim, C.L., Brakeman, P.R., Fukuda, M., Mostov, K.E., Martín-Belmonte, F. (2012) Synaptotagmin-like proteins control the formation of a single apical membrane domain in epithelial cells. *Nature cell biology*. **14**(8), 838–49.

Gassama-Diagne, A., Yu, W., ter Beest, M., Martin-Belmonte, F., Kierbel, A., Engel, J., Mostov, K. (2006) Phosphatidylinositol-3,4,5-trisphosphate regulates the formation of the basolateral plasma membrane in epithelial cells. *Nature cell biology*. **8**(9), 963–70.

Geiger, T., Wehner, A., Schaab, C., Cox, J., Mann, M. (2012) Comparative proteomic analysis of eleven common cell lines reveals ubiquitous but varying expression of most proteins. *Molecular & cellular proteomics : MCP*. **11**(3), M111.014050.

Giebel, B., Wodarz, A. (2012) Notch signaling: Numb makes the difference. *Current Biology*. **22**(4).

Gloerich, M., Bianchini, J.M., Siemers, K.A., Cohen, D.J., Nelson, W.J. (2017) Cell division orientation is coupled to cell–cell adhesion by the E-cadherin/LGN complex. *Nature communications*. **8**(13996), 1–11.

Glotzer, M. (2009) The 3Ms of central spindle assembly: microtubules, motors and MAPs. *Nature reviews. Molecular cell biology*. **10**(1), 9–20.

Gonzalez, A., Rodriguez-Boulan, E. (2009) Clathrin and AP1B: Key roles in basolateral trafficking through trans-endosomal routes. *FEBS Letters*. **583**(23), 3784–3795.

Grant, B.D., Donaldson, J.G. (2009) Pathways and mechanisms of endocytic recycling. *Nature reviews. Molecular cell biology*. **10**(9), 597–608.

Green, R.A., Paluch, E., Oegema, K. (2012) Cytokinesis in animal cells. *Annual review of cell and developmental biology*. **28**, 29–58.

Gromley, A., Yeaman, C., Rosa, J., Redick, S., Chen, C.-T., Mirabelle, S., Guha, M., Sillibourne, J., Doxsey, S.J. (2005) Centriolin anchoring of exocyst and SNARE complexes at the midbody is required for secretory-vesicle-mediated abscission. *Cell*. **123**(1), 75–87.

Grönroos, T., Teppo, S., Mehtonen, J., Laukkanen, S., Liuksiala, T., Nykter, M., Heinäniemi, M., Lohi, O. (2017) Overexpression of PTP4A3 in ETV6-RUNX1 acute lymphoblastic leukemia. *Leuk Res.*. **54**, 1–6.

Guizetti, J., Gerlich, D.W. (2012) ESCRT-III polymers in membrane neck constriction. *Trends in Cell Biology*. **22**(3), 133–140.

Guo, K., Li, J., Wang, H., Osato, M., Tang, J.P., Quah, S.Y., Gan, B.Q., Zeng, Q. (2006) PRL-3 initiates tumor angiogenesis by recruiting endothelial cells in vitro and in vivo. *Cancer research*. **66**(19), 9625–35.

Guzińska-Ustymowicz, K., Pryczynicz, A. (2011) PRL-3, an emerging marker of carcinogenesis, is strongly associated with poor prognosis. *Anti-cancer agents in medicinal chemistry*. **11**(1), 99–108.

Haag, M., Schmidt, A., Sachsenheimer, T., Brügger, B. (2012) Quantification of Signaling Lipids by Nano-Electrospray Ionization Tandem Mass Spectrometry (Nano-ESI MS/MS). *Metabolites*. **2**(4), 57–76.

Hammond, G.R. V., Fischer, M.J., Anderson, K.E., Holdich, J., Koteci, A., Balla, T., Irvine, R.F. (2012) PI4P and PI(4,5)P2 Are Essential But Independent Lipid Determinants of Membrane Identity. *Science*. **337**(6095), 727–730.

Hao, Y., Du, Q., Chen, X., Zheng, Z., Balsbaugh, J.L., Maitra, S., Shabanowitz, J., Hunt, D.F., Macara, I.G. (2010) Par3 Controls Epithelial Spindle Orientation by aPKC-Mediated Phosphorylation of Apical Pins. *Current Biology*. **20**(20), 1809–1818.

Harper, C.B., Popoff, M.R., McCluskey, A., Robinson, P.J., Meunier, F.A. (2013) Targeting membrane trafficking in infection prophylaxis: Dynamin inhibitors. *Trends in Cell Biology*. **23**(2), 90–101.

Harris, T.W., Hartwieg, E., Horvitz, H.R., Jorgensen, E.M. (2000) Mutations in synaptojanin disrupt synaptic vesicle recycling. *Journal of Cell Biology*. **150**(3), 589–599.

Haucke, V., De Camilli, P. (1999) AP-2 recruitment to synaptotagmin stimulated by tyrosine-based endocytic motifs. *Science (New York, N.Y.)*. **285**(5431), 1268–71.

Helms, J.B., Rothman, J.E. (1992) Inhibition by brefeldin A of a Golgi membrane enzyme that catalyses exchange of guanine nucleotide bound to ARF. *Nature*. **360**(6402), 352–354.

Hendriks, W.J. a J., Elson, A., Harroch, S., Pulido, R., Stoker, A., den Hertog, J. (2013) Protein tyrosine phosphatases in health and disease. *The FEBS journal*. **280**(2), 708–30.

Henne, W.M., Boucrot, E., Meinecke, M., Evergren, E., Vallis, Y., Mittal, R., McMahon, H.T. (2010) FCHo proteins are nucleators of clathrin-mediated endocytosis. *Science*. **328**(5983), 1281–1284.

Henry, L., Sheff, D. (2008) Rab8 regulates basolateral secretory, but not recycling, traffic at the recycling endosome. *Molecular biology of the cell*. **19**, 2059–2068.

Hinrichsen, L., Meyerholz, A., Groos, S., Ungewickell, E.J. (2006) Bending a membrane: how clathrin affects budding. *Proceedings of the National Academy of Sciences of the United States of America*. **103**(23), 8715–20.

Hirokawa, N., Noda, Y., Tanaka, Y., Niwa, S. (2009) Kinesin superfamily motor proteins and intracellular transport. *Nature reviews. Molecular cell biology*. **10**(10), 682–96.

Hoeger, B., Diether, M., Ballester, P.J., Köhn, M. (2014) Biochemical evaluation of virtual screening methods reveals a cell-active inhibitor of the cancer-promoting phosphatases of regenerating liver. *European journal of medicinal chemistry*. **88**, 89–100.

Hofmann, I., Schlechter, T., Kuhn, C., Hergt, M., Franke, W.W. (2009) Protein p0071 – an armadillo plaque protein that characterizes a specific subtype of adherens junctions. *Journal of cell science*. **122**, 21–24.

Hollander, P. Den, Rawls, K., Tsimelzon, A., Shepherd, J., Mazumdar, A., Hill, J., Fuqua, S.A.W., Chang, J.C., Osborne, C.K., Hilsenbeck, S.G., Mills, G.B., Brown, P.H. (2016) Phosphatase PTP4A3 promotes triple-negative breast cancer growth and predicts poor patient survival. *Cancer Research*. **76**(7), 1942–1953.

Honda, A., Al-Awar, O.S., Hay, J.C., Donaldson, J.G. (2005) Targeting of Arf-1 to the early Golgi by membrin, an ER-Golgi SNARE. *Journal of Cell Biology*. **168**(7), 1039–1051.

Höning, S., Ricotta, D., Krauss, M., Späte, K., Spolaore, B., Motley, A., Robinson, M., Robinson, C., Haucke, V., Owen, D.J. (2005) Phosphatidylinositol-(4,5)-bisphosphate regulates sorting signal recognition by the clathrin-associated adaptor complex AP2. *Molecular Cell*. **18**(5), 519–531.

Hu, C.-K., Coughlin, M., Mitchison, T.J. (2012) Midbody assembly and its regulation during cytokinesis. *Molecular Biology of the Cell*. **23**(6), 1024–1034.

Humphreys, R.C., Krajewska, M., Krnacik, S., Jaeger, R., Weiher, H., Krajewski, S., Reed, J.C., Rosen, J.M. (1996) Apoptosis in the terminal endbud of the murine mammary gland: a mechanism of ductal morphogenesis. *Development*. **122**(12), 4013–4022.

Ikezoe, T., Yang, J., Nishioka, C., Tasaka, T., Taniguchi, A., Kuwayama, Y., Komatsu, N., Bandobashi, K., Togitani, K., Koeffler, H.P., Taguchi, H. (2007) A novel treatment strategy targeting Aurora kinases in acute myelogenous leukemia. *Molecular Cancer Therapeutics*. **6**(6), 1851–1857.

Ivanov, A.I., Hopkins, A.M., Brown, G.T., Gerner-Smidt, K., Babbin, B. a, Parkos, C. a, Nusrat, A. (2008) Myosin II regulates the shape of three-dimensional intestinal epithelial cysts. *Journal of cell science*. **121**(Pt 11), 1803–1814.

Jacob, R., Naim, H.Y. (2001) Apical membrane proteins are transported in distinct vesicular carriers. *Current Biology*. **11**(18), 1444–1450.

Jaffe, A.B., Kaji, N., Durgan, J., Hall, A. (2008) Cdc42 controls spindle orientation to position the apical surface during epithelial morphogenesis. *The Journal of cell biology*. **183**(4), 625–33.

Jaulin, F., Kreitzer, G. (2010) KIF17 stabilizes microtubules and contributes to epithelial morphogenesis by acting at MT plus ends with EB1 and APC. *The Journal of cell biology*. **190**(3), 443–460.

Jaulin, F., Xue, X., Rodriguez-Boulan, E., Kreitzer, G. (2007) Polarization-dependent selective transport to the apical membrane by KIF5B in MDCK cells. *Developmental cell*. **13**(4), 511–522.

Jiang, Y., Liu, X.-Q., Rajput, A., Geng, L., Ongchin, M., Zeng, Q., Taylor, G.S., Wang, J. (2011) Phosphatase PRL-3 is a direct regulatory target of TGFbeta in colon cancer metastasis. *Cancer Research*. **71**(1), 234–244.

Jinguji, Y., Ishikawa, H. (1992) Electron microscopic observations on the maintenance of the tight junction during cell division in the epithelium of the mouse small intestine. *Cell Struct Funct*. **17**(1), 27–37.

Johnson, A.E., Chen, J.S., Gould, K.L. (2013) CK1 is required for a mitotic checkpoint that delays cytokinesis. *Current Biology*. **23**(19), 1920–1926.

Jovic, M., Sharma, M., Rahajeng, J., Caplan, S. (2010) The early endosome: A busy sorting station for proteins at the crossroads. *Histology and Histopathology*. **25**(1), 99–112.

Ketel, K., Krauss, M., Nicot, A.-S., Puchkov, D., Wieffer, M., Müller, R., Subramanian, D., Schultz, C., Laporte, J., Haucke, V. (2016) A phosphoinositide conversion mechanism for exit from endosomes. *Nature*. **529**(7586), 408–412.

Kirchhausen, T., Owen, D., Harrison, S.C. (2014) Molecular structure, function, and dynamics of clathrin-mediated membrane traffic. *Cold Spring Harbor Perspectives in Biology*. **6**(5).

Kirchner, F., Schuetz, A., Boldt, L.-H., Martens, K., Dittmar, G., Haverkamp, W., Thierfelder, L., Heinemann, U., Gerull, B. (2012) Molecular insights into arrhythmogenic right ventricular cardiomyopathy caused by plakophilin-2 missense mutations. *Circulation. Cardiovascular genetics*. **5**(4), 400–11.

Kluger, R., Alagic, A. (2004) Chemical cross-linking and protein-protein interactions-a review with illustrative protocols. *Bioorganic chemistry*. **32**(6), 451–72.

Knorre, D.G., Kudryashova, N. V, Godovikova, T.S. (2009) Chemical and functional aspects of posttranslational modification of proteins. *Acta naturae*. **1**(3), 29–51.

Kosaka, T., Ikeda, K. (1983) Reversible blockage of membrane retrieval and endocytosis in the garland cell of the temperature-sensitive mutant of Drosophila melanogaster , shibirets1. *Journal of Cell Biology*. **97**, 499–507.

Krndija, D., Münzberg, C., Maass, U., Hafner, M., Adler, G., Kestler, H.A., Seufferlein, T., Oswald, F., von Wichert, G. (2012) The phosphatase of regenerating liver 3 (PRL-3) promotes cell migration through Arf-activity-dependent stimulation of integrin α5 recycling. *Journal of cell science*. **125**(Pt 16), 3883–92.

Kuo, T.-C., Chen, C.-T., Baron, D., Onder, T.T., Loewer, S., Almeida, S., Weismann, C.M., Xu, P., Houghton, J.-M., Gao, F.-B., Daley, G.Q., Doxsey, S. (2011) Midbody accumulation through evasion of autophagy contributes to cellular reprogramming and tumorigenicity. *Nature Cell Biology*. **13**(10), 1214–1223.

Kwon, S.-H., Nedvetsky, P.I., Mostov, K.E. (2011) Transcriptional profiling identifies TNS4 function in epithelial tubulogenesis. *Current biology : CB*. **21**(2), 161–6.

Laprise, P., Chailler, P., Houde, M., Beaulieu, J.-F., Boucher, M.-J., Rivard, N. (2002) Phosphatidylinositol 3-kinase controls human intestinal epithelial cell differentiation by promoting adherens junction assembly and p38 MAPK activation. *The Journal of biological chemistry*. **277**(10), 8226–8234.

Le-Roy, C., Wrana, J.L. (2005) Clathrin- and non-clathrin-mediated endocytic regulation of cell signalling. *Nature reviews. Molecular cell biology*. **6**(2), 112–26.

Lee, G.Y., Kenny, P.A., Lee, E.H., Bissell, M.J. (2007) Three-dimensional culture models of normal and malignant breast epithelial cells. *Nature methods*. **4**(4), 359–65.

Leslie, N.R., Batty, I.H., Maccario, H., Davidson, L., Downes, C.P. (2008) Understanding PTEN regulation: PIP2, polarity and protein stability. *Oncogene*. **27**(41), 5464–5476.

Leung, C.T., Brugge, J.S. (2012) Outgrowth of single oncogene-expressing cells from suppressive epithelial environments. *Nature*. **482**(7385), 410–3.

Li, D., Mangan, A., Cicchini, L., Margolis, B., Prekeris, R. (2014) FIP5 phosphorylation during mitosis regulates apical trafficking and lumenogenesis. *EMBO reports*. **15**(4), 428–437.

Li, D., Mangan, A., Cicchini, L., Margolis, B., Prekeris, R. (2014) FIP5 phosphorylation during mitosis regulates apical trafficking and lumenogenesis. *EMBO Rep.*, 1–10.

Li, X., Wilmanns, M., Thornton, J., Köhn, M. (2013) Elucidating human phosphatase-substrate networks. *Science signaling*. **6**(275), rs10.

Lian, S., Meng, L., Xing, X., Yang, Y., Qu, L., Shou, C. (2016) PRL-3 promotes cell adhesion by interacting with JAM2 in colon cancer. *Oncology Letters*. **12**(3), 1661–1666.

Liang, F., Liang, J., Wang, W.-Q., Sun, J.-P., Udho, E., Zhang, Z.-Y. (2007) PRL3 promotes cell invasion and proliferation by down-regulation of Csk leading to Src activation. *The Journal of Biological Chemistry*. **282**(8), 5413–5419.

Liberti, S., Sacco, F., Calderone, A., Perfetto, L., Iannuccelli, M., Panni, S., Santonico, E., Palma, A., Nardozza, A.P., Castagnoli, L., Cesareni, G. (2013) HuPho: The human phosphatase portal. *FEBS Journal*. **280**(2), 379–387.

Lin, D.T.S., Conibear, E. (2015) ABHD17 proteins are novel protein depalmitoylases that regulate N-Ras palmitate turnover and subcellular localization. *eLife*. **4**(DECEMBER2015).

Linder, M.E., Deschenes, R.J. (2007) Palmitoylation: policing protein stability and traffic. *Nature reviews. Molecular cell biology*. **8**(1), 74–84.

Liu, J., Fairn, G.D., Ceccarelli, D.F., Sicheri, F., Wilde, A. (2012) Cleavage furrow organization requires PIP 2-mediated recruitment of anillin. *Current Biology*. **22**(1), 64–69.

Liu, Y., Wang, Y., Yamakuchi, M., Masuda, S., Tokioka, T., Yamaoka, S., Maruyama, I., Kitajima, I. (2001) Phosphoinositide-3 kinase-PKB/Akt pathway activation is involved in fibroblast Rat-1 transformation by human T-cell leukemia virus type I tax. *Oncogene*. **20**(20), 2514–2526.

Liu, Y., Zhou, J., Chen, J., Gao, W., Le, Y., Ding, Y., Li, J. (2009) PRL-3 promotes epithelial mesenchymal transition by regulating cadherin directly. *Cancer biology & therapy*. **8**(14), 1352–1359.

Loerke, D., Mettlen, M., Schmid, S.L., Danuser, G. (2011) Measuring the hierarchy of molecular events during clathrin-mediated endocytosis. *Traffic*. **12**(7), 815–825.

Loerke, D., Mettlen, M., Yarar, D., Jaqaman, K., Jaqaman, H., Danuser, G., Schmid, S.L. (2009) Cargo and Dynamin Regulate Clathrin-Coated Pit Maturation. *PLoS Biology*. **7**(3).

Lubarsky, B., Krasnow, M.A. (2003) Tube morphogenesis: making and shaping biological tubes. *Cell*. **112**(1), 19–28.

Maacha, S., Anezo, O., Foy, M., Liot, G., Mery, L., Laurent, C., Sastre-Garau, X., Piperno-Neumann, S., Cassoux, N., Planque, N., Saule, S. (2016) Protein tyrosine phosphatase 4A3 (PTP4A3) promotes human uveal melanoma aggressiveness through membrane accumulation of matrix metalloproteinase 14 (MMP14). *Investigative Ophthalmology and Visual Science*. **57**(4), 1982–1990.

Macia, E., Ehrlich, M., Massol, R., Boucrot, E., Brunner, C., Kirchhausen, T. (2006) Dynasore, a Cell-Permeable Inhibitor of Dynamin. *Developmental Cell*. **10**(6), 839–850.

Maddox, A.S., Lewellyn, L., Desai, A., Oegema, K. (2007) Anillin and the Septins Promote Asymmetric Ingression of the Cytokinetic Furrow. *Developmental Cell*. **12**(5), 827–835.

Maehama, T. (1998) The Tumor Suppressor, PTEN/MMAC1, Dephosphorylates the Lipid Second Messenger, Phosphatidylinositol 3,4,5-Trisphosphate. *Journal of Biological Chemistry*. **273**(22), 13375–13378.

Mailleux, A.A., Overholtzer, M., Schmelzle, T., Bouillet, P., Strasser, A., Brugge, J.S. (2007) BIM regulates apoptosis during mammary ductal morphogenesis, and its absence reveals alternative cell death mechanisms. *Developmental cell*. **12**(2), 221–234.

Majerus, P.W., York, J.D. (2009) Phosphoinositide phosphatases and disease. *Journal of lipid research*. **50 Suppl**, S249–54.

Maliga, Z., Junqueira, M., Toyoda, Y., Ettinger, A., Mora-Bermúdez, F., Klemm, R.W., Vasilj, A., Guhr, E., Ibarlucea-Benitez, I., Poser, I., Bonifacio, E., Huttner, W.B., Shevchenko, A., Hyman, A.A. (2013) A genomic toolkit to investigate kinesin and myosin motor function in cells. *Nature cell biology*. **15**(3), 325–34.

Mangia, A., Saponaro, C., Malfettone, A., Bisceglie, D., Bellizzi, A., Asselti, M., Popescu, O., Reshkin, S.J., Paradiso, A., Simone, G. (2012) Involvement of nuclear NHERF1 in colorectal cancer progression. *Oncology Reports*. **28**(3), 889–894.

Margadant, C., Monsuur, H.N., Norman, J.C., Sonnenberg, A. (2011) Mechanisms of integrin activation and trafficking. *Current Opinion in Cell Biology*. **23**(5), 607–614.

Mariscal, J., Alonso-Nocelo, M., Muinelo-Romay, L., Barbazan, J., Vieito, M., Abalo, A., Gomez-Tato, A., Maria de Los Angeles, C. de C., Garcia-Caballero, T., Rodriguez, C., Brozos, E., Baron, F., Lopez-Lopez, R., Abal, M. (2016) Molecular Profiling of Circulating Tumour Cells Identifies Notch1 as a Principal Regulator in Advanced Non-Small Cell Lung Cancer. *Scientific reports*. **6**, 37820.

Martin, B., Pallen, C.J., Wang, J.H., Graves, D.J. (1985) Use of fluorinated tyrosine phosphates to probe the substrate specificity of the low molecular weight phosphatase activity of calcineurin. *The Journal of biological chemistry*. **260**(28), 14932–14937.

Martin, B.R., Wang, C., Adibekian, A., Tully, S.E., Cravatt, B.F. (2011) Global profiling of dynamic protein palmitoylation. *Nature Methods*. **9**(1), 84–89.

Martin-Belmonte, F., Gassama, A., Datta, A., Yu, W., Rescher, U., Gerke, V., Mostov, K. (2007) PTEN-mediated apical segregation of phosphoinositides controls epithelial morphogenesis through Cdc42. *Cell*. **128**(2), 383–97.

Martinez-Garay, I., Rustom, A., Gerdes, H.-H., Kutsche, K. (2006) The novel centrosomal associated protein CEP55 is present in the spindle midzone and the midbody. *Genomics*. **87**(2), 243–53.

Matter, K., Balda, M.S. (2003) Signalling to and from tight junctions. *Nature Reviews Molecular Cell Biology*. **4**(3), 225–36.

Matter, W.F., Estridge, T., Zhang, C., Belagaje, R., Stancato, L., Dixon, J., Johnson, B., Bloem, L., Pickard, T., Donaghue, M., Acton, S., Jeyaseelan, R., Kadambi, V., Vlahos, C.J. (2001) Role of PRL-3, a human muscle-specific tyrosine phosphatase, in angiotensin-II signaling. *Biochemical and biophysical research communications*. **283**(5), 1061–8.

Mattheyses, A.L., Simon, S.M., Rappoport, J.Z. (2010) Imaging with total internal reflection fluorescence microscopy for the cell biologist. *Journal of cell science*. **123**(Pt 21), 3621–8.

Mattila, P.E., Youker, R.T., Mo, D., Bruns, J.R., Cresawn, K.O., Hughey, R.P., Ihrke, G., Weisz, O.A. (2012) Multiple Biosynthetic Trafficking Routes for Apically Secreted Proteins in MDCK Cells. *Traffic*. **13**(3), 433–442.

Mayor, S., Pagano, R.E. (2007) Pathways of clathrin-independent endocytosis. *Nat Rev Mol Cell Biol*. **8**(8), 603–612.

McCaffrey, L.M., Macara, I.G. (2011) Epithelial organization, cell polarity and tumorigenesis. *Trends in cell biology*. **21**(12), 727–35.

McCaffrey, L.M., Macara, I.G. (2009) Widely conserved signaling pathways in the establishment of cell polarity. *Cold Spring Harbor perspectives in biology*. **1**(2), a001370.

McCart, A.E., Mahony, D., Rothnagel, J. a (2003) Alternatively spliced products of the human kinesin light chain 1 (KNS2) gene. *Traffic (Copenhagen, Denmark)*. **4**(8), 576–580.

McLaughlin, S., Wang, J., Gambhir, A., Murray, D. (2002) PIP2 and proteins: interactions, organization, and information flow. *Annual Review of Biophysics and Biomolecular Structure*. **31**, 151–75.

McMahon, H.T., Boucrot, E. (2011) Molecular mechanism and physiological functions of clathrin-mediated endocytosis. *Nature reviews. Molecular cell biology*. **12**(8), 517–533.

McNamara, C.R., Degterev, A. (2011) Small-molecule inhibitors of the PI3K signaling network. *Future medicinal chemistry*. **3**(5), 549–65.

McParland, V., Varsano, G., Li, X., Thornton, J., Baby, J., Aravind, A., Meyer, C., Pavic, K., Rios, P., Köhn, M. (2011) The metastasis-promoting phosphatase PRL-3 shows activity toward phosphoinositides. *Biochemistry*. **50**(35), 7579–90.

McPherson, P., Ritter, B., Wendland, B. (2013) Clathrin-Mediated Endocytosis. In: Madame Curie Bioscience Database [Internet]. Austin (TX): *Landes Bioscience*, 2000–2013.

Meder, D., Shevchenko, A., Simons, K., Füllekrug, J. (2005) Gp135/podocalyxin and NHERF-2 participate in the formation of a preapical domain during polarization of MDCK cells. *The Journal of cell biology*. **168**(2), 303–313.

Mele, M., Ferreira, P.G., Reverter, F., DeLuca, D.S., Monlong, J., Sammeth, M., Young, T.R., Goldmann, J.M., Pervouchine, D.D., Sullivan, T.J., Johnson, R., Segre, A. V., Djebali, S., Niarchou, A., Consortium, T.G., Wright, F. a., Lappalainen, T., Calvo, M., Getz, G., Dermitzakis, E.T., Ardlie, K.G., Guigo, R. (2015) The human transcriptome across tissues and individuals. *Science*. **348**(6235), 660–665.

Mellman, D.L., Gonzales, M.L., Song, C., Barlow, C.A., Wang, P., Kendziorski, C., Anderson, R.A. (2008) A PtdIns4,5P2-regulated nuclear poly(A) polymerase controls expression of select mRNAs. *Nature*. **451**(7181), 1013–1017.

Mellman, I., Nelson, W. (2008) Coordinated protein sorting, targeting and distribution in polarized cells. *Nat Rev Mol Cell Biol*. **9**(11), 833–845.

Mendes Pinto, I., Rubinstein, B., Li, R. (2013) Force to divide: Structural and mechanical requirements for actomyosin ring contraction. *Biophysical Journal*. **105**(3), 547–554.

Miller, SG., Carnell, L., Moore, HH.(1992) Post-Golgi membrane traffic: brefeldin A inhibits export from distal Golgi compartments to the cell surface but not recycling. *J Cell Biol.*. **118**(2), 267–83.

Min, S.-H., Kim, D.M., Heo, Y.-S., Kim, H.M., Kim, I.-C., Yoo, O.-J. (2010) Downregulation of p53 by phosphatase of regenerating liver 3 is mediated by MDM2 and PIRH2. *Life Sciences*. **86**(1-2), 66–72.

Ming, J., Liu, N., Gu, Y., Qiu, X., Wang, E.-H. (2009) PRL-3 facilitates angiogenesis and metastasis by increasing ERK phosphorylation and up-regulating the levels and activities of Rho-A/C in lung cancer. *Pathology*. **41**(2), 118–26.

Mishra, R., Grzybek, M., Niki, T., Hirashima, M., Simons, K. (2010) Galectin-9 trafficking regulates apical-basal polarity in Madin-Darby canine kidney epithelial cells. *Proceedings of the National Academy of Sciences of the United States of America*. **107**(41), 17633–8.

Mizuuchi, E., Semba, S., Kodama, Y., Yokozaki, H. (2009) Down-modulation of keratin 8 phosphorylation levels by PRL-3 contributes to colorectal carcinoma progression. *International journal of cancer*. **124**(8), 1802–10.

Morais-de-Sá, E., Sunkel, C. (2013) Adherens junctions determine the apical position of the midbody during follicular epithelial cell division. *EMBO reports*. **14**(8), 696–703.

Moravec, R., Conger, K.K., D'Souza, R., Allison, A.B., Casanova, J.E. (2012) BRAG2/GEP100/IQSec1 interacts with clathrin and regulates ??5??1 integrin endocytosis through activation of ADP ribosylation factor 5 (Arf5). *Journal of Biological Chemistry*. **287**(37), 31138–31147.

Morfini, G., Szebenyi, G., Elluru, R., Ratner, N., Brady, S.T. (2002) Glycogen synthase kinase 3 phosphorylates kinesin light chains and negatively regulates kinesin-based motility. *EMBO Journal*. **21**(3), 281–293.

Morita, E. (2012) Differential requirements of mammalian ESCRTs in multivesicular body formation, virus budding and cell division. *FEBS Journal*. **279**(8), 1399–1406.

Nagano, M., Hoshino, D., Koshikawa, N., Akizawa, T., Seiki, M. (2012) Turnover of focal adhesions and cancer cell migration. *International Journal of Cell Biology*.

Nagaraj, N., Wisniewski, J.R., Geiger, T., Cox, J., Kircher, M., Kelso, J., Pääbo, S., Mann, M. (2011) Deep proteome and transcriptome mapping of a human cancer cell line. *Molecular systems biology*. **7**(548), 548.

Nakatsu, F., Perera, R.M., Lucast, L., Zoncu, R., Domin, J., Gertler, F.B., Toomre, D., De Camilli, P. (2010) The inositol 5-phosphatase SHIP2 regulates endocytic clathrin-coated pit dynamics. *Journal of Cell Biology*. **190**(3), 307–315.

Nakayama, N., Yamashita, K., Tanaka, T., Kawamata, H., Ooki, A., Sato, T., Nakamura, T., Watanabe, M. (2016) Genomic gain of the PRL-3 gene may represent poor prognosis of primary colorectal cancer, and associate with liver metastasis. *Clinical and Experimental Metastasis*. **33**(1), 3–13.

Neisch, A.L., Fehon, R.G. (2011) Ezrin, Radixin and Moesin: key regulators of membrane-cortex interactions and signaling. *Current Opinion in Cell Biology*. **23**(4), 377–382.

Neto, H., Collins, L.L., Gould, G.W. (2011) Vesicle trafficking and membrane remodelling in cytokinesis. *The Biochemical journal*. **437**(1), 13–24.

Nishimura, A., Linder, M.E. (2013) Identification of a novel prenyl and palmitoyl modification at the CaaX motif of Cdc42 that regulates RhoGDI binding. *Molecular and Cellular Biology*. **33**(7), 1417–1429.

Noatynska, A., Gotta, M., Meraldi, P. (2012) Mitotic spindle (DIS)orientation and DISease: cause or consequence? *The Journal of cell biology*. **199**(7), 1025–35.

Noda, Y., Okada, Y., Saito, N., Setou, M., Xu, Y., Zhang, Z., Hirokawa, N. (2001) KIFC3, a microtubule minus end-directed motor for the apical transport of annexin XIIIb-associated Triton-insoluble membranes. *The Journal of cell biology*. **155**(1), 77–88.

Orsatti, L., Forte, E., Tomei, L., Caterino, M., Pessi, A., Talamo, F. (2009) 2-D Difference in gel electrophoresis combined with Pro-Q Diamond staining: a successful approach for the identification of kinase/phosphatase targets. *Electrophoresis*. **30**(14), 2469–2476.

Overeem, A.W., Bryant, D.M., van IJzendoorn, S.C.D. (2015) Mechanisms of apical-basal axis orientation and epithelial lumen positioning. *Trends in cell biology*. **25**(8), 476–85.

Özbalci, C., Sachsenheimer, T., Brügger, B. (2013) Quantitative analysis of cellular lipids by nano-electrospray ionization mass spectrometry. *Methods in molecular biology (Clifton, N.J.)*. **1033**, 3–20.

Ozkucur, N., Perike, S., Sharma, P., Funk, R.H.W. (2011) Persistent directional cell migration requires ion transport proteins as direction sensors and membrane potential differences in order to maintain directedness. *BMC cell biology*. **12**, 4.

Parmar, H.B., Barry, C., Duncan, R. (2014) Polybasic trafficking signal mediates golgi export, ER retention or ER export and retrieval based on membrane-proximity. *PLoS ONE*. **9**(4).

Patterson, K.I., Brummer, T., Brien, P.M.O., Daly, R.J. (2009) Dual-specificity phosphatases : critical regulators with diverse cellular targets. *Biochemstry journal*. **418**(3), 475–489.

Paul, N.R., Jacquemet, G., Caswell, P.T. (2015) Endocytic Trafficking of Integrins in Cell Migration. *Current Biology*. **25**(22), R1092–R1105.

Pavicic-Kaltenbrunner, V., Mishima, M., Glotzer, M. (2007) Cooperative assembly of CYK-4/MgcRacGAP and ZEN-4/MKLP1 to form the centralspindlin complex. *Mol Biol Cell*. **18**(12), 4992–5003.

Pease, J.C., Tirnauer, J.S. (2011) Mitotic spindle misorientation in cancer - out of alignment and into the fire. *Journal of Cell Science*. **124**(7), 1007–1016.

Pease, J.C., Tirnauer, J.S. (2011) Mitotic spindle misorientation in cancer--out of alignment and into the fire. *Journal of cell science*. **124**(Pt 7), 1007–16.

Peng, L., Jin, G., Wang, L., Guo, J., Meng, L., Shou, C. (2006) Identification of integrin alpha1 as an interacting protein of protein tyrosine phosphatase PRL-3. *Biochemical and Biophysical Research Communications*. **342**(1), 179–183.

Peng, L., Xing, X., Li, W., Qu, L., Meng, L., Lian, S., Jiang, B., Wu, J., Shou, C. (2009) PRL-3 promotes the motility, invasion, and metastasis of LoVo colon cancer cells through PRL-3-integrin β1-ERK1/2 and-MMP2 signaling. *Molecular Cancer*. **8**, 110.

Petrie, R.J., Doyle, A.D., Yamada, K.M. (2009) Random versus directionally persistent cell migration. *Nature reviews. Molecular cell biology*. **10**(8), 538–49.

Piekny, A., Werner, M., Glotzer, M. (2005) Cytokinesis: Welcome to the Rho zone. *Trends in Cell Biology*. **15**(12), 651–658.

Piekny, A.J., Glotzer, M. (2008) Anillin Is a Scaffold Protein That Links RhoA, Actin, and Myosin during Cytokinesis. *Current Biology*. **18**(1), 30–36.

Piekny, A.J., Maddox, A.S. (2010) The myriad roles of Anillin during cytokinesis. *Seminars in Cell and Developmental Biology*. **21**(9), 881–891.

De Pinto, V., Messina, A., Lane, D.J.R., Lawen, A. (2010) Voltage-dependent anion-selective channel (VDAC) in the plasma membrane. *FEBS Letters*. **584**(9), 1793–1799.

Polacheck, W.J., Zervantonakis, I.K., Kamm, R.D. (2013) Tumor cell migration in complex microenvironments. *Cellular and Molecular Life Sciences*. **70**(8), 1335–1356.

Pollarolo, G., Schulz, J.G., Munck, S., Dotti, C.G. (2011) Cytokinesis remnants define first neuronal asymmetry in vivo. *Nature neuroscience*. **14**(12), 1525–33.

Polo, S., Pece, S., Di Fiore, P.P. (2004) Endocytosis and cancer. *Current Opinion in Cell Biology*. **16**(2), 156–161.

Posor, Y., Eichhorn-Gruenig, M., Puchkov, D., Schöneberg, J., Ullrich, A., Lampe, A., Müller, R., Zarbakhsh, S., Gulluni, F., Hirsch, E., Krauss, M., Schultz, C., Schmoranzer, J., Noé, F., Haucke, V. (2013) Spatiotemporal control of endocytosis by phosphatidylinositol-3,4-bisphosphate. *Nature*. **499**, 233–7.

Posor, Y., Eichhorn-Grünig, M., Haucke, V. (2015) Phosphoinositides in endocytosis. *Biochimica et Biophysica Acta - Molecular and Cell Biology of Lipids*. **1851**(6), 794–804.

Pulido, R., Stoker, A.W., Hendriks, W.J.A.J. (2013) PTPs emerge as PIPs: protein tyrosine phosphatases with lipid-phosphatase activities in human disease. *Human molecular genetics*. **22**(R1), R66–76.

Qu, Y., Han, B., Yu, Y., Yao, W., Bose, S., Karlan, B.Y., Giuliano, A.E., Cui, X. (2015) Evaluation of MCF10A as a reliable model for normal human mammary epithelial cells. *PLoS ONE*. **10**(7).

Ragkousi, K., Gibson, M.C. (2014) Cell division and the maintenance of epithelial order. *Journal of Cell Biology*. **207**(2), 181–188.

Ren, T., Jiang, B., Xing, X., Dong, B., Peng, L., Meng, L., Xu, H., Shou, C. (2009) Prognostic significance of phosphatase of regenerating liver-3 expression in ovarian cancer. *Pathology and Oncology Research*. **15**(4), 555–560.

Rios, P., Li, X., Köhn, M. (2013) Molecular mechanisms of the PRL phosphatases. *The FEBS journal*. **280**(2), 505–24.

Ríos, P., Nunes-Xavier, C.E., Tabernero, L., Köhn, M., Pulido, R. (2014) Dual-specificity phosphatases as molecular targets for inhibition in human disease. *Antioxidants & redox signaling*. **20**(14), 2251–73.

Robinson, M.S. (2004) Adaptable adaptors for coated vesicles. *Trends in Cell Biology*. **14**(4), 167–174.

Rodríguez-Fraticelli, A.E., Bagwell, J., Bosch-Fortea, M., Boncompain, G., Reglero-Real, N., García-León, M.J., Andrés, G., Toribio, M.L., Alonso, M.A., Millán, J., Perez, F., Bagnat, M., Martín-Belmonte, F. (2015) Developmental regulation of apical endocytosis controls epithelial patterning in vertebrate tubular organs. *Nature cell biology*. **17**(3), 241–50.

Rodriguez-Fraticelli, A.E., Vergarajauregui, S., Eastburn, D.J., Datta, A., Alonso, M.A., Mostov, K., Martín-Belmonte, F. (2010) The Cdc42 GEF Intersectin 2 controls mitotic spindle orientation to form the lumen during epithelial morphogenesis. *The Journal of cell biology*. **189**(4), 725–38.

Roignot, J., Peng, X., Mostov, K. (2013) Polarity in mammalian epithelial morphogenesis. *Cold Spring Harbor perspectives in biology*. **5**, a013789.

Romá-Mateo, C., Raththagala, M., Gentry, M., Sanz, P. (2016) Assessing the Biological Activity of the Glucan Phosphatase Laforin. *Methods Mol Biol*. **1447**, 107–119.

Roskoski, R. (2004) Src protein-tyrosine kinase structure and regulation. *Biochemical and Biophysical Research Communications*. **324**(4), 1155–1164.

Rothberg, K.G., Heuser, J.E., Donzell, W.C., Ying, Y.-S., Glenney, J.R., Anderson, R.G.W. (1992) Caveolin, a protein component of caveolae membrane coats. *Cell*. **68**(4), 673–682.

Rothberg, K.G., Ying, Y.S., Kamen, B.A., Anderson, R.G.W. (1990) Cholesterol controls the clustering of the glycophospholipid-anchored membrane receptor for 5-methyltetrahydrofolate. *Journal of Cell Biology*. **111**(6 PART 2), 2931–2938.

Rouleau, C., Roy, A., St Martin, T., Dufault, M.R., Boutin, P., Liu, D., Zhang, M., Puorro-Radzwill, K., Rulli, L., Reczek, D., Bagley, R., Byrne, A., Weber, W., Roberts, B., Klinger, K., Brondyk, W., Nacht, M., Madden, S., Burrier, R., Shankara, S., Teicher, B. a (2006) Protein tyrosine phosphatase PRL-3 in malignant cells and endothelial cells: expression and function. *Molecular cancer therapeutics*. **5**(2), 219–29.

Le Roy, C., Wrana, J.L. (2005) Clathrin- and non-clathrin-mediated endocytic regulation of cell signalling. *Nature reviews. Molecular cell biology*. **6**(2), 112–26.

Rubio, T., Köhn, M. (2016) Regulatory mechanisms of phosphatase of regenerating liver (PRL)-3. *Biochem Soc Trans*. **44**(5), 1305–1312. DOI: 10.1042/BST20160146

Ruchaud, S., Carmena, M., Earnshaw, W.C. (2007) Chromosomal passengers: conducting cell division. *Nat Rev Mol Cell Biol*. **8**(10), 798–812.

Saarikangas, J., Zhao, H., Lappalainen, P. (2010) Regulation of the actin cytoskeleton-plasma membrane interplay by phosphoinositides. *Physiological Reviews*. **90**(1), 259–289.

Saffarian, S., Cocucci, E., Kirchhausen, T. (2009) Distinct dynamics of endocytic clathrin-coated pits and coated plaques. *PLoS Biology*. **7**(9).

Saha, S., Bardelli, A., Buckhaults, P., Velculescu, V.E., Rago, C., St Croix, B., Romans, K.E., Choti, M.A., Lengauer, C., Kinzler, K.W., Vogelstein, B. (2001) A Phosphatase Associated with Metastasis of Colorectal Cancer formed global gene expression profiles of. *Science*. **294**(5545), 1343–1346.

Sakurai, A., Jian, X., Lee, C.J., Manavski, Y., Chavakis, E., Donaldson, J., Randazzo, P.A., Gutkind, J.S. (2011) Phosphatidylinositol-4-phosphate 5-kinase and GEP100/Brag2 protein mediate antiangiogenic signaling by semaphorin 3E-plexin-D1 through Arf6 protein. *Journal of Biological Chemistry*. **286**(39), 34335–34345.

Schlossman, D.M., Schmid, S.L., Braell, W.A., Rothman, J.E. (1984) An enzyme that removes clathrin coats: Purification of an uncoating ATPase. *Journal of Cell Biology*. **99**(2), 723–733.

Schlu, M.A., Pfarr, C.S., Pieczynski, J., Whiteman, E.L., Hurd, T.W., Fan, S., Liu, C., Margolis, B. (2009) Trafficking of Crumbs3 during Cytokinesis Is Crucial for Lumen Formation. *Mol. Biol. Cell*. **20**, 4652–4663.

Schlüter, M.A., Margolis, B. (2009) Apical lumen formation in renal epithelia. *Journal of the American Society of Nephrology : JASN*. **20**(7), 1444–52.

Schlüter, M.A., Pfarr, C.S., Pieczynski, J., Whiteman, E.L., Hurd, T.W., Fan, S., Liu, C.-J., Margolis, B. (2009) Trafficking of Crumbs3 during cytokinesis is crucial for lumen formation. *Molecular biology of the cell*. **20**(22), 4652–63.

Schmid, I., Sakamoto, K.M. (2001) Analysis of DNA content and green fluorescent protein expression. *Current protocols in cytometry / editorial board, J. Paul Robinson, managing editor ... [et al.]*. **Chapter 7**, Unit 7.16.

Schmid, S.L., Mettlen, M. (2013) Cell biology: Lipid switches and traffic control. *Nature*. **499**(7457), 161–2.

Schramp, M., Hedman, A., Li, W., Tan, X., Anderson, R. (2015) PIP kinases from the cell membrane to the nucleus. *Sub-Cellular Biochemistry*. **58**, 25–59.

Seifried, A., Schultz, J., Gohla, A. (2013) Human HAD phosphatases: Structure, mechanism, and roles in health and disease. *FEBS Journal*. **280**(2), 549–571.

Semba, S., Mizuuchi, E., Yokozaki, H. (2010) Requirement of phosphatase of regenerating liver-3 for the nucleolar localization of nucleolin during the progression of colorectal carcinoma. *Cancer Science*. **101**(10), 2254–2261.

Shahbazi, M.N., Perez-Moreno, M. (2015) Connections between cadherin-catenin proteins, spindle misorientation, and cancer. *Tissue Barriers*. **3**(3), e1045684.

Sharma, N., Low, S.H., Misra, S., Pallavi, B., Weimbs, T. (2006) Apical targeting of syntaxin 3 is essential for epithelial cell polarity. *The Journal of cell biology*. **173**(6), 937–948.

Shattil, S.J., Kim, C., Ginsberg, M.H. (2010) The final steps of integrin activation: the end game. *Nature Reviews Molecular Cell Biology*. **11**(4), 288–300.

Shewan, A., Eastburn, D.J., Mostov, K. (2011) Phosphoinositides in cell architecture. *Cold Spring Harbor perspectives in biology*. **3**(8), a004796.

Shi, Y. (2009) Serine/Threonine Phosphatases: Mechanism through Structure. *Cell*. **139**(3), 468–484.

Shoshan-Barmatz, V., Ben-Hail, D. (2012) VDAC, a multi-functional mitochondrial protein as a pharmacological target. *Mitochondrion*. **12**(1), 24–34.

Shukla, A.K., Westfield, G.H., Xiao, K., Reis, R.I., Huang, L.-Y., Tripathi-Shukla, P., Qian, J., Li, S., Blanc, A., Oleskie, A.N., Dosey, A.M., Su, M., Liang, C.-R., Gu, L.-L., Shan, J.-M., Chen, X., Hanna, R., Choi, M., Yao, X.J., Klink, B.U., Kahsai, A.W., Sidhu, S.S., Koide, S., Penczek, P. a., Kossiakoff, A. a., Woods Jr, V.L., Kobilka, B.K., Skiniotis, G., Lefkowitz, R.J. (2014) Visualization of arrestin recruitment by a G-protein-coupled receptor. *Nature*. **512**(7513), 218–222.

Singh, R.D., Puri, V., Valiyaveettil, J.T., Marks, D.L., Bittman, R., Pagano, R.E. (2003) Selective caveolin-1-dependent endocytosis of glycosphingolipids. *Molecular biology of the cell*. **14**(8), 3254–3265.

Skinner, A.L., Vartia, A. a, Williams, T.D., Laurence, J.S. (2009) Enzyme activity of phosphatase of regenerating liver is controlled by the redox environment and its C-terminal residues. *Biochemistry*. **48**(20), 4262–72.

Skretting, G., Torgersen, M.L., van Deurs, B., Sandvig, K. (1999) Endocytic mechanisms responsible for uptake of GPI-linked diphtheria toxin receptor. *Journal of cell science*. **112 (Pt 2**, 3899–909.

Van der Sluijs, P., Bennett, M.K., Antony, C., Simons, K., Kreis, T.E. (1990) Binding of exocytic vesicles from MDCK cells to microtubules in vitro. *Journal of cell science*. **95 (Pt 4)**, 545–53.

Snider, J. (2013) Overview of Post-Translational Modifications (PTMs). *Thermo Scientific*.

Song, M.S., Salmena, L., Pandolfi, P.P. (2012) The functions and regulation of the PTEN tumour suppressor. *Nature Reviews Molecular Cell Biology*. **13**(5), 283–296.

Spangenberg, L., Shigunov, P., Abud, A.P.R., Cofré, A.R., Stimamiglio, M.A., Kuligovski, C., Zych, J., Schittini, A. V., Costa, A.D.T., Rebelatto, C.K., Brofman, P.R.S., Goldenberg, S., Correa, A., Naya, H., Dallagiovanna, B. (2013) Polysome profiling shows extensive posttranscriptional regulation during human adipocyte stem cell differentiation into adipocytes. *Stem Cell Research*. **11**(2), 902–912.

Spano, D., Heck, C., De Antonellis, P., Christofori, G., Zollo, M. (2012) Molecular networks that regulate cancer metastasis. *Seminars in Cancer Biology*. **22**(3), 234–249.

St Johnston, D., Ahringer, J. (2010) Cell polarity in eggs and epithelia: parallels and diversity. *Cell*. **141**(5), 757–74.

Standaert, M.L., Bandyopadhyay, G., Farese, R. (1995) Studies with wortmannin suggest a role for phosphatidylinositol 3-kinase in the activation of glycogen synthase and mitogen-activated protein kinase by insulin in rat adipocytes: comparison of insulin and protein kinase C modulators. *Biochem Biophys Res Commun.*. **209**(3), 1082–1088.

Stechly, L., Morelle, W., Dessein, A.F., Andr??, S., Grard, G., Trinel, D., Dejonghe, M.J., Leteurtre, E., Drobecq, H., Trugnan, G., Gabius, H.J., Huet, G. (2009) Galectin-4-regulated delivery of glycoproteins to the brush border membrane of enterocyte-like cells. *Traffic*. **10**(4), 438–450.

Steigemann, P., Gerlich, D.W. (2009) Cytokinetic abscission: cellular dynamics at the midbody. *Trends in cell biology*. **19**(11), 606–16.

Steigemann, P., Wurzenberger, C., Schmitz, M.H.A., Held, M., Guizetti, J., Maar, S., Gerlich, D.W. (2009) Aurora B-mediated abscission checkpoint protects against tetraploidization. *Cell*. **136**(3), 473–84.

Stephens, B.J., Han, H., Gokhale, V., Von Hoff, D.D. (2005) PRL phosphatases as potential molecular targets in cancer. *Molecular cancer therapeutics*. **4**(11), 1653–61.

Stimpson, H.E.M., Toret, C.P., Cheng, A.T., Pauly, B.S., Drubin, D.G. (2009) Early-arriving Syp1p and Ede1p function in endocytic site placement and formation in budding yeast. *Molecular biology of the cell*. **20**(22), 4640–51.

Sun, F., Li, W., Wang, L., Jiao, C. (2017) Expression of phosphatase of regenerating liver-3 is associated with prognosis of Wilms tumor. *Onco Targets Ther.*. **10**, 311–317.

Sun, J.-P., Luo, Y., Yu, X., Wang, W.-Q., Zhou, B., Liang, F., Zhang, Z.-Y. (2007) Phosphatase activity, trimerization, and the C-terminal polybasic region are all required for PRL1-mediated cell growth and migration. *The Journal of biological chemistry*. **282**(39), 29043–51.

Sun, Y., Carroll, S., Kaksonen, M., Toshima, J.Y., Drubin, D.G. (2007) PtdIns(4,5)P2 turnover is required for multiple stages during clathrin- and actin-dependent endocytic internalization. *Journal of Cell Biology*. **177**(2), 355–367.

Suzuki, A., Ohno, S. (2006) The PAR-aPKC system: lessons in polarity. *Journal of cell science*. **119**(Pt 6), 979–87.

Sweitzer, S.M., Hinshaw, J.E. (1998) Dynamin undergoes a GTP-dependent conformational change causing vesiculation. *Cell*. **93**(6), 1021–1029.

Takada, Y., Ye, X., Simon, S. (2007) The integrins. *Genome Biology*. **8**(5), 215.

Tamguney, T., Stokoe, D. (2007) New insights into PTEN. *Journal of cell science*. **120**(Pt 23), 4071–9.

Teckchandani, A., Toida, N., Goodchild, J., Henderson, C., Watts, J., Wollscheid, B., Cooper, J.A. (2009) Quantitative proteomics identifies a Dab2/integrin module regulating cell migration. *Journal of Cell Biology*. **186**(1), 99–111.

Thapa, N., Anderson, R.A. (2012) PIP2 signaling, an integrator of cell polarity and vesicle trafficking in directionally migrating cells. *Cell Adhesion and Migration*. **6**(5), 409–412.

Tian, W., Qu, L., Meng, L., Liu, C., Wu, J., Shou, C. (2012) Phosphatase of regenerating liver-3 directly interacts with integrin β1 and regulates its phosphorylation at tyrosine 783. *BMC biochemistry*. **13**(1), 22.

Tonks, N.K. (2013) Protein tyrosine phosphatases - From housekeeping enzymes to master regulators of signal transduction. *FEBS Journal*. **280**(2), 346–378.

Tonks, N.K. (2006) Protein tyrosine phosphatases: from genes, to function, to disease. *Nature reviews. Molecular cell biology*. **7**(11), 833–846.

Tonks, N.K. (2003) PTP1B: From the sidelines to the front lines! *FEBS Letters*. **546**(1), 140–148.

Torkko, J.M., Manninen, A., Schuck, S., Simons, K. (2008) Depletion of apical transport proteins perturbs epithelial cyst formation and ciliogenesis. *Journal of cell science*. **121**(Pt 8), 1193–1203.

Townley, A. K., Schmidt, K., Hodgson, L., Stephens, D.J. (2012) Epithelial organization and cyst lumen expansion require efficient Sec13-Sec31-driven secretion. *Journal of Cell Science*. **125**(3), 673–684.

Traub, L.M. (2009) Tickets to ride: selecting cargo for clathrin-regulated internalization. *Nature reviews. Molecular cell biology*. **10**(9), 583–96.

Tremblay, M.L. (2009) The PTP family photo album. *Cell*. **136**(2), 213–4.

Treyer, A., Müsch, A. (2013) Hepatocyte Polarity. *Comprehensive Physiology*. **3**(1), 243–287.

Ungewickell, E., Ungewickell, H., Holstein, S.E., Lindner, R., Prasad, K., Barouch, W., Martin, B., Greene, L.E., Eisenberg, E. (1995) Role of auxilin in uncoating clathrin-coated vesicles. *Nature*. **378**(6557), 632–5.

Vagnoni, A., Rodriguez, L., Manser, C., De Vos, K.J., Miller, C.C.J. (2011) Phosphorylation of Kinesin Light Chain 1 at Serine 460 Modulates Binding and Trafficking of Calsyntenin-1. *Journal of Cell Science*. **124**, 1032–1042.

Vandsemb, E.N., Bertilsson, H., Abdollahi, P., Størkersen, Ø., Våtsveen, T.K., Rye, M.B., Rø, T.B., Børset, M., Slørdahl, T.S. (2016) Phosphatase of regenerating liver 3 (PRL-3) is overexpressed in human prostate cancer tissue and promotes growth and migration. *Journal of translational medicine*. **14**, 71.

Varnai, P., Thyagarajan, B., Rohacs, T., Balla, T. (2006) Rapidly inducible changes in phosphatidylinositol 4,5-bisphosphate levels influence multiple regulatory functions of the lipid in intact living cells. *The Journal of cell biology*. **175**(3), 377–82.

Vernia, S., Solaz-Fuster, M.C., Gimeno-Alcañiz, J.V., Rubio, T., García-Haro, L., Foretz, M., Rodríguez de Córdoba, S., Sanz, P. (2009) AMP-activated protein kinase phosphorylates R5/PTG, the glycogen targeting subunit of the R5/PTG-protein phosphatase 1 holoenzyme, and accelerates its down-regulation by the laforin-malin complex. *Journal of Biological Chemistry*. **284**(13), 8247–8255.

Wakayama, Y., Miura, K., Sabe, H., Mochizuki, N. (2011) EphrinA1-EphA2 signal induces compaction and polarization of Madin-Darby canine kidney cells by inactivating Ezrin through negative regulation of RhoA. *The Journal of biological chemistry*. **286**(51), 44243–53.

Wang, E., Brown, P.S., Aroeti, B., Chapin, S.J., Mostov, K.E., Dunn, K.W., Dunn, K.W. (2000) Apical and Basolateral Endocytic Pathways of MDCK Cells Meet in Acidic Common Endosomes Distinct from a Nearly-Neutral Apical Recycling Endosome. *Traffic*. **1**, 480–493.

Wang, H., Quah, S.Y., Dong, J.M., Manser, E., Tang, J.P., Zeng, Q. (2007) PRL-3 down-regulates PTEN expression and signals through PI3K to promote epithelial-mesenchymal transition. *Cancer research*. **67**(7), 2922–6.

Wang, H., Vardy, L.A., Tan, C.P., Loo, J.M., Guo, K., Li, J., Lim, S.G., Zhou, J., Chng, W.J., Ng, S.B., Li, H.X., Zeng, Q. (2010) PCBP1 suppresses the translation of metastasis-associated PRL-3 phosphatase. *Cancer cell*. **18**(1), 52–62.

Wang, T., Yanger, K., Stanger, B.Z., Cassio, D., Bi, E. (2014) Cytokinesis defines a spatial landmark for hepatocyte polarization and apical lumen formation. *Journal of cell science*. **127**(Pt 11), 2483–92.

Wang, X., Yue, P., Young, A.K., Fu, H., Khuri, F.R., Sun, S.Y. (2008) Enhancing mammalian target of rapamycin (mTOR)-targeted cancer therapy by preventing mTOR/raptor inhibition-initiated, mTOR/rictor-independent Akt activation. *Cancer Research*. **68**(18), 7409–7418.

Wang, X., Zhao, B.S., Roundtree, I.A., Lu, Z., Han, D., Ma, H., Weng, X., Chen, K., Shi, H., He, C. (2015) N^6-methyladenosine modulates messenger RNA translation efficiency. *Cell*. **161**(6), 1388–1399.

Warner, A.K., Keen, J.H., Wang, Y.L. (2006) Dynamics of membrane clathrin-coated structures during cytokinesis. *Traffic*. **7**(2), 205–215.

Webb, D.J., Horwitz, A.F. (2003) New dimensions in cell migration. *Nature cell biology*. **5**(8), 690–692.

Webb, M.R. (1992) A continuous spectrophotometric assay for inorganic-phosphate and for measuring phosphate release kinetics in biological-systems. *Proceedings Of The National Academy Of Sciences Of The United States Of America*. **89**(11), 4884–4887.

Wei, C., Bhattaram, V.K., Igwe, J.C., Fleming, E., Tirnauer, J.S. (2012) The LKB1 tumor suppressor controls spindle orientation and localization of activated AMPK in mitotic epithelial cells. *PloS one*. **7**(7), e41118.

Weisz, O. a, Rodriguez-Boulan, E. (2009) Apical trafficking in epithelial cells: signals, clusters and motors. *Journal of cell science*. **122**(Pt 23), 4253–4266.

Wenk, M.R., Pellegrini, L., Klenchin, V.A., Di Paolo, G., Chang, S., Daniell, L., Arioka, M., Martin, T.F., De Camilli, P. (2001) PIP kinase Igamma is the major PI(4,5)P2 synthesizing enzyme at the synapse. *Neuron*. **32**(1), 79–88.

Wong, R., Hadjiyanni, I., Wei, H.C., Polevoy, G., McBride, R., Sem, K.P., Brill, J.A. (2005) PIP2 hydrolysis and calcium release are required for cytokinesis in Drosophila spermatocytes. *Current Biology*. **15**(15), 1401–1406.

Worby, C.A., Gentry, M.S., Dixon, J.E. (2006) Laforin, a dual specificity phosphatase that dephosphorylates complex carbohydrates. *Journal of Biological Chemistry*. **281**(41), 30412–30418.

Woźniak, M.J., Allan, V.J. (2006) Cargo selection by specific kinesin light chain 1 isoforms. *The EMBO journal*. **25**(23), 5457–68.

Wu, J.-Q.Q., Pollard, T.D. (2005) Counting cytokinesis proteins globally and locally in fission yeast. *Science New York NY*. **310**(5746), 310–314.

Xie, L.H., Takano, M., Kakei, M., Okamura, M., Noma, A. (1999) Wortmannin, an inhibitor of phosphatidylinositol kinases, blocks the MgATP-dependent recovery of Kir6.2/SUR2A channels. *Journal of Physiology*. **514**(3), 655–665.

Xing, C., Lu, X.X., Guo, P. Da, Shen, T., Zhang, S., He, X.S., Gan, W.J., Li, X.M., Wang, J.R., Zhao, Y.Y., Wu, H., Li, J.M. (2016) Ubiquitin-specific protease 4-mediated deubiquitination and stabilization of PRL-3 is required for potentiating colorectal oncogenesis. *Cancer Research*. **76**(1), 83–95.

Xiong, J., Li, Z., Zhang, Y., Li, D., Zhang, G., Luo, X., Jie, Z., Liu, Y., Cao, Y., Le, Z., Tan, S., Zou, W., Gong, P., Qiu, L., Li, Y., Wang, H., Chen, H. (2016) PRL-3 promotes the peritoneal metastasis of gastric cancer through the PI3K/Akt signaling pathway by regulating PTEN. *Oncology Reports*. **36**(4), 1819–1828.

Xu, C., Wang, X., Liu, K., Roundtree, I.A., Tempel, W., Li, Y., Lu, Z., He, C., Min, J. (2014) Structural basis for selective binding of m6A RNA by the YTHDC1 YTH domain. *Nature chemical biology*. **10**(11), 927–929.

Xu, J., Cao, S., Wang, L., Xu, R., Chen, G., Xu, Q. (2011) VEGF promotes the transcription of the human PRL-3 gene in HUVEC through transcription factor MEF2C. *PLoS ONE*. **6**(11), e27165.

Yeh, H.-C., Li, C.-C., Huang, C.-N., Hour, T.-C., Yeh, B.-W., Li, W.-M., Liang, P.-I., Chang, L.-L., Li, C.-F., Wu, W.-J. (2015) PTP4A3 Independently Predicts Metastasis and Survival in Upper Tract Urothelial Carcinoma Treated with Radical Nephroureterectomy. *The Journal of urology*. **194**(5), 1449–55.

Yeh, M., Huang, C., Li, C., Chang, L., Lin, H., Ke, H., Huang, A., Liang, P., Li, C., Wu, W. (2016) Overexpression of PTP4A3 is associated with metastasis and unfavorable prognosis in bladder cancer. *World J Urol.*. **34**(6), 835–846.

Yu, A., Rual, J.F., Tamai, K., Harada, Y., Vidal, M., He, X., Kirchhausen, T. (2007) Association of Dishevelled with the Clathrin AP-2 Adaptor Is Required for Frizzled Endocytosis and Planar Cell Polarity Signaling. *Developmental Cell*. **12**(1), 129–141.

Yuan, T.L., Cantley, L.C. (2008) PI3K pathway alterations in cancer: variations on a theme. *Oncogene*. **27**(41), 5497–510.

Zanini, I.M.Y., Soneson, C., Lorenzi, L.E., Azzalin, C.M. (2017) Human cactin interacts with DHX8 and SRRM2 to assure efficient pre-mRNA splicing and sister chromatid cohesion. *J Cell Sci*. **130**, 767–778.

Zeng, Q., Si, X., Horstmann, H., Xu, Y., Hong, W., Pallen, C.J. (2000) Prenylation-dependent association of protein-tyrosine phosphatases PRL-1, -2, and -3 with the plasma membrane and the early endosome. *The Journal of biological chemistry*. **275**(28), 21444–52.

Zhang, C., Tian, W., Meng, L., Qu, L., Shou, C. (2015) PRL-3 promotes gastric cancer migration and invasion through a NF-kappaB-HIF-1alpha-miR-210 axis. *Journal of molecular medicine (Berlin, Germany)*, 401–415.

Zhang, H., Kozlov, G., Li, X., Wu, H., Gulerez, I., Gehring, K. (2017) PRL3 phosphatase active site is required for binding the putative magnesium transporter CNNM3. *Scientific reports*. **7**(48), 1–9.

Zhang, X.C., Piccini, A., Myers, M.P., Van Aelst, L., Tonks, N.K. (2012) Functional analysis of the protein phosphatase activity of PTEN. *The Biochemical journal*. **444**(3), 457–64.

Zhao, W.-B., Li, Y., Liu, X., Zhang, L.-Y., Wang, X. (2008) Evaluation of PRL-3 expression, and its correlation with angiogenesis and invasion in hepatocellular carcinoma. *International Journal of Molecular Medicine*. **22**(2), 187–192.

Zheng, P., Liu, Y.-X., Chen, L., Liu, X.-H., Xiao, Z.-Q., Zhao, L., Li, G.-Q., Zhou, J., Ding, Y.-Q., Li, J.-M. (2010) Stathmin, a new target of PRL-3 identified by proteomic methods, plays a key role in progression and metastasis of colorectal cancer. *Journal of Proteome Research*. **9**(10), 4897–4905.

Zheng, Z., Zhu, H., Wan, Q., Liu, J., Xiao, Z., Siderovski, D.P., Du, Q. (2010) LGN regulates mitotic spindle orientation during epithelial morphogenesis. *The Journal of cell biology*. **189**(2), 275–88.

Zhou, J., Chong, P.S., Lu, X., Cheong, L.-L., Bi, C., Liu, S.-C., Zhou, Y., Tan, T.Z., Yang, H., Chung, T.-H., Zeng, Q., Chng, W.-J. (2014) Phosphatase of regenerating liver-3 is regulated by signal transducer and activator of transcription 3 in acute myeloid leukemia. *Experimental Hematology*. **42**(12), 1041–1052.e2.

Zhu, L., Crothers, J., Zhou, R., Forte, J.G. (2010) A possible mechanism for ezrin to establish epithelial cell polarity. *American journal of physiology. Cell physiology*. **299**(2), C431–C443.

Zimmerman, M.W., Homanics, G.E., Lazo, J.S. (2013) Targeted deletion of the metastasis-associated phosphatase Ptp4a3 (PRL-3) suppresses murine colon cancer. *PloS one*. **8**(3), e58300.

Zimmerman, M.W., McQueeney, K.E., Isenberg, J.S., Pitt, B.R., Wasserloos, K.A.,

Homanics, G.E., Lazo, J.S. (2014) Protein-tyrosine phosphatase 4A3 (PTP4A3) promotes vascular endothelial growth factor signaling and enables endothelial cell motility. *Journal of Biological Chemistry*. **289**(9), 5904–5913.

Zuo, X., Guo, W., Lipschutz, J.H. (2009) The exocyst protein Sec10 is necessary for primary ciliogenesis and cystogenesis in vitro. *Molecular biology of the cell*. **20**(10), 2522–2529.